Experimental and Theoretical Studies of Reactions Important in Photochemical Smog: Aromatics and Alkanes

Thesis by

Jean M. Andino

In Partial Fulfillment of the Requirements

for the Degree of

Doctor of Philosophy

California Institute of Technology

Pasadena, California

1996

Defended: January 2, 1996

Acknowledgments

There are many people that I would like to acknowledge. First, I would like to thank my primary advisors, John Seinfeld and Richard Flagan for the support that they gave me in establishing the new Indoor Photochemical Reactor and carrying out the research in this thesis. I will always be proud to have been a part of the "Air Pollution/Aerosols Group" family. Thanks to Richard Eastvedt for his handiness and patience...without him, the dream of the Indoor Photochemical Reactor would have been just that...a dream. Many thanks to group members Lynn Russell, Shou Hua Zhang, and Donald Dabdub for lending a helpful suggestion...or just an ear when I really needed it.

Special thanks to Connie Calderón, Michelle Medley, and Sue Bunker for countless hours of support. Each of you has, in your own way, helped me to grow as an individual, and I am grateful to have learned from and worked with each of you.

I am indebted to all of my brothers and sisters from Caltech, especially Danny Howard, for the unwavering support, words of encouragement, and occasional weekend diversions at *La Casa*. As I leave Caltech, my hopes are

that each of you will stay dedicated, keep the faith, and always remember where you came from as you continue up your respective ladders of success.

Most importantly, my thanks go to my mother, Maria Victoria Andino, whose love, support, caring, and inspiration have brought me as far as I have come! This thesis and my Ph.D. are dedicated to you for all of the sacrifices that you have made throughout my life.

Appearing below are two quotes that guided me in the past, and became even more meaningful during my time at Caltech.

El que no busca, no encuentra.

El que no escucha, no aprende.

El que no trata, fracasa, con el alma y con la mente.

Cuando hay fé, hay con que hacer lo que hay que hacer. - Rubén Blades

Knowledge of the effort required to carry us this distance should propel us in the right direction and help us bear up under our own burdens.

Continuing the struggle is the best way we have of saying thank you to those who struggled for us. -Eric V. Copage

Abstract

The development of effective ozone control strategies requires the use of atmospheric models. There is general agreement within the scientific community that several aspects of the chemistry within these models has yet to be fully elucidated, and is influential in their predictions. The work in this thesis is aimed at trying to determine some of the unknown aspects of the mechanisms of important atmospheric species. Specifically, the gas-phase reactions of two large alkanes, 2,2,4-trimethylpentane and 2,2,5-trimethylhexane are investigated. These two alkanes are present in urban air, and are potential aerosol presursors. The chemistry of several aromatic hydrocarbons are also studied using both theoretical and experimental techniques. The effects of NO_2 on the photooxidation of toluene, m-xylene, and p-xylene are examined, and mechanisms of each of these organics are thouroughly evaluated through closely coordinated laboratory work and computer modeling. In addition, product studies of the photooxidation of 1,2,4-trimethylbenzene and m-ethyltoluene are conducted. These studies provide the first identification of ring-retained products from 1,2,4-trimethylbenzene, and ring-retained and fragmented products from m-ethyltoluene.

A new indoor experimental reactor was designed to investigate gas-phase reaction kinetics and mechanisms. This new system has served to launch the atmospheric chemistry program at Caltech into a wide variety of new research topics.

Contents

List of Tables

List of Figures

Chapter 1

Introduction

With the advent of industrialization came an increase in the emission of primary pollutants such as hydrocarbons and oxides of nitrogen. In the presence of sunlight, these primary pollutants react to form photochemical smog. To date, photochemical smog has been identified as the cause of adverse health effects in humans, phytotoxicity, the deterioration of buildings, and the reduction of visibility and solar radiation, among other things. For these reasons, it is important to fully understand and characterize the components leading to the formation of photochemical smog.

In order to control and abate the harmful effects of photochemical smog, its main components must be defined, and limits to their concentrations established. National ambient air quality standards (NAAQS) have been set for photochemical smog components such as ozone, nitrogen dioxide, and nitric oxide. The level and frequency of exceedences in particular areas of the country determine when air pollution control strategies are necessary. In the Los Angeles area, the main concern has focused particularly on extremely high levels of ozone. Agencies such as the Air Quality Management District and the California Air Resources Board have encouraged an increase in carpooling efforts and decreased use of items that result in high evaporative emissions of hydrocarbons (such as lighter fluid, commonly used in barbecues). The efforts of these two agencies have resulted in the improvement of air quality in Los Angeles, and a reduction in the number of exceedences of the NAAQS for ozone over the last decade.

Predictive computer modeling has been used to establish and evaluate proposed air pollution control strategies. However, many important issues related to these predictive models have yet to be fully elucidated. Mod-

els which currently exist include four components: chemistry, meteorology, transport mechanisms, and emissions data. In order to devise an effective air pollution control strategy, each of these components must reasonably represent the actual conditions present in the atmosphere. The work in this thesis is aimed at addressing two of the important, and as of yet unsettled issues in the chemistry portion of atmospheric models: the atmospheric chemistry of large alkanes and aromatic compounds.

The major loss processes for hydrocarbons in the atmosphere involve reaction with the oxidants O_3, OH, and NO_3. Rate constants for the reactions of many organics with these oxidants have been determined, and compilations of these values appear in Atkinson, 1989 and Atkinson, 1994. From these rates constants, and assuming concentrations of O_3, OH, and NO_3 of 7×10^{11}, 1.5×10^6, and 5×10^8 molecules cm^{-3}, respectively, lifetimes of organic compounds with respect to reaction with the three major oxidants can be determined [5]. Table 1.1, adapted from Seinfeld et al., 1995, details the tropospheric lifetimes of selected hydrocarbons. For the aromatics and the alkanes listed, it is evident that the major atmospheric loss process for these two classes of compounds are reactions with hydroxyl radicals. Thus, it is these reactions with hydroxyl radicals that are the focus of this thesis.

When hydrocarbons react in the atmosphere, they inevitably form peroxy radicals. In the polluted troposphere, these peroxy radicals convert NO to NO_2. The formation of NO_2 is significant in that its subsequent photolysis is the principal mechanism for ozone formation. The reactions can be summarized as:

Table 1.1: Tropospheric Lifetimes of Selected Organics

Organic	Lifetime due to reaction with:		
	OH	NO_3	O_3
Methane	9.6 yr	>120 yr	
Ethane	60 d	> 12 yr	
Propane	13d	>2.5 yr	
Ethene	1.8 d	225 d	9.7 d
Propene	7.0 h	4.9 d	1.5 d
Methanol	17 d	> 77 d	
Ethanol	4.7 d	> 51 d	
Benzene	12.5 d	> 6 yr	> 4.5 yr
Toluene	2.6 d	1.9 yr	> 4.5 yr
m-Xylene	7.8 h	200 d	> 4.5 yr

$$\text{Hydrocarbon} + \cdot\text{OH} \rightarrow \text{R}\cdot$$

$$\text{R}\cdot + O_2 \rightarrow RO_2^{\cdot}$$

$$RO_2^{\cdot} + NO \rightarrow RO\cdot + NO_2$$

$$NO_2 + h\nu \rightarrow O\cdot + NO$$

$$O\cdot + O_2 \rightarrow O_3$$
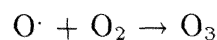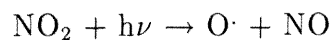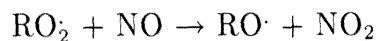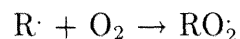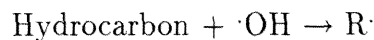
Thus NO_2 plays an important role in the formation of photochemical smog.

The kinetics and mechanisms of small alkanes have been widely characterized[2]. However, the only available literature data concerning the larger alkanes (> C_8) are kinetic data [3, 1]. The mechanisms of large alkane photooxidation have not been widely investigated. Many of these compounds are used in gasoline and industries. The potential for release of alkanes into the atmosphere is thus quite high. These alkanes can react in the atmosphere according to the reactions detailed above to eventually generate ozone and adversely affect air quality. The large alkanes are especially important. In

addition to their ozone forming potential, compounds with more than six carbons have been identified as potential aerosol precursors. It is therefore important to fully characterize the gas-phase mechanism of the large alkane reactions. This thesis focuses on the gas-phase OH radical reactions of two large, branched alkanes: 2,2,4-trimethylpentane and 2,2,5-trimethylhexane.

The atmospheric chemistry of several of the more common aromatics (benzene, toluene, m- and p-xylene) have been investigated in the past[2]. The major atmospheric sink of this class of compounds is reaction with hydroxyl radicals via both the addition of OH to the ring and abstraction of an H atom from the ring. However, the addition pathway dominates to form a methyl substituted hydroxycyclohexadienyl radical. It is this radical and its subsequent fate that are in question. Our approach to the question of the fate of the radical was two-fold: experimental and theoretical in nature. From the experimental perspective, our goal was to investigate the effect of NO_2 on the reactions of the aromatic-oh adduct. Recent evidence has suggested that the role of NO_2 may be more important than previously believed [4]. We therefore undertook a systematic laboratory study of the effects of NO_2 on the toluene, m-xylene, p-xylene, m-ethyltoluene, and 1,2,4-trimethylbenzene systems. From the theoretical perspective, our goal was to identify the intermediates believe to form from the susequent reactions of the methyl substituted hydroxycyclohexadienyl radicals. Semi-empirical and *ab initio* techniques were used to determine the energies of all possible intermediates in the same aromatic systems which were studied experimentally. The results of the theoretical calculations were compared to available product data, and full mechanisms, from initial OH radical attack to stable

product formation, were developed for each aromatic.

Bibliography

[1] Atkinson, R., Gas-Phase Tropospheric Chemistry of Organic Compounds, *J. Phys.Chem. Ref. Data*, **Mongraph 2**, 1 (1994).

[2] Atkinson, R., Gas-Phase Tropospheric Chemistry of Organic Compounds: A Review, *Atmos. Environ.*, **24A**, 1(1990).

[3] Atkinson, R., Kinetics and Mechanisms of the Gas-Phase Reactions of the Hydroxyl Radical Reaction with Organic Compounds, *J. Phys. Chem. Ref. Data.*, **Monograph 1**, 1 (1989).

[4] Atkinson,R. Aschmann,S., Arey, J., Carter,W., Formation of Ring Retaining Products from the OH Radical-Initiated Reactions of Benzene and Toluene *Int. J. Chem. Kinet.*, **21**, 801 (1989).

[5] Seinfeld, J.H., Andino, J.M., Bowman, F.M., Forstner, H.J., Pandis, S., Tropospheric Chemistry, *Adv. Chem. Eng.*, **19**, 325 (1995).

[6] Lurman, F.W. and Main, H.H., "Analysis of the Ambient VOC Data Collected in the Southern Air Quality Study," Final Report, Contract

No. A832-130. State of California Air Resources Board, Sacramento (1992).

Chapter 2

Experimental System

2.1 Photochemical Reactor

A new indoor photochemical reactor was designed and constructed to study detailed gas-phase kinetics and mechanisms. A schematic of the reactor appears in Figure 2.1, and a photograph of the chamber is in Figure 2.2. The system provides for excellent control of experimental parameters such as light intensity and temperature. The reaction chamber is a batch reactor composed of 2 mil Teflon FEP film, with a volume of approximately 1000 liters. Teflon film has a low absorbance in the ultraviolet wavelength region of critical importance to reactions in the troposphere (in the region around 350 nm), and is sufficiently versatile to allow for ease in cleaning or disposal. An absorbance spectrum of the teflon used appears in Figure 2.3. This spectrum was generated using a variable wavelength Fourier transform spectrometer (Nicolet SX 400).

Artificial light (two banks of 24 Sylvania F30T8BL black lamps) is used to initiate the chemistry within the chamber. The lamps are mounted on a specially designed reflective surface to provide uniformity in irradiation. There are many different types of lamps which could have been used to generate artificial light. These particular ultraviolet lamps were chosen because of the similarity of their spectral distribution to that of the radiation reaching the earth. The sun emits a variety of wavelengths of light. Radiation reaching the stratosphere contains wavelengths greater than 180 nm. Through the stratosphere, the radiation is filtered by ozone so that only wavelengths greater than 290 nm actually reach the earth. These particular black lamps emit most of their light in wavelength regions which are crucial for tropo-
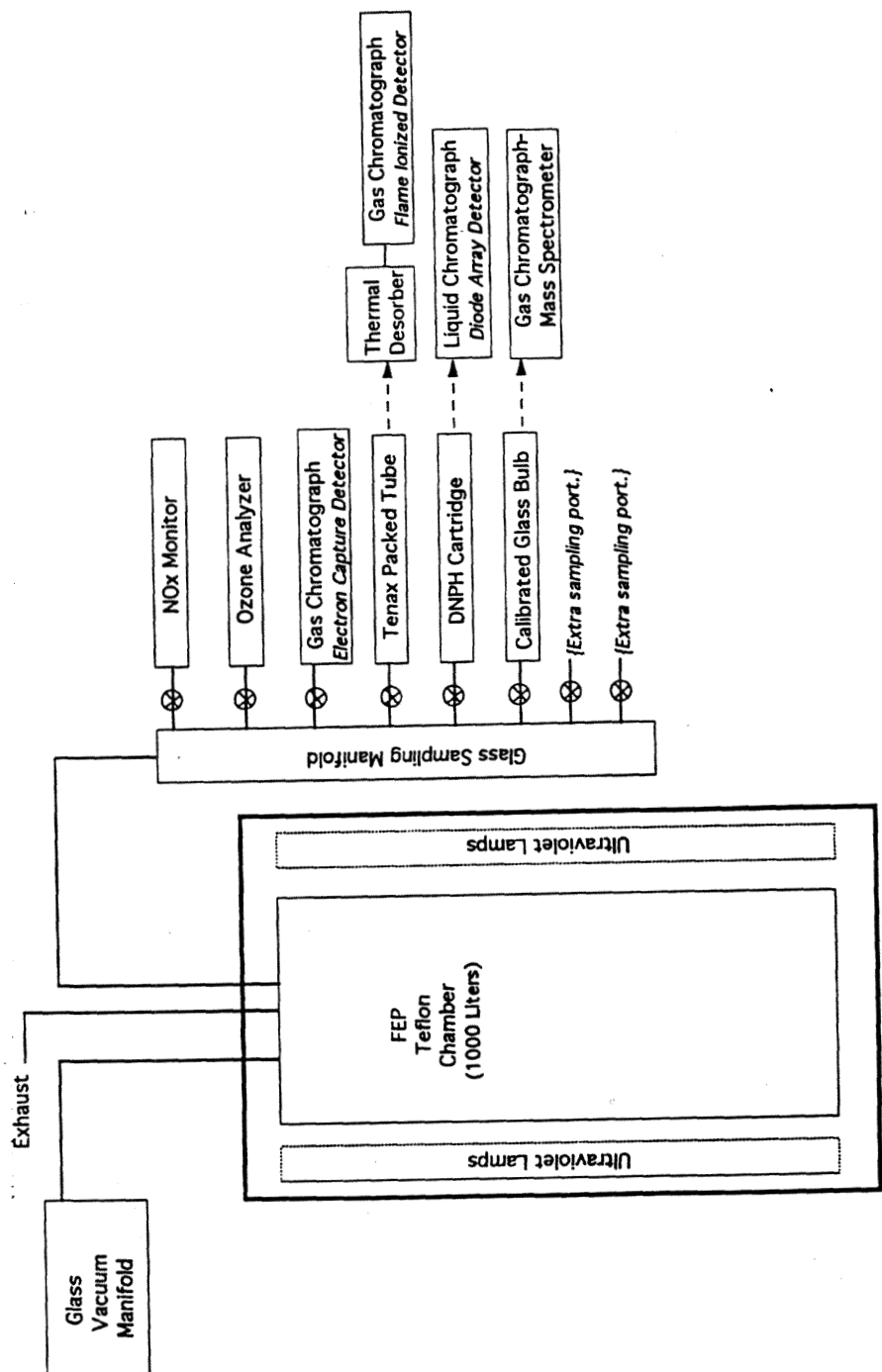
Figure 2.1: Schematic of the Indoor Photochemical Reactor.
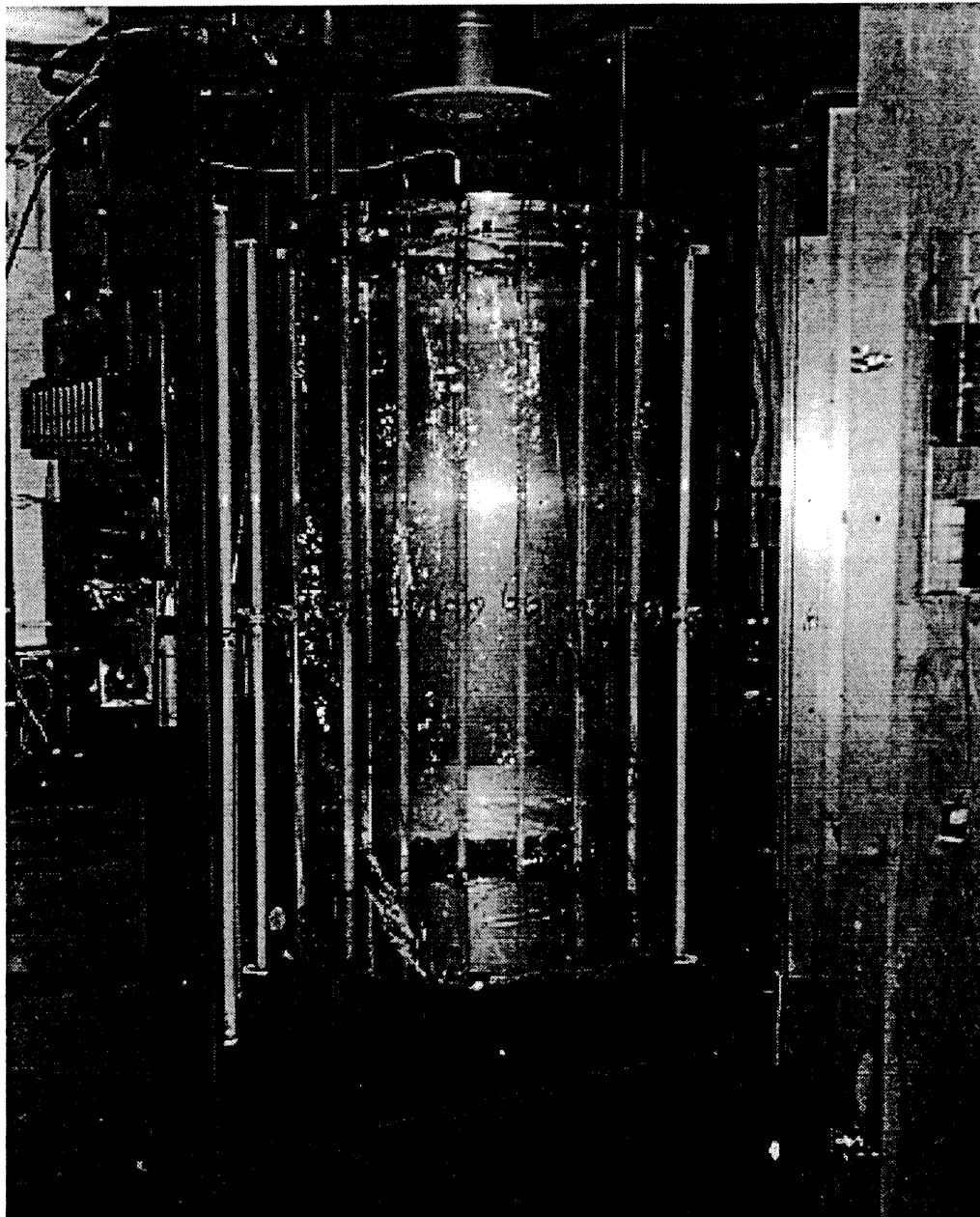
Figure 2.2: Photograph of the Indoor Photochemical Reactor.
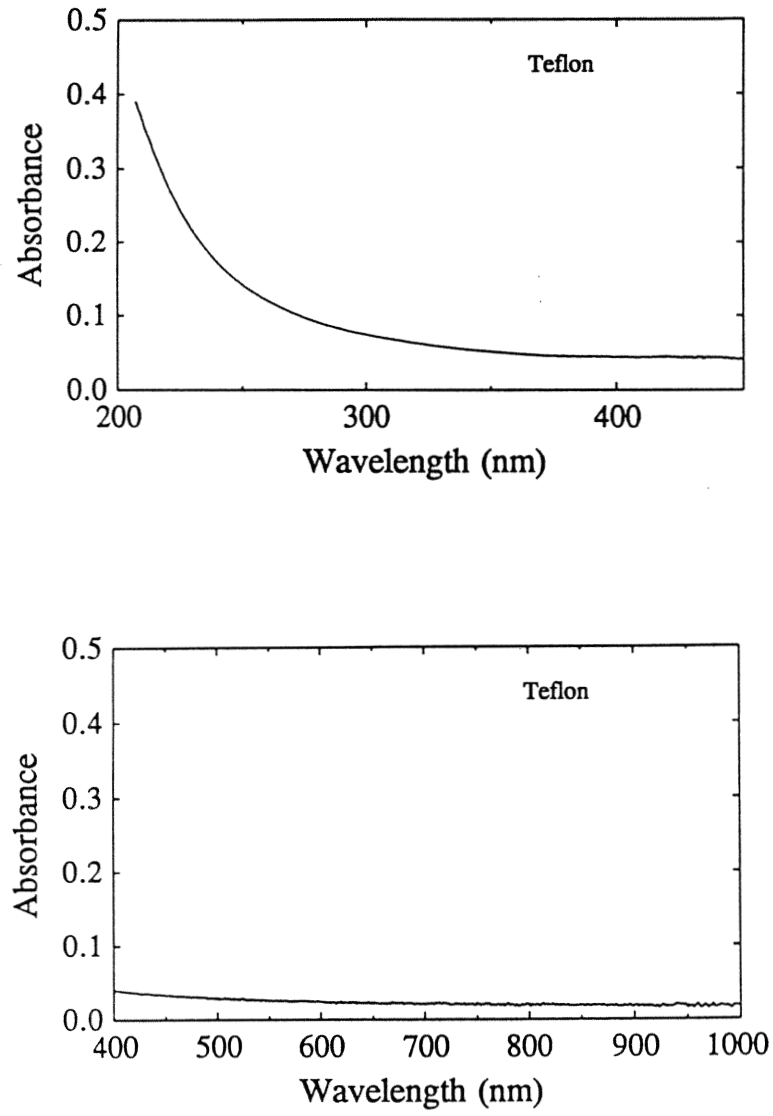
Figure 2.3: Absorbance spectrum of 2 mil FEP teflon film.

spheric chemistry, thereby allowing for the simulation of atmospheric activity. The spectral distribution of a Sylvania F30T8BL black lamp appears in Figure 2.4, spectrum (A), and was obtained directly from Sylvania. The sharp features in the lamp spectrum are mercury absorption lines which can be attributed to the material used to construct the lamps. For comparison, the spectral absorption of NO_2, formaldehyde, and methyl glyoxal appear in Figure 2.4, (B), (C), and (D), respectively. The spectral data for these plots were obtained from Bass et al., 1983 and Moortgat et al., 1983 for formaldehyde, NASA, 1987 for NO_2, and Plum et al., 1993 for methyl glyoxal. These three compounds are significant to atmospheric processes, and are representative of the types of compounds that would be present in indoor chamber studies. A comparison of the spectral distribution of sun at two different zenith angles, 0 and 40 degrees, and the black lights appears in Figure 2.5. The light intensity within the chamber can be adjusted by varying the number of lamps from the minimum of 2 lamps to a maximum of 48 lamps.

A feedback-controlled cooling system which blows cool air around the chamber is used to control the temperature within the chamber. Temperature probes are located both inside of the bag and between the bag and the lamps. The temperature probe located on the outside of the bag is used to control the temperture of the system. The probe inside of the bag is used to record the actual bag temperature. The system is ordinarily set to operate at 298 ± 2 K.

The reaction chamber is coupled to a glass vacuum manifold (input) and a glass sampling manifold (output). The glass vacuum manifold, pictured in Figure 2.6, has several detachable calibrated bulbs (only one is pictured)
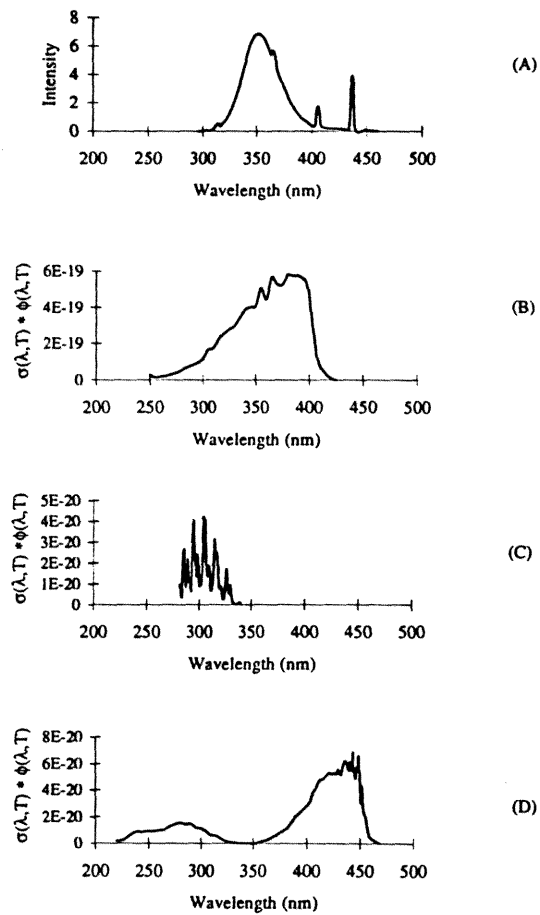
Figure 2.4: (A) Spectral distribution of black lamps. (B) Absorbance Coefficient * Quantum Yield for NO_2. (C) Absorbance Coefficient * Quantum Yield for HCHO. (D) Absorbance Coefficient * Quantum Yield for methyl glyoxal.
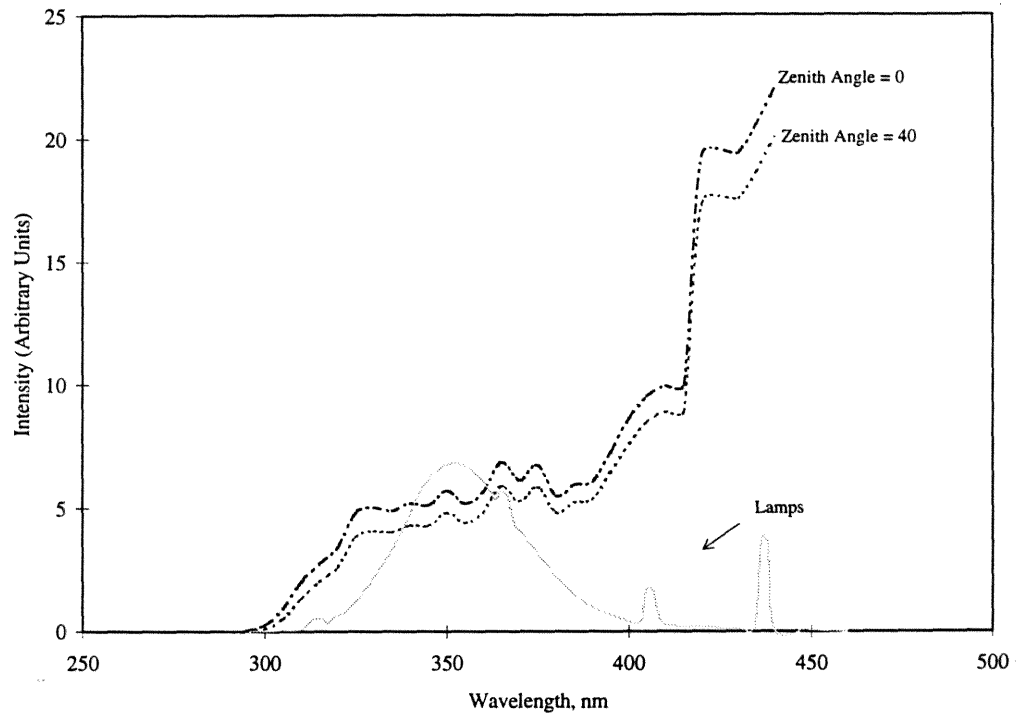
Figure 2.5: Scaled spectral distribution of sun at zenith angles of 0 and 40 degrees as compared to Sylvania F30T8BL lamps.

Table 2.1: Equipment For Indoor Photochemical Reactor Experiments

Name	Manufacturer/Model Number
NO$_x$ monitor	Thermo Environmental / Model 42
Ozone Analyzer	Dasibi / Model 1003PC
Gas Chromatograph (ECD)	Shimadzu / Mini GC II
Gas Chromatograph (FID)	Hewlett Packard / Model 5890 Series II
Liquid Chromatograph (DAD)	Hewlett Packard / Model 1090
Gas Chromatograph (MS)	Hewlett Packard / Models 5890 and 5898

which are used to admit known amounts of volatile reactants (such as methyl or ethyl nitrite) to the chamber. The evaporation bulb is used to admit organics by gently evaporating liquid samples with a heat gun while flowing air through the bulb. The sampling manifold has several ports (with stopcocks on them) which are used to deliver gas chamber samples to various on- and off-line analytical instruments. The schematic (Figure 2.1) shows how each port is used. Note that the dashed arrows indicate off-line analytical capabilites. In addition, because of the set up of our laboratory, it is possible to alter our system so that the GC-FID operates on-line rather than off-line (through the tenax packed tubes and the thermal desorber). Table 2.1 lists the manufacturers and model numbers of the equipment typically available for use with the indoor photochemical reactor.

An air purification system is used to deliver contaminant-free air to the chamber and the glass vacuum manifold. The system is made up of three stainless steel tubes. Tubes 1,2, and 3 are filled with 50% molecular sieves/50% drierite, purafil, and activated carbon, respectively. Scrubbed air fed to the chamber typically contains less than approximately 1-2 ppb of ozone, NO$_x$, or hydrocarbons.
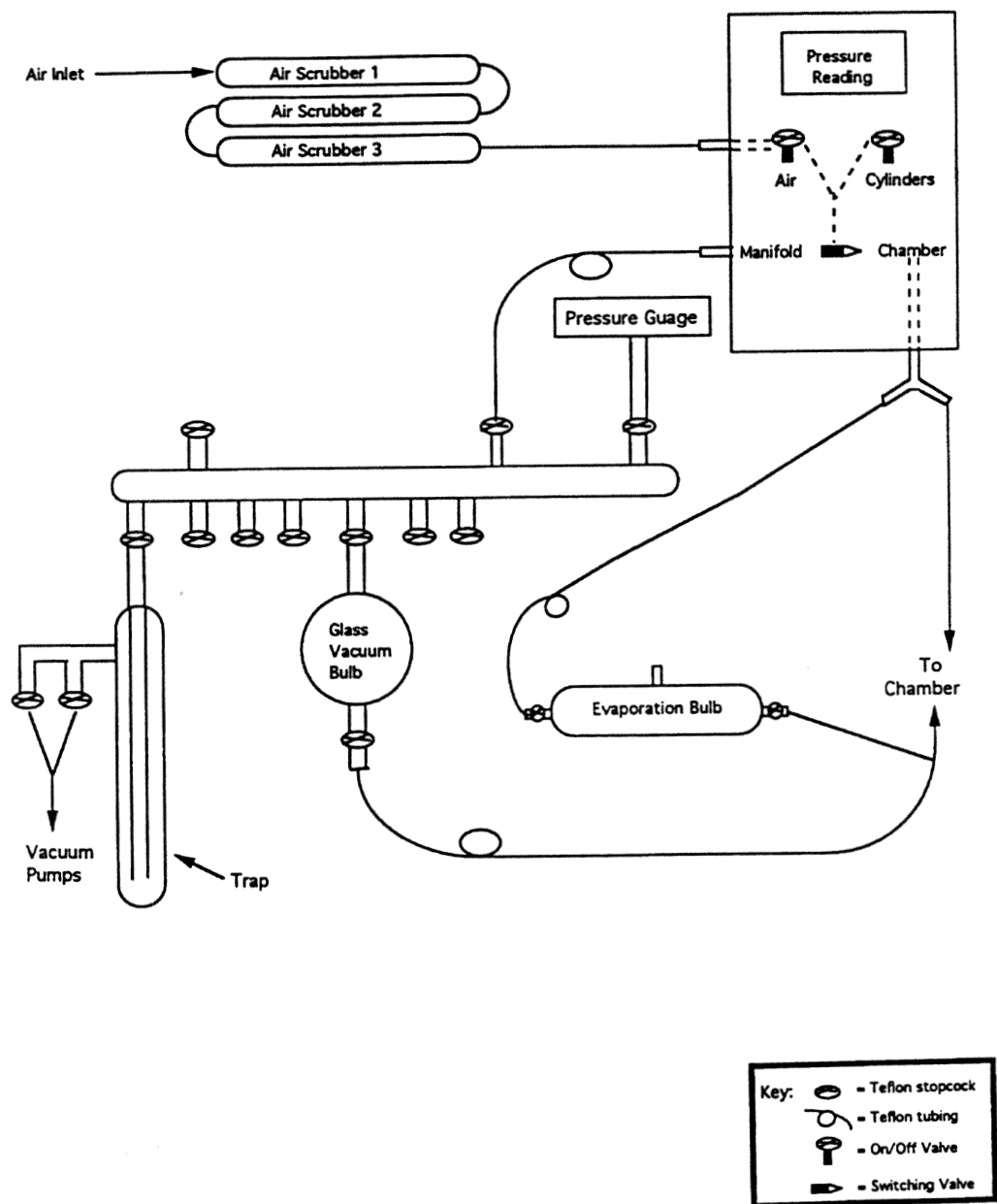
Figure 2.6: Schematic of the glass vacuum manifold which is used to admit reactants to the chamber.

2.2 Experimental System Characterization

2.2.1 Ultraviolet Light Intensity

One of the most important considerations in an indoor system lies in the determination of the ultraviolet intensity. This determination is crucial in ensuring that during the computer modeling of the experiments, all loss processes of photolyzing species are accurately accounted for. The ultraviolet intensity within the chamber is related to the photolysis rate constant through the following mathematical relationship:

$$k(T) = \int \sigma(\lambda, T)\phi(\lambda, T)I(\lambda)d\lambda, \tag{2.1}$$

where: $\sigma(\lambda, T)$ = absorption coefficient

$\phi(\lambda, T)$ = quantum yield

$I(\lambda)$ = lamp intensity.

A calculation of the photolysis rate constants for various species can be made given the absorption coefficients and the quantum yields, but an experimental determination of the value is needed in order take into account the age and decreasing intensity of the lamps. The most widely accepted technique of determining the ultraviolet intensity of black lamps is a chemistry-based technique which relies on the photolysis of NO_2 [3]. As mentioned earlier, NO_2 is a critical component in the formation of ozone in the troposphere. In addition, nitrogen dioxide absorbs most of its energy in the wavelength region

were a large portion of tropospheric chemistry takes place (see Figure 2.4, B) and where the black lamp output is a maximum. Although other atmospheric species such as formaldehyde and ozone absorb in wavelength regions of crucial importance to tropospheric chemistry, their absorption coefficients are an order of magnitude lower than that of NO_2 in the same region.

By investigating the reaction of NO_2 in pure nitrogen diluent, a measure of the ultraviolet lamp intensity can be determined. The pertinent reactions in such a system are:

(1) $NO_2 + h\nu \rightarrow O + NO$

(2) $O + O_2 + M \rightarrow O_3 + M$

(3) $O_3 + NO \rightarrow O_2 + NO_2$

(4) $O + NO_2 \rightarrow O_2 + NO$

(5) $O + NO_2 + M \rightarrow NO_3 + M$

(6) $NO_3 + NO \rightarrow NO_2 + NO_2$

(7) $O + NO + M \rightarrow NO_2 + M$
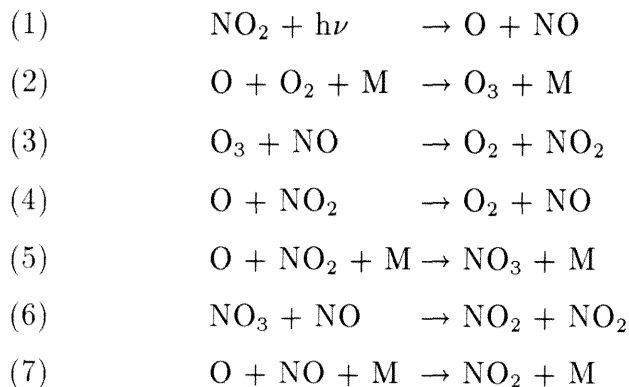
If O_2 is not initially present in the system, one can assume that $[O]$, $[NO_3]$, and $[O_3]$ are at steady state. In addition, one can state that $[NO] = [NO]_o + [NO_2]_o - [NO_2]$. An expression for k_1, a measure of the light intensity, can then be obtained as [4]:

$$k_1 = \frac{1}{2\Delta t} \left\{ [1 + R_1 + R_2] \ln \frac{[NO_2]_o}{[NO_2]} + R_2 \left(\frac{[NO_2]_o}{[NO_2]} - 1 \right) \right\}$$

where

$$\Delta t = t_{final} - t_{initial}$$

$$R_1 = \frac{k_5[M]}{k_4}$$

$$R_2 = \frac{k_7[M]}{k_4}$$

assuming that [NO] and [O_2] are initially zero. (Note that if oxygen is initially present in the system, the above equation no longer holds since the steady-state assumptions do not necessarily apply. It has been estimated that concentrations above 20 ppm of oxygen will affect the determination of k_1 for the NO_2 system [4]). By measuring the concentration of NO_2 using a calibrated NO_x monitor, and knowing the total diluent concentration, k_1 can be determined. A complete derivation of k_1 appears in Appendix 1.

Although the use of NO_2 as a determination of the uv light intensity is a widely accepted practice, one should also note that it does not fully characterize the photolysis rates of other compounds in the system. Various other compounds which can potentially form and photolyze in the reaction chamber have absorption spectra and wavelength dependencies which are quite different from that of NO_2. A measure of k_1 is thus not necessarily an accurate measure of the photolysis rates of these other compounds. However, the Carter modeling program[2] used in this thesis incorporates the absorption spectra and quantum yields of these compounds in conjunction with a normalization factor (determined by ratioing the experimentally and mathematically determined values of k_1) to determine the photolysis rate constants of the additional compounds. Rate constant derived from the Carter program for several compounds are presented in Table 2.2.

Table 2.2: Rate constants generated from the Carter program after normalization.

Compound	Rate Constant (min^{-1})
NO_2	4×10^{-2}
HONO	1.119×10^{-2}
HCHO	7.039×10^{-5}
H_2O_2	2.994×10^{-5}
$O_3(O^3P)$	1.942×10^{-4}
$O_3(O^1D)$	4.020×10^{-5}

2.2.2 Methyl Nitrite Chemistry

Methyl nitrite, CH_3ONO, is commonly used as a source of OH radicals in chamber studies [3]. A spectrum of the absorbance of methyl nitrite (as compared to another important nitrite, t-butyl nitrite), taken from Pitts and Pitts, 1986, appears in Figure 2.7. (The quantum yield is taken as 1, so this figure is directly comparable to the spectra of Figure 2.4.) At wavelengths > 320 nm, methyl nitrite photolyzes according to the following:

$$CH_3ONO + h\nu \rightarrow CH_3O\cdot + NO$$
$$CH_3O\cdot + O_2 \rightarrow HCHO + HO_2$$
$$HO_2^\cdot + NO \rightarrow OH\cdot + NO_2$$
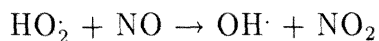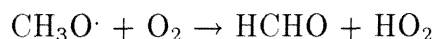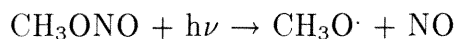
In order to adequately model the experimental studies presented in this thesis, it is important to characterize the photolysis rate constant for methyl nitrite (j_{CH_3ONO}). Thus, experiments were conducted by photolyzing CH_3ONO-air and CH_3ONO-NO-air systems and monitoring concentrations using a NO_x monitor. The photolysis rate constant for methyl nitrite was determined by fits of experimental data for NO to theoretical time-concentration profiles
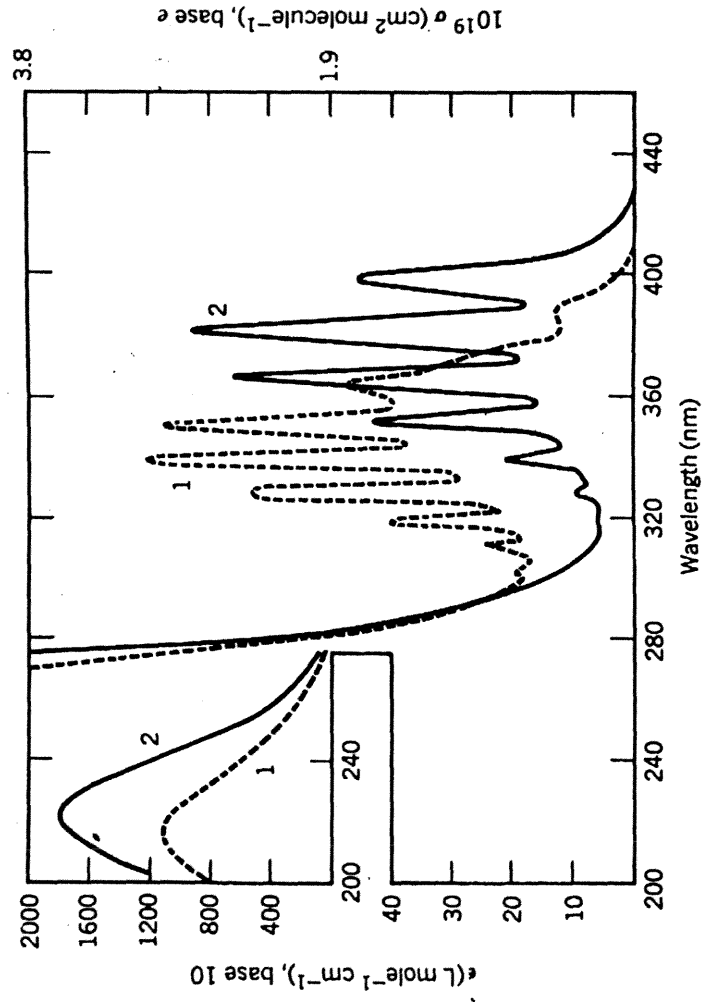
Figure 2.7: Absorbance spectra at 300 K of methyl nitrite (1) and t-butyl nitrite (2), taken from Pitts and Pitts, 1986.

23

Table 2.3: Simplified CH_3ONO mechanism used in modeling.

No.	Reaction	Rate Constant (@ 298 K) $cm^3molecule^{-1}s^{-1}$
	Methyl Nitrite Photolysis	
MN1)	$CH_3ONO + h\nu \rightarrow CH_3O + HCHO$	Experiment
MN2)	$CH_3O + O_2 \rightarrow HCHO + HO_2$	$1.9*10^{-15}$
MN3)	$HO_2 + NO \rightarrow OH + NO_2$	$3.7*10^{-12}$
	Formaldehyde Reactions	
F1)	$HCHO + h\nu = 2\ HO2 + CO$	PHOT=HCHO
F2)	$HCHO + OH = HO2 + CO + H2O$	$1.125*10^{-12}$, -1.288, 2.0
	Inorganic Reactions	
1)	$NO_2 + h\nu \rightarrow NO + O$	$PHOT = NO_2$
2)	$O + O_2 + M \rightarrow O_3 + M$	$6.093*10^{-34}$
3)	$O + NO_2 \rightarrow NO + O_2$	$6.459*10^{-12}$
4)	$O + NO_2 + M \rightarrow NO_3 + M$	FALLOFF F= 0.600, N= 1.000
		K0: $3.232*10^{-03}$ 0.00 -4.000
		KI: $3.229*110^{+04}$ 0.00 -1.000
5)	$O_3 + NO + M \rightarrow NO_2 + O_2 + M$	$1.977*10^{-12}$
6)	$NO + NO_3 \rightarrow 2\ NO_2$	$1.690*10^{-11}$
7)	$NO_2 + NO_3 \rightarrow NO + NO_2 + O_2$	$4.946*10^{-15}$

generated using the Carter modeling program[2]. Table 2.3 is a simplified version of the mechanism used to model the CH_3ONO chemistry, including only the most important reactions. Figure 2.8 shows the agreement between the experimental and theoretical data for NO in one of the CH_3ONO systems. The photolysis rate constant for methyl nitrite was determined to be 0.06 min^{-1} for 24 lamps. Several additional modeling studies were conducted with the methyl nitrite mechanism to determine the importance of the intial NO concentration and the reactions of HCHO in the CH_3ONO experimental system. In all cases, the starting methyl nitrite concentration was 1.1 ppm. Three different simulations were conducted:

- HCHO reactions not included in the mechanism, $[NO]_o > 0$.

Methyl Nitrite Chemistry
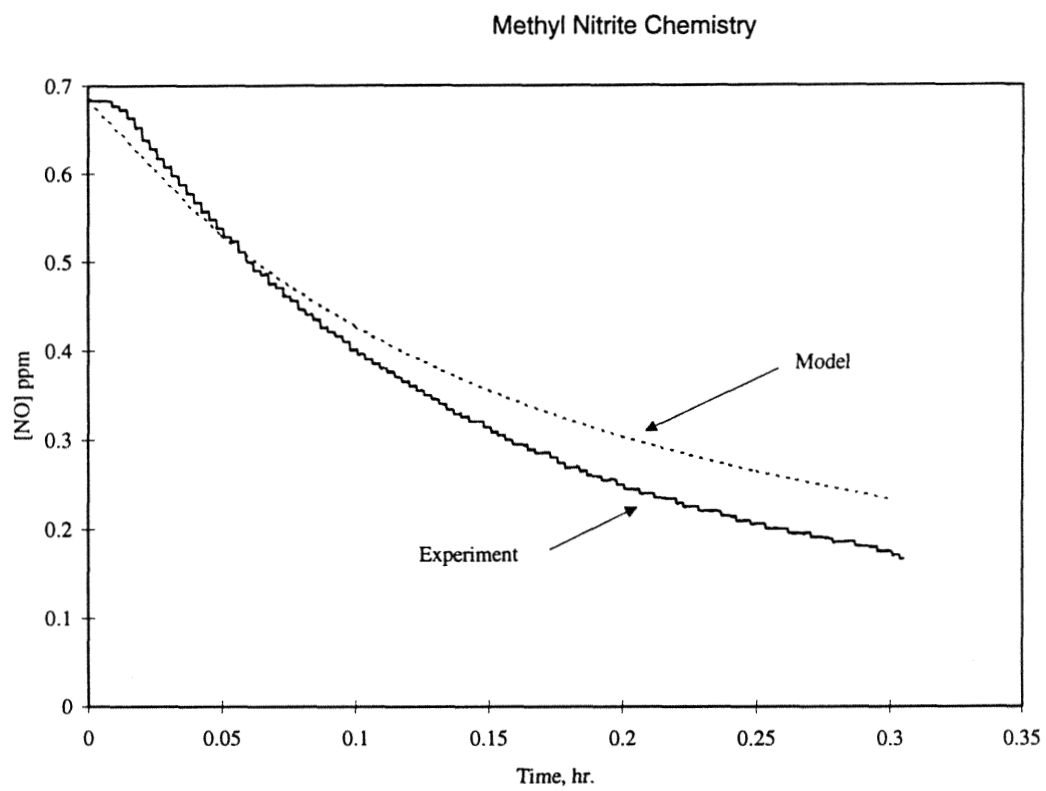
Figure 2.8: Experimental and theoretical data for NO for the photolysis of CH$_3$ONO.

- HCHO reactions included in the mechanism, $[NO]_o > 0$.

- HCHO reactions included in the mechanism, $[NO]_o = 0$.

The time concentration profiles for these three conditions appear in Figures 2.9-2.11. In addition, Figure 2.12 shows the effect of NO on ozone concentrations. Comparison of Figures 2.9 and 2.10 indicates that the inclusion of HCHO reactions in a methyl nitrite mechanism has a significant effect on the NO and NO_2 concentrations predicted in the system. The NO concentration is decreased and the NO_2 concentration is increased by the reaction of HCHO. Comparison of Figures 2.10 and 2.11 indicates that the presence of an intial amount of NO increases the overall concentration of NO_2 in the system. However, the HCHO concentration remains essentially the same. This result may indicate that despite the presence of NO, which would enhance the conversion of HO_2 to OH and produce NO_2, the resulting OH preferentially reacts with compounds other than HCHO. Thus, the OH+HCHO is not a dominant reaction in the CH_3ONO system. Figure 2.12 indicates that O_3 concentrations are not significant in any of the three systems. The effect of NO is intially opposite to that which we might expect from examination of the mechanism alone, since the presence of NO should decrease the amount of O_3 in the system. After a while, though, there is a cross over in curves (b) and (c), indicating that NO is effectively scavenging the O_3 in the system. Thus, the addition of NO as a reactant to a methyl nitrite system does indeed result in the lowering of O_3 concentrations once a critical level of O_3 is reached .

Methyl Nitrite Simulation
(no HCHO rxns)
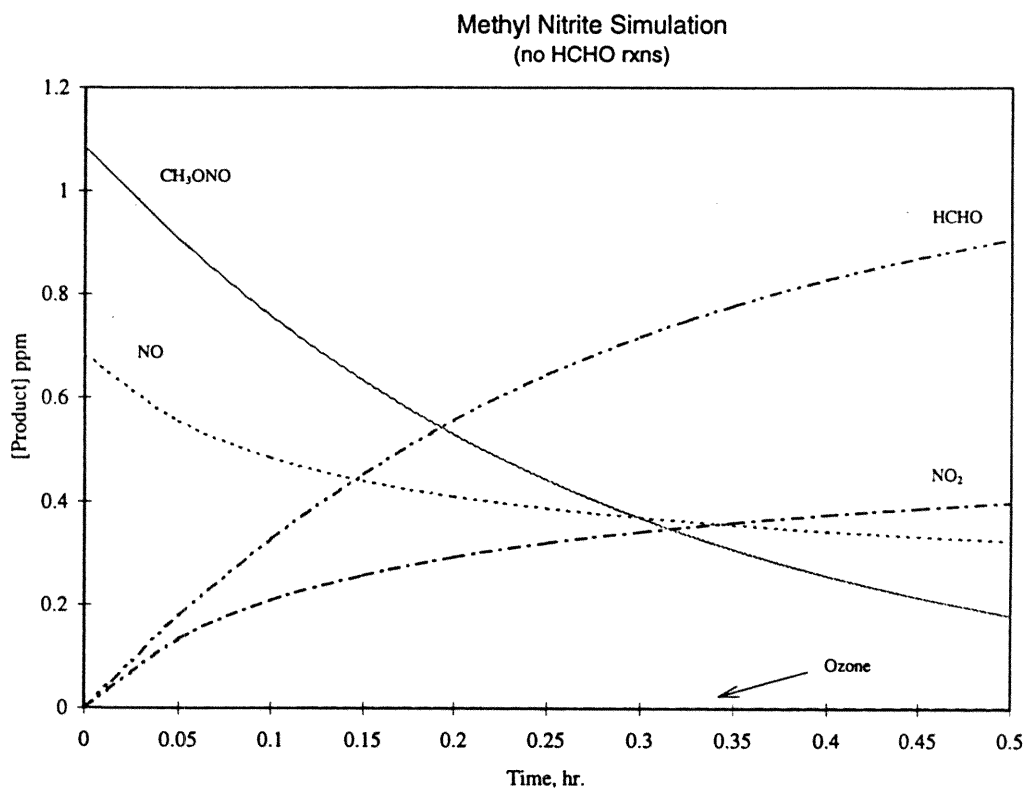
Figure 2.9: Simulation of CH_3ONO system. HCHO reactions are excluded from the mechanism, and $[NO]_o > 0$.

Methyl Nitrite Simulation
(HCHO rxns, intial [NO] > 0)
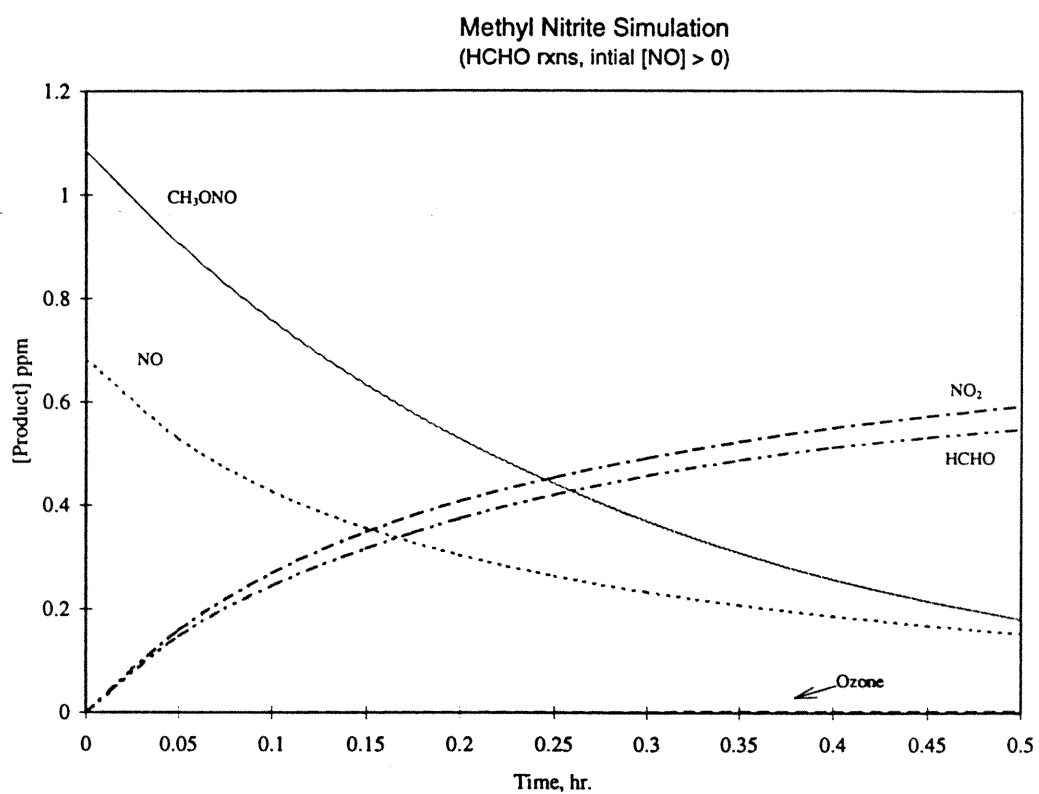
Figure 2.10: Simulation of CH_3ONO system. HCHO reactions are included in the mechanism, and $[NO]_o > 0$.
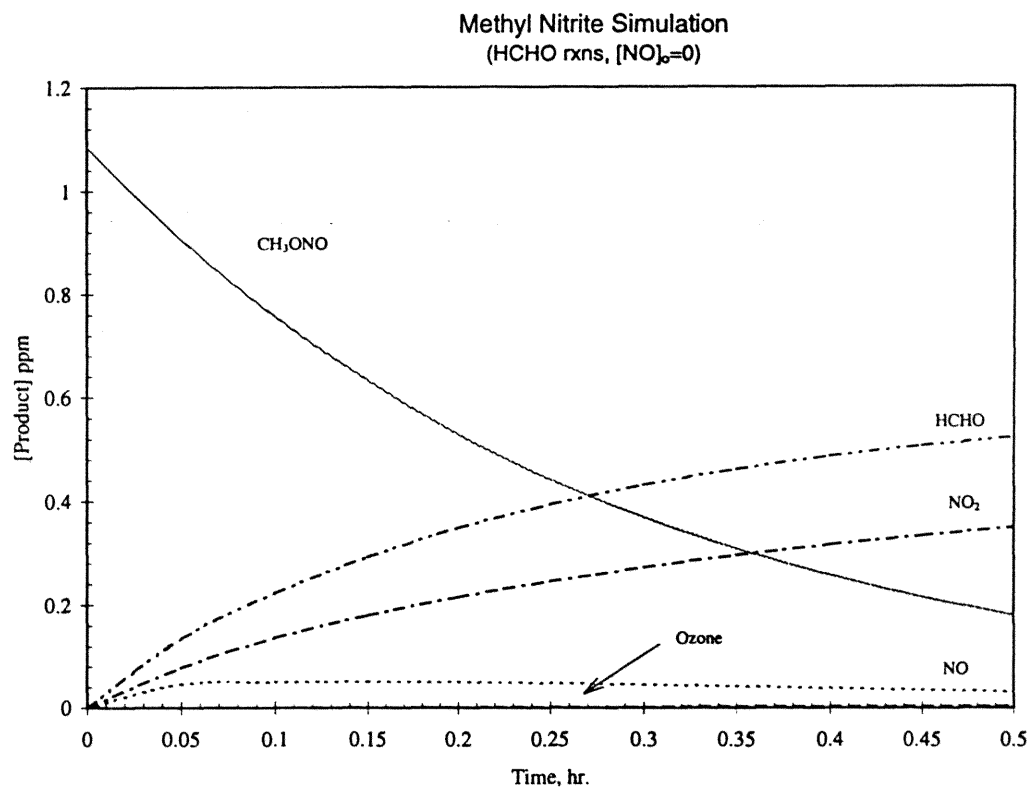
Figure 2.11: Simulation of CH_3ONO system. HCHO reactions are included in the mechanism, and $[NO]_o = 0$.

Methyl Nitrite Simulations
Variation in [Ozone]
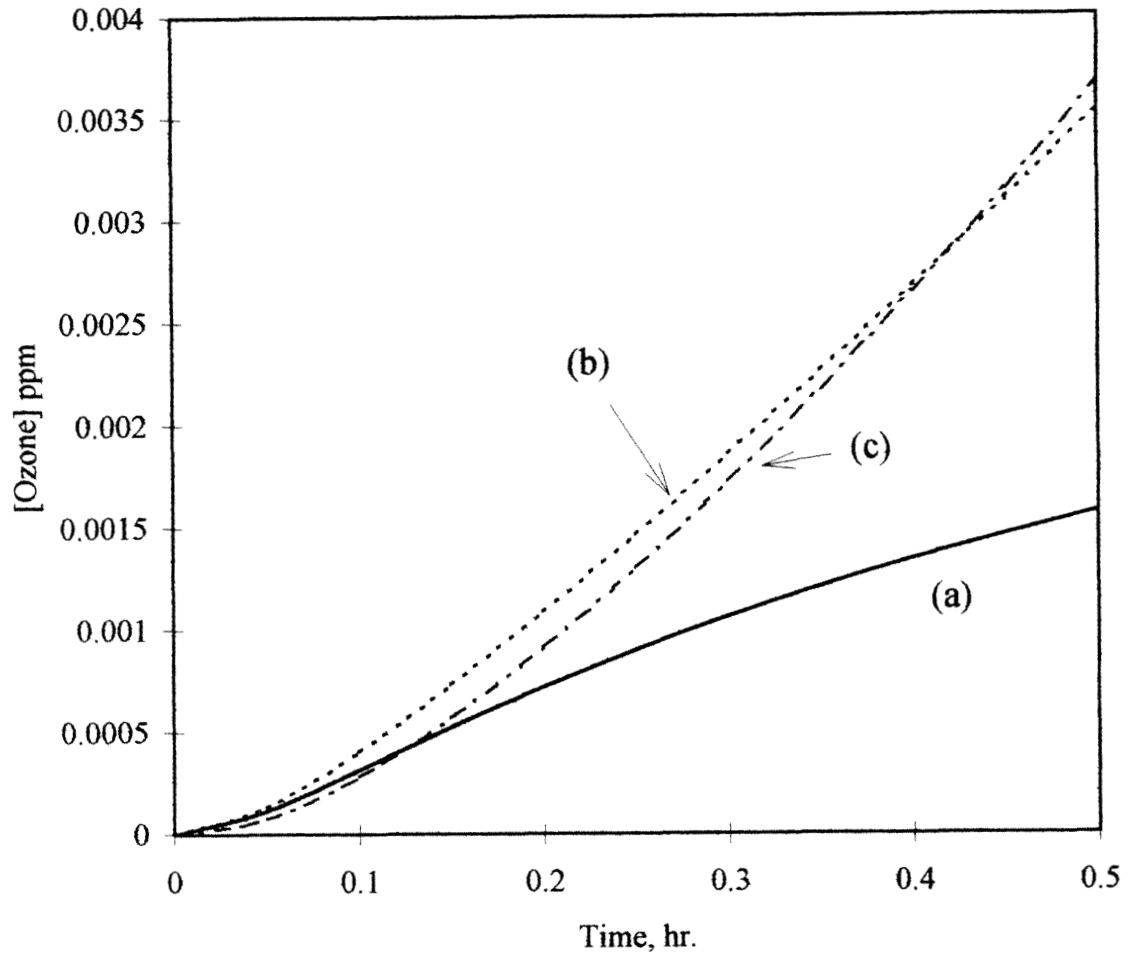
Figure 2.12: Comparison of O_3 data from simulations of CH_3ONO chemistry (a) excluding HCHO chemistry with $[NO]_o > 0$, (b) including HCHO chemistry with $[NO]_o > 0$, and (c) including HCHO chemistry with $[NO]_o = 0$.

2.2.3 t-Butyl Alcohol Experiments

To determine whether the new experimental system behaved similar to other indoor chambers, the photooxidation of t-butyl alcohol (tBA) was re-investigated. [5] Specifically, the goals of these experiments were to determine whether or not we could generate OH radicals by the photolysis of methyl nitrite, successfully react these radicals with a relatively well-studied compound, and reproduce the results of other research groups. In addition, these experiments served as a test of our analytical instruments.

The atmospheric chemistry of t-butyl alcohol has become quite important since this compound is being considered as a fuel additive in order to reduce the reactivity of vehicle emissions. [5, 8] The tBA-OH reaction mechanism proceeds via an abstraction mechanism :

(1) $(CH_3)_3COH + \cdot OH \quad \rightarrow \cdot CH_2C(CH_3)_2OH$

(2) $\cdot CH_2C(CH_3)_2OH + O_2 + M \rightarrow \cdot O_2CH_2C(CH_3)_2OH + M$

(3) $\cdot O_2CH_2C(CH_3)_2OH + NO \rightarrow \cdot OCH_2C(CH_3)_2OH + NO_2$

(4) $\cdot OCH_2C(CH_3)_2OH \quad \rightarrow HCHO + \cdot C(CH_3)_2OH$

(5) $\cdot C(CH_3)_2OH + O_2 \quad \rightarrow HO_2\cdot + CH_3C(O)CH_3$
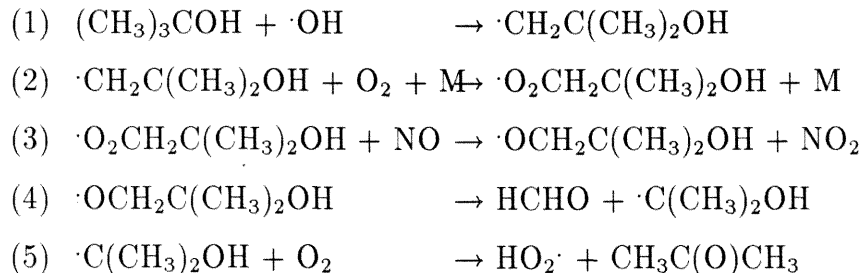
The consumption of one molecule of tBA results in the formation of approximately one molecule of formaldehyde and one molecule of acetone.[5]

Four tBA-OH experiments were conducted in the indoor photochemical reactor, and had typical starting concentrations of 20-40 mtorr and 0.1-0.2 torr of tBA and methyl nitrite, respectively. The reaction was monitored using the GC-MS. Standards of tBA and acetone in methanol were generated

and used for calibration of the system. To account for the secondary loss of acetone via reaction with OH radicals, the following formula was used:

$$F = \frac{k_1 - k_2}{k_1} \frac{1 - \frac{[Hydrocarbon]_t}{[Hydrocarbon]_o}}{\frac{[Hydrocarbon]_t}{[Hydrocarbon]_o}^{\frac{k_2}{k_1}} - \frac{[Hydrocarbon]_t}{[Hydrocarbon]_o}} \tag{2.2}$$

The rate constants k_1 and k_2 correspond to the reactions of tBA and acetone with OH, respectively, and have values of $1.12*10^{-12}$ and $2.26*10^{-13}$. A plot of the corrected acetone concentration versus the loss of tBA appears in Figure 2.13. The plot is a straight line, with slope of 0.910 ± 0.051, as expected from the reaction mechanism and previously published experimental results.[5] We were able to successfully react tBA with methyl nitrite, and, given that our results agreed with previously published data, found that there were no abnormalities within our system (such as unexplained losses within our chamber), or with our sampling methods.
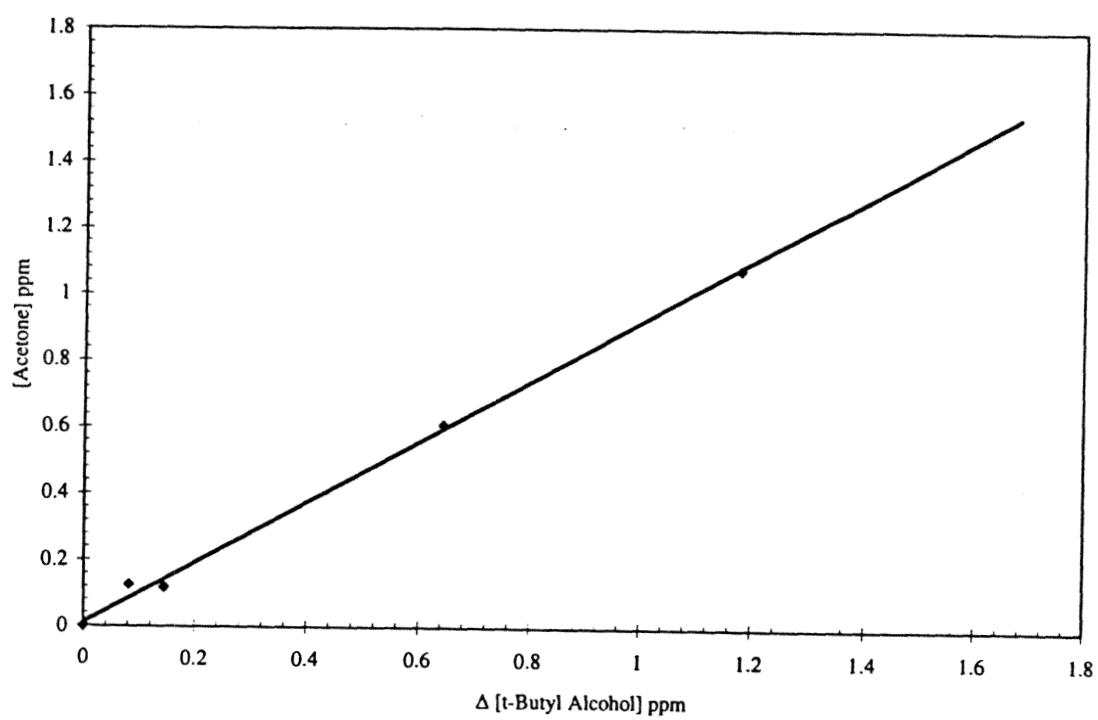
Figure 2.13: Yield of acetone from the phtooxidation of t-Butyl Alcohol.

Bibliography

[1] Bass,A.M., Glasgow,L.C., Miller,C., Jesson,J.P., Filken,D.L., Temperature Dependent Absorption Cross Sections for Formaldehyde (CH_2O): The Effect of Formaldehyde on Stratospheric Chlorine Chemistry, *Planet. Space Sci.*, **28**, 675 (1980).

[2] Carter, W.P. Documentation for the SAPRC Atmospheric Photochemical Mechanism Preparation and Emissions Processing Programs for Implementation in Air-Shed Models, California Air Resources Board, Contract No. A5-122-32, October 1988.

[3] Finlayson-Pitts, B.J., Pitts Jr., J.N., Atmospheric Chemistry: Fundamentals and Experimental Techniques, Wiley, New York, 1986.

[4] Holmes,J.R., O'Brien,R.J., Crabtree,J.H., Hecht,T.A., Seinfeld,J.H., Measurement of Ultraviolet Radiation Intensity in Photochemical Smog Studies, *Environ. Sci. Tech.*, **7**, 519 (1973).

[5] Japar, S.M , Wallignton, T.J., Richert, J.F.O., Ball, J.C., The Atmospheric Chemistry of Oxygenated Fuel Additives: t-Butyl Alcohol,

Dimethyl Ether, and Methyl-t-Butyl Ether, *Int. J. Chem. Kinet.*, **22**, 1257 (1991).

[6] Moortgat, G.K., Seiler,W., Warneck, P., Photodissociation of HCHO in Air: CO and H_2 Quantum Yields at 220 and 300 K, *J. Chem. Phys.*, **78**, 1185 (1983).

[7] NASA,"Chemical Kinetics and Photochemical Data For Use in Stratospheric Modeling. Evaluation 8," JPL Publication 87-41.

[8] Seinfeld, J.H., Andino, J.M., Bowman, F.M., Forstner, H.J., Pandis, S., Tropospheric Chemistry, *Adv. Chem. Eng.*, **19**, 325 (1995).

Chapter 3

Photooxidation of 2,2,4-Trimethylpentane and 2,2,5- Trimethylhexane: A Product Study

Abstract

Hydroxyl radical-initiated photooxidation of 2,2,4-trimethylpentane and 2,2,5-tri-methylhexane in the presence of NO_x has been investigated. Primary products detected from the reaction of 2,2,4-trimethylpentane with OH radicals are 2-methyl-1-propanal, acetone, and formaldehyde, with molar yields of 0.190, 0.264, and 1.114, respectively. Acetaldehyde was also positively detected as a product.

Both the kinetics and mechanism of 2,2,5-trimethylhexane photooxidation were studied. The relative rate method, using 2,2,4-trimethylhexane as a reference, was used in order to make the first determination of the rate constant for OH radical reaction with 2,2,5-trimethylhexane. This rate constant was determined to be $(5.27\pm0.15)x10^{-12}$ cm^3 molecule^{-1} s^{-1}, in excellent agreement with the predicted value of $5.7x10^{-12}$ cm^3 molecule^{-1} s^{-1} as determined from Atkinson's structure reactivity relationship. Primary products detected from the reaction of 2,2,5-trimethylhexane with OH radicals were 3,3-dimethylbutyraldehyde, acetone, acetaldehyde, and formaldehyde, with molar yields of 0.208, 0.169, 0.014 and 1.111, respectively. 2,2-Dimethyl-1-propanal was also detected in the 2,2,5-trimethylhexane system. Based on the 2,2,4-trimethylpentane study, model predictions, and 3,3-dimthylbutyraldehyde + OH experiments, the formation of 2,2-dimethyl-1-propanal is, however, believed to be a secondary, rather than a primary product. We saw no evidence for the formation of 3-methyl-1-propanal or 2-methyl-1-propanal. The results obtained are discussed in terms of their implications for the atmospheric reactions of alkoxy radicals.

3.1 Introduction

Kinetics and mechanisms of the atmospheric reactions of a number of the smaller alkanes have been investigated[1]. Studies of larger ($> C_8$) alkanes, however, have focused primarily on rate constant determinations [1], and mechanisms have yet to be fully determined. We have undertaken a study of the photooxidation mechanism of two branched alkanes, 2,2,4-trimethylpentane (iso-octane) and 2,2,5-trimethylhexane. Both compounds were identified in the 1987 Southern California Air Quality Study (SCAQS)[2]. Of the total morning composition of non-methane organic compounds, 2,2,4-trimethylpentane and 2,2,5-trimethylhexane represented 1.414% and 0.170% of the total carbon, respectively. In addition, 2,2,4-trimethylpentane is listed as one of the 25 most abundant species in the fall episode of SCAQS, based on the fraction of non-methane organic carbon.

Hydroxyl radical reaction with alkanes proceeds via H-atom abstraction. The peroxy radicals formed after the initial H-atom abstraction are, in the presence of NO, rapidly converted to alkoxy radicals. The reaction pathways of the alkoxy radicals are crucial to the overall mechanisms for alkane reactions. These resulting alkoxy radicals can react with NO, NO_2, O_2, unimolecularly decompose, or isomerize [1, 3, 4, 5, 6, 7, 8]. While estimates of the reaction rates of the O_2 and decomposition pathways have been made [1, 4, 5, 8], alkoxy radical isomerization reactions, on the other hand, still have not been completely characterized. Alkoxy radicals with greater than

five carbons are believed to undergo 1,4- or 1,5- H atom shift isomerization reactions via 5- and 6-member rings, respectively [1, 3, 5, 7] to eventually form hydroxy carbonyls. Rate constant data exist for the 1,5-H atom isomerization reactions of alkoxy radicals, but have not been tested against a wide variety of alkanes [1].

We report here the investigation of the photooxidation of 2,2,4- trimethylpentane and 2,2,5-trimethylhexane. The first determination of the rate constant of the OH + 2,2,5-trimethylhexane reaction is presented and compared to the theoretical value derived from Atkinson's structure reactivity relationship[16, 15]. Experimental studies of the photooxidation of 2,2,4-trimethylpentane and 2,2,5-trimethylhexane are presented, and product yields are compared to those predicted by photooxidation mechanisms.

3.2 Experimental

The Caltech Indoor Photochemical Reactor has been described in detail elsewhere[1]. Briefly, the chamber is a 1 m^3 reactor constructed of 2 mil FEP Teflon. Artificial light (two banks of 24 Sylvania F30T8BL black lamps) is used to initiate the chemistry within the chamber. The lamps are mounted on a cylindrical surface to provide for uniformity in irradiation. The light intensity within the chamber can be adjusted by varying the number of lamps that are used. These experiments were conducted using 50% of the total intensity available.

---

[1]See Chapter 2.

Relative Rate Experiment

A relative rate experiment was conducted to determine the rate constant of hydroxyl radical reaction with 2,2,5-trimethylhexane. The relative rate method is a standard method for determining the rate constant of a compound given a known rate constant of a reference compound[12]. The reference used in this study was 2,2,4-trimethylpentane, with a known rate constant of 3.59×10^{-12} cm^3 molecule^{-1} s^{-1} [1]. Provided that the sole loss process for 2,2,4- trimethylpentane (Reference) and 2,2,5-trimethylhexane (Reactant) is reaction with OH radicals, the following relations hold:

$$\text{Reactant} + \cdot OH \overset{1}{\to} \text{Products}$$
$$\text{Reference} + \cdot OH \overset{2}{\to} \text{Products}$$
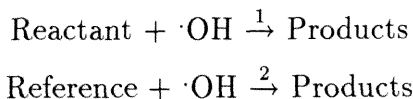
$$\ln \frac{[Reactant]_o}{[Reactant]_t} = \frac{k_1}{k_2} \ln \frac{[Reference]_o}{[Reference]_t}, \qquad (3.1)$$

where k_1 and k_2 are the rate constants for reactions (1) and (2), respectively. If the logarithmic terms are plotted against each other, the slope is the ratio, $\frac{k_1}{k_2}$. The rate constant, k_1 can then be placed on an absolute basis using the known rate constant, k_2.

Three experiments were conducted with initial mixing ratios of 2-5 ppm of 2,2,4-trimethylpentane and 2,2,5-trimethylhexane, respectively, 3-6 ppm of methyl nitrite, and 1-3 ppm of NO.

Product Determinations

Methyl nitrite was initially used as the OH radical precursor in these experiments. Formaldehyde cannot be determined exclusively as a product from alkane-CH_3ONO-NO experimental systems because HCHO is also produced in the photolysis of CH_3ONO. Thus, ethyl nitrite was used as the OH presursor in several experiments. Methyl and ethyl nitrite photolyze according to the following mechanism:

$$RCH_2ONO + h\nu \rightarrow RCH_2O\cdot + NO$$
$$RCH_2O\cdot + O_2 \rightarrow RCHO + HO_2\cdot$$
$$HO_2\cdot + NO \rightarrow OH\cdot + NO_2 \; ,$$
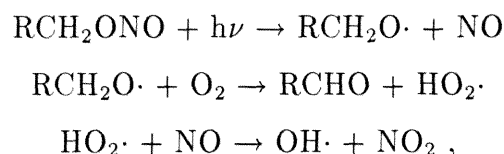
where R = H for methyl nitrite, or R = CH_3 for ethyl nitrite.

To minimize ozone production, and maximize the conversion of peroxy radicals to alkoxy radicals, NO was added to the chamber. Typical initial mixing ratios were approximately 2-4 ppm and 2-5 ppm for 2,2,4-trimethylpentane and 2,2,5-trimethylhexane, respectively, 3-10 ppm CH_3ONO (or C_2H_5ONO), and 2-5 ppm NO. 2,2,4-Trimethylpentane was obtained from Aldrich with a stated purity of 99+%, and 2,2,5-trimethylhexane was obtained from Wiley Organics with a stated purity of 99.8%. Nitric oxide was taken from a standard cylinder generated by Scott Marin. The nitrites were prepared by the dropwise addition of 50% sulfuric acid to a saturated alcohol(methanol for methyl nitrite and ethanol for ethyl nitrite) /sodium nitrite solution, and were vacuum purified and stored under liquid N_2[13].

The mixture was photolyzed and sampled periodically for analyses by an on-line GC-FID (HP 5890) and NO_x analyzer (Thermo Environmental Model 42). The column used in the GC was a J&W Scientific DB-5 column of dimension 30m x 0.25mm x 0.25μm. The temperature program used started at 35° C. The oven temperature was maintained at 35° C for 6 min., and then increased by 30° C/min. until 200° C. The final temperature of 200° C was maintained for 1 min.. Retention times for 2,2,4-trimethylpentane and 2,2,5-trimethylhexane were 4.0 min. and 5.0 min., respectively. Typical irradiation times for the branched alkane study ranged from 5 to 20 min..

At the end of each experiment, a sample from the chamber was collected on a 2,4-dinitrophenylhydrazine (DNPH) impregnated C_{18}-cartridge (Waters Co.). The samples were eluted using 2 ml of acetonitrile, and analyzed using a Hewlett Packard Model 1090 Series II liquid chromatograph, with a diode array detector. A reversed-phase Axxiom LC column of dimension 5 μm x 150 cm was used to obtain adequate separation. HPLC grade acetonitrile and water were used as the solvents in a ratio of 55% to 45%, with a total flowrate of 1 ml/min. Typical observed pressures were between 109 and 112 bar. Authentic standards were compared to the experimental samples to identify and quantify the products. Formaldehyde-, acetaldehyde-, acetone-, and 3-methyl-1-butanal-DNPH hydrazone standards in acetonitrile were obtained from Radian corporation at a concentration of 3 μg/ml. Crystalline 2-methyl-1-propanal-DNPH hydrazone was obtained from Radian corporation, and was used to generate standard solutions using HPLC grade acetonitrile. Both the standard solutions and the crystalline hydrazones had stated purities of at least 99%. They were used without further purification.

2,2-Dimethyl-1-propanal and 3,3-dimethylbutyraldehyde DNPH hydrazones (crystalline forms) were synthesized in our laboratory according to the methods of Druzik et al. [14]. The hydrazones were combined with HPLC grade acetonitrile to form standard solutions of each. 2,2-Dimethyl-1-propanal and 3,3-dimethylbutyraldehyde were obtained from Aldrich, with stated purities of 97% and 95%, respectively. While the aldehydes themselves were not purified, the resulting hydrazones were recrystallized twice to remove any impurities. Based on LC-diode array analyses, these standard solutions had purities of at least 99% .

Interferences from Primary Carbonyl Product Reactions

Several experiments were performed to investigate the product yield interferences that may arise from carbonyl reaction with OH radicals or photolysis. 2,2-Dimethyl-1-propanal-, 3,3-dimethylbutyraldehyde-, 2-methyl-1-propanal-, and 3-methyl-1-butanal-CH_3ONO-NO mixtures were placed in the chamber and photolyzed. Samples were taken on DNPH impregnated cartridges for analysis by HPLC. The results were analyzed, and results indicate that the OH reactions with 3,3-dimethylbutyraldehyde and 3-methyl-1-butanal result in the formation of 2,2-dimethyl-1-propanal and 2-methyl-1-propanal, respectively. The OH reactions with 2,2-dimethyl-1-propanal and 2-methyl-1-propanal did not result in compounds that interfere with product analyses in the alkane studies. Separate experiments were conducted to investigate the photolysis lifetimes of aldehydes under the conditions used

in these studies. Under typical time periods used in this study, significant losses in the aldehyde concentration were not detected.

3.3 Rate Constant of 2,2,5-Trimethylhexane-OH Reaction

Plotting the logarithmic terms of Equation 3.1 against each other results in a straight line with a slope of 1.467 ± 0.041 (see Figure 3.1). This slope corresponds to the ratio of rate constants, $\frac{k_1}{k_2}$, and the error corresponds to 2σ. Using the known rate constant for 2,2,4-trimethylpentane of $3.59\text{x}10^{-12}$ $cm^3molecule^{-1}s^{-1}$ [1], a rate constant for the OH-initiated photooxidation of 2,2,5-trimethylhexane of $(5.27\pm0.15)\text{x}10^{-12}$ $cm^3molecule^{-1}s^{-1}$ is determined, and does not include errors due to the rate constant of the reference reaction. This determination of the rate constant for OH reaction with 2,2,5-trimethylhexane is in excellent agreement with the predicted value of $5.7\text{x}10^{-12}$ $cm^3molecule^{-1}s^{-1}$ as determined from structure reactivity relationships [16, 15].

3.4 Photooxidation Products

The structure reactivity relationship [16, 15] predicts the following percentage distribution for OH attack sites on 2,2,4-trimethylpentane: tertiary carbon = 51%, secondary carbon = 29%, and primary carbon = 20%. Similarly, the structure reactivity relationship predicts the percentages of OH radical at-
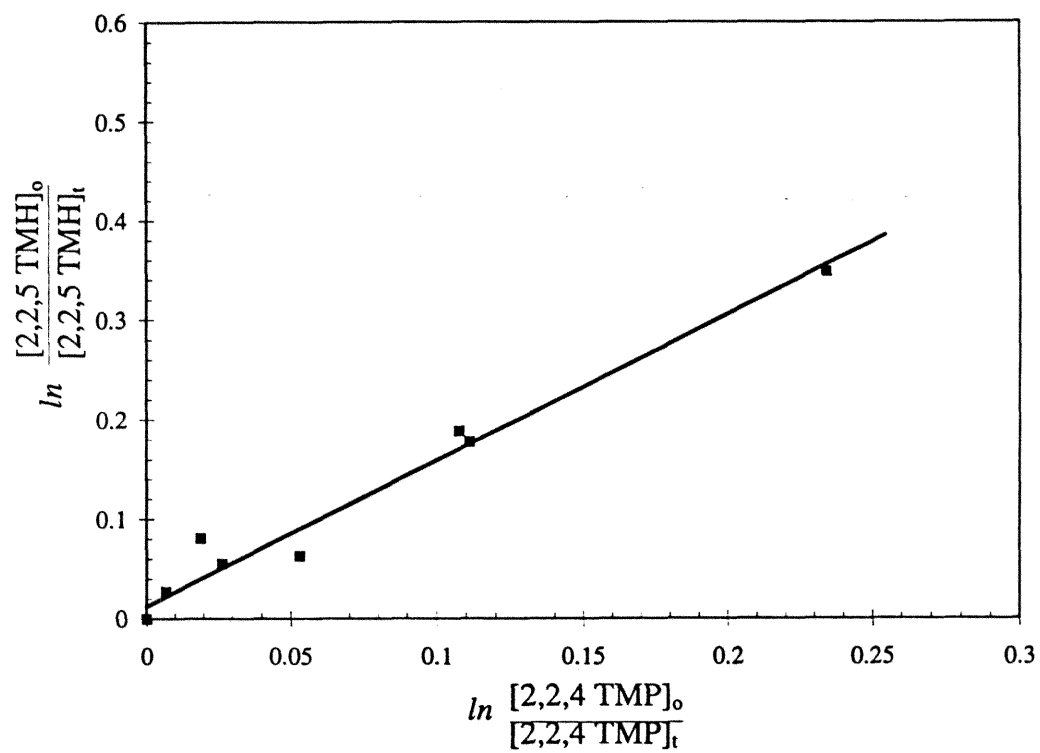
Figure 3.1: Relative rate study to determine k_{OH} for 2,2,5-trimethylhexane.

tack on the tertiary, secondary, and primary carbons of 2,2,5-trimethylhexane as 40%, 45%, and 15%, respectively. Proposed mechanisms for the tertiary, secondary, and primary OH reactions for each alkane, indicating the dominant pathways for decomposition, and excluding isomerization reactions , are shown in Figures 3.2-3.5 for 2,2,4-trimethylpentane and Figures 3.6-3.10 for 2,2,5-trimethylhexane. Additional decomposition pathways are included in the mechanisms which will be discussed subsequently.

3.4.1 2,2,4 Trimethylpentane

Products identified in the 2,2,4-trimethylpentane-OH-NO_x system include formaldehyde, acetone, and 2-methyl-1-propanal. These aldehydes are themselves capable of photolyzing and reacting with OH radicals. The interference studies discussed earlier indicate the photolysis loss of these products is not significant over the photolysis time periods considered in these experiments. The yield of each of the products identified was corrected for losses due to reaction with OH radicals, according to the method of Atkinson et al. [15]. The correction factor, F, was calculated using Equation 3.2 along with the rate constants in Table 3.1. Raw yields were multiplied by F to produce corrected yields,

$$
F = \frac{k_1 - k_2}{k_1} \frac{1 - \frac{[Hydrocarbon]_t}{[Hydrocarbon]_o}}{\frac{[Hydrocarbon]_t}{[Hydrocarbon]_o}^{\frac{k_2}{k_1}} - \frac{[Hydrocarbon]_t}{[Hydrocarbon]_o}}
\tag{3.2}
$$

where k_1 and k_2 are the rate constants of the following reactions:

$$
\text{Hydrocarbon} + \text{OH} \xrightarrow{1} \text{Product}
$$
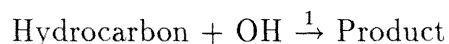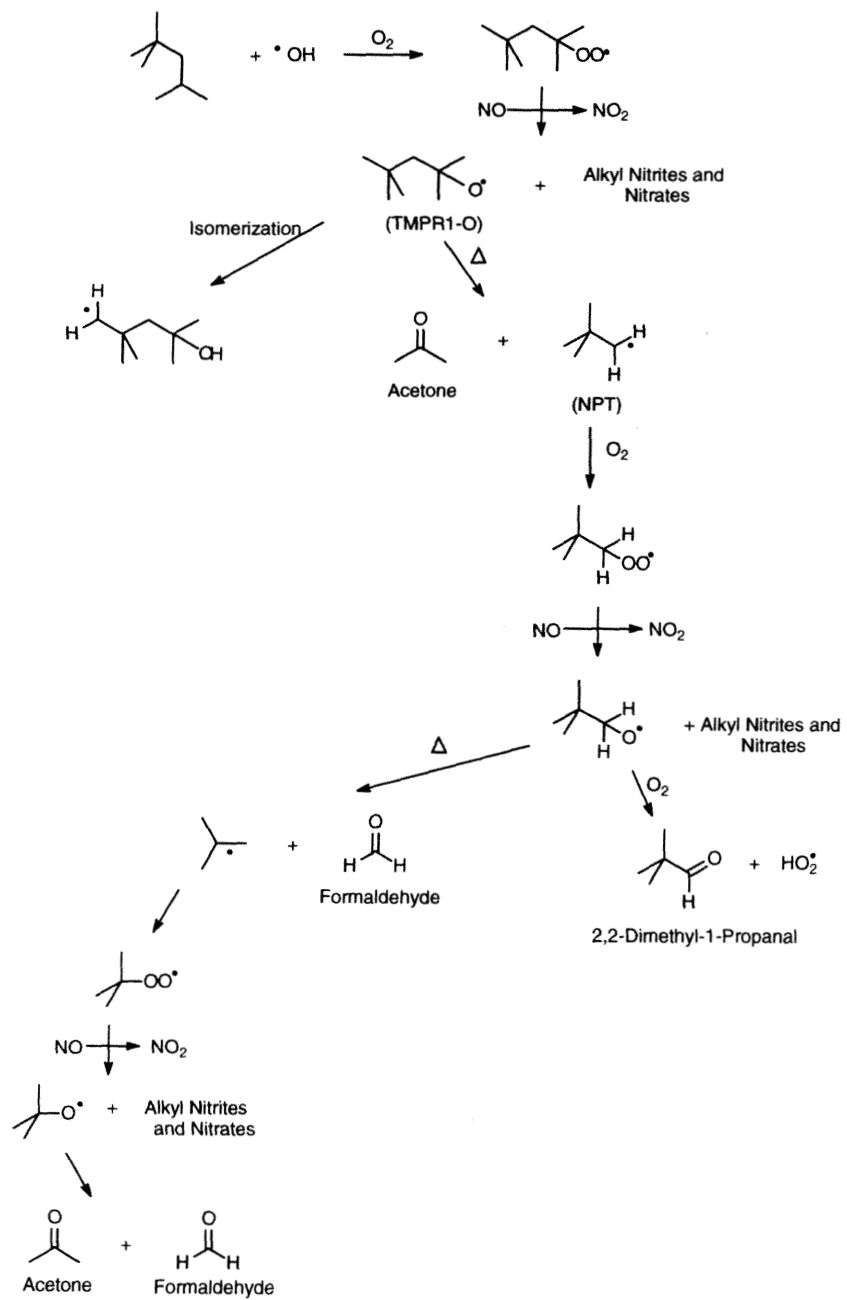
Figure 3.2: 2,2,4-Trimethylpentane + OH Reactions , Tertiary
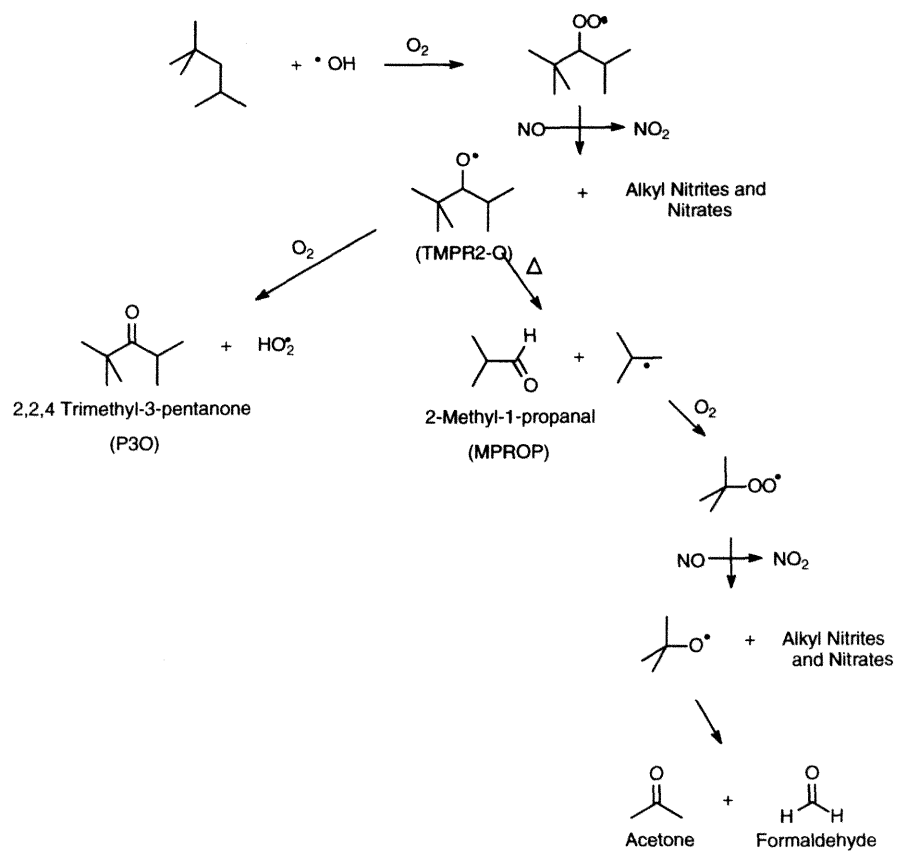
Figure 3.3: 2,2,4-Trimethylpentane + OH Reactions , Secondary
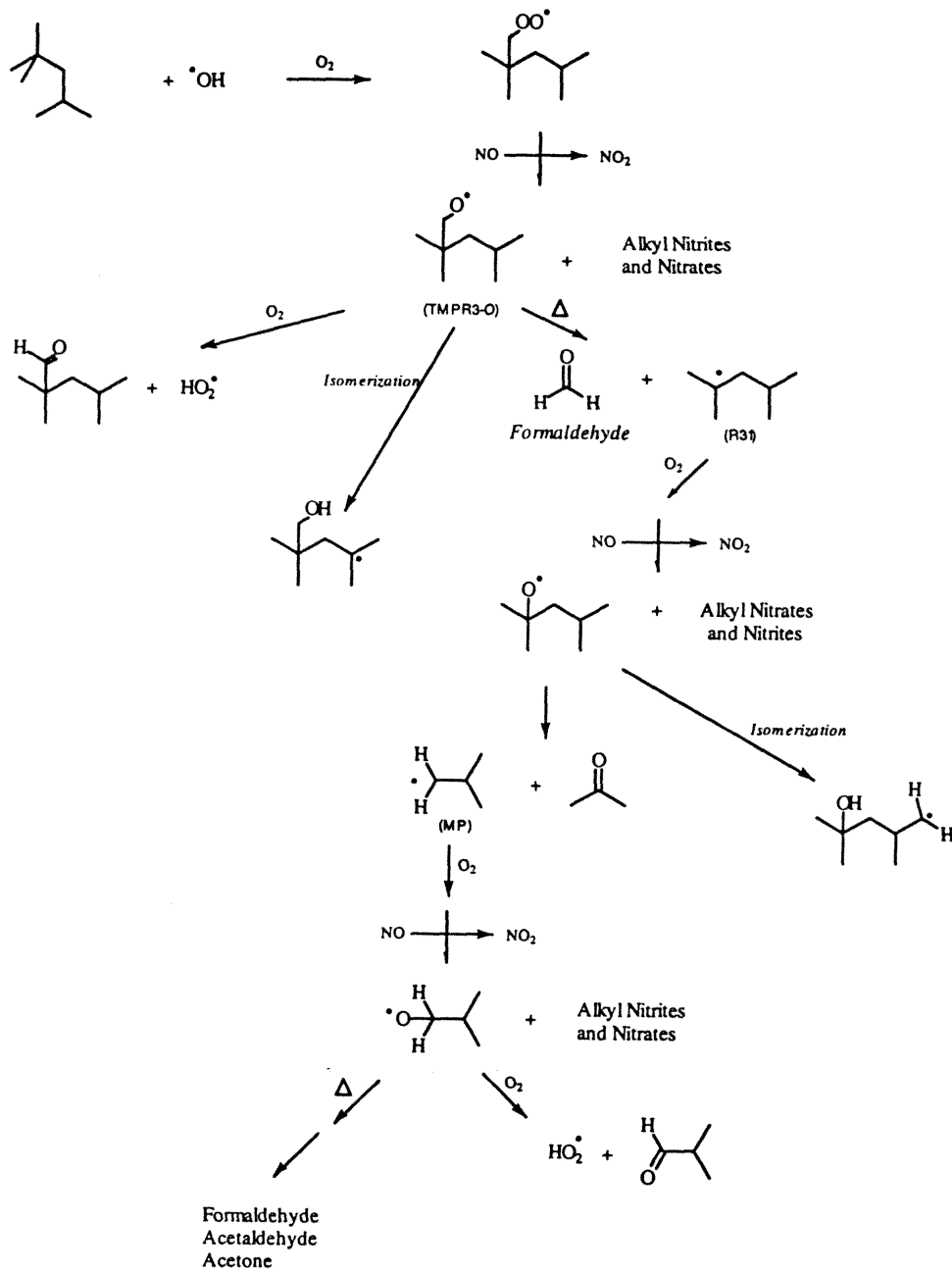
Figure 3.4: 2,2,4-Trimethylpentane + OH Reactions , Primary
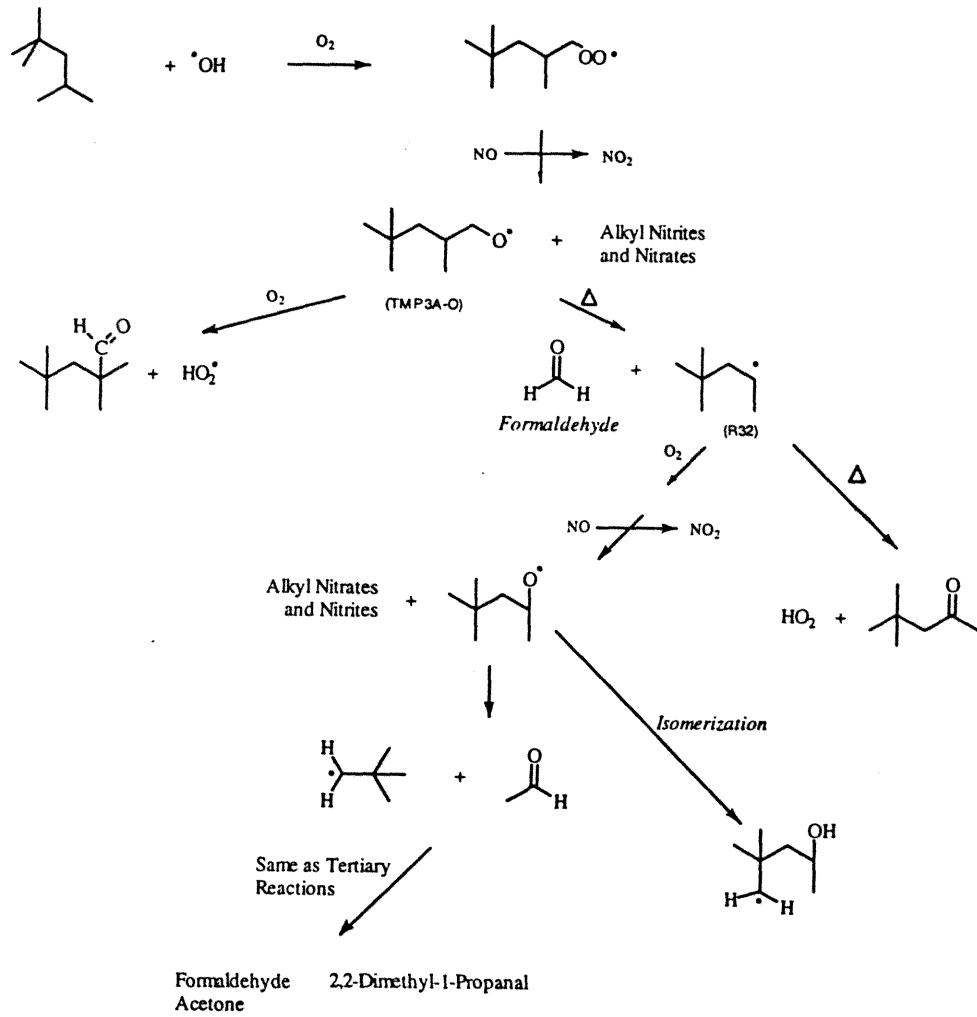
Figure 3.5: 2,2,4-Trimethylpentane + OH Reactions , Primary
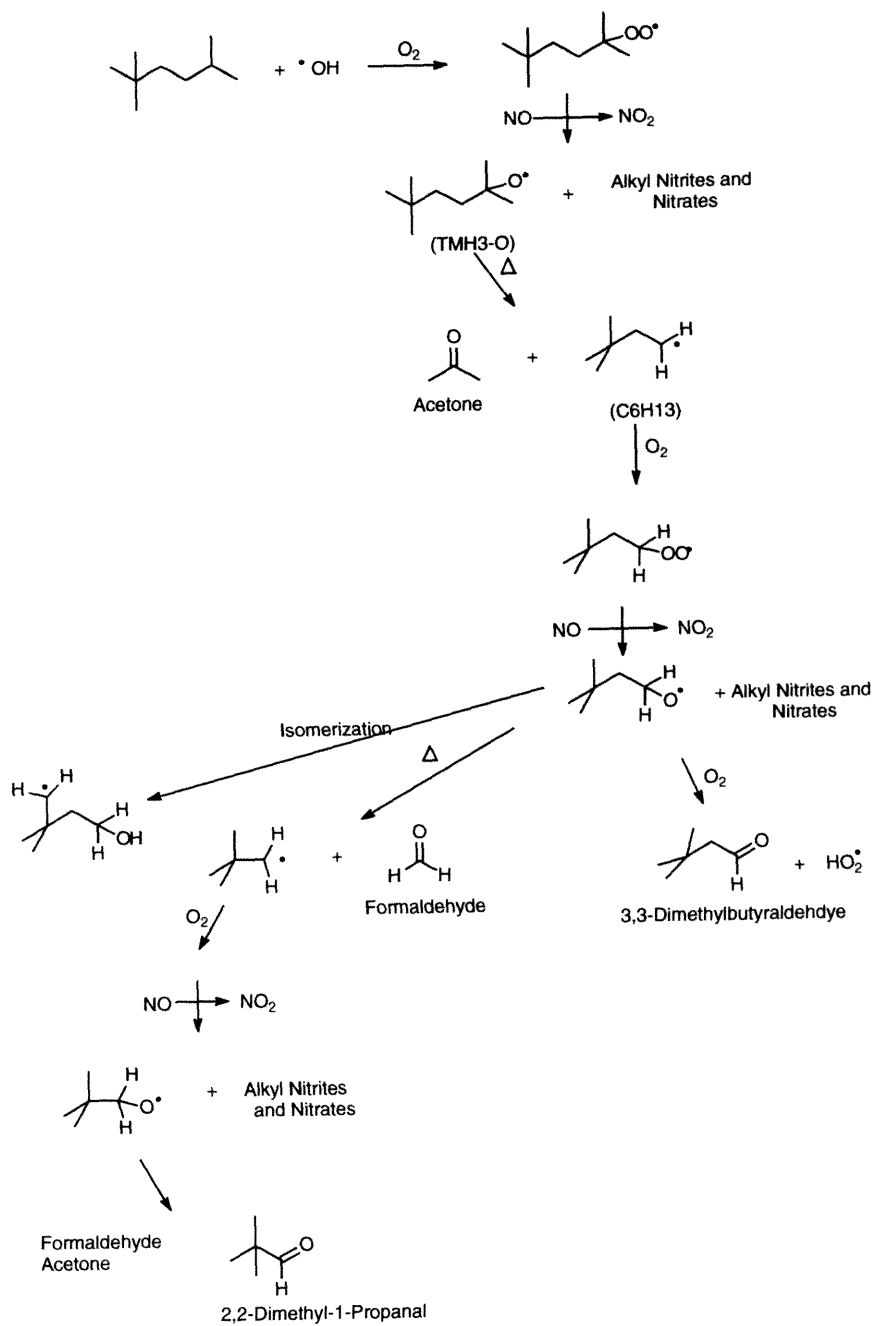
Figure 3.6: 2,2,5-Trimethylhexane + OH Reactions, Tertiary
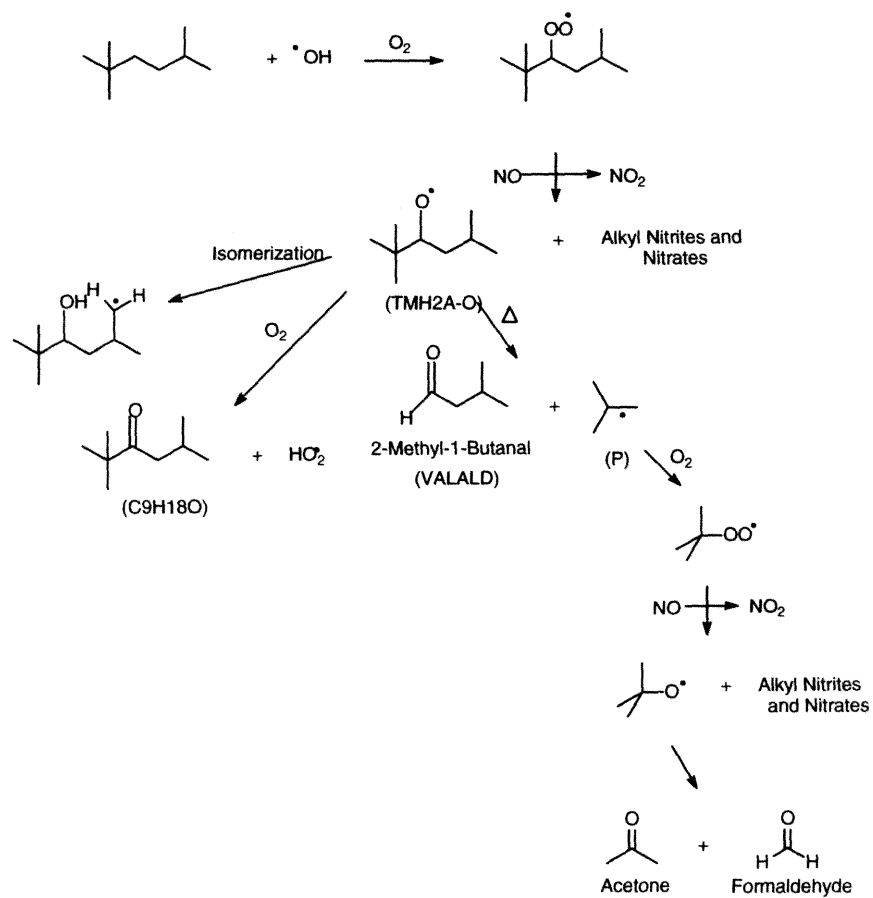
Figure 3.7: 2,2,5-Trimethylhexane + OH Reactions, Secondary
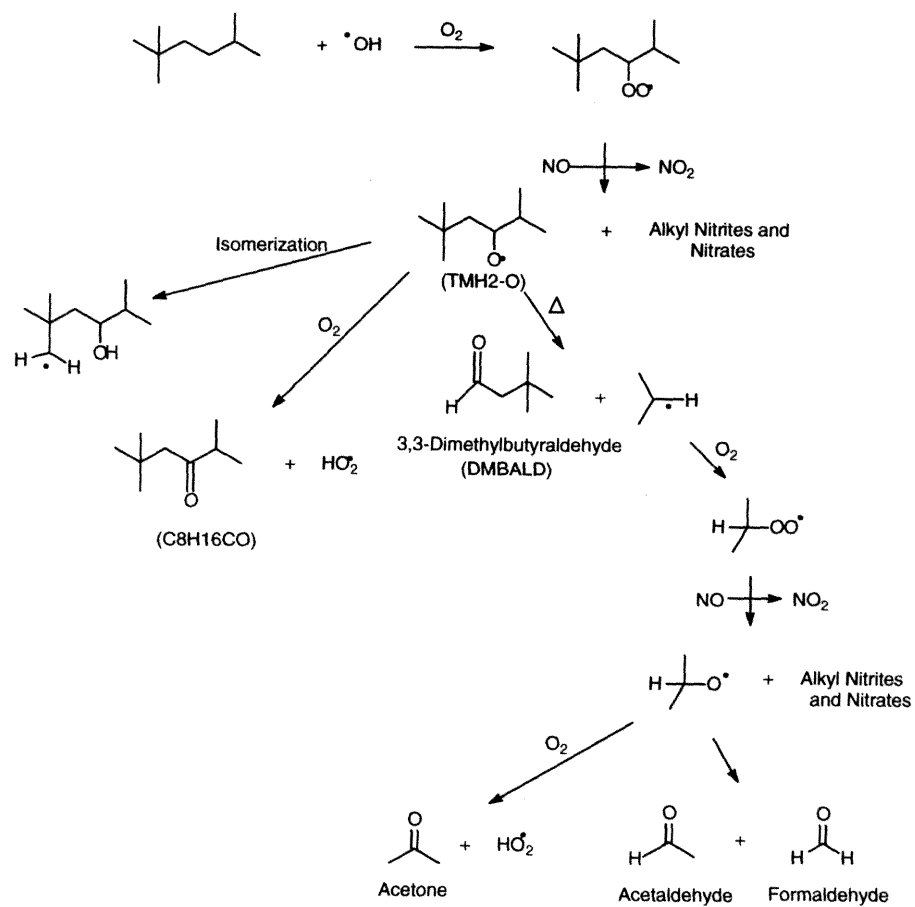
Figure 3.8: 2,2,5-Trimethylhexane + OH Reactions, Secondary
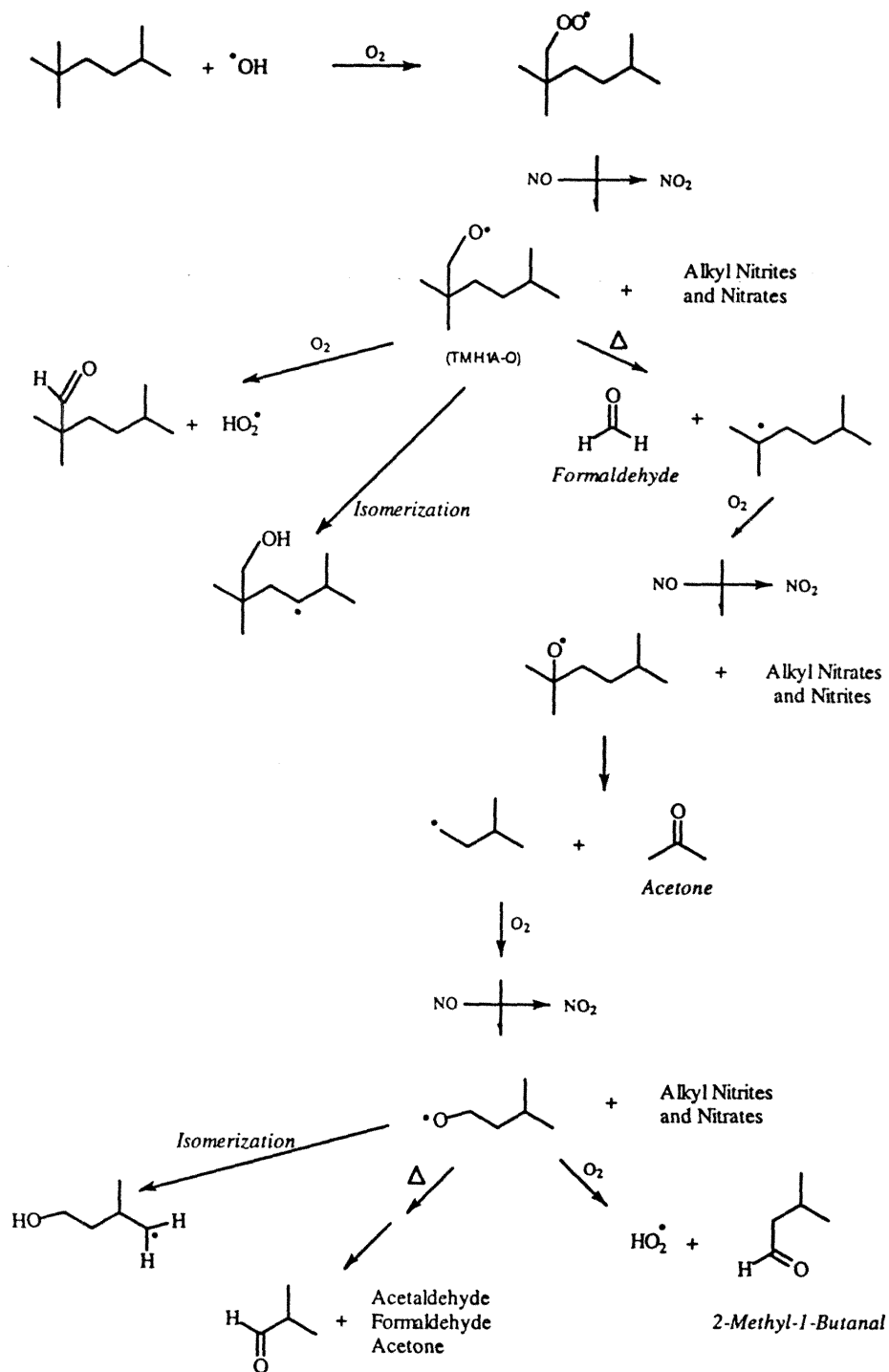
Figure 3.9: 2,2,5-Trimethylhexane + OH Reactions, Primary
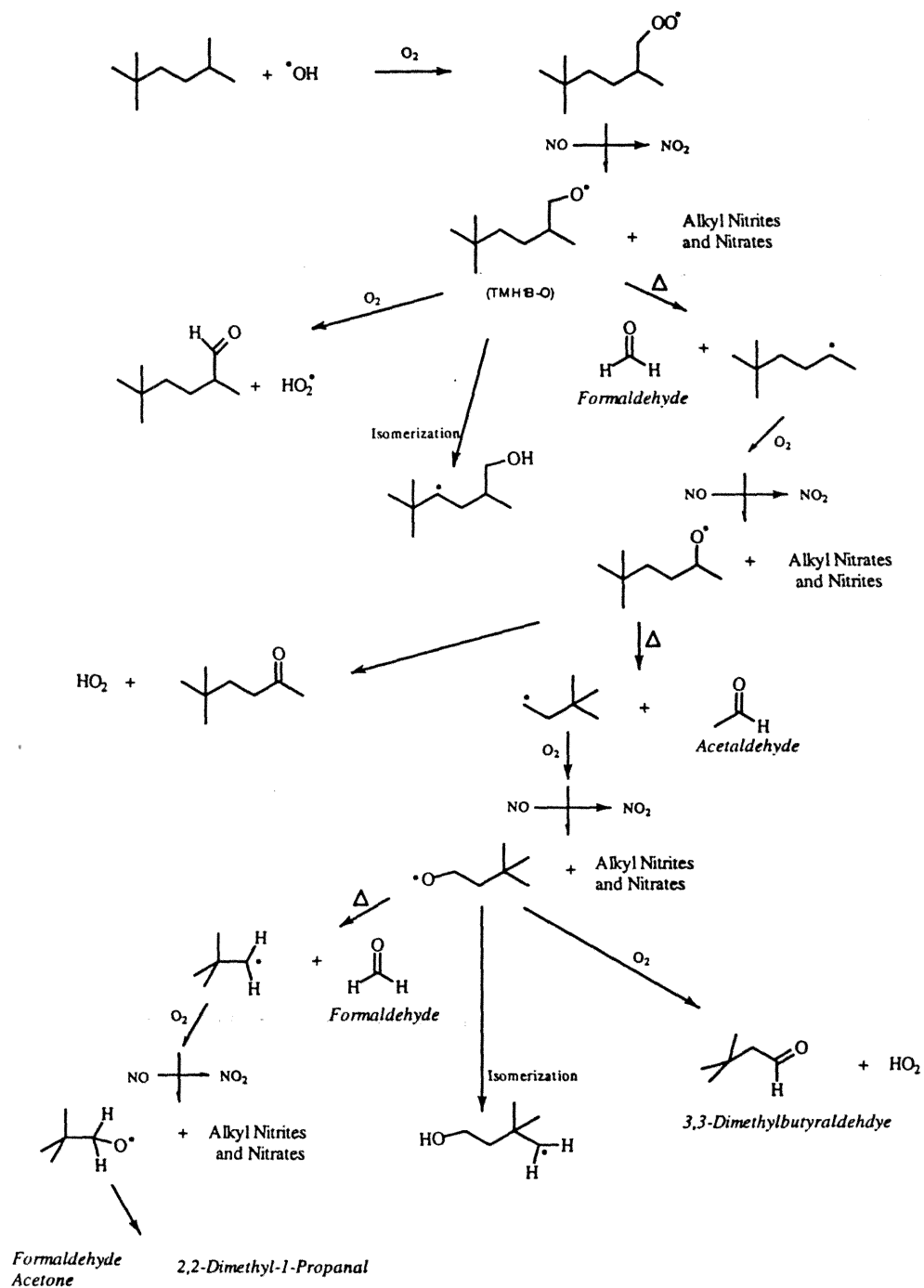
Figure 3.10: 2,2,5-Trimethylhexane + OH Reactions, Primary

Table 3.1: OH Radical rate constants used to correct product yields.

Compound	Rate constant ($cm^3 molecule^{-1} s^{-1}$)	Reference
Alkanes		
2,2,4-Trimethylpentane	3.59×10^{-12}	[1]
2,2,5-Trimethylhexane	5.267×10^{-12}	This work.
Products		
Formaldehyde	9.37×10^{-12}	[1]
Acetaldehyde	1.58×10^{-12}	[8, 1]
Acetone	2.19×10^{-13}	[1]
2-Methyl-1-propanal	2.63×10^{-12}	[8, 1]
3-Methyl-1-butanal	2.74×10^{-11}	[8]
2,2-Dimethyl-1-propanal	2.65×10^{-11}	[8, 1]

$$\text{Product} + \text{OH} \xrightarrow{2} \text{Secondary Products}$$

The primary radical produced in the photooxidation of 2,2,4-trimethylpentane is the neopentyl peroxy radical. In the presence of significant NO, this radical will react with NO to form the corresponding alkoxy radical. The neopentyl alkoxy radical can react with O_2 to form 2,2-dimethyl-1-propanal or decompose to eventually form acetone and formaldehyde (see Figure 3.2). With the use of authentic samples of 2,2-dimethyl-1-propanal-DNPH, we were able to confirm that there was no evidence for the formation of 2,2-dimethyl-1-propanal in the 2,2,4-trimethylpentane photooxidation system. This finding is consistent with that of Wallington et al. [20] who saw no significant evidence for the formation of 2,2-dimethyl-1-propanal during their studies of the neopentyl radical in the presence of NO_x. They did, however, notice significant formation of this product in systems without NO_x. Our results

Table 3.2: Corrected Carbonyl Photooxidation Product Yields

Alkane	Product	Molar Yield
2,2,4-Trimethylpentane	2-Methyl-1-propanal	0.190
	Acetone	0.264
	Formaldehyde	1.114
	Acetaldehyde	Detected
2,2,5-Trimethylhexane	3,3-Dimethylbutyraldehyde	0.208
	2,2-Dimethyl-1-propanal	See text.
	Acetone	0.169
	Acetaldehyde	0.014
	Formaldehyde	1.111

indicate that the major pathway for the neopentyl alkoxy radical is decomposition rather than reaction with O_2. Thus, the major products obtained from the tertiary carbon reactions of 2,2,4-trimethylpentane are acetone and formaldehyde.

The major product from OH attack on the secondary carbon of 2,2,4-trimethylpentane is 2-methyl-1-propanal, whereas formaldehyde and acetone are major products from the primary carbon reactions. Acetaldehyde was also detected as a secondary product in a few of the experiments. Without standards, the larger aldehydes and ketones believed to be formed from the primary reactions could not be positively identified. However, several carbonyl compounds with relatively long retention times (consistent with large compounds) were detected by the LC. Yields of each of the quantified products are given in Table 3.2.

3.4.2   2,2,5 Trimethylhexane

The major products identified from 2,2,5-trimethylhexane photooxidation include formaldehyde, acetone, acetaldehyde, 2,2-dimethyl-1-propanal, and 3,3-dimethylbutyraldehyde. Yields for each of the detected carbonyls were corrected using Equation 3.2 and the rate constants in Table 3.1. The corrected yields are presented in Table 3.2.

The most abundant radicals formed in the 2,2,5-trimethylhexane system are those resulting from OH attack on the tertiary carbon of 2,2,5-trimethylhexane. Based on the mechanism presented in Figure 3.6, the possible products formed from attack on the tertiary carbon include 3,3- dimethyl-butyraldehyde, 2,2-dimethyl-1-propanal, formaldehyde, and acetaldehyde. Each of these products was detected in the photooxidation studies of 2,2,5-trimethylhexane. However, the 2,2-dimethyl-1-propanal formed is believed to be a secondary, rather than a dominant, product. The only pathway for formation of the 2,2-dimethyl-1-propanal is via the neopentyl alkoxy radical. The 2,2,4-trimethylpentane study presented in this paper and the neopentyl peroxy study of Wallington et al.[20] indicate that neopentyl radicals are not a precursor to 2,2-dimethyl-1-propanal in the presence of significant NO_x. In addition, the interference study reported in this work indicates that 2,2-dimethyl-1-propanal is formed as a product of OH reaction with 3,3-dimethylbutyraldehyde. Thus, the 2,2-dimethyl-1-propanal identified is a result of secondary reactions of 3,3-dimethylbutyraldehyde, and has been included in the calculation of the total 3,3-dimethylbutyraldehyde concentration. It is important to note that the F factor was not used to correct

the 3,3-dimethylbutyraldehyde yield, since the addition of the corrected 2,2-dimethyl-1-propanal yield to the 3,3-dimethylbutyraldehyde yield accounts for the losses due to OH reaction. More detail will be given in the next section regarding the direct formation of 2,2-dimethyl-1-propanal.

Based on Figure 3.7, OH attack on the secondary carbon of 2,2,5- trimethylhexane could result in the formation of 3-methyl-1-butanal, formaldehyde, and acetone from the alkoxy radical decomposition route, or the ketone, $(CH_3)_3CC(O)$-$CH_2C(CH_3)_2$, from the alkoxy radical reaction with O_2. Authentic DNPH derivatized samples were not available to investigate the formation of the C_9 ketone. However, with the use of authentic DNPH derivatized samples of 3-methyl-1-butanal, we were able to confirm that, under the conditions of the study presented in this paper, there was no evidence for the formation of 3-methyl-1-butanal from the photooxidation of 2,2,5-trimethylhexane.

Attack on the primary carbon centers of 2,2,5-trimethylhexane can result in the formation of a variety of carbonyl products. From Figure 3.9, possible photooxidation products include 2-methyl-1-propanal, acetaldehyde, formaldehyde, acetone, and 3-methyl-1-butanal from the decomposition pathway of the intial C_9 alkoxy radical formed, or the C_9 carbonyl from reaction of this same alkoxy radical with O_2. Authentic DNPH derivatized samples of the C_9 carbonyl depicted in Figure 3.9 were not available. However, authentic DNPH derivatized samples were available for the other possible carbonyl products. There was no evidence for the formation of 2-methyl-1-butanal or 3-methyl-1-butanal in OH-intiated photooxidation of 2,2,5-trimethylhexane in the presence of NO_x.

3.5 Atmospheric Reaction Mechanisms

2,2,4-Trimethylpentane and 2,2,5-trimethylhexane photooxidation mechanisms were developed using the SAPRC Atmospheric Photochemical Mechanism Preparation Program[16]. To simplify the mechanisms slightly, we included all species leading to nitrite (with the exception of CH_3ONO) or nitrates in two general categories entitled "Nitrites" and "Nitrates", respectively, and did not include the secondary reactions of the major products formed in the two studies (see Table 3.2). Since all of the major products were corrected for losses using Equation 3.2, the exclusion of secondary loss processes in the mechanisms facilitated the direct comparison between observed and predicted yields of major products. The mechanisms used for 2,2,4-trimethylpentane and 2,2,5-trimethylhexane appear in Tables 3.3 and 3.4, respectively. Note that while the inorganic reactions (those involving NO_x) were included in the actual mechanisms used for simulating the experiments, to conserve space, they are not included in Tables 3.3 and 3.4. Rate constants used for all reactions except those involving the alkoxy radicals were obtained directly from Atkinson [1]. The rate constants for the alkoxy radical reactions were derived using ΔH estimates obtained from Stein et al. [25] in conjuction with the estimation technique of Atkinson [1]. Units for all of the rate constants with the exception of those corresponding to the isomerization and decomposition reactions are cm^3 molecule^{-1} s^{-1}. The isomerization and decomposition reaction rate constants are in units of s^{-1}. All rate constants are at 298 K.

Table 3.3: 2,2,4-Trimethylpentane Mechanism

(Units: cm^3, molecule, s)

No.	k @ 298K	Reaction
		2,2,4-Trimethylpentane Reactions
1A)	1.83×10^{-12}	TMP + OH → TMPR1 + H2O
1B)	1.04×10^{-12}	TMP + OH → TMPR2 + H2O
1C)	4.314×10^{-13}	TMP + OH → TMPR3 + H2O
1D)	2.87×10^{-13}	TMP + OH → TMP3A + H2O
		Tertiary Radical Reactions
2)	1×10^{-12}	TMPR1 + O2 → TMPR1-O2
3)	2.0×10^{-17}	TMPR1-O2 + TMPR1-O2 → TMPR1-O + TMPR1-O + O2
4)	7.65×10^{-12}	TMPR1-O2 + NO → TMPR1-O + NO2
4A)	1.25×10^{-12}	TMPR1-O2 + NO → Nitrate
5)	6.7×10^4	TMPR1-O → Isomerization
6)	3.8×10^{-11}	TMPR1-O + NO → Nitrite
7)	3.8×10^{-11}	TMPR1-O + NO2 → Nitrate
8)	3×10^4	TMPR1-O → ACETONE + NPT
		Secondary Radical Reactions
9)	1×10^{-12}	TMPR2 + O2 → TMPR2-O2
10A)	2.25×10^{-15}	TMPR2-O2 + TMPR2-O2 → TMPR2-O + TMPR2-O + O2
10B)	2.75×10^{-15}	TMPR2-O2 + TMPR2-O2 → ALCOHOL1 + P3O
11)	5.79^{-12}	TMPR2-O2 + NO → TMPR2-O + NO2
11A)	3.11×10^{-12}	TMPR2-O2 + NO → Nitrate
12)	3.8×10^{-11}	TMPR2-O + NO → Nitrite
13)	3.8×10^{-11}	TMPR2-O + NO2 → Nitrate

14)	2.48×10^{-14}	TMPR2-O + O2 → P3O + HO2
15)	5.66×10^{5}	TMPR2-O → (CH3)3C + MPROP
15A)	Varied	TMPR2-O →1,4-Isomerization

Primary Radical Reactions

16)	1×10^{-12}	TMPR3 + O2 → TMPR3-O2
17A)	1.125×10^{-13}	TMPR3-O2 + TMPR3-O2 → TMPR3-O + TMPR3-O + O2
17B)	1.375×10^{-13}	TMPR3-O2 + TMPR3-O2 → ALCOHOL2 + ALDEHYDE2
18)	7.3×10^{-12}	TMPR3-O2 + NO → TMPR3-O + NO2
18A)	1.60×10^{-12}	TMPR3-O2 + NO → Nitrate
19)	3.8×10^{-11}	TMPR3-O + NO → Nitrite
20)	3.8×10^{-11}	TMPR3-O + NO2 → Nitrate
21)	8.82×10^{-15}	TMPR3-O + O2 → HO2 + ALDEHYDE2
22)	6.3×10^{4}	TMPR3-O → HCHO + R31
23)	4.1×10^{6}	TMPR3-O → 1,5-Isomerization
24)	1×10^{-12}	R31 + O2 → R31-O2
25)	2.0×10^{-17}	R31-O2 + R31-O2 → R31-O + R31-O + O2
26)	7.97×10^{-12}	R31-O2 + NO → R31-O + NO2
26A)	9.34×10^{-13}	R31-O2 + NO → Nitrate
27)	3.8×10^{-11}	R31-O + NO → Nitrite
28)	3.8×10^{-11}	R31-O + NO2 → Nitrate
29)	4.9×10^{4}	R31-O → ACETONE + MP
30)	2.9×10^{-12}	MP + O2 → MP-O2
31)	1.125×10^{-13}	MP-O2 + MP-O2 → MP-O + MP-O + O2
31A)	1.375×10^{-13}	MP-O2 + MP-O2 → ALCOHOL3 + MPROP + O2
32)	8.9×10^{-12}	MP-O2 + NO → MP-O + NO2
33)	3.8×10^{-11}	MP-O+ NO → Nitrite
34)	3.8×10^{-11}	MP-O + NO2 → Nitrate
35)	1.1×10^{3}	MP-O → HCHO + P
36)	8.5×10^{-15}	MP-O + O2 → MPROP + HO2

37)	11×10^{-12}	$P + O2 \rightarrow P\text{-}O2$
38)	5.5×10^{-16}	$P\text{-}O2 + P\text{-}O2 \rightarrow P\text{-}O + P\text{-}O + O2$
38A)	5.4×10^{-16}	$P\text{-}O2 + P\text{-}O2 \rightarrow ALCOHOL4 + ACETONE$
39)	8.9×10^{-12}	$P\text{-}O2 + NO \rightarrow P\text{-}O + NO2$
40)	3.4×10^{-11}	$P\text{-}O + NO \rightarrow Nitrite$
41)	3.5×10^{-11}	$P\text{-}O + NO2 \rightarrow Nitrate$
42)	8.0×10^{-15}	$P\text{-}O + O2 \rightarrow ACETONE + HO2$
43)	1.5×10^{-1}	$P\text{-}O \rightarrow CH3 + CH3CHO$

Primary Radical Reactions

44)	1×10^{-12}	$TMP3A + O2 \rightarrow TMP3A\text{-}O2$
45)	1.125×10^{-13}	$TMP3A\text{-}O2 + TMP3A\text{-}O2 \rightarrow TMP3A\text{-}O + TMP3A\text{-}O + O2$
45A)	1.375×10^{-13}	$TMP3A\text{-}O2 + TMP3A\text{-}O2 \rightarrow ALCOHOL5 + ALDEHYDE3$
46)	7.30×10^{-12}	$TMP3A\text{-}O2 + NO \rightarrow TMP3A\text{-}O + NO2$
46A)	1.60×10^{-12}	$TMP3A\text{-}O2 + NO \rightarrow Nitrate$
47)	3.8×10^{-11}	$TMP3A\text{-}O + NO \rightarrow Nitrite$
48)	3.8×10^{-11}	$TMP3A\text{-}O + NO2 \rightarrow Nitrate$
49)	1.1×10^{-14}	$TMP3A\text{-}O + O2 \rightarrow HO2 + ALDEHYDE3$
50)	1.6×10^{4}	$TMP3A\text{-}O \rightarrow HCHO + R32$
51)	1×10^{-12}	$R32 + O2 \rightarrow R32\text{-}O2$
52)	2.0×10^{-17}	$R32\text{-}O2 + R32\text{-}O2 \rightarrow R32\text{-}O + R32\text{-}O + O2$
53)	6.39×10^{-12}	$R32\text{-}O2 + NO \rightarrow R32\text{-}O + NO2$
53A)	2.51×10^{-12}	$R32\text{-}O2 + NO \rightarrow Nitrate$
54)	3.8×10^{-11}	$R32\text{-}O + NO \rightarrow Nitrite$
55)	3.8×10^{-11}	$R32\text{-}O + NO2 \rightarrow Nitrate$
56)	4.5×10^{3}	$R32\text{-}O \rightarrow CH3CHO + NPT$

Neopentyl Radical Reactions

NP1)	2.4×10^{-12}	$NPT + O2 \rightarrow NPTO2$
NP2A)	6.0×10^{-13}	$NPTO2 + NPTO2 \rightarrow DMP + DMPA + O2$
NP2B)	4.0×10^{-13}	$NPTO2 + NPTO2 \rightarrow NPTO + NPTO + O2$

NP3) 1.5x10⁻¹¹ NPTO2 + HO2 → R-OOH + O2

NP4) 7.6x10⁻¹² NPTO2 + NO → NPTO + NO2

NP5) 9.4x10⁵ NPTO → (CH3)3C + HCHO

NP6) 4.7x10⁻¹⁵ NPTO + O2 → DMP + HO2

NP7) 3.0x10⁻¹² (CH3)3C + O2 → (CH3)3CO2

NP8) 2.0x10⁻¹⁷ (CH3)3CO2 + (CH3)3CO2 → (CH3)3CO + (CH3)3CO

NP9) 4.8x10⁻¹² (CH3)3CO2 + HO2 → R-OOH + O2

NP10) 7.6x10⁻¹² (CH3)3CO2 + NO → (CH3)3CO + NO2

NP11) 500 (CH3)3CO → ACETONE + CH3

NP12) 3.8x10⁻¹¹ NPTO + NO → Nitrite

NP13) 3.8x10⁻¹¹ NPTO + NO2 → Nitrate

NP14) 3.8x10⁻¹¹ (CH3)3CO + NO → Nitrite

NP15) 3.8x10⁻¹¹ (CH3)3CO + NO2 → Nitrate

Methyl Radical Reactions

M2) 1.0x10⁻¹² CH3 + O2 → CH3O2

M3A) 1.19x10⁻¹³ CH3O2 + CH3O2 → CH3O + CH3O + O2

M3B) 1.98x10⁻¹³ CH3O2 + CH3O2 → HCHO + CH3OH + O2

M4) 4.8x10⁻¹² CH3O2 + HO2 → R-OOH + O2

M5) 7.6x10⁻¹² CH3O2 + NO → CH3O + NO2

M6) 4.11x10⁻¹² CH3O2 + NO2 → CH3O2NO2

M7) 1.92x10⁻¹⁵ CH3O + O2 → HCHO + HO2

M8) 1.4x10⁻¹¹ CH3O + NO → CH3ONO

M9) 3.8x10⁻¹¹ CH3O + NO2 → Nitrate

Table 3.4: 2,2,5-Trimethylhexane Mechanism

(Units: cm³, molecule, s)

No.	k @ 298K	Reaction
		2,2,5-Trimethylhexane Reactions
1A)	2.11×10^{-12}	TMH + OH → TMH3 + H2O
1B)	1.16×10^{-12}	TMH + OH → TMH2A + H2O
1C)	1.21×10^{-12}	TMH + OH → TMH2B + H2O
1D)	4.74×10^{-13}	TMH + OH → TMH1A + H2O
1E)	3.16×10^{-13}	TMH + OH → TMH1B + H2O
		Tertiary Radical Reactions
2)	1×10^{-12}	TMH3 + O2 → TMH3-O2
3)	1.87×10^{-17}	TMH3-O2 + TMH3-O2 → TMH3-O + TMH3-O + O2
4)	7.56×10^{-12}	TMH3-O2 + NO → TMH3-O + NO2
4a)	1.34×10^{-12}	TMH3-O2 + NO → Nitrate
5)	1.4×10^{5}	TMH3-O → ACETONE + C6H13
6)	3.8×10^{-11}	TMH3-O + NO → Nitrite
7)	3.8×10^{-11}	TMH3-O + NO$_2$ → Nitrate
8)	1×10^{-12}	C6H13 + O2 → C6H13O2
9)	5×10^{-14}	C6H13O2 + C6H13O2 → C6H13O + C6H13O + O2
9a)	5×10^{-14}	C6H13O2 + C6H13O2 → DMBALD + ALCOHOL1
10)	8.15×10^{-12}	C6H13O2 + NO → C6H13O + NO2
10a)	7.53×10^{-13}	C6H13O2 + NO → Nitrate
11)	1.67×10^{-14}	C6H13O + O2 → HO2 + DMBALD
12)	1.37×10^{2}	C6H13O → NPT + HCHO
12A)	6.7×10^{4}	C6H13O → 1,5-Isomerization

13) 3.8×10^{-11} C6H13O + NO → Nitrite

14) 3.8×10^{-11} C6H13O + NO$_2$ → Nitrate

Secondary Radical Reactions

15) 1×10^{-12} TMH2A + O2 → TMH2A-O2

16) 4.98×10^{-16} TMH2A-O2 + TMH2A-O2 → TMH2A-O + TMH2A-O + O2

16a) 4.98×10^{-16} TMH2A-O2 + TMH2A-O2 → C8H18CO + ALCOHOL2

17) 5.6×10^{-12} TMH2A-O2 + NO → TMH2A-O + NO2

17a) 3.3×10^{-12} TMH2A-O2 + NO → Nitrate

18) 2.91×10^{-14} TMH2A-O + O2 → HO2 + C8H18CO

19) 8.02×10^{5} TMH2A-O → (CH3)3C + VALALD

19A) 6.7×10^{4} TMH2A-O → 1,5-Isomerization

20) 3.8×10^{-11} TMH2A-O + NO → Nitrite

21) 3.8×10^{-11} TMH2A-O + NO$_2$ → Nitrate

Secondary Radical Reactions

22) 1×10^{-12} TMH2B + O2 → TMH2B-O2

23) 4.98×10^{-16} TMH2B-O2 + TMH2B-O2 → TMH2B-O + TMH2B-O + O2

23a) 4.98×10^{-16} TMH2B-O2 + TMH2B-O2 → C8H18CO + ALCOHOL3

24) 5.6×10^{-12} TMH2B-O2 + NO → TMH2B-O + NO2

24a) 3.3×10^{-12} TMH2B-O2 + NO → Nitrate

25) 3.65×10^{-14} TMH2B-O + O2 → HO2 + C8H18CO

26) 1.82×10^{5} TMH2B-O → DMBALD + P

26A) 6.7×10^{4} TMH2B-O → 1,5-Isomerization

27) 3.8×10^{-11} TMH2B-O + NO → Nitrite

28) 3.8×10^{-11} TMH2B-O + NO$_2$ → Nitrate

Primary Radical Reactions

29) 1×10^{-12} TMH1A + O2 → TMH1A-O2

30) 5×10^{-14} TMH1A-O2 + TMH1A-O2 → TMH1A-O + TMH1A-O + O2

30a) 5×10^{-14} TMH1A-O2 + TMH1A-O2 → C8H17CHO + ALCOHOL4

31) 7.2×10^{-12} TMH1A-O2 + NO → TMH1A-O + NO2

31a) 1.7×10^{-12} TMH1A-O2 + NO → Nitrate

32) 8.82×10^{-15} TMH1A-O + O2 → HO2 + C8H17CHO

33) 2.16×10^{4} TMH1A-O → HCHO + C8H17

33A) 8.4×10^{6} TMH1A-O → 1,5-Isomerization

34) 3.8×10^{-11} TMH1A-O + NO → Nitrite

35) 3.8×10^{-11} TMH1A-O + NO$_2$ → Nitrate

36) 1×10^{-12} C8H17 + O2 → C8H17-O2

37) 1.87×10^{-17} C8H17-O2 + C8H17-O2 → C8H17-O + C8H17-O + O2

38) 7.75×10^{-12} C8H17-O2 + NO → C8H17-O + NO2

38a) 1.15×10^{-12} C8H17-O2 + NO → Nitrate

39) 4.9×10^{4} C8H17-O → ACETONE + C5H11

39) 4.1×10^{6} C8H17-O → 1,5 Isomerization

40) 3.8×10^{-11} C8H17-O + NO → Nitrite

41) 3.8×10^{-11} C8H17-O + NO$_2$ → Nitrate

42) 1×10^{-12} C5H11 + O2 → C5H11-O2

43) 5×10^{-14} C5H11-O2 + C5H11-O2 → C5H11-O + C5H11-O + O2

43a) 5×10^{-14} C5H11-O2 + C5H11-O2 → VALALD + ALCOHOL5

44) 8.43×10^{-12} C5H11-O2 + NO → C5H11-O + NO$_2$

44a) 4.74×10^{-13} C5H11-O2 + NO → Nitrate

45) 1.3×10^{-14} C5H11-O + O2 → HO2 + VALALD

46) 2.9×10^{2} C5H11-O → HCHO + MP

46A) 6.7×10^{4} C5H11-O → 1,5-Isomerization

47) 3.8×10^{-11} C5H11-O + NO → Nitrite

48) 3.8×10^{-11} C5H11-O + NO$_2$→ Nitrate

49) 2.9×10^{-12} MP + O2 → MP-O2

50) 1.125×10^{-13} MP-O2 + MP-O2 → MP-O + MP-O + O2

50a) 1.375×10^{-13} MP-O2 + MP-O2 → ALCOHOL3 + MPROP + O2

51) 8.9×10^{-12} MP-O2 + NO → MP-O + NO2

52) 3.8×10^{-11} MP-O+ NO → Nitrite

53) 3.8×10^{-11} MP-O + NO2 → Nitrate

54) 1.1×10^{3} MP-O → HCHO + P

55) 8.5×10^{-15} MP-O + O2 → MPROP + HO2

Primary Radical Reactions

56) 1×10^{-12} TMH1B + O2 → TMH1B-O2

57) 5×10^{-14} TMH1B-O2 + TMH1B-O2 → TMH1B-O + TMH1B-O + O2

57a) 5×10^{-14} TMH1B-O2 + TMH1B-O2 → C8CHO + ALCOHOL7

58) 7.2×10^{-12} TMH1B-O2 + NO → TMH1B-O + NO2

58a) 1.7×10^{-12} TMH1B-O2 + NO → Nitrate

59) 1.1×10^{-14} TMH1B-O + O2 → HO2 + C8CHO

60) 1.93×10^{3} TMH1B-O → HCHO + C8

60A) 8.4×10^{6} TMH1B-O → 1,5-Isomerization

61) 3.8×10^{-11} TMH1B-O + NO → Nitrite

62) 3.8×10^{-11} TMH1B-O + NO$_2$ → Nitrate

63) 1×10^{-12} C8 + O2 → C8-O2

64) 4.98×10^{-16} C8-O2 + C8-O2 → C8-O + C8-O + O2

64a) 4.98×10^{-16} C8-O2 + C8-O2 → C8H16O

65) 5.95×10^{-12} C8-O2 + NO → C8-O + NO2

65a) 2.95×10^{-12} C8-O2 + NO → C8-O + NO2

66) 1.8×10^{-14} C8-O + O2 → HO2 + C8H16O

67) 4.5×10^{3} C8-O → CH3CHO + C6H13

68) 3.8×10^{-11} C8-O + NO → Nitrite

69) 3.8×10^{-11} C8-O + NO$_2$ → Nitrate

Reactions of the i-Propyl Radical

j37) 11×10^{-12} P + O2 → P-O2

j38) 5.5×10^{-16} P-O2 + P-O2 → P-O + P-O + O2

j38A) 5.4×10^{-16} P-O2 + P-O2 → ALCOHOL4 + ACETONE

j39) 8.9×10^{-12} P-O2 + NO → P-O + NO2

j40) 3.4×10^{-11} P-O + NO → Nitrite

j41) 3.5×10^{-11} P-O + NO2 → Nitrate

j42) 8.0×10^{-15} P-O + O2 → ACETONE + HO2

j43) 1.5×10^{-1} P-O → CH3 + CH3CHO

Neopentyl Radical Reactions

Same as in 2,2,4-Trimethylpentane mechanism.

Methyl Radical Reactions

Same as in 2,2,4-Trimethylpentane mechanism.

3.5.1 2,2,4-Trimethylpentane

A mechanism for 2,2,4-trimethylpentane that does not include alkoxy radical isomerization reactions overpredicts, by a factor of 2, the yield of acetone, the major carbonyl formed from attack on the tertiary carbon of 2,2,4-trimethylpentane. Since the majority of the acetone is generated from the tertiary reactions of 2,2,4-trimethylpentane, this overprediction indicates that alkoxy radical isomerization pathways are important. The major isomerization pathway is via 1,5-H atom shift, and in the case of 2,2,4-trimethylpentane, the only radicals that are likely to undergo this shift are the tertiary and primary alkoxy radicals. Rate constants for 1,5-H atom isomerizations are available in Atkinson [1]. Incorporating the alkoxy radical isomerization reactions into the mechanism produces predicted yields that agree reasonably well with measured concentrations of acetone and 2-methyl-1-propanal, errors of +1.5% and +16%, as compared to observed results, respectively. The mechanism consistently underpredicts formaldehyde formation. Observed and predicted concentrations of acetone, 2-methyl-1-propanal, and formaldehyde are presented in Figures 3.11, 3.12, and 3.13, respectively.

The elevated experimental formaldehyde yields relative to those predicted by the mechanism may be attributed to reactions of isomerization products for which standards were not available. Each product formed from 1,5-H atom isomerization is expected to result in the formation of at least one HCHO molecule. Examination of the mechanisms in Figures 3.2- 3.4 shows that each 1,5-isomerization for an alkoxy radical either bypasses or delays the
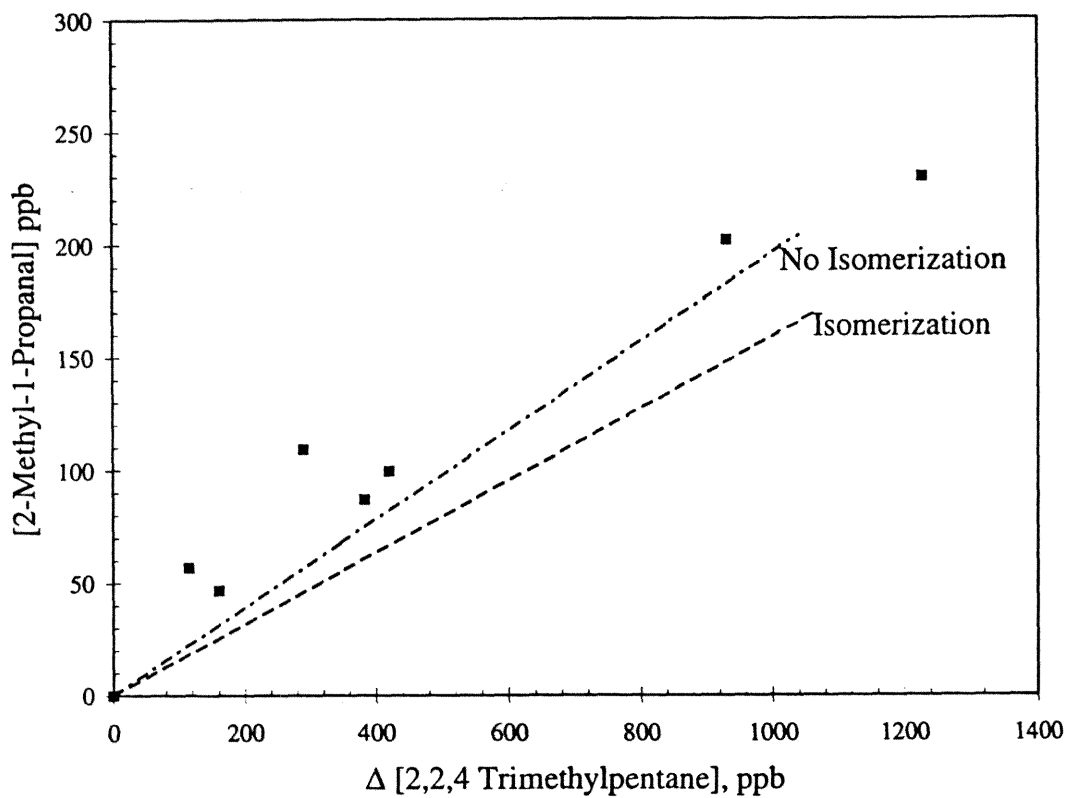
Figure 3.11: Observed data (points) and predicted concentrations excluding alkoxy radical isomerization and including 1,5-isomerization for 2-methyl-1-propanal from 2,2,4- trimethylpentane photooxidation.
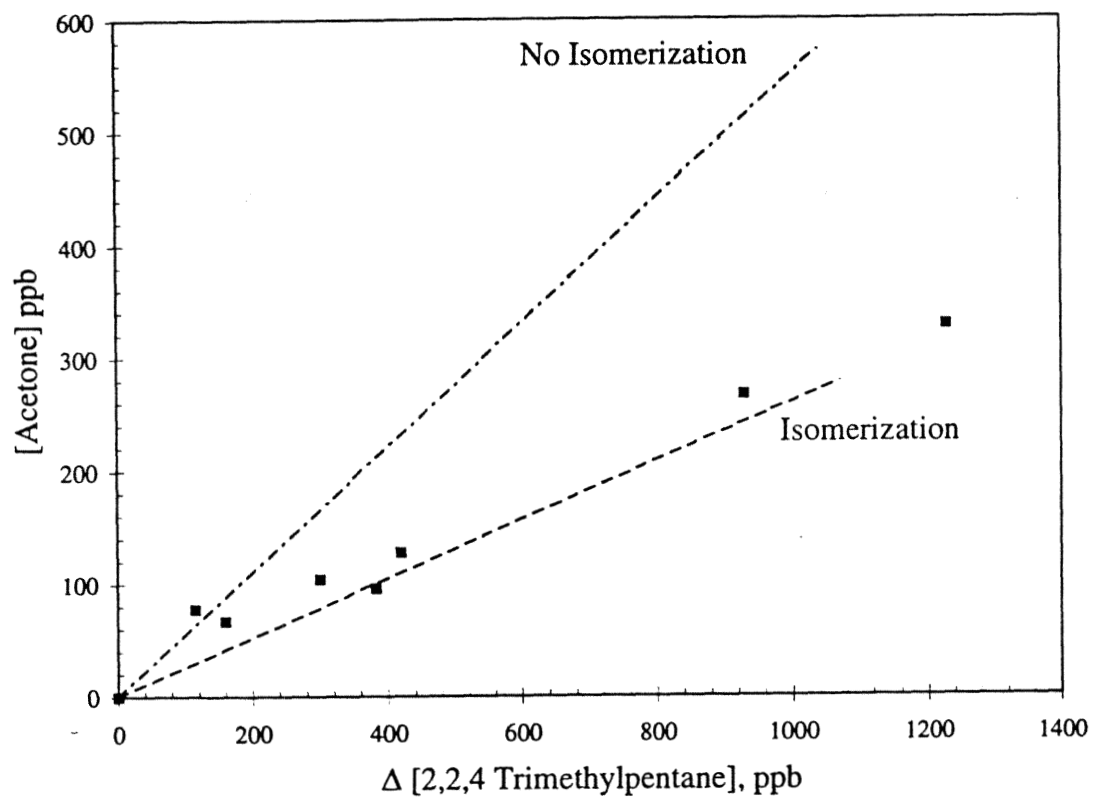
Figure 3.12: Observed data (points) and predicted concentrations excluding alkoxy radical isomerization and including 1,5-isomerization for acetone from 2,2,4-trimethylpentane photooxidation.
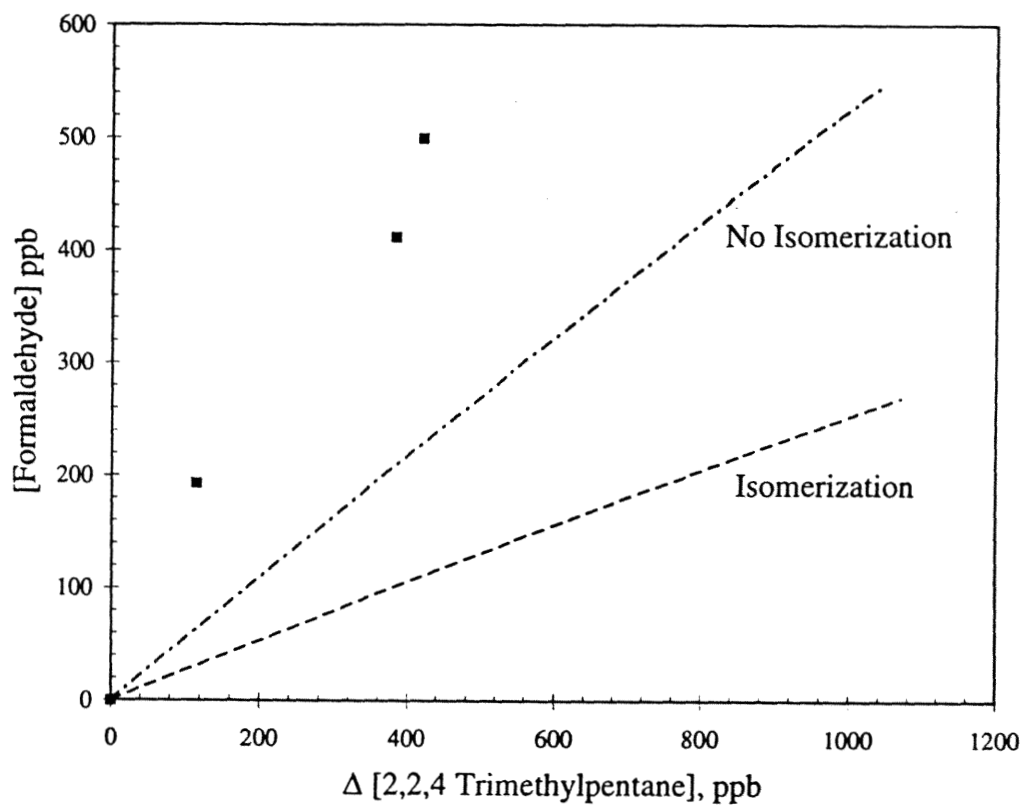
Figure 3.13: Observed data (points) and predicted concentrations excluding alkoxy radical isomerization and including 1,5-isomerization for formaldehyde from 2,2,4- trimethylpentane photooxidation.

formation of one molecule of HCHO. Thus, the line labeled "No Isomerization" in Figure 3.13 actually represents the HCHO production resulting from isomerization when HCHO formation is accounted for from further reactions of isomerization products.

A 1,5-H atom isomerization step for the secondary alkoxy radical from 2,2,4-trimethylpentane is not possible. However, another type of isomerization, 1,4- H atom shift, may be possible for the secondary radical in the 2,2,4-trimethylpentane system. Given the reasonably good agreement between the predicted yield, including isomerization pathways for the tertiary and primary radicals, and the experimental yield for 2-methyl propanal, it is unlikely that there is a significant 1,4- H atom shift pathway for the secondary alkoxy radical. Such a pathway would result in poor agreement between observations and predictions for the yield of 2-methyl propanal. An estimate for the rate constant for a 1,4-H atom shift with abstraction from a -CH_3 group can be made from comparisons of observed and predicted concentrations of 2-methyl propanal. 1,4-Isomerization reactions for the secondary alkoxy radical , TMPR2-O, and the primary alkoxy radical, TMPR3-O, resulting in abstraction of H-atoms from a -CH_3 and a -CH_2 group, respectively, were included in the 2,2,4-trimethylpentane mechanism. The rate constant for 1,4-isomerization corresponding to H-atom abstraction from a -CH_3 group was varied from $1x10^1$- $1x10^5$ s^{-1}. From previous studies, the ratio of rate constants for 1,5-isomerization corresponding to abstraction from a -CH_3 group is approximately a factor of 100 smaller than the corresponding abstraction from a -CH_2 group [1, 18]. Thus, the rate constant for 1,4-isomerization of the primary alkoxy radical was varied from $1x10^3$-$1x10^7$ s^{-1}, simultaneous

to the variation of the rate constant for 1,4-isomerization of the secondary alkoxy radical. The resulting 2-methyl-1-propanal yield was compared to the experimentally derived yield, and an estimate for this isomerization step was obtained by calculating the error between the yields. Upper limits to the rate constants for 1,4-isomerization with H-atom abstraction from a -CH_3 and a -CH_2 group were determined to be $1x10^3$ and $1x10^5$ s^{-1}, respectively. Initial comparisons of the 1,4- isomerization rate constant for abstraction from a -CH_3 group determined in this work to literature data [7] show that the value determined here is approximately an order of magnitude larger than the value reported in the literature. However, the uncertainty factor of 60 reported by Baldwin et al. [7] places the value for 1,4-isomerization with abstraction from a -CH_3 group reported in this work in reasonable agreement with previous estimates.

3.5.2   2,2,5-Trimethylhexane

Initially, the mechanism for the 2,2,5-trimethylhexane system included all of the reactions except the isomerization reactions. Once again, comparisons of the predicted and observed yields of the major products formed (acetone and 3,3 dimethylbutyraldehyde) indicate that the mechanism without alkoxy radical isomerization overpredicts the observed yields. Once isomerization reaction steps corresponding to 1,5-H atom shifts are added to the mechanism, the experimental results are more closely represented. The predicted yield for 3,3-dimethylbutyraldehyde is approximately 22% larger than the observed yield. However, the mechanism predictions for acetone are

still approximately 150% larger than the experimental results. This observation indicates either that additional and significant isomerization reactions other than 1,5-H shifts are possible with the radicals formed in the photooxidation of larger alkanes, rate constants corresponding to 1,5-H atom shifts for branched compounds are too low, or decomposition and O_2 reaction rate constants for the alkoxy radicals are too high. Because there was excellent agreement between observed and predicted concentrations for the case of 2,2,4-trimethylpentane using rate constant data available for 1,5-isomerization, decomposition, and O_2 reactions of the alkoxy radicals, we must conclude that there are additional isomerization pathways for 2,2,5-trimethylhexane that are insignificant for 2,2,4-trimethylpentane. Therefore, 1,4-isomerization alkoxy radical reactions were included in the mechanisms, and the results compared to the observed data. The rate constants used for the 1,4-isomerizations were those determined from fits of the 2-methyl-1-propanal data from the photooxidation of 2,2,4-trimethylpentane (see the previous section). Inclusion of 1,4-isomerization steps, where applicable, provide a better fit to the acetone data. The predicted acetone yield is only 18% larger than the observed yield. The 3,3-dimethylbutyraldehyde data remained unchanged. In all cases, however, the formaldehyde and acetaldehyde yields are underpredicted. Experimental data and mechanism predictions for 3,3-dimethylbutyraldehyde, acetone, acetaldehyde, and formaldehyde appear in Figures 3.14-3.17, respectively.

The underpredicted yields for acetaldehyde and formaldehyde, as in the case of 2,2,4-trimethylpentane, is likely a result of reactions of isomerization products from the alkoxy radicals. To examine this, we used the predicted
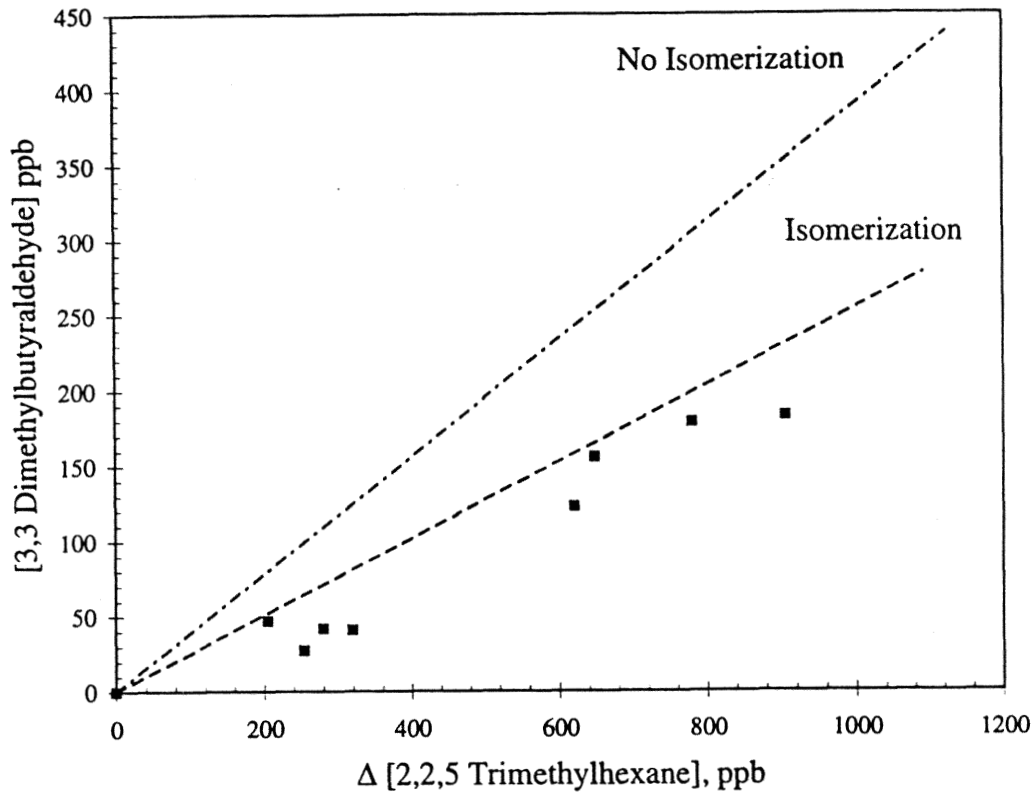
Figure 3.14: Depicted are the observed and the predicted concentrations for 3,3- dimethylbutyraldehdye from 2,2,5-trimethylhexane photooxidation. The predicted concentrations are based on mechanisms that exclude isomerizations and include both 1,4- and 1,5- isomerizations.
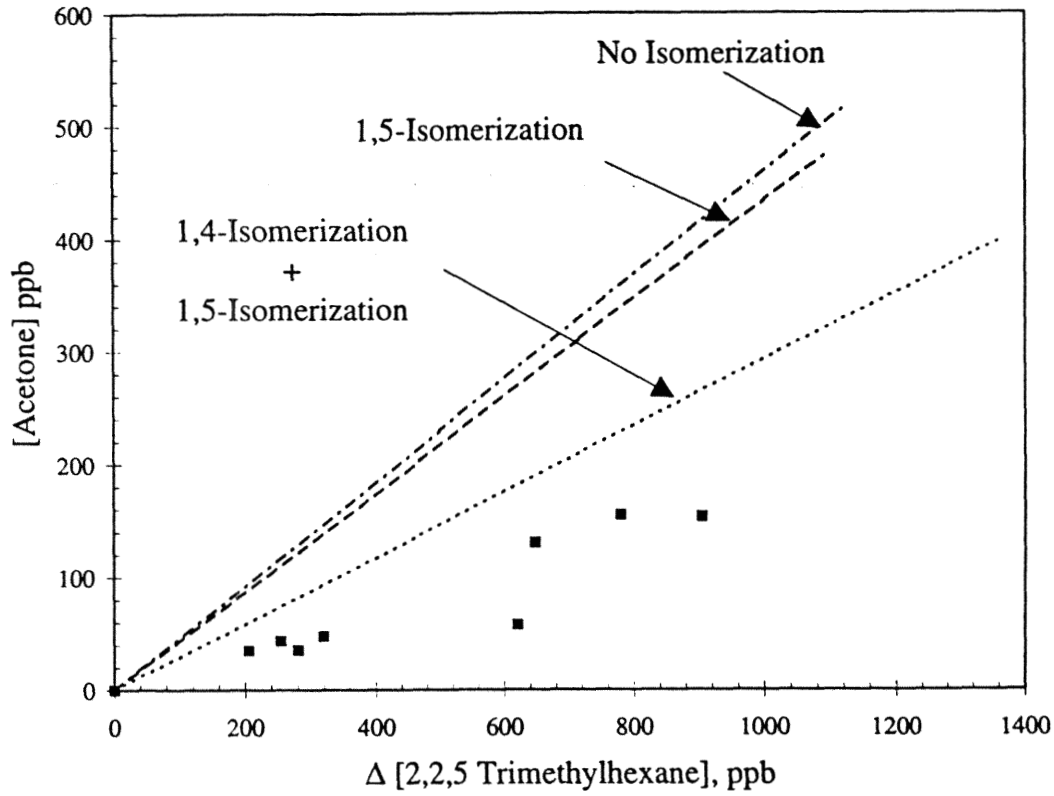
Figure 3.15: Observed and predicted concentrations for acetone from 2,2,5-trimethylhexane photooxidation. The predicted concentrations are based on mechanisms that exclude all alkoxy radical isomerizations, include only 1,5-isomerizations, and include both 1,4- and 1,5-isomerizations.
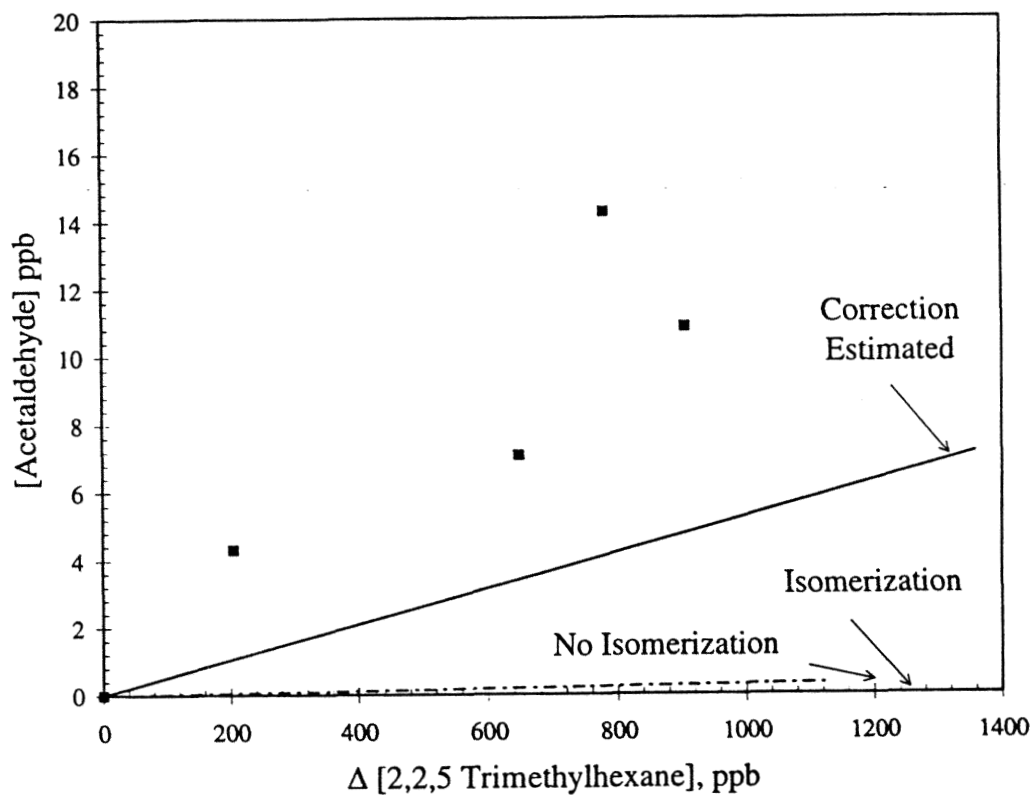
Figure 3.16: Observed and predicted concentrations for acetaldehyde from 2,2,5-trimethylhexane photooxidation. The line labeled "Correction Estimated" takes into account the formation of acetaldehyde from the reactions of alkoxy radical isomerization products.
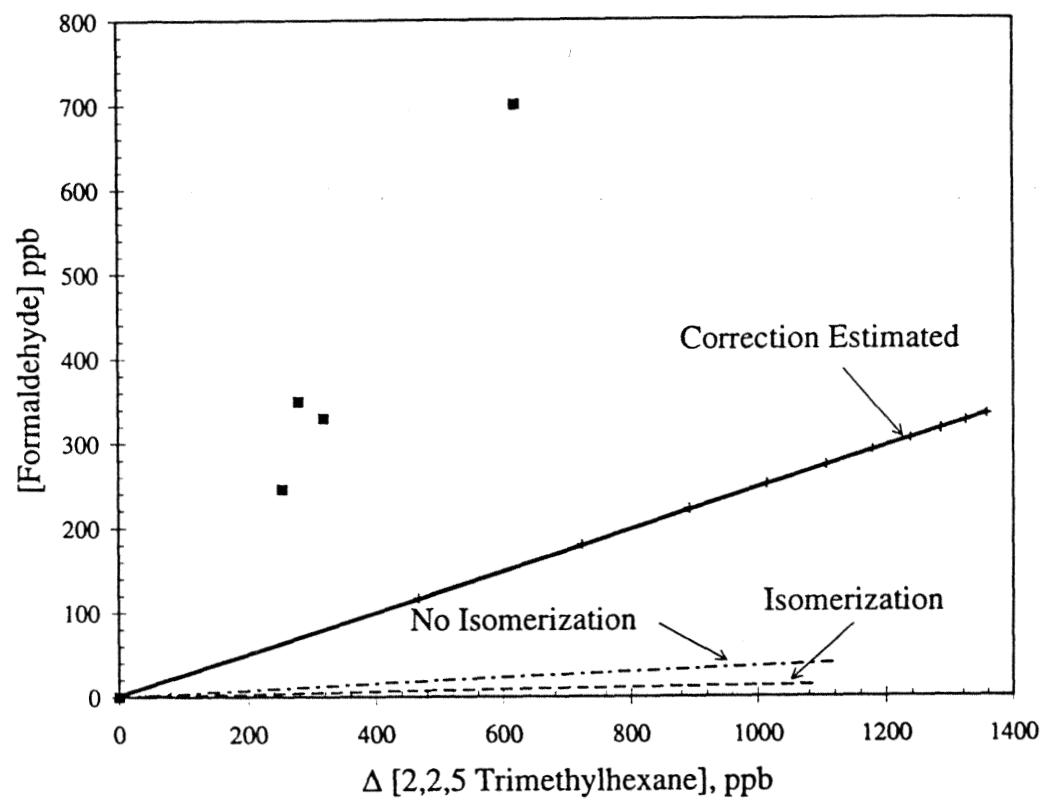
Figure 3.17: Observed and predicted concentrations for formaldehyde from 2,2,5-trimethylhexane photooxidation . The line labeled "Correction Estimated" takes into account the formation of formaldehyde from the secondary reactions of alkoxy radical isomerization products.

concentrations of products resulting from the alkoxy radical 1,4- and 1,5-isomerization steps to calculate the amount of HCHO that would result from continued reaction of these products. Most of the pathways that are capable of undergoing 1,4- and 1,5-isomerizations lead to the direct formation of at least one molecule of HCHO. In addition, acetaldehyde is generated from the reaction of the 1,5-isomerization product resulting from the alkoxy radical, TMH2A-O (see Figure 3.7). Assuming that only one HCHO molecule is formed in any of the reactions of the products of alkoxy radical isomerizations, a lower bound estimate for the production of HCHO is possible, and included in Figure 3.17. The yield of the isomerization products from the single alkoxy radical isomerization reaction producing CH_3CHO as a product was used to correct the CH_3CHO yield, and the result appears in Figure 3.16. The predicted yields based on the formation of only one HCHO or CH_3CHO molecule per reaction of alkoxy radical isomerization product are still lower than the observed yields, but it is important to note that we have not taken into account the full reaction mechanisms of these products.

As discussed earlier, the neopentyl radicals are not expected to react to form 2,2-dimethyl-1-propanal in the presence of NO_x. Regardless of whether or not isomerization reactions are included in the overall mechanisms for 2,2 4-trimethylpentane or 2,2,5-trimethylhexane, the predicted yields of 2,2-dimethyl-1-propanal are negligible. This result lends credence to the supposition that the 2,2-dimethyl-1-propanal detected in the photooxidation of 2,2,5-trimethylhexane is a result of secondary reaction of OH with 3,3-dimethylbutyraldehyde, rather than primary formation from the neopentyl radical.

3.6 Conclusions

Experiments have been performed to investigate the photooxidation of two relatively large alkanes, 2,2,4- trimethylpentane and 2,2,5-trimethylhexane. The first kinetic study of the OH + 2,2,5-trimethylhexane reaction resulted in a rate constant of $(5.267 \pm 0.147) \times 10^{-12}$ cm^3 $molecule^{-1}$ s^{-1}, in excellent agreement with a predicted value of 5.7 $\times 10^{-12}$ cm^3 $molecule^{-1}$ s^{-1}, using Atkinson's structure reactivity relationship[15]. Carbonyl products have been identified from laboratory experiments with each alkane, and the major products observed are consistent with those expected from the mechanisms. Mechanisms for each of the alkanes were developed to examine the effect of alkoxy radical isomerization reactions on predicted carbonyl yields. Using the mechanism for 2,2,4-trimethylpentane photooxidation, upper limits for the rate constants of 1,4-H atom isomerization with abstraction from $-CH_3$ and $-CH_2$ groups have been determined as 1×10^3 and 1×10^5 s^{-1}, respectively.

Acknowledgement

Bibliography

[1] Atkinson, R., *J. Phys. Chem.* , **Monograph 2**, 1 (1994).

[2] Lurmann, F.W. and Main, H.H., "Analysis of the Ambient VOC Data Collected in the Southern Air Quality Study," Final Report, Contract No. A832-130. State of California Air Resources Board, Sacramento (1992).

[3] Atkinson, R., Kwok, E.S.C., Arey, J. , Aschmann, S.M., *Disscussions Faraday Society*, **100**, In Press (1994).

[4] Atkinson, R., Carter, W.P.L., *J. Atm. Chem.*, **13**, 195 (1991).

[5] Atkinson, R., *Atmos. Environ.*, **24A**, 1(1990).

[6] Dobe, S., Berces,T., Reti, F., Marta,F., *Int. J. Chem. Kinet.*, **19**, 895 (1987).

[7] Baldwin, A.C., Barker, J.R., Golden, D.M., Hendry,D.G., *J. Phys. Chem.*, **81**, 2483 (1977).

[8] Atkinson, R., *J. Phys. Chem. Ref. Data*, **Monograph 1**,1 (1989).

[9] Kwok, E.S.C., Atkinson, R., *Atm. Environ.*, **24**, 1685 (1995).

[10] Atkinson, R., *Int. J. Chem. Kinet.*, **19**, 799 (1987).

[11] Holmes,J.R., O'Brien,R.J., Crabtree,J.H., Hecht,T.A., Seinfeld,J.H., *Environ. Sci. Tech.*, **7**, 519 (1973).

[12] Finlayson-Pitts, B.J., Pitts Jr., J.N., Atmospheric Chemistry: Fundamentals and Experimental Techniques, Wiley, New York, 1986.

[13] Taylor, W.D., Allston, T.D., Moscato, M.J., Fazekas, G.B., Kozlowski,R., Takacs,G.A., *Int. J. Chem. Kinet.*, **12**, 231 (1980).

[14] Druzik, C.M., Grosjean,D., Van Neste, A., Parmar, S.S., *Int. J. Environ. Anal. Chem.*, **38**, 495 (1990).

[15] Atkinson, R., Aschmann,S.M., Carter,W.P.L., Winer,A.M., Pitts Jr., J.N., *J.Phys. Chem.*, **86**, 4563 (1982).

[16] Carter, W.P. Documentation for the SAPRC Atmospheric Photochemical Mechanism Preparation and Emissions Processing Programs for Implementation in Air-Shed Models, California Air Resources Board, Contract No. A5-122-32, October 1988.

[17] Stein, S.E.; Rukkers, J.M.; Brown, R.L., "NIST Standard Reference Database 25: NIST Structures and Properties Database and Estimation Program", 1991.

[18] Eberhard, J., Muller, C., Stocker,D.W., Alistair Kerr,J., *Env. Sci. Tech.*, **29**, 232 (1995).

[19] Atkinson, R., Aschmann,S.M., *Env. Sci. Tech.*, *29*, 528 (1995).

[20] Wallington,T.J., Andino,J.M., Potts,A.R., Nielsen,O.J., *Int. J. Chem. Kinet.*, *24*, 649 (1992).

Chapter 4

Mechanism of Atmospheric Photooxidation of Aromatics: A Theoretical Study

Abstract

The mechanisms of atmospheric photooxidation of aromatic compounds are of seminal importance in the chemistry of the urban and regional atmosphere. It has been difficult to experimentally account for the full spectrum of oxidation products in laboratory studies. In an effort to fully elucidate the atmospheric reaction pathways for the aromatic-OH reaction, we have conducted theoretical calculations on aromatic intermediates. Energies have been determined for these intermediates using semi-empirical UHF/PM3 geometry optimizations combined with *ab initio* calculations using density functional theory (DFT). A hybrid DFT model, the Becke 3 parameter functional with the non-local correlation functional of Lee, Yang and Parr, was used in conjunction with the 6-31G(d,p) basis set to study the intermediate structures. Full mechanisms for the OH-initiated photooxidation of toluene, *m*-xylene, *p*-xylene, 1,2,4- trimethylbenzene and *m*-ethyltoluene are developed. The lowest energy intermediates have been determined and predicted products from these structures are compared to available experimental product data. These studies serve to refine proposed mechanisms currently available for toluene, *m*-xylene and *p*-xylene, while providing new information on the 1,2,4- trimethylbenzene and *m*- ethyltoluene reaction pathways.

4.1   Introduction

Aromatic compounds are of great interest in atmospheric chemistry because of their abundance in motor vehicle emissions and because of their reactivity with respect to ozone and organic aerosol formation. Understanding the atmospheric oxidation mechanisms of aromatics has long been cited as the most critical need in further development of reaction mechanisms for the urban and regional atmosphere[1]. The major atmospheric sink for aromatics is reaction with the hydroxyl radical. Whereas rate constants for the OH reaction with aromatics have been well characterized [2], mechanisms of aromatic oxidation following the initial OH attack have been highly uncertain. In experimental photooxidation studies of toluene, m-xylene, and p-xylene (summaries of which are available in [2, 3, 4]), typically less than 50% of the reacted carbon has been identified as products. A difficulty in accounting for the remaining fraction of reacted carbon lies in the fact that the intermediates involved in aromatic-OH oxidation have not been unambiguously identified. Consequently, theoretical studies can be extremely useful in evaluating the possible mechanisms of oxidation. We present here theoretical calculations on possible structural intermediates formed in the OH-initiated reactions of toluene, m-xylene, p- xylene, 1,2,4- trimethylbenzene, and m-ethyltoluene. The aromatics chosen correspond to ones which our group has studied in the laboratory. From these energy determinations, the most likely intermediate species have been identified, and overall mechanisms for the photooxidation of these aromatics are proposed.

The aromatic-OH reaction proceeds by both abstraction and addition

pathways (see [2] and [3] and references therein). The addition pathway, occurring roughly 90% of the time, is the more prevalent route. Products identified in the OH addition reactions of toluene, m-xylene, and p-xylene in previous laboratory studies appear in Tables 4.1-4.3. The yields presented in the tables are defined as the ratio of the molar concentration of the product to that of reacted aromatic. As noted above, generally less than 50% of the carbon in these systems has been accounted for experimentally. In the current study, we compare available experimental product data for the toluene, p-xylene, and m-xylene systems to our proposed mechanisms to evaluate the extent of agreement between the theoretical mechanisms and observed product data. The theory is then used to predict additional products that might be found in these three systems. Since only two studies on products resulting from 1,2,4- trimethylbenzene photooxidation are available [5, 6], neither considering the full mechanism for photooxidation, and no product data on the reactions of m-ethyltoluene are available, we develop plausible atmospheric reaction mechanisms for both of these species based on theory alone.

4.2   Calculation Methods

The essential element of the theoretical approach is to employ semi-empirical and *ab initio* quantum mechanical techniques to determine the most energetically favored intermediates in the reaction mechanisms, taking into account transition state complexes. These methods are used to determine the lowest energy structures in the most computationally efficient manner, balancing the desire for reasonable computational times with the highest level of the-

Table 4.1: Toluene Photooxidation Products: Molar Yields

Compound	Yield	Reference
Glyoxal	0.105 ± 0.019	[6]
	0.058	[7]
	0.150 ± 0.040	[8]
	0.080	[9]
Methyl Glyoxal	0.146 ± 0.006	[6]
	0.077	[7]
	0.140 ± 0.04	[8]
	0.075	[9]
Methylbutenedial	0.058	[7]
Hydroxymethylbutenedial	0.034	[7]
Oxoheptadienal	0.027	[7]
Methylhydroperoxide	0.018	[7]
Formaldehyde	0.010	[7]
Hexadienyl	0.010	[7]
Hydroxyoxoheptadienal	0.010	[7]
Maleic Anhydride	0.040 ± 0.004	[8]
o-Cresol	0.204 ± 0.027	[10]
m- and p-Cresol	0.048 ± 0.009	[10]
m-Nitrotoluene	$(0.0135 \pm 0.0029) + (1.90 \pm 0.25) * 10^{-16} [NO_2]$	[10]
o-Nitrotoluene	$0.07 * [m\text{-nitrotoluene}]$	[10]
p-Nitrotoluene	$0.35 * [m\text{-nitrotoluene}]$	[10]

Table 4.2: m-Xylene Photooxidation Products: Molar Yields

Compound	Yield	Reference
Glyoxal	0.13 ± 0.03	[11]
	0.086	[12]
	0.086 ± 0.011	[6]
Methylglyoxal	0.42 ± 0.05	[11]
	0.375	[12]
	0.319 ± 0.009	[6]
Formaldehyde	0.17 ± 0.02	[11]
2,4 Dimethylphenol	0.099	[13]
2,6 Dimethylphenol	0.111	[13]
4-Nitro-m-xylene	0.0018	[13]
5-Nitro-m-xylene	$0.0032 + 1.6 * 10^{-17} [NO_2]$	[13]

Table 4.3: p-Xylene Photooxidation Products: Molar Yields

Compound	Yield	Reference
Glyoxal	0.24 ± 0.02	[11]
	0.225 ± 0.039	[6]
Methylglyoxal	0.12 ± 0.02	[11]
	0.105 ± 0.034	[6]
3-Hexene-2,5 Dione	Detected	[11]
Formaldehyde	0.17 ± 0.02	[11]
2,5 Dimethylphenol	0.188	[13]
2-Nitro-p-xylene	$0.0120 + 2.8 \times 10^{-17}[NO_2])$	[13]

ory. Semi-empirical optimizations require less computational time, and, given that all of the structures studied are similar in nature (aromatic structures with C, N, O, and H atoms), semi-empirical optimizations are adequate for screening and optimizing the structures, while *ab initio* calculations provide accurate energy determinations.

To examine the effectiveness of semi-empirical optimizations followed by *ab initio* calculations, studies were conducted on a variety of compounds, including methylhydroxycyclohexadienyl radicals resulting from toluene photooxidation, alkyl radicals, alkoxy radicals and nitroalkenes, using different geometry optimization and single point energy calculation schemes. The first study compared the use of high and low level computational techniques to examine methylhydroxycyclohexadienyl radical formation from OH addition to toluene. Since experimental data for the energies of these radicals are not available, comparisons of theoretical and experimental results are not possible. However, these calculations were used in order to find a balance between the highest level of theory and the computational time required to accurately predict the stability of radicals that are similar to those studied

in this work, assuming that the most rigorous computational method adequately reflects the true energy of the species. The second study compared the results of the chosen computational technique to experimental values to provide a calibration of the technique.
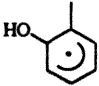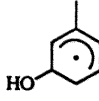
Techniques used for geometry optimization include density functional theory (DFT)[14] using the hybrid density functional, Becke3LYP, of Becke [15, 16] and Lee *et al.* [17, 18] and a 6-31G(d,p) basis set, restricted open-shell Hartree Fock (ROHF) optimization using a 6-31G(d,p) basis set, a semi-empirical unrestricted Hartree-Fock PM3 (UHF/PM3) optimization[19], and a molecular mechanics optimization using the MM+ functional form[20]. Of the semi-empirical techniques, the PM3 parameterization, a Modified Neglect of Diatomic Overlap (MNDO) method, is most often cited as producing the best optimizations for hydrocarbon systems and complexes containing nitrogen and oxygen[19, 21]. In addition to providing an accurate geometry, PM3 has also been shown to provide accurate vibrational frequencies that can be compared directly to experiment without *post hoc* correction[22]. These vibrational frequencies allow for the calculation of zero-point energies. The MM+ functional form of the potential was used in the molecular mechanics optimizations since it is most appropriate for small organic molecules[20]. The DFT and ROHF optimizations were performed on HP 9000/735 workstations using Gaussian 92[18] and PSGVB, version 2.13[23], respectively, while the UHF/PM3 and molecular mechanics optimizations were performed on a personal computer using Hyperchem, release 4.0[24]. Single point calculations were performed following geometry optimizations utilizing either the ROHF method or density functional theory[14] using the Becke3LYP hybrid

density functional. Both types of calculations employed a 6-31G(d,p) basis set, and were performed on HP 9000/735 workstations using Gaussian 92[18]. The results for the methylhydroxycyclohexadienyl radicals are given in Table 4.4, with relative energy defined as the difference in energy between any given structural isomer and the lowest energy structural isomer. Table 4.4 indicates that the MM+ optimization, followed by the DFT calculation, does not reproduce the results of the high-level DFT optimization followed by the DFT calculation. The UHF/PM3 geometry optimization method, however, gives relative energies that are quite close to the DFT values. Of the techniques studied, a semi-empirical UHF/PM3 geometry optimization, followed by a single point calculation using the Becke3LYP density functional and a 6-31G(d,p) basis set, exhibits the best combination of computational efficiency and accuracy. This method was therefore chosen for all of the calculations that are presented in this study.

To calibrate the chosen computational scheme, a second study was performed. Geometry optimizations using the UHF/PM3 method followed by a single point calculation using the Becke3LYP density functional and a 6-31G(d,p) basis set were performed on radicals and stable species for which experimental energy data exist. The relative energies of isomers of the structures were compared, and are tabulated in Table 4.5. From this table it is evident that the PM3/Becke3LYP technique adequately reproduces the relative energies between structural isomers for several different classes of compounds. In addition, we can obtain an estimate of our accuracy by comparing experimentally derived and theoretical relative energies. These values differ at most by 1.6 kcal/mol (which can be rounded to 2 kcal/mol). As a further

Table 4.4: Relative energies in kcal/mol for isomers of the methylhydroxycyclohexadienyl radical using various computational methods. The 6-31G(d,p) basis set was used for all *ab initio* calculations.
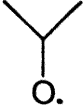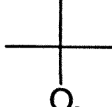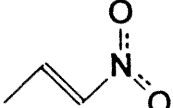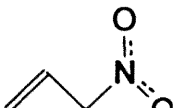
Geometry Opt./ Single Pt. Calc. Methods	Structure	HO— ⬡(·) (methyl top)	⬡(·) —OH (methyl top)	HO— ⬡(·) (methyl top)
Becke3LYP / Becke3LYP		0 [a]	1.1	1.8 ·
ROHF / Becke3LYP		0 [b]	0.9	1.7
ROHF / ROHF		0 [c]	0.8	0.7
UHF-PM3 / Becke3LYP		0 [d]	1.2	1.6
MM+ / Becke3LYP		0.1	0 [e]	0.4

Absolute energies: (a) -347.3406 a.u., (b) -347.3364 a.u., (c) -345.1331 a.u., (d) -347.3374 a.u., (e) -347.3318 a.u.

calibration, ΔH_{rxn} values derived from literature data [25] and PM3/DFT calculations for the toluene + OH reaction resulting in the formation of cresol isomers are compared. These data appear in Table 4.6, and show agreement between experiment and theory to within 2 kcal/mol. Although the ΔH_{rxn} comparisons between experiment and theory are within 2 kcal/mol agreement for the case presented in Table 4.6, it is difficult to say that the agreement between experiment and theory will be at the level of 2 kcal/mol for all cases studied in this work. However, because literature data were not available to indicate a reasonable level of error for ΔH_{rxn} values, and we have not performed a variety of ΔH_{rxn} calculations on reactions involving the alteration of carbon centers, interpretations of inclusions/exclusions of reaction pathways are limited to those which involve large differences between ΔH_{rxn} values for different reaction pathways.

Because molecular mechanics provides a fast, first approximation to the optimized structure, this technique was used before employing the UHF/PM3 method in the present study of aromatic mechanisms. To examine whether the individual structures investigated were at global rather than local minima, several starting geometries of each structure were subjected to geometry optimization calculations. The heats of formation (obtained at the PM3 level) of the different geometries were compared, and the lowest energy structure was chosen for subsequent single point *ab initio* calculations. In cases where the semi-empirically derived heats of formation were similar, several conformations were subjected to single point *ab initio* calculations to locate the lowest energy conformation. All structures were characterized as being genuine minima (i.e. having no imaginary frequencies) at the PM3 level. The
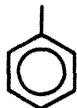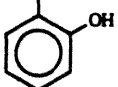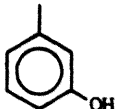
Table 4.5: A comparison of relative energies of different structural isomers based on experimental data and theoretical calculations.

Structure	Relative Energy - Experiment [a] (kcal/mol)	Relative Energy - Calculated [b] (kcal/mol)
	3.8 0	4.3 0
	4.9 0	3.3 0
	6.6 0	6.1 0
	2.6 0	3.3 0
	5 0	5.1 0

(a) Experimental data from NIST Standard Reference Database 25 [28].
(b) Relative energies determined using UHF/PM3 geometry optimization followed by Becke3LYP single point energy calculation.

Table 4.6: A comparison of experimentally and theoretically derived ΔH_{rxn} values for the Toluene + OH reaction.

Reactants	Products	ΔH_{rxn}, Theoretical (kcal/mol)	ΔH_{rxn}, Experimental (kcal/mol)
(toluene) + OH	(2-methylphenol, OH ortho) + H	+ 1.38	+ 0.8 ± 0.4
	(3-methylphenol, OH meta) + H	+ 1.25	- 0.8 ± 0.7
	(4-methylphenol, OH para) + H	+ 1.94	+ 0.9 ± 0.4

Becke3LYP energy was subsequently corrected to 298 K using the normal mode vibrational frequencies and thermal corrections obtained at the PM3 level. Thus, it is this corrected energy that is used to determine the lowest energy intermediate species in a particular step of the reaction mechanism.

Transition states were calculated with a constrained optimization procedure at the UHF/PM3 level using Gaussian 92. Conventional direct optimization schemes available through Gaussian 92 were attempted. However, because of the complexity of the structures studied, it was difficult to locate the structure with an initial geometry corresponding to a single negative eigenvalue of the second derivative matrix, a condition which is necessary before a conventional transition state optimization can proceed. The constrained optimization method relies on the assumption that the transition states are governed by the formation of a single bond in each step (for example, the C-O bond in the formation of the methylhydroxycyclohexadienyl radicals). Thus, the bond distance is adjusted by small increments (0.1 Å steps, in this case), and frozen while the geometry of the molecule is optimized. At the end of each optimization, the PM3-derived energy of the structure is noted. This procedure is repeated until a point of maximum energy is obtained. The constrained optimization procedure at the UHF/PM3 level was used to obtain an initial estimate of the transition state. Once this estimated transition state structure was found, DFT single point calculations were performed on this structure and small geometrical perturbations of the structure to ensure that the UHF/PM3 constrained optimization was successful in determining an estimate for the transition state geometry. This estimate of the true transition state is assumed to be an upper limit to the

first-order saddle point due to the elementary means of accounting for electron correlation. Because of the large number of structures considered in this study, transition states were located for representative cases and subsequently applied to homologous transition state complexes.

4.3 Results of Calculations

A generalized summary of the steps considered in the OH-aromatic mechanism appears in Figure 4.1. Each reaction is subsequently treated individually. Figures 4.2 - 4.6 show the reaction coordinate diagrams (Relative energy in kcal/mol versus reaction path) for the lowest energy structures found for each of the five aromatic-OH reactions. Energy and geometry data for the various structures studied in this work are available throughout this manuscript for comparison. Additional data are available from the authors upon request.

4.3.1 Initial Hydroxyl Radical Attack

There are several possible sites of attack for the OH radical in each of the aromatics considered. Some sites are less sterically hindered than others or are favored because of stabilizations as a result of group interactions. If we consider the transition states leading to the formation of the substituted hydroxycyclohexadienyl radicals, the aromatic-OH adducts formed in Reaction 1b, we find that the barrier heights are essentially negligible. Several different geometries were considered for each aromatic. Shown in Table 4.7 are
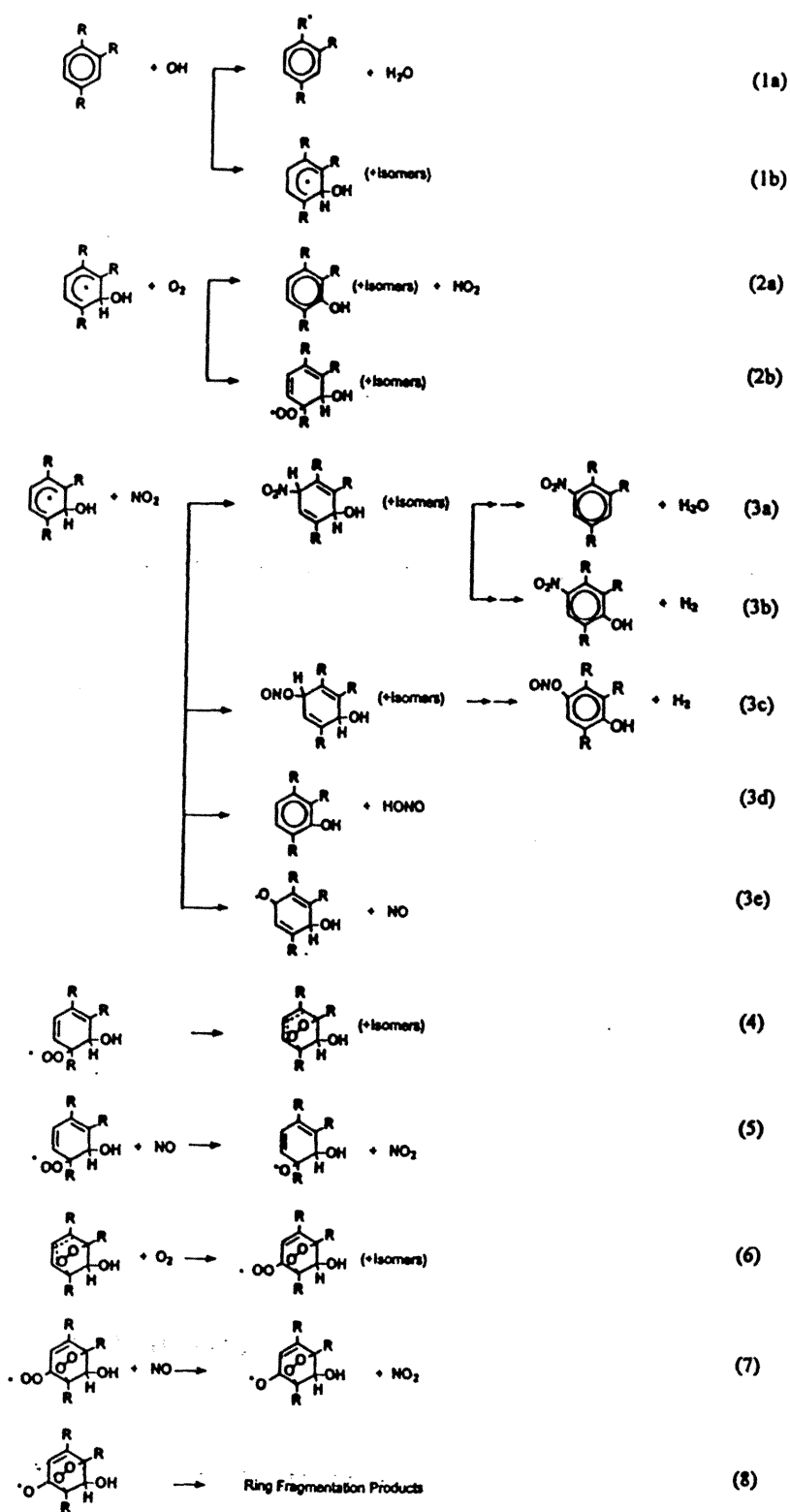
Figure 4.1: Possible reactions in a generalized mechanism of Aromatic-OH photooxidation. "R" represents either an H atom or a methyl/ethyl group, depending on the aromatic considered.
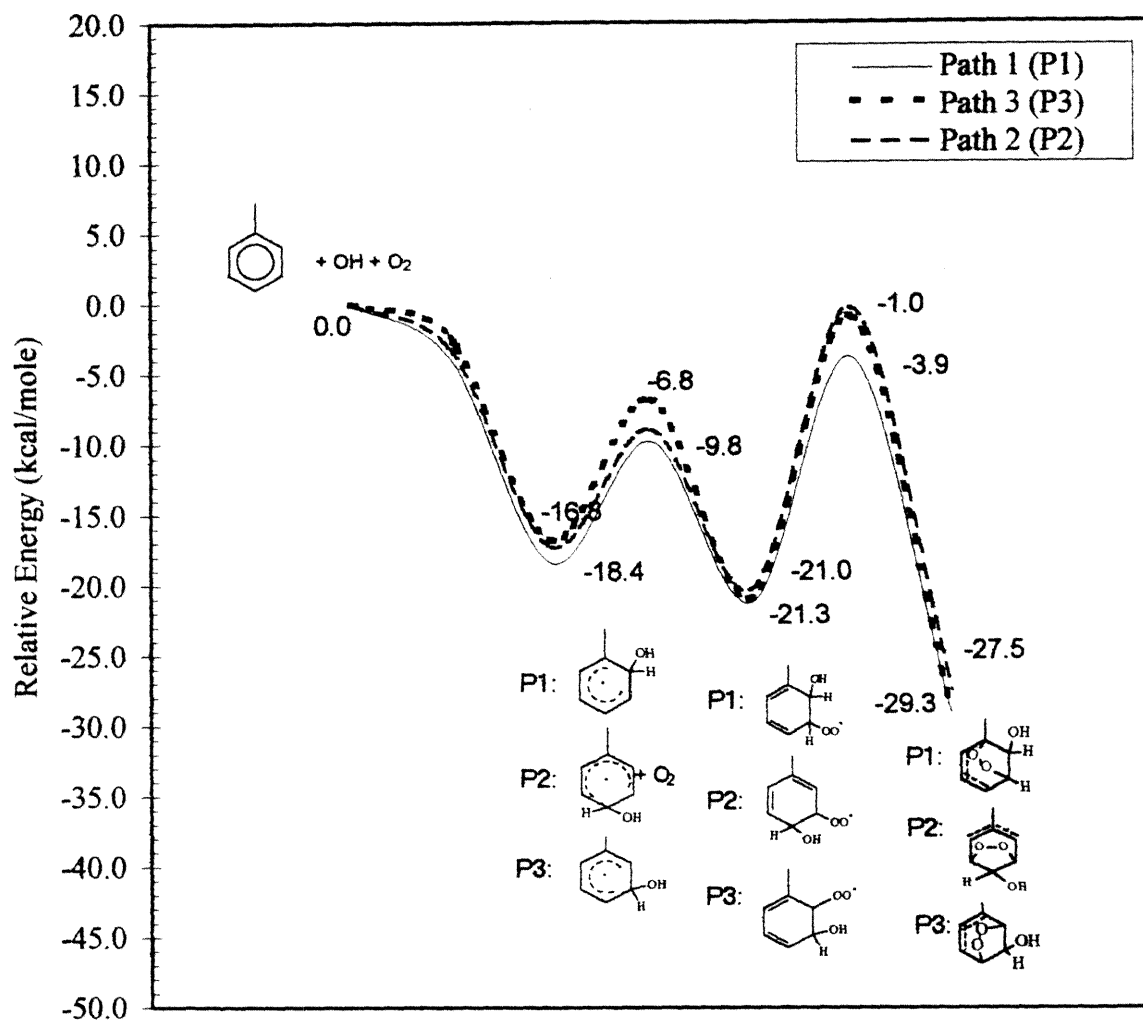
Figure 4.2: Reaction coordinate diagram for toluene. Indicated are the three favored pathways. Shown below the plots are the corresponding aromatic-OH adduct, peroxy radical, and bicyclic radical corresponding to the pathways. The structures are labeled P1, P2, P3 corresponding to paths 1, 2, and 3, respectively.
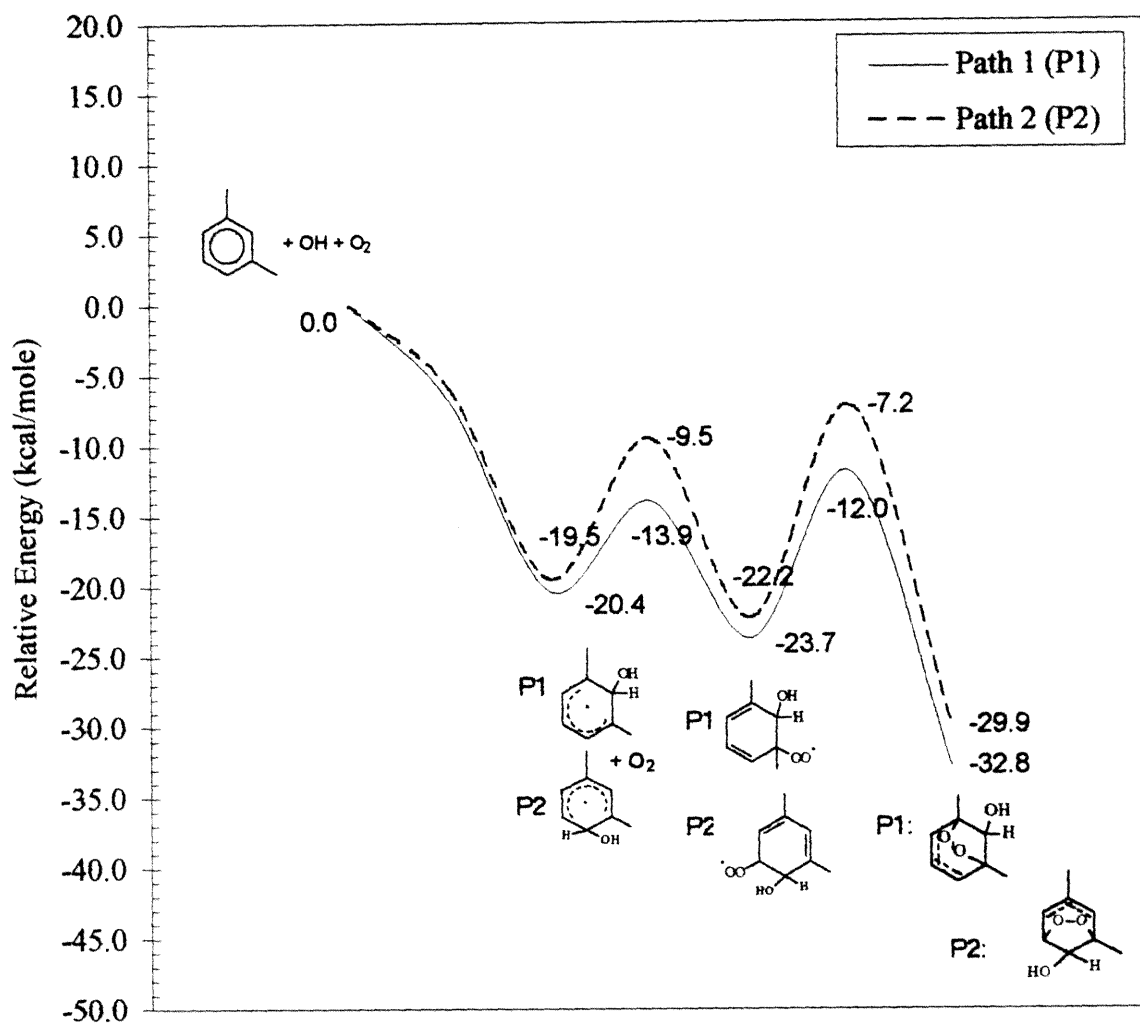
Figure 4.3: Reaction coordinate diagram for *m*- xylene. Indicated are the energies of the two favored pathways. Shown below the plots are the corresponding aromatic-OH adduct, peroxy radical, and bicyclic radical corresponding to the pathways. The structures are labeled P1 and P2 corresponding to paths 1 and 2, respectively.
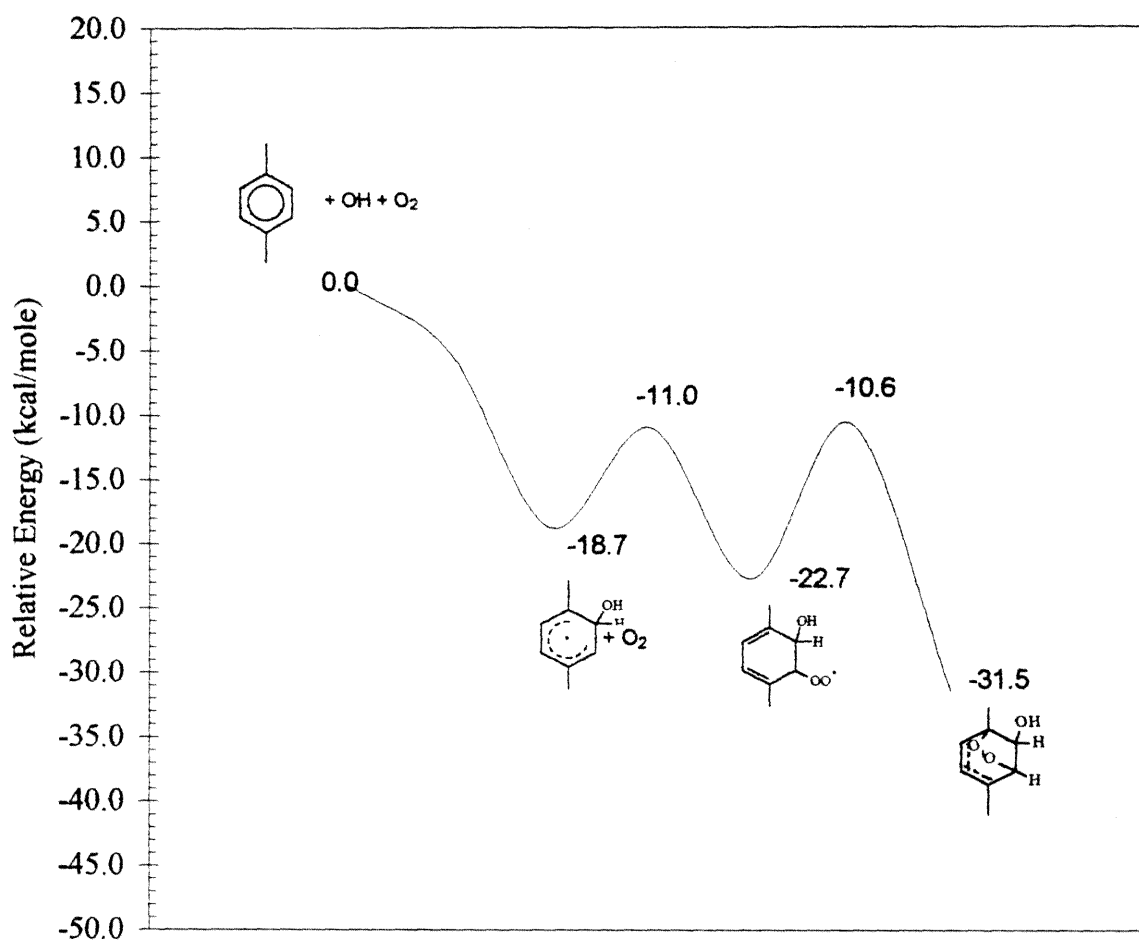
Figure 4.4: Reaction coordinate diagram for *p*- xylene. Shown below the path are the corresponding aromatic-OH adduct, peroxy radical, and bicyclic radical corresponding to the favored pathway.
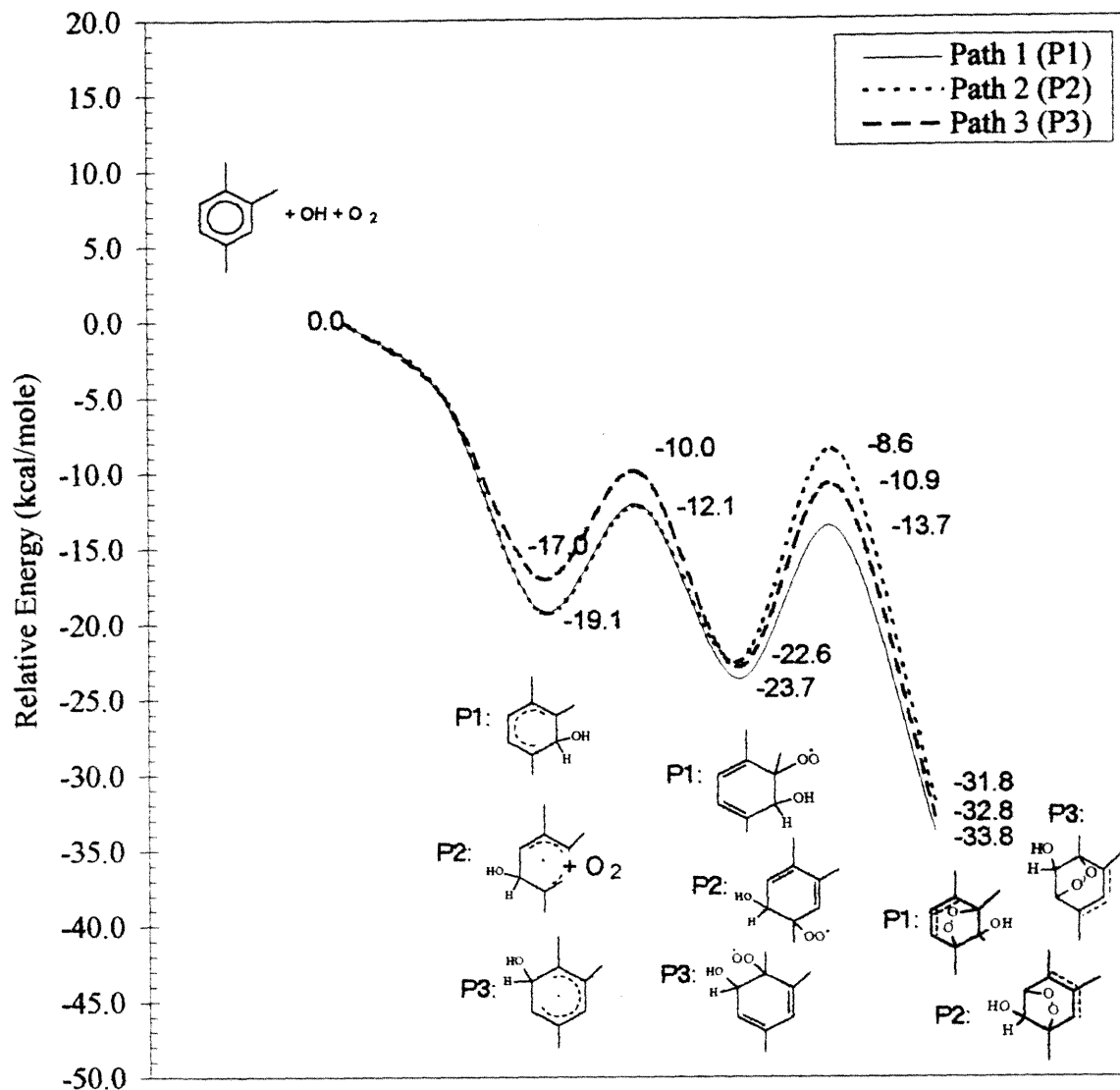
Figure 4.5: Reaction coordinate diagram for 1,2,4- trimethylbenzene. Indicated are the energies of the three favored pathways. Shown below the diagram are the corresponding aromatic-OH adduct, peroxy radical, and bicyclic radical corresponding to the pathways. The structures are labeled P1, P2, and P3 corresponding to paths 1, 2 and 3, respectively.
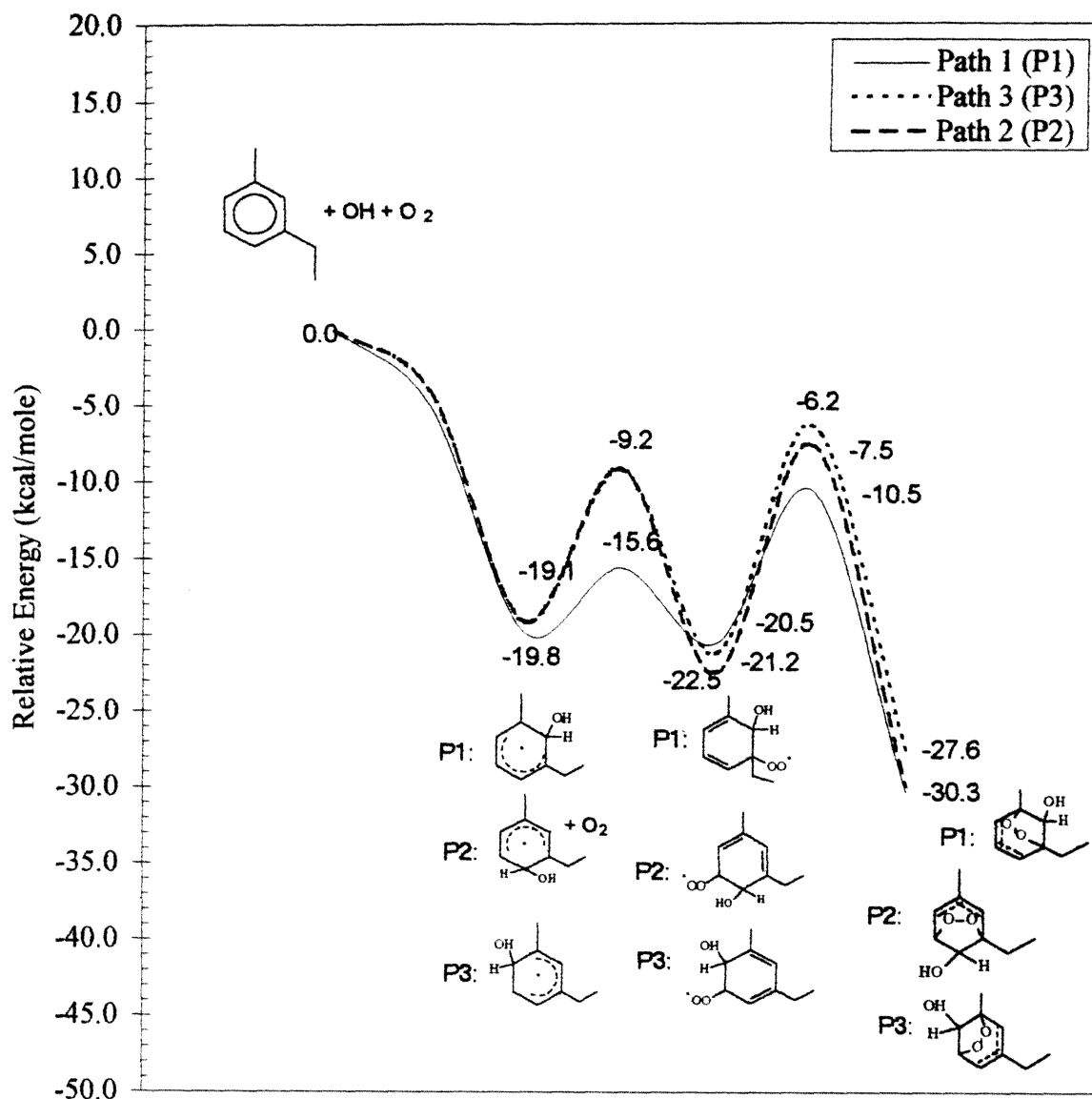
Figure 4.6: Reaction coordinate diagram for *m*-ethyltoluene. Indicated are the energies of the three favored pathways. Shown below the diagram are the corresponding aromatic-OH adduct, peroxy radical, and bicyclic radical corresponding to the pathways. The structures are labeled P1, P2, P3 corresponding to paths 1, 2, and 3, respectively.

the PM3-derived equilibrium structures for a representative sample of the most stable aromatic-OH adducts. Total energies for aromatic-OH adducts are tabulated in Table 4.8. Indicated are single point energies at 0 K derived using density functional theory, and energies corrected to 298 K using vibrational information generated at the PM3 level. In general, the preferred place of OH addition, based on total energies of the aromatic-OH adducts, is a position ortho to a substituent methyl group. In considering the total energies of the each of the aromatic- OH isomers, we did, however, find that there were some cases where isomers had energies within 2 kcal/mol of the lowest energy structures. So, whereas the structures with OH attachment at the ortho position are lowest in energy, pathways that include aromatic-OH structures whose relative energy falls within ±2 kcal/mol of the lowest energy isomer will also be considered. Throughout our discussion, we compare available experimental product data to results predicted by the theoretical calculations. This comparison serves two purposes: to lend credence to our uncertainty limit of 2 kcal/mol and to show that the theoretical predictions are adequate representations of atmospheric and/or experimental conditions.

Toluene

The lowest energy aromatic-OH structure for toluene is that resulting from addition to the ortho position. However, OH additions to the meta and para positions yield structures that are only 1.6 and 1.2 kcal/mol higher in energy than addition at the ortho site. Thus, based on theoretical considerations, additions to the meta and para positions cannot be excluded from reaction

Table 4.7: PM3 equilibrium structures for a representative selection of the most stable aromatic-OH adducts formed from OH addition to the aromatic ring (Reaction 1b). Bond distances are in Å, and angles are in degrees.

Parameter	toluene	m-xylene	p-xylene	m-ethyl-toluene
$r(C_1,C_2)$	1.505	1.507	1.505	1.507
$r(C_2,O_1)$	1.414	1.416	1.415	1.416
$r(C_2,C_3)$	1.498	1.507	1.497	1.507
$r(C_3,C_4)$	1.370	1.379	1.377	1.379
$r(C_4,C_5)$	1.411	1.407	1.416	1.408
$r(C_5,C_6)$	1.406	1.407	1.405	1.407
$r(C_6,C_1)$	1.381	1.379	1.381	1.379
$r(C_1,C_7)$	1.479	1.479	1.478	1.479
$r(C_3,C_8)$	-	1.479	-	1.490
$r(C_4,C_9)$	-	-	1.486	-
$\angle(C_1,C_2,C_3,O_1)$	128	127	127	128

Parameter	1,2,4-tmb
$r(C_1,C_2)$	1.388
$r(C_3,O_1)$	1.417
$r(C_2,C_3)$	1.507
$r(C_3,C_4)$	1.506
$r(C_4,C_5)$	1.378
$r(C_5,C_6)$	1.406
$r(C_6,C_1)$	1.413
$r(C_1,C_7)$	1.486
$r(C_2,C_8)$	1.480
$r(C_4,C_9)$	1.479
$\angle(C_2,C_3,C_4,O_1)$	127
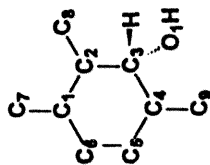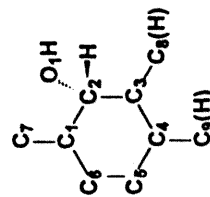
Table 4.8: Calculated energies (in a.u.) of the most stable reaction intermediates for the pathway leading to the formation of the bicyclic peroxy radicals. (a) Addition sites in parenthesis indicate comparable low energy structures.

	Aromatic		OH Addition (Rxn. 1b)			O$_2$ Addition (Rxn. 2b)			O$_2$ Bridge Formation (Rxn. 4)		
Molecule	$E_e°$	E^{298}	Site	$E_e°$	E^{298}	Site^a	$E_e°$	E^{298}	Sites	$E_e°$	E^{296}
toluene	-271.5774	-271.4454	3	-347.3348	-347.1876	2 (4,6)	-497.6616	-497.5035	2,4	-497.6750	-497.5168
			4	-347.3355	-347.1883	3 (1)	-497.6606	-497.5025	3,5	-497.6721	-497.5139
			2	-347.3374	-347.1902	3 (1,5)	-497.6621	-497.5040	3,1	-497.6751	-497.5169
m-xylene	-310.8971	-310.7363	4	-386.6589	-386.4826	5 (3,1)	-536.9828	-536.7963	5,3	-536.9962	-536.8086
			2	-386.6603	-386.4840	3	-536.9851	-536.7986	3,1	-537.0008	-536.8132
p-xylene	-310.8969	-310.7359	2	-386.6253	-386.4492	3 (1,5)	-536.9848	-536.7968	3,1	-536.9988	-536.8108
1,2,4-	-350.2154	-350.0250	6	-425.9739	-425.7671	1	-576.3036	-576.0861	1,5	-576.3194	-576.1019
trimethyl-			3	-425.9773	-425.7705	2	-576.3049	-576.0874	2,4	-576.3210	-576.1035
benzene			5	-425.9774	-425.7706	4 (2)	-576.3031	-576.0856	4,6	-576.3177	-576.1002
m-ethyl-	-350.2116	-350.0216	4	-425.9740	-425.7675	5 (3,1)	-576.2976	-576.0801	5,3	-576.3077	-576.0902
toluene			6	-425.9742	-425.7677	5 (1,3)	-576.2996	-576.0821	5,1	-576.3114	-576.0939
			2	-425.9751	-425.7686	3 (1,5)	-576.2967	-576.0792	3,1	-576.3121	-576.0946

mechanism considerations. Following formation of the adduct, molecular oxygen can abstract a hydrogen atom to form a cresol. There is experimental evidence for o-, m-, and p-cresol, with the o-cresol yield dominating cresol formation (Table 4.1), consistent with the theoretical predictions.

m-*Xylene*

The lowest energy aromatic-OH structure for m-xylene also corresponds to OH addition to the 2- position. Additions to the 4- and 5- positions are 0.88 and 3.5 kcal/mol higher in energy than addition to the 2- position. Additions to the 6- and 4- positions create identical structures. Based on these results, the lowest energy adducts for m-xylene correspond to OH addition to the 2- and 4- positions, both of which are ortho to one of the substituent methyl groups. The reaction coordinate diagram for m-xylene, Figure 4.3, depicts the lowest energy adducts formed. Comparing the theoretical predictions to experimentally determined products in Table 4.2, we note experimental evidence for 2,6- and 2,4- dimethylphenol (with the 2,6- dimethylphenol yield dominating), consistent with OH addition to the 2- and 4- positions. There is no experimental evidence for 3,5- dimethylphenol, consistent with our finding that OH addition to the 5- position can be excluded.

p-*Xylene*

Because of the high degree of symmetry of p-xylene, only one structure was considered. The experimental evidence for O_2 reaction with the p-xylene-OH adduct leading to the formation of only 2,5-dimethylphenol (see Table

4.3), indicates that there is only one possible pathway for OH addition to the ring. The reaction coordinate diagram for *p*-xylene (Figure 4.4) and Table 4.7 show the structure for the OH-aromatic adduct.

1,2,4-Trimethylbenzene

The lowest energy aromatic-OH adducts for trimethylbenzene correspond to OH additions at the 3- and 5- positions. The energies of these two adducts are identical. Addition to the 6- position is 2.1 kcal/mol higher in energy than the other two adducts. The reaction coordinate diagram for 1,2,4-trimethylbenzene, Figure 4.5, details the path of the favored OH-aromatic adduct structures. Given that there are no experimental data available on the ring-retaining products of 1,2,4- trimethylbenzene, the given energy calculations can be used to predict the phenolic compounds formed. Thus, we predict the formation of 2,3,6- trimethylphenol, 2,3,5-trimethylphenol and 2,4,5- trimethylphenol from the O_2 reaction with the adducts formed from OH addition to the 3-, 6- and 5- positions, respectively (according to Reaction 2a).

m-Ethyltoluene

The lowest energy aromatic-OH adduct for *m*-ethyltoluene corresponds to OH addition to the 2- position. The energies for the adducts formed from addition to the 4-,5-, and 6- positions are 0.69, 3.0, and 0.56 kcal/mol higher than that for addition to the 2- position. From these values, we conclude that the aromatic-OH adducts to be included in the reaction mechanism for *m*-

ethyltoluene include addition of OH to the 2-,4-, and 6- positions. Note that these results are very similar to those of *m*-xylene; addition of OH to the 5-position is the least favored radical. Substituent methyl groups have a considerable effect on the favored addition sites for OH. Figure 4.6 details the paths of the three lowest energy aromatic-OH structures. As with the case of 1,2,4-trimethylbenzene, there are no experimental data available for ring-retaining products formed from the *m*-ethyltoluene-OH reaction. Based on our energy determinations, we predict the formation of 2-ethyl-6-methylphenol, 2-ethyl-4-methylphenol, and 4-ethyl-6- methylphenol from the O_2 reaction with the adducts formed from OH addition to the 2-, 4-, and 6- positions, respectively.

4.3.2   Fate of the OH-Aromatic Adduct: NO_2 Reaction

It has been suggested that aromatic-OH adducts react with NO_2 to yield nitroaromatics according to Reaction 3a of the generalized mechanism.[29] To explain the observed variation of aromatic photooxidation product yields with varying NO_2 concentration, alternative paths for aromatic-OH adduct reaction with NO_2 that results in the formation of oxy type radicals (Reaction 3e)[27], or the formation of a phenolic type compound and HONO (Reaction 3d) [27] have been proposed. Two additional pathways can be suggested for Reaction 3, pathway 3c forming the hydroxyaromatic nitrite, and 3b forming the hydroxy nitroaromatic (nitrophenol, nitro-dimethylphenol, etc.) .

Experimental evidence has been found for the presence of nitroaromatic compounds in the photooxidation of toluene, *m*- xylene, and *p*-xylene (see
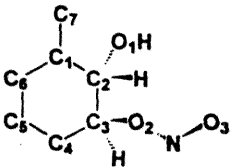
Tables 4.1- 4.3). While calculations were not performed on all of the nitroaromatic compounds, it will be shown in the discussion that follows that ΔH_{rxn} for Reaction 3a is -26.3 for the case of toluene. Thus, the reaction of NO_2 with the OH-aromatic adduct is assumed to be exothermic for all aromatics in this study. The nitroaromatics that are predicted to form involve NO_2 reaction with the most stable OH-aromatic adducts, using the conventional wisdom that NO_2 addition to an alkyl hydroxycyclohexadienyl radical will be at a site ortho to the hydroxyl substituent group[29]. Consistent with the theoretical prediction that all three possible toluene-OH adducts form, experimental evidence exists for three different nitrotoluene products. Similarly, consistent with the prediction that only two of the possible m-xylene-OH adducts form, experimental evidence exists for only two nitro-m-xylene products. Hydroxyl radical addition to the 2-position of m-xylene, with subsequent reaction with NO_2, yields 4-nitro-m-xylene, whereas addition to the 4-position yields 5-nitro-m-xylene. Observations of the nitroaromatics from the p-xylene photooxidation systems are also consistent with theory. Only one nitroaromatic, 2-nitro-p- xylene, is detected in laboratory studies. Since experimental data are not available for the nitroaromatics resulting from the 1,2,4- trimethylbenzene and m-ethyltoluene systems, the results of the previous section, indicating the favored aromatic-OH adducts, can predict the nitroaromatic species expected to form in photooxidation studies of 1,2,4-trimethylbenzene and m-ethyltoluene. From OH addition to the 3-position and 5- positions, 4-nitro-1,2,4- trimethylbenzene and 6-nitro-1,2,4- trimethylbenzene are predicted to form, and 5-nitro-1,2,4- trimethylbenzene should not form. For m-ethyltoluene, the formation of 4-nitro-m-ethyltoluene from OH
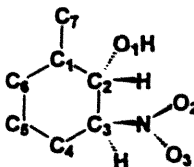
addition to the 2-position, 5-nitro-m-ethyltoluene from OH addition to the 4-position, and 2-nitro-m-ethyltoluene from addition to the 6-position are predicted.
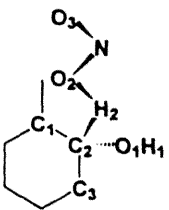
To examine the stabilities of the five competing pathways for aromatic-OH adduct reaction with NO_2, theoretical calculations were performed for the case of toluene. Energies were calculated for nitrotoluene (Reaction 3a), nitrophenol (Reaction 3b), phenol nitrite (Reaction 3c), phenol (Reaction 3d), and oxy radicals (Reaction 3e). Only one structural isomer for each reaction (3a-3d) was considered. Transition states were determined for the first steps of Reactions 3a-3c, and for Reactions 3d and 3e. Geometrical information for these reaction intermediates as well as the transition states appear in Table 4.9. The second steps of reactions 3a-3c were not subjected to transition state analyses since these reactions involve processes (rearrangement and the subsequent loss of water or molecular hydrogen) which are difficult to analyze using the constrained optimization procedure, and are subject to interpretation. Clearly, much additional work is required to completely elucidate the transition states of the second steps of Reactions 3a-3c. Even though transition states are not included for the second steps of Reactions 3a-3c, valuable information can be gained regarding the relative stability of intermediates as well as the overall heats of reactions for the reactions considered.

The compounds, NO, NO_2, H_2O and HONO were subjected to the same type of calculations as each of the intermediate species. A PM3 geometry optimization was conducted followed by a Becke3LYP single point calculation. The single point energy was subsequently corrected to 298 K using

Table 4.9: PM3 derived geometries for (a) equilibrium and (b) approximate transition state structures for the reactions of aromatic-OH adducts with NO_2. All bond distances are in Å, and angles are in degrees.

Parameter	Opt. Value[a]	TS Value[b]
$r(C_1,C_2)$	1.512	
$r(C_2,O_1)$	1.408	
$r(C_2,C_3)$	1.560	
$r(C_3,O_2)$	1.436	2.2
$r(C_3,C_4)$	1.500	
$r(O_2,N)$	1.411	
$r(N,O_3)$	1.164	
$\angle(C_3,O_2,N)$	113	
$\angle(O_2,N,O_3)$	108	
$\angle(C_1,C_2,C_3,O_1)$	127	
$\angle(C_2,C_3,C_4,O_2)$	119	100

Parameter	Opt. Value	TS Value
$r(C_1,C_2)$	1.509	
$r(C_2,O_1)$	1.407	
$r(C_2,C_3)$	1.556	
$r(C_3,N)$	1.549	2.6
$r(C_3,C_4)$	1.492	
$r(N,O_2)$	1.211	
$r(N,O_3)$	1.213	
$\angle(C_3,N,O_2)$	120	
$\angle(O_2,N,O_3)$	123	
$\angle(C_1,C_2,C_3,O_1)$	127	
$\angle(C_2,C_3,C_4,N)$	124	101

Parameter	TS Value
$r(C2,H2)$	1.0
$r(H2,O2)$	1.7
$\angle(C_1,C_2,C_3,H_2)$	37
$\angle(H_2,O_2,N)$	104
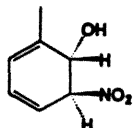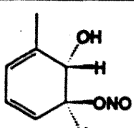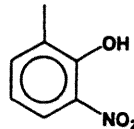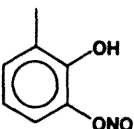
the normal mode vibrational frequencies and thermal corrections obtained at the PM3 level. Table 4.10 shows the uncorrected energy at O K (from the Becke3LYP single point calculation) and the corrected energy at 298 K for NO, NO_2, H_2O HONO, and each of the other species participating in a reaction with an aromatic intermediate. Table 4.11 contains the energies (O K and 298 K) of all of the products formed in the aromatic-OH adduct reaction with NO_2.

For the case of toluene as an example, the ΔH_{rxn} for the first steps of pathways 3a-3c, and overall pathways 3d and 3e are -26.3, -26.3, -24.5, -52.8, and +38.3 kcal/mol, respectively. The barrier heights for pathways 3a,b (first step), 3c (first step), 3d are 5, 1, 2 kcal/mol, respectively. Note that Reactions 3c and 3e are assumed to have the same transition state. Based on this information for the initial steps of Reactions 3a-3c, and the overall Reactions 3d and 3e, the only pathway that can be unambiguously excluded is Reaction 3e, because of its endothermic nature. In the absence of additional transition state data regarding the second steps of Reactions 3a-3c, it impossible to recommend the exclusion of one of these pathways. Therefore, until additional data can be obtained for Reactions 3a-3c, we recommend the inclusion of Reactions 3a-3d in overall mechanisms for aromatic-OH photooxidation. As mentioned previously, it is clear that additional computational work is required to fully elucidate the pathways of aromatic-OH reaction with NO_2.

Table 4.10: Calculated energy (in a.u.) of molecules involved in reactions with aromatic intermediates. Structures optimized using PM3 and energies determined using Becke3LYP/6-31g(d,p). (a) Electronic energy at 0 K. (b) Corrected energy at 298 K, which includes zero point energies and thermal corrections determined using PM3 normal mode vibrations.

Molecule	E_e^o [a]	E^{298} [b]
OH	-75.7268	-75.7153
O_2	-150.3165	-150.3093
H_2O	-76.4190	-76.3943
HONO	-205.6981	-205.6736
NO_2	-205.0700	-205.0573
NO	-129.8879	-129.8803

Table 4.11: Calculated energies (in a.u.) of the products formed by the reaction of NO_2 with the toluene-OH adduct.

Molecule	E_e°	E^{298}
3-nitrotoluene	-476.0749	-475.9356
2-cresol	-346.7967	-346.6581
	-552.4537	-552.2865
	-552.4548	-552.2894
	-551.2802	-551.1439
	-551.2802	-551.1342

Aromatic Peroxy Radical

Under atmospheric conditions, oxygen is expected to rapidly add to the aromatic-OH adduct, forming a peroxy radical (Reaction 2b in the generalized mechanism)[26]. Semi-empirical geometry optimizations and *ab initio* calculations were performed on all of the resulting peroxy radicals for each of the five aromatics considered. Transition state analyses indicate that the transition state energies are governed by consideration of the type of carbon atom being bonded to (secondary versus tertiary) and the steric nature of the site of attachment. The energies of the approximated transition states for the reactions of aromatic-OH adducts with O_2 are available in Table 4.12. From this table, it can be seen that addition of O_2 to a site adjacent to the OH group (such as O_2 addition to the 3-position with OH at the 2-position for *p*-xylene) results in a transition state energy that is roughly 10 kcal/mol higher than the parent aromatic-OH adduct + O_2 energy. Additions of O_2 to a tertiary carbon give a transition state energy that is roughly 7 kcal/mol higher than the parent aromatic-OH + O_2 energy. Additions to a secondary carbon site not adjacent to the OH radical addition site give a transition state energy that is roughly 5 kcal/mol higher than the parent aromatic-OH + O_2 energy. These barrier heights are consistent with the low rate constants observed by Knispel *et al.*[26]. Table 4.13 contains the geometrical information for the structures of a representative set of the peroxy radicals. Energies for the most stable peroxy radical structures appear in Table 4.8. Examination of the relative energies of each of the peroxy radicals for a given aromatic reveals that the energies of the intermediate peroxy radicals are all similar.

Given this fact, all structural isomers of the aromatic peroxy radicals are equally likely to form.

4.3.3 Fate of the Peroxy Radical: Cyclization vs NO Reaction

Alkyl peroxy radicals present in polluted atmospheres generally react with NO to form alkoxy radicals[2, 28]. Aromatic peroxy radicals, in contrast, were postulated to cyclize forming bicyclic radicals in order to rationalize the observed formation of α-dicarbonyls from the aromatic hydrocarbon reactions [29]. To test this hypothesis, we examined the ΔH_{rxn} for reactions 4 and 5 in the generalized mechanism for aromatic-OH reaction.

Calculations were performed for Reaction 4 on all possible bicyclic radicals, regardless of whether or not they originated from the lowest energy aromatic-OH adduct, with the exception of those radicals containing a four-membered oxygen ring. The ring strain energies associated with the formation of such radicals were assumed to be much higher than those of the corresponding five- and six- membered rings. Structural information for selected bicyclic peroxy radicals resulting from the aromatic-OH reaction appear in Table 4.14. Energies of the most stable bicyclic peroxy radical intermediates appear in Table 4.8, under the heading of "O_2 Bridge formation". In all of the cases studied, the allylically stabilized five-membered bicyclic radicals are the lowest energy bicylic radicals formed. In fact, all other non-allylically stabilized bicyclic radicals are about 20 kcal higher in energy than the lowest energy allylically stabilized bicyclic radical, and are approximately

Table 4.12: Approximate transition state energies for the reactions of aromatic-OH adducts with O_2, represented in terms of the local structure of the aromatic-OH adduct, (a)at the addition site (Add'n Site), where all tertiary carbons (C_t) are bound to methyl (Me) groups unless otherwise indicated, and (b) in the two positions ortho to the addition site. (c) Transition state bond distance for the C-O bond which is formed during the addition of O_2 to the aromatic-OH adduct.

Aromatic	Add'n Site [a]	Ortho Groups [b]	$E_e°$(TS) (a.u.)	E^{298}(TS) (a.u.)	r(C-O) [c] (Å)	E^{298}(Reactants) (a.u.)	Barrier Ht. (kcal/mol)
p-xylene	C_s	Me,OH	-536.9635	-536.7780	1.90	-536.7904	7.8
	C_t	H,OH	-536.9673	-536.7818	1.85	-536.7904	5.4
	C_s	H,Me	-536.9669	-536.7814	1.85	-536.7904	5.6
toluene	C_s	H,OH	-497.6406	-497.4857	1.90	-497.4995	8.7
	C_t	H,OH	-497.6454	-497.4905	1.85	-497.4995	5.6
	C_s	H,H	-497.6491	-497.4942	1.80	-497.4995	3.3
m-xylene	C_t	H,OH	-536.9686	-536.7833	1.90	-536.8023	11.9
m-ethyl-	C_t(Et)	H,OH	-576.2861	-576.0711	1.80	-576.0779	4.3
toluene	C_t	H,OH	-576.2803	-576.0631	1.85	-576.0779	9.3
	C_s	H,H	-576.2892	-576.0742	1.80	-576.0779	2.3

Table 4.13: PM3 equilibrium structures for a representative selection of the most stable reaction products of aromatic-OH adducts with O_2 (Reaction 2b). All bond distances are in Å, angles are in degrees.

Parameter	toluene	m-xylene	p-xylene	m-ethyl-toluene
r(C$_1$,C$_2$)	1.510	1.514	1.510	1.513
r(C$_2$,O$_1$)	1.411	1.409	1.410	1.420
r(C$_2$,C$_3$)	1.555	1.563	1.556	1.562
r(C$_3$,O$_2$)	1.478	1.494	1.478	1.496
r(O$_2$,O$_3$)	1.253	1.253	1.255	1.252
r(C$_3$,C$_4$)	1.494	1.504	1.501	1.503
r(C$_4$,C$_5$)	1.345	1.343	1.356	1.345
r(C$_5$,C$_6$)	1.443	1.448	1.440	1.445
r(C$_6$,C$_1$)	1.351	1.349	1.354	1.350
r(C$_1$,C$_7$)	1.482	1.481	1.481	1.482
r(C$_3$,C$_8$)	-	1.525	-	1.543
r(C$_4$,C$_9$)	-	-	1.482	-
∠(C$_3$,O$_2$,O$_3$)	114	116	114	117
∠(C$_1$,C$_2$,C$_3$,O$_1$)	125	124	125	121
∠(C$_2$,C$_3$,C$_4$,O$_2$)	118	117	117	122

Parameter	1,2,4-tmb
r(C$_1$,C$_2$)	1.512
r(C$_3$,O$_1$)	1.409
r(C$_2$,C$_3$)	1.566
r(C$_2$,O$_2$)	1.497
r(O$_2$,O$_3$)	1.252
r(C$_3$,C$_4$)	1.512
r(C$_4$,C$_6$)	1.354
r(C$_5$,C$_6$)	1.440
r(C$_6$,C$_1$)	1.358
r(C$_1$,C$_7$)	1.483
r(C$_2$,C$_8$)	1.526
r(C$_4$,C$_9$)	1.480
∠(C$_2$,O$_2$,O$_3$)	116
∠(C$_2$,C$_3$,C$_4$,O$_1$)	125
∠(C$_1$,C$_2$,C$_3$,O$_2$)	118

10 kcal/mol higher in energy than the corresponding peroxy radicals from which they are formed. Thus, the reactions forming the allylically stabilized bicyclics are the only exothermic reactions determined in this step of the mechanisms. The barrier heights for bicyclic ring closure seem to be governed by the attachment sites of the O_2 bridge. Representative transition state energies for the bicyclic radical intermediates appear in Table 4.15. A transition state that results in the attachment of an O_2 bridge to two tertiary carbons results in a lower energy transition state than that which results in the attachment to one tertiary and one secondary carbon. The energy of the transition state which results in a O_2 bridge between two tertiary carbons is approximately 10 kcal/mol higher than that of the parent peroxy radical. A transition state that results in O_2 attachment to a secondary carbon, with O_2 originating from a tertiary site, results in a transition state energy that is approximately 12 kcal/mol higher than the parent peroxy radical. A transition state that results in O_2 attachment to a tertiary carbon, with O_2 originating from a secondary carbon site, results in a transition state energy that is approximately 17 kcal higher than the parent peroxy radical.

Energy data for a representative selection of aromatic oxy radicals formed in the reaction of NO with the aromatic peroxy radicals appear in Table 4.16. Representative aromatic peroxy radicals, bicyclic radicals , and aromatic oxy radicals, along with the ΔH_{rxn} values for Reactions 4 and 5 are presented in Figure 4.7. Not all of the lowest energy aromatic peroxy radicals (which appear in the reaction coordinate diagrams) appear in Figure 4.7. The peroxy radicals chosen for Figure 4.7 are representative cases chosen to give the reader an indication that the two pathways for peroxy radical reaction

Table 4.14: PM3 equilibrium structures for a representative selection of the most stable reaction products in the formation of bicyclic peroxy radicals from peroxy radical intermediates (Reaction 2b). Bond distances are in units of Å, and angles are in degrees.

Parameter	toluene	m-xylene	p-xylene	m-ethyl-toluene
r(C₁,C₂)	1.577	1.572	1.577	1.570
r(C₂,O₁)	1.388	1.389	1.388	1.389
r(C₂,C₃)	1.565	1.572	1.565	1.572
r(C₃,O₂)	1.403	1.424	1.402	1.423
r(O₂,O₃)	1.595	1.580	1.595	1.580
r(C₁,O₃)	1.422	1.424	1.422	1.423
r(C₃,C₄)	1.505	1.510	1.511	1.511
r(C₄,C₅)	1.393	1.393	1.402	1.393
r(C₅,C₆)	1.393	1.393	1.389	1.393
r(C₆,C₁)	1.511	1.510	1.510	1.511
r(C₁,C₇)	1.519	1.519	1.519	1.519
r(C₃,C₈)	-	1.519	-	1.532
r(C₄,C₉)	-	-	1.471	-
∠(C₁,C₂,C₃,O₁)	125	125	114	114
∠(C₂,C₃,C₄,O₂)	114	112	114	112
∠(C₆,C₁,C₂,O₃)	116	115	115	116

Parameter	1,2,4-tmb
r(C₁,C₂)	1.518
r(C₃,O₁)	1.389
r(C₂,C₃)	1.574
r(C₂,O₂)	1.424
r(O₂,O₃)	1.580
r(C₄,O₃)	1.423
r(C₃,C₄)	1.570
r(C₄,C₅)	1.509
r(C₅,C₆)	1.387
r(C₆,C₁)	1.404
r(C₁,C₇)	1.473
r(C₂,C₈)	1.521
r(C₄,C₉)	1.520
∠(C₂,C₃,C₄,O₁)	114
∠(C₁,C₂,C₃,O₂)	115
∠(C₃,C₄,C₅,O₃)	112
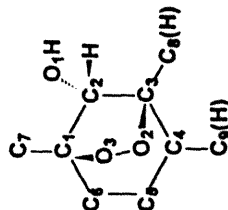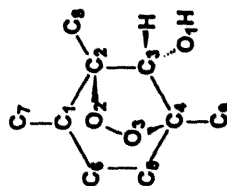
Table 4.15: Approximate transition states for the addition reactions of bicyclic peroxy radicals with O_2, represented in terms of the local structure of the bicyclic peroxy radical (a) at the addition site, and (b) in the two positions ortho to the addition site. "Me" represents a methyl group bond to a tertiary carbon, whereas "CO" represents an attachment site for the O_2 bridge. (c) Transition state bond distance for C-O bond which is formed in the addition of O_2.

Aromatic	Add'n Site [a]	Ortho Groups [b]	$E_e°$(TS) (a.u.)	E^{298}(TS) (a.u.)	r(C-O) [c] (Å)	E^{298}(reactants) (a.u.)	Barrier Ht. (kcal/mol)
toluene	C_s	Me, H	-647.9641	-647.7973	1.9	-647.8262	18.2
	C_s	CO, H	-647.9643	-647.7975	1.9	-647.8262	18.0
p-xylene	C_t	CO, H	-687.3104	-687.1114	1.9	-687.1201	5.5

are both possible, and that Reaction 5 cannot be unambiguously excluded from a generalized reaction mechanism. Inclusion of Reaction 5 results in the formation of oxy radicals. These radicals can go on to react according the scheme in Figure 4.8 to yield ring-retained hydroxy carbonyl compounds or decompose by C-C bond scission to ultimately form a di-unsaturated dicarbonyl. These carbonyl compounds can serve to account for part of the carbon unaccounted for in laboratory studies of aromatic-OH systems.

4.3.4 Bicyclic Peroxy Radicals

After bicyclic radical formation, oxygen quickly adds to the radical, forming a bicyclic peroxy radical. Transition state energies for a representative selection of bicyclic peroxy radicals appear in Table 4.17. Energy calculations were performed on each of the resulting possible bicyclic peroxy radicals. Note that O_2 addition to rings that result in bicyclic peroxy structures with two radical sites are unlikely to form, and were thus not subjected to single point calculations. The energies determined for the bicyclic peroxy radicals are all similar in magnitude; thus, all bicyclic peroxy structures resulting from the lowest energy bicyclic radicals must be considered in an overall mechanism. Given the steric hindrance problems associated with another cyclization, the bicyclic peroxy radical reacts with NO to form a bicyclic oxy radical and NO_2.

Toluene:
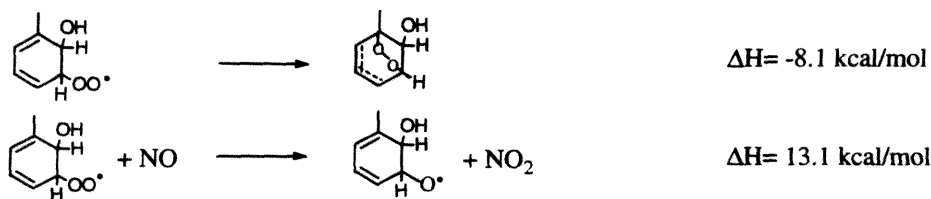
$\Delta H= -8.1$ kcal/mol

$\Delta H= 13.1$ kcal/mol

m-Xylene:

$\Delta H= -9.1$ kcal/mol

$\Delta H= -12.4$ kcal/mol

p-Xylene:

$\Delta H= -8.8$ kcal/mol

$\Delta H= 4.2$ kcal/mol

1,2,4 Trimethylbenzene:

$\Delta H= -9.2$ kcal/mol

$\Delta H= -13.5$ kcal/mol

m-Ethyltoluene:

$\Delta H= -6.4$ kcal/mol

$\Delta H= -1.0$ kcal/mol
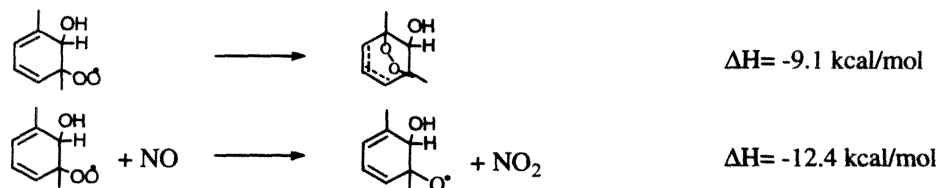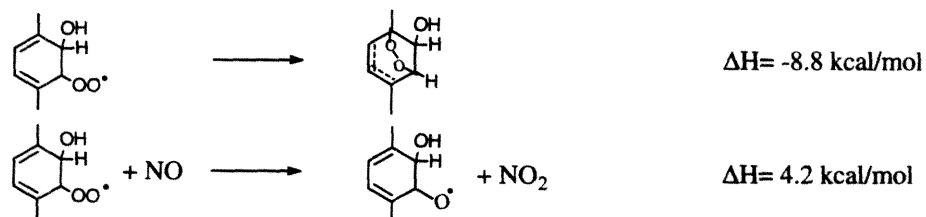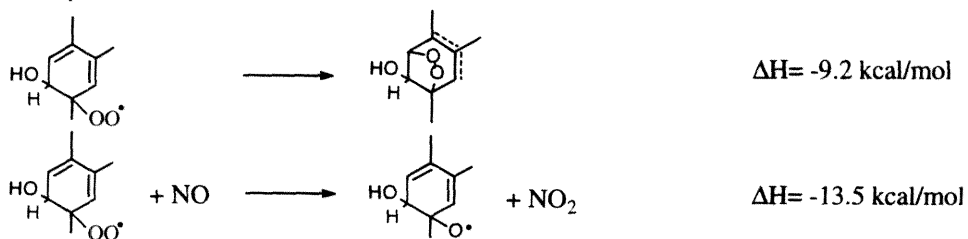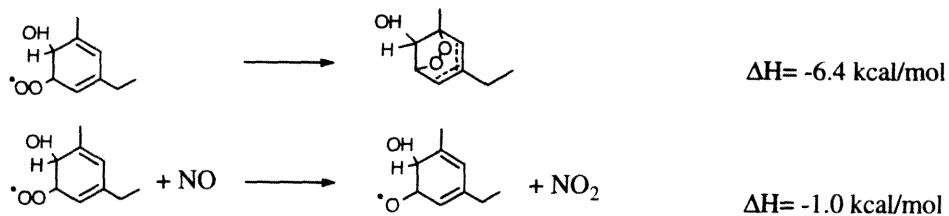
Figure 4.7: ΔH_{rxn} values for Reactions 4 and 5 for different aromatic systems.
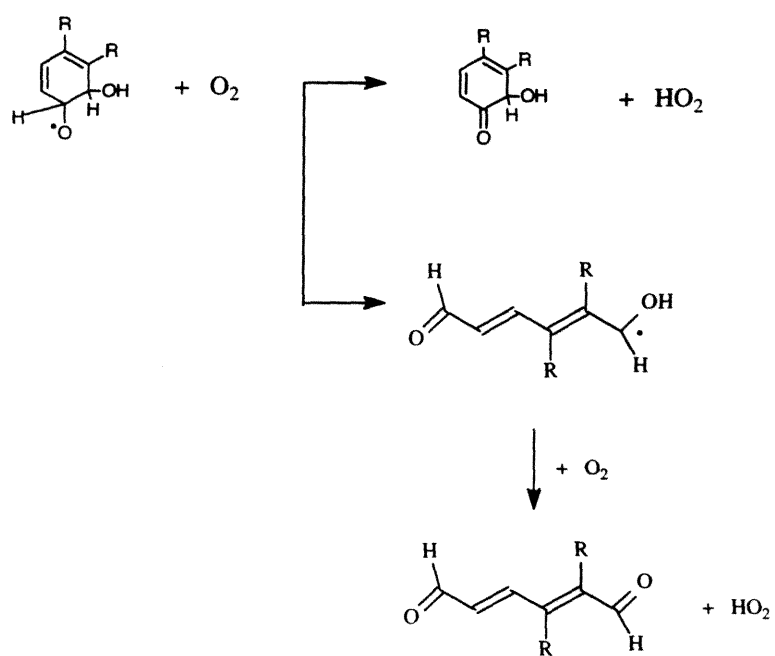
Figure 4.8: Subsequent reaction of oxy radicals formed from Reaction 5 of the generalized mechanism.

Table 4.16: Calculated energies (in a.u.) for the products of the reaction of NO with a representative selection of the most stable peroxy intermediates and for the products of the reaction of O_2 with a representative selection of the most stable bicyclic intermediates.

Molecule	OH Site	O· Site	E_e°	E^{298}	OH Site	O_2 Bridge Sites	O_2 Addition Site	E_e°	E^{298}
toluene	2	3	-422.4566	-422.3062	2	3,1	4	-648.0151	-647.8483
m-xylene	2	3	-461.8238	-461.6413	2	3,1	4	-687.3402	-687.1399
p-xylene	2	3	-461.7941	-461.6131	2	3,1	6	-687.3344	-687.1354
1,2,4-trimethylbenzene	5	4	-501.1425	-500.9301	5	4,6	3	-726.6533	-726.4208
m-ethyltoluene	6	5	-501.1191	-500.9067	6	5,1	2	-726.6518	-726.4236

Table 4.17: Approximate transition states for the formation of the bicyclic peroxy radical, represented in terms of the type of carbon that is bound to an oxygen (a) at the original site of O_2 addition to the peroxy radical, and (b) at the bond which is created when the O_2 bridge is formed. (c) Transition state bond distance for the bond which is created when the O_2 bridge is formed.

Aromatic	Peroxy Site[a]	Bicyclic Peroxy Attachment Site[b]	$E_o°$(TS) (a.u.)	E^{298}(TS) (a.u.)	r(C-O)[c] (Å)	E^{298}(peroxy) (a.u.)	Barrier Ht. (kcal/mol)
m-xylene	C_t	C_t	-536.9672	-536.7800	2.20	-536.7986	11.7
toluene	C_s	C_t	-497.6318	-497.4764	2.10	-497.5040	17.3
	C_t	C_s	-497.6396	-497.4842	2.05	-497.5040	12.4
p-xylene	C_t	C_s	-536.9625	-536.7775	2.05	-536.7968	12.1

4.3.5 Ring Fragmentation Products

The only path for the resulting bicyclic oxy radicals is fragmentation via favorable β- scission reactions. These fragmentation reactions yield an acyclic radical and eventually dicarbonyl products (see Table 4.1 - 4.3. Shown in Figure 4.9 is an example of the β-scission process for a bicyclic oxy radical formed in the photooxidation of toluene. The key issue is the method of fragmentation of the resulting acyclic radical. Calculations of the ΔH_{rxn}, for the decomposition of the acylic radical were conducted using the NIST Structures and Properties estimation program [25]. This program is based on the group additivity theory of Benson [30]. Based on the calculations, each acyclic radical fragments at the bond between the carbon attached to the oxygen atom and the saturated carbon center rather than the unsaturated carbon center. This point is clearly shown in Figure 4.9. Decomposition path A, illustrating fragmentation between the carbon with the oxygen atom attached to it and the unsaturated carbon center, is the favored path based on group additivity calculations. Decomposition path B is the unlikely method of fragmentation based on group additivity considerations. Shown in Figure 4.10 are the bicyclic oxy radicals and the products that are predicted to form following the β-scission process analogous to that depicted in Figure 4.9. It is well known that α-hydroxy carbonyls subsequently react with O_2 to form HO_2 and the corresponding dicarbonyl product[29]. Note from Tables 4.1 - 4.3 that a number of the ring fragmentation products theoretically predicted for toluene, m- xylene, and p-xylene have been identified experimentally.
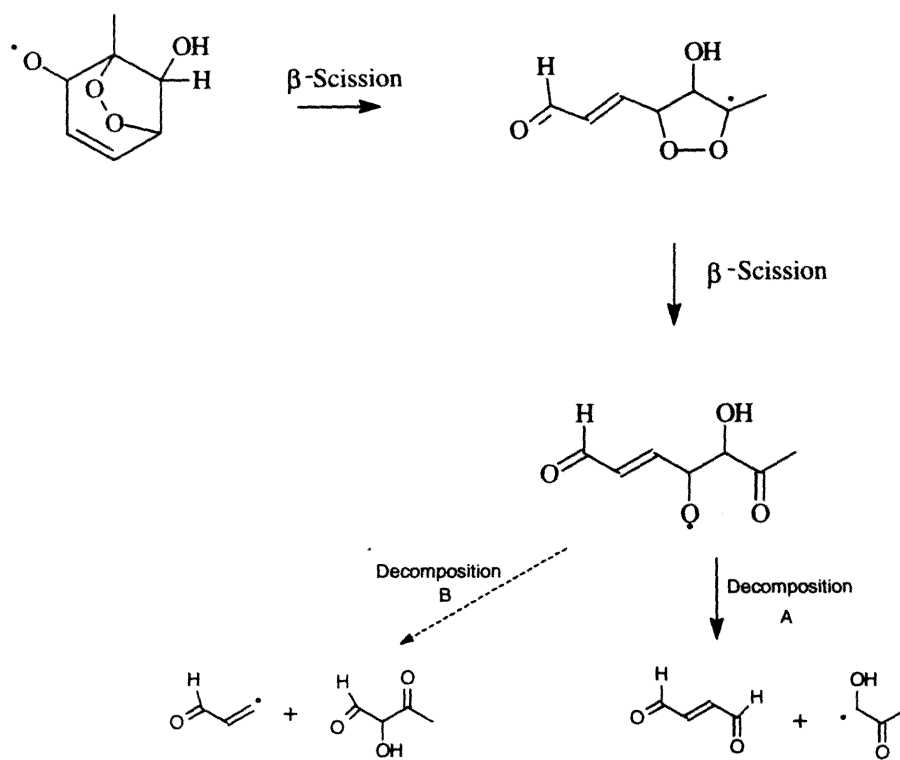
Figure 4.9: β-Scission of a bicyclic oxy radical of toluene to give ring fragmentation products. Decomposition path A is the favored path for fragmentation of the acyclic radical.
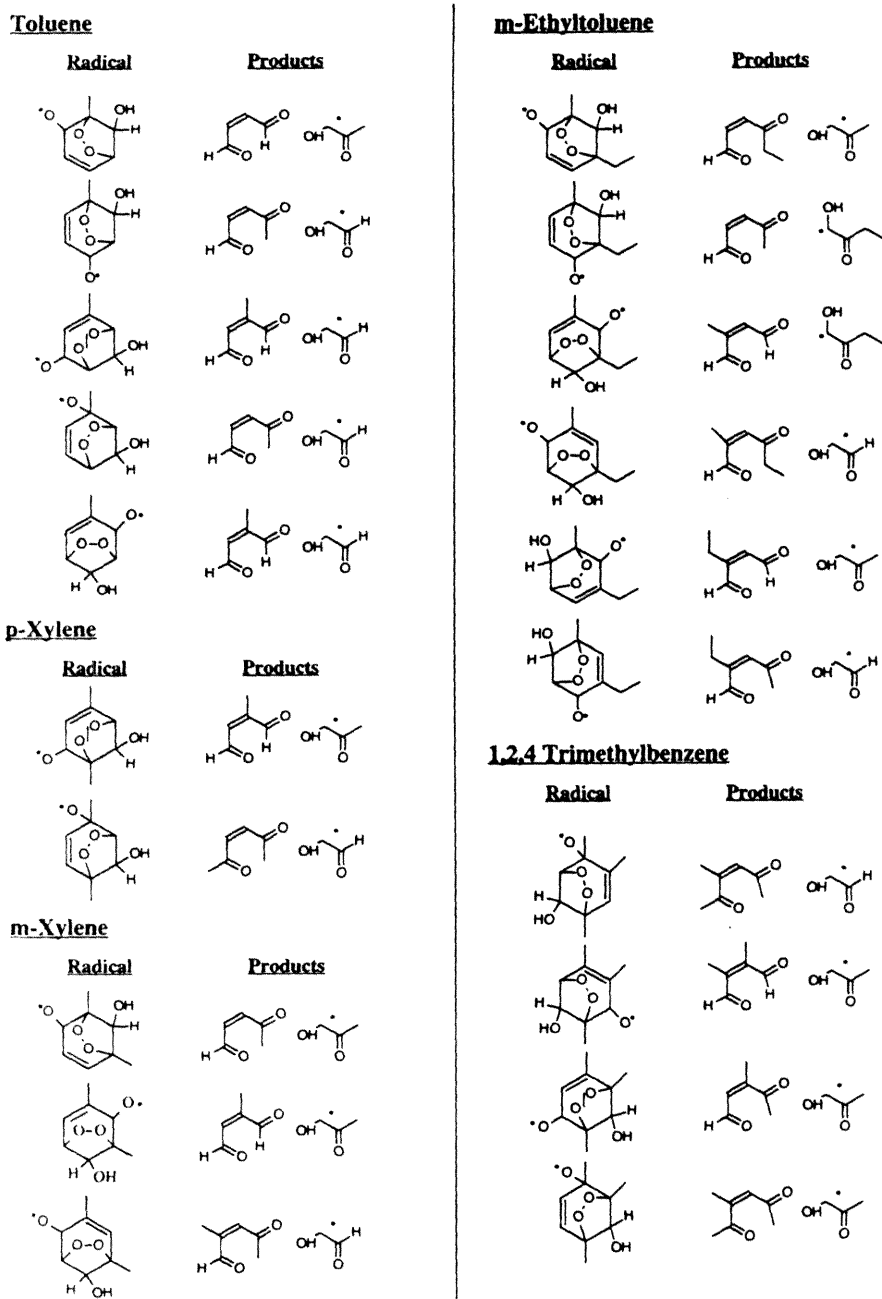
Figure 4.10: Fragmentation products formed from the bicyclic oxy radicals.

4.4 Conclusion

We have elucidated the intermediates in five atmospheric aromatic-OH photooxidation systems, using theoretically-based calculations. In general we find that the predicted site of initial OH attack is ortho to a substituent group attached to the ring. In addition, we have investigated the NO_2 reaction with the aromatic-OH adduct, and have shown that this reaction proceeds via four pathways, forming the nitroaromatic (Reaction 3a), hydroxy nitroaromatic (Reaction 3b), hydroxy aromatic nitrite (Reaction 3c), and the phenolic compound (Reaction 3d). Reaction 3e is not energetically favored, and is thus excluded from a general aromatic-OH mechanism. All peroxy radicals formed from the reaction of the aromatic adduct with O_2 have approximately the same energy. Therefore, it is difficult to exclude a particular structure. However, it is clear that if the original aromatic-OH adduct is not favored, then the resulting peroxy radicals will not be formed. The allylically stabilized five-membered ring bicyclic radicals are, in all cases, approximately 20 kcal/mol more stable than any other bicyclic radical, including those with six-membered rings. Thus, these bicyclic radicals should be included in overall aromatic reaction mechanisms. The aromatic peroxy radical reaction with NO (Reaction 5) is determined to be a plausible reaction to include in aromatic-OH reaction mechanisms. Subsequent reaction of the oxy radicals formed in Reaction 5 can lead to ring-retaining hydroxy carbonyl compounds. These additional ring-retaining compounds can account for part of the remaining carbon unaccounted for in laboratory studies of aromatics. When compared to available product data, the theoretical results

for the intermediates formed and the subsequent reactions for toluene, *m*-xylene, and *p*-xylene are found to be consistent with experimental results. The theoretical technique has been applied to two important, yet relatively unstudied, aromatics, 1,2,4- trimethylbenzene and *m*-ethyltoluene, to predict their reaction intermediates and stable products.

Acknowledgments

Bibliography

[1] National Research Council, "Rethinking the Ozone Problem in Urban and Regional Air Pollution", National Academy Press, Washington D.C. , 1991.

[2] Atkinson, R., *J. Phys. Chem. Ref. Data.*, **1989**, *Monograph 1*, 1.

[3] Atkinson, R., *J. Phys.Chem. Ref. Data*, **1994**, *Mongraph 2*, 1.

[4] Atkinson, R., *Atmos. Environ.*, **1990**, *24A*, 1.

[5] Bandow, H.; Washida, N., *Bull. Chem. Soc. Jpn.*, **1985**,*58*, 2549.

[6] Tuazon, E.; Mac Leod, H.; Atkinson, R.; Carter, W., *Environ. Sci. Tech.*, **1986**, *20*, 383.

[7] Dumdei, B.; Kenny, D.; Shepson, P.; Kleindienst, T.; Nero, C.; Cupitt, L.; Claxton, L., *Environ. Sci. Tech.*, **1988**, *22*, 1493.

[8] Bandow, H.; Washida, N.; Akimoto, H., *Bull. Chem. Soc. Jpn.*, **1985**, *58*, 2531.

[9] Shepson, P.; Edney, E.; Corse, E., *J. Phys. Chem.*, **1984**, *88*, 4122.

136

[10] Atkinson, R.; Aschmann, S.; Arey, J.; Carter, W.,*Int. J. Chem. Kinet.*, **1989**, *21*, 801.

[11] Bandow, H.; Washida, N., *Bull. Chem. Soc. Jpn.*, **1985**, *58*, 2541.

[12] Gery, M.; Fox, D.; Kamens, R.; Stockburger, L., *Environ. Sci. Technol.*, **1987**, *21*, 339.

[13] Atkinson, R.; Aschmann, S.; Arey, J., *Int. J. Chem. Kinet.*, **1991**, *23*, 77.

[14] Parr, R.G.; Yang,W., "Density Functional Theory of Atoms and Molecules", Oxford University Press, New York, 1989; Chapter 3.

[15] Becke, A.D., *Phys. Rev. A*, **1988**, *38*, 3098.

[16] Becke, A.D.. *ACS Symposium Series*, **1989**, *394*, 165.

[17] Lee, H.; Lee, C.; Parr, R.G., *Phys. Rev. A*, **1991**, *44*, 768.

[18] Frisch, M.J.; Trucks, G.W.; Schlegel, H.B.; Gill, P.M.W.; Johnson, B.G.; Wong, M.W.; Foresman, J.B.; Robb, M.A.; Head-Gordon, M.; Replogle, E.S.; Gompert, R.; Andres, I.L.; Raghavachari, K.; Binkley, J.S.; Gonzalez, C.; Martin, R.L.; Fox, D.J.; Defrees, D.J.; Baker, J.; Stewart, J.J.P.; Pople, J.A. "Gaussian 92/DFT, Revision F.4", Gaussian,Inc., Pittsburg,PA., 1993.

[19] Stewart, J.J.P. *J. Comp. Chem.*, **1989**, *10*, 209.

[20] Allinger,N.L., *J. Am. Chem. Soc.*, **1977**, *99*, 8127.

[21] Plummer, B.F.; Steffen, W.C.; Herndon, W.C., *Struct. Chem.*, **1993**, *4*, 279.

[22] Coolidge, M.B.; Marlin, J.E.; Stewart, J.J.P., *J. Comp. Chem.*, **1991**, *12*, 948.

[23] Ringnalda, M.N., Langlois, J.M., Greeley, B.H., Murphy, R.B., Russo, T.V., Cortis, C., Muller, R.P., Martin, B., Donnelly, Jr., R.E., Mainz, D.T., Wright, J.R., Pollard, W.T., Cao, Y., Won, Y., Miller, G.H., Goddard, III, W.A., Friesner, R.A., "PSGVB version 2.1", Schrodinger, Inc. (1995).

[24] Hyperchem Release 4.0, Autodesk, Inc., 1994.

[25] Stein, S.E.; Rukkers, J.M.; Brown, R.L., "NIST Standard Reference Database 25: NIST Structures and Properties Database and Estimation Program", 1991.

[26] Knispel, R.; Koch, R.; Siese, M.; Zetzsch, C., *Ber. Bunsenges. Phys. Chem.*, **1990**, *94*, 1375.

[27] Atkinson, R.; Aschmann, S.M., *Int. J. Chem. Kinet.*, **1994**, *26*, 929.

[28] Wallington, T.J.; Dagaut, P.; Kurylo, M.J., *Chem. Rev.*, **1992**, *92*, 667.

[29] Atkinson, R., Lloyd, A., *J. Phys. Chem. Ref. Data*, **1984**, *13*, 315.

[30] Benson, S.W., "Thermochemical Kinetics, 2nd Ed.", John Wiley & Sons, New York, 1976.

Chapter 5

Photooxidation of Aromatic Compounds: Evidence for an NO$_2$ Effect

Abstract

Atmospheric reaction pathways in the NO_x-air photooxidation of aromatics remain one of the most uncertain elements of urban atmospheric chemistry. This work examines the effect of NO_2 on the product distribution formed after the initial aromatic-OH reaction of toluene, m-xylene, and p-xylene. Results of experiments conducted in a 1 m^3 photochemical reactor are used to evaluate key branching steps in atmospheric aromatic photooxidation mechanisms.

5.1 Introduction

Aromatics are an important class of compounds in urban air. Notably, in the Southern California Air Quality Study of 1987, aromatics were found to compromise approximately 25% of the carbon in the South Coast Air Basin[1]. Despite the prevalence of these compounds in the atmosphere and their importance in ozone formation, the reaction mechanisms of these species are one of the greatest uncertainties in urban atmospheric chemistry[2].

The major atmospheric sink of aromatics is reaction with the OH radical [3, 4]. Approximately 10% of the hydroxyl radical reaction with an aromatic proceeds via the abstraction route, the remainder by addition. The abstraction route produces ring-retaining products such as aromatic aldehydes and nitrated compounds. The first step in the OH reaction with toluene (as an example) is shown in Figure 5.1. The addition route results in ring fragmentation products such as dicarbonyls and ring-retaining products such as nitroaromatics and phenols. In general, the preferred site of OH addition to the aromatic ring is at positions ortho to the carbon that is substituted with an electron donating group[5].

Molecular oxygen and NO_2 can react with the substituted methylcyclohexadienyl (MHCD) radical that results from the OH addition pathway. Present indications are that the O_2 pathway proceeds via two routes: addition to form a peroxy radical and H-atom abstraction to form a phenolic type compound. The peroxy radical stabilizes itself by cyclicizing. The cyclicized radical adds oxygen, forming another peroxy radical which subsequently undergoes a series of favorable β- scission reactions to form ring
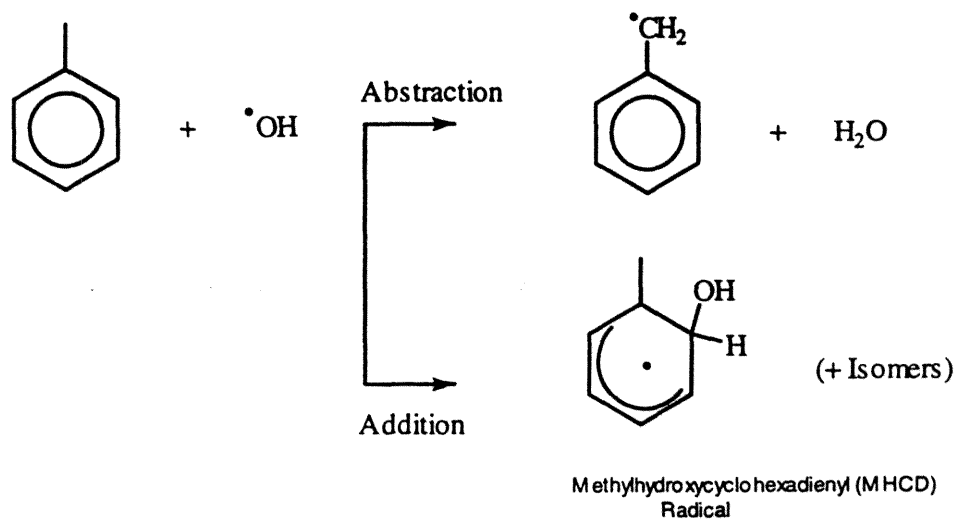
Figure 5.1: Initial steps in the toluene-OH reaction.

Table 5.1: Toluene Photooxidation Products: Molar Yields

Compound	Yield	Reference
Glyoxal	0.105 ± 0.019	[15]
	0.058	[16]
	0.150 ± 0.040	[17]
	0.080	[18]
Methyl Glyoxal	0.146 ± 0.006	[15]
	0.077	[16]
	0.140 ± 0.04	[17]
	0.075	[18]
Benzaldehyde	0.0645 ± 0.0080	[19]
	0.05	[16]
	0.054	[18]
Benzyl Nitrate	0.0084 ± 0.0017	[19]
Formaldehyde	0.010	[16]
o-Cresol	0.204 ± 0.027	[19]
m- and p-Cresol	0.048 ± 0.009	[19]
m-Nitrotoluene	$0.0135 \pm 0.0029 + 1.90 \pm 0.25 \times 10^{-16}[NO_2]$	[19]
o-Nitrotoluene	$0.07 \times [m\text{-nitrotoluene}]$	[19]
p-Nitrotoluene	$0.35 \times [m\text{-nitrotoluene}]$	[19]

fragmentation products. Recently, through *ab initio* calculations, Andino et al. [5] identified the energetically favored intermediate species formed in the OH-initiated photooxidation of aromatic comounds, and examined their ring fragmentation pathways. NO_2 reaction with the substituted MHCD radical leads to the formation of nitroaromatic compounds. Atkinson and Aschmann [6] have suggested that the NO_2 pathway also results in the formation of phenolic type compounds. Several of the products identified in laboratory studies of toluene, m-xylene, and p-xylene photooxidation are listed in Tables 5.1-5.3; these products are consistent with the theoretical study of Andino et al.[5].

Table 5.2: *m*-xylene Photooxidation Products: Molar Yields

Compound	Yield	Reference
Glyoxal	0.13 ± 0.03	[20]
	0.086	[21]
	0.086 ± 0.011	[15]
Methylglyoxal	0.42 ± 0.05	[20]
	0.375	[21]
	0.319±0.009	[15]
Formaldehyde	0.17 ± 0.02	[20]
m-Tolualdehyde	0.0331	[22]
	0.12 ± 0.059	[21]
3-Methylbenzyl nitrate	0.0061	[22]
2,4 Dimethylphenol	0.099	[22]
2,6 Dimethylphenol	0.111	[22]
Dimethylphenol	0.178 ± 0.065 [1]	[21]
4-Nitro-*m*-xylene	0.0018	[22]
5-Nitro-*m*-xylene	See Note[2]	[22]
Nitro-*m*-xylene	0.033 ± 0.025 [3]	[21]

Table 5.3: *p*-xylene Photooxidation Products: Molar Yields

Compound	Yield	Reference
Glyoxal	0.24 ± 0.02	[20]
	0.225 ± 0.039	[15]
Methylglyoxal	0.12 ± 0.02	[20]
	0.105 ± 0.034	[15]
3-Hexene-2,5 Dione	Detected	[20]
Formaldehyde	0.17 ± 0.02	[20]
p-Tolualdehyde	0.0701	[22]
4-Methylbenzyl nitrate	0.0082	[22]
2,5 Dimethylphenol	0.188	[22]
2-Nitro-*p*-xylene	$(0.0120 + 2.8x10^{-17}[NO_2])$	[22]

Recent evidence has suggested that the level of NO_2 will significantly affect the yields of aromatic-OH reaction products [6]. While there have been a series of investigations of the photooxidation of toluene, m-xylene, and p-xylene, the only systematic study of effects of NO_2 on aromatic systems is that of Atkinson and Aschmann [6], examining the reactions of toluene, o-xylene, and 1,2,3-trimethylbenzene.

Examination of the product yields in Tables 5.1-5.3 shows that, in several cases, discrepancies exist between reported yields. As examples, note the yields of methyl glyoxal from toluene and m-xylene and glyoxal from m-xylene. Even if the error limits on the yields are considered, these discrepancies can be significant, and may be attributed to the neglect of secondary reactions or differences in NO_2 concentrations in the experimental systems. When considering the mechanism of aromatic photooxidation, there are several junctures where the NO_2 level might affect observed product yields. The most influential reaction involving NO_2 is that with the substituted MHCD radical. The branching ratio between the reactions of O_2 and NO_2 with this radical is of crucial importance to product yields. We present here the results of a systematic laboratory study on the effects of NO_2 on selected product yields in toluene, m-xylene, and p-xylene photooxidations. Based on these results, we have developed plausible reaction mechanisms for the photooxidation of these aromatics, and have estimated the branching ratio between the MCHD radical reaction with NO_2 and O_2.

5.2 Experimental Procedure

The Caltech Indoor Photochemical Reactor has been described in detail elsewhere[4]. Briefly, the chamber is a 1 m^3 reactor composed of 2 mil FEP Teflon. Artificial light (two banks of 24 Sylvania F30T8BL black lamps) is used to initiate the chemistry within the chamber. The lamps are mounted on a cylindrical surface to provide for uniformity in irradiation. The light intensity within the chamber can be adjusted by varying the number of lamps that are used (minimum of 2 lamps, and maximum of 48 lamps). Typical irradiation times for toluene, m-xylene, and p-xylene were 1-6 min., 1-5 min., and 1-10 min., respectively.

To study the hydroxyl radical-aromatic reactions in the presence of NO_x, methyl nitrite was introduced to the chamber along with the aromatic of interest via a calibrated glass vacuum manifold. Methyl nitrite generates OH radicals according to the following reactions:

$$CH_3ONO + h\nu \rightarrow CH_3O\cdot + NO$$
$$CH_3O\cdot + O_2 \rightarrow HCHO + HO_2\cdot$$
$$HO_2\cdot + NO \rightarrow \cdot OH + NO_2$$
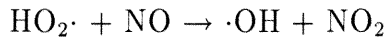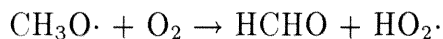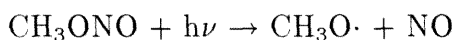
In order to minimize ozone production, and maximize the conversion of peroxy radicals to alkoxy radicals, NO was added to the chamber. Typical starting mixing ratios were 4-5 ppm aromatic, 1-5 ppm CH_3ONO, and 1 ppm NO. Toluene, m- xylene, and p-xylene were obtained from Aldrich with stated purities of 99+%, 99+%, and 99+%. All were used without further

---

[4]See Chapter 2.

purification. Nitric oxide was taken from a standard cylinder (generated by Scott-Marin). Methyl nitrite was prepared by the dropwise addition of 50% sulfuric acid to a saturated methanol/sodium nitrite solution. Using high purity N_2, the resulting gas was bubbled through a NaOH solution to neutralize the acid, and then passed through $CaCl_2$ to dry it. The nitrite was trapped in a bulb which was immersed in a dry ice/ethanol slush bath, purified using the glass vacuum manifold, and stored at liquid N_2 temperatures.

To study aromatic-OH reactions in the absence of NO_x, ozone-olefin reactions were used to generate OH radicals. The olefin-ozone reaction has been shown to yield significant amounts of hydroxyl radicals [7]. α-Pinene was chosen for the current study because its photooxidation products have been reasonably well charaterized, and it produces a high yield of OH radicals[7, 8, 9]. Hydroxyl radical yield from the ozone reaction with α-pinene is 0.85, much higher than other readily available alkenes and monoterpenes. Dark reactions of ozone, α-pinene, and aromatic were carried out to generate OH radicals for NO_x-free experiments. The ozone was produced by an ozone generator (Enmett Inc.), and α-pinene was purchased from Aldrich with a stated purity of 99%. It was used without further purification.

The chamber was sampled periodically for analyses by the on-line ozone analyzer (Dasibi 1008) and NO_x analyzer (Thermo Environmental Model 42). Samples were also collected onto Tenax packed stainless steel tubes for desorption and subsequent analysis by GC-FID. Desorption was accomplished using a Tekmar Model 6000 Aerotrap desorber with an attached cryofocusing unit. The column used in the GC-FID was a J&W Scientific DB-5 column of dimension 30 m x 0.25 mm x 0.25 μm. The GC-FID oven temperature

was held at 50°C for 1 min and increased by 20°C/min. until the final temperature of 275°C was reached. The oven was then held at 275°C for 1 min

.

The GC-FID was calibrated for the aromatics by using standard cylinders (generated by Scott-Marrin) of each aromatic. Standard concentrations of the aromatic were introduced into a small (4 liter) teflon bag. Tenax packed tube samples were taken from this bag and analyzed in the same manner as the experimental samples. Calibrations of the products were carried out in a slightly different manner. Liquid samples of the products were vaporized into the chamber along with an aromatic. The calibration amount of aromatic introduced into the chamber was used to calculate the bag volume, and the product concentration was obtained. Response factors were obtained for each product identified by evaporating a known amount of the product, in liquid form, into the chamber along with an aromatic. The aromatic concentration was calibrated, and the value obtained was used to determine the bag volume. This volume was then used to calculate the product concentration. Response factors were subsequently generated from these calculated concentrations.

At the end of each experiment, a sample from the chamber was collected on a 2,4-dinitrophenylhydrazine (DNPH) impregnated C_{18} cartridge. The DNPH method was the only method used to analyze for aldehydes in these studies. The samples were eluted using 3 ml of acetonitrile, and analyzed using a Hewlett Packard Model 1090 Series II liquid chromatograph with a diode array detector. A reversed-phase ODS Axxiom LC column of dimension 0.5 μm x 150 cm was used to obtain adequate separation. HPLC grade acetonitrile and water were used as the solvents in a ratio of 55% to 45%,

with a total flowrate of 1 ml/min. Typical observed pressures were between 109 and 112 mbar.

Authentic DNPH derivatized carbonyl standards for the LC were purchased from Radian Corporation for comparison to the experimental samples. Additional standard samples for glyoxal and methyl glyoxal were synthesized in our laboratory according to the method of Druzik et al. [10].

5.3   Effect of NO$_2$ on Product Yields in Aromatic Photooxidation

The primary products detected and quantified from the OH-addition pathway in the toluene photoxidation system are o-,m-,p-cresol, methyl glyoxal, and glyoxal . Average NO$_2$ concentrations before correction for the OH-NO$_2$ reaction were determined using the following equation, incorporating the contribution of methyl nitrite photolysis and NO to NO$_2$ conversion :

$$\overline{[NO_2]} = \frac{1}{n} \sum_{i=1}^{n} ([CH_3ONO]_o(\ 1- \ e^{-kt_i}) + \Delta[\ NO]_i)$$

where: k = photolysis rate constant for methyl nitrite, as measured experimentally, $\Delta [NO]_n = [NO]_o - [NO]_t$, and n = number of data points. This expression assumes that the initial NO$_2$ concentration is zero. Because a NO$_x$ monitor was used as the method of monitoring the inorganic compound concentrations, the actual amount of NO$_2$ initially present was not quantifiable. Use of a NO$_x$ monitor does not allow for the direct measurement of NO$_2$.

In addition, organic nitrites and nitrates can (and do) effect a response on the NO_2 channel. The average concentration of NO_2 obtained in the above formula was corrected to account for the OH-NO_2 reaction. This correction term was derived using modeling predictions determined with the aid of the mechanisms appearing in Tables 7-9. The mechanisms will be discussed subsequently. For completeness, the OH reactions of products appearing in Table 5.4 were also included in these simulations. Mechanism predictions of the NO_2 concentrations resulting from both the inclusion and exclusion of the OH + NO_2 reaction for each aromatic were plotted against each other, and regression analyses yielded straight lines with excellent correlation coefficients ($R^2 > 0.999$). The average NO_2 concentration determined by taking into account the formation of NO_2 from methyl nitrite photolysis and NO to NO_2 conversion (denoted as $[NO_2]_{average}$) was then corrected using the following linear relationships for the given aromatics:

$$\text{Toluene: } [NO_2]_{corrected} = (0.8487)([NO_2]_{average}) + 0.0157$$

$$\text{m-Xylene: } [NO_2]_{corrected} = (0.9175)([NO_2]_{average}) + 0.0358$$

$$\text{p-Xylene: } [NO_2]_{corrected} = (0.8717)([NO_2]_{average}) + 0.056$$

From these relationships, it is clear that the correction term increases as the concentration of NO_2 in the system increases.

The range of NO_2 mixing ratios used in the toluene study was 200-1650 ppb. Yields of major species versus average $[NO_2]$ for toluene are presented in Figures 5.2-5.4. The data points in Figures 5.2-5.4, and subsequent figures represent the measured data from experiments with and without NO_x. The

lines in these figures will be discussed subsequently.

The primary OH-addition pathway products that were detected and quantified from the photooxidation of m-xylene are glyoxal, methyl glyoxal, nitro-m-xylene, 2,4-dimethylphenol, and 2,6-dimethylphenol. The average NO_2 mixing ratios ranged from 200 ppb to 1100 ppb. Yields of major species versus average $[NO_2]$ for m-xylene are presented in Figures 5.5-5.8.

The primary products resulting from the addition pathway of the photooxidation of p-xylene that were detected and quantified are glyoxal, methyl glyoxal, and 2,5-dimethylphenol. Average NO_2 mixing ratios in these experiments ranged from 200 ppb to 1050 ppb. Yields of major species versus average $[NO_2]$ for p-xylene are presented in Figures 5.9-5.11.

Because the detection limit of the GC-FID/thermal desorber towards nitroaromatics was not adequate to see these species, only limited data are available for nitroaromatics, in particular, only those resulting from the m-xylene system.

Since all products identified are capable of undergoing secondary reactions with hydroxyl radicals, raw product yields must be corrected. Using the method of Atkinson et al. [11], the following formula,

$$F = \frac{k_1 - k_2}{k_1} \frac{1 - \frac{[Aromatic]_t}{[Aromatic]_o}}{\frac{[Aromatic]_t}{[Aromatic]_o}^{\frac{k_2}{k_1}} - \frac{[Aromatic]_t}{[Aromatic]_o}} \tag{5.1}$$

where k_1 and k_2 are the rate constants of the following reactions:

$$\text{Aromatic} + \text{OH} \xrightarrow{1} \text{Product}$$

$$\text{Product} + \text{OH} \xrightarrow{2} \text{Secondary Products}$$
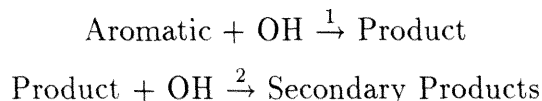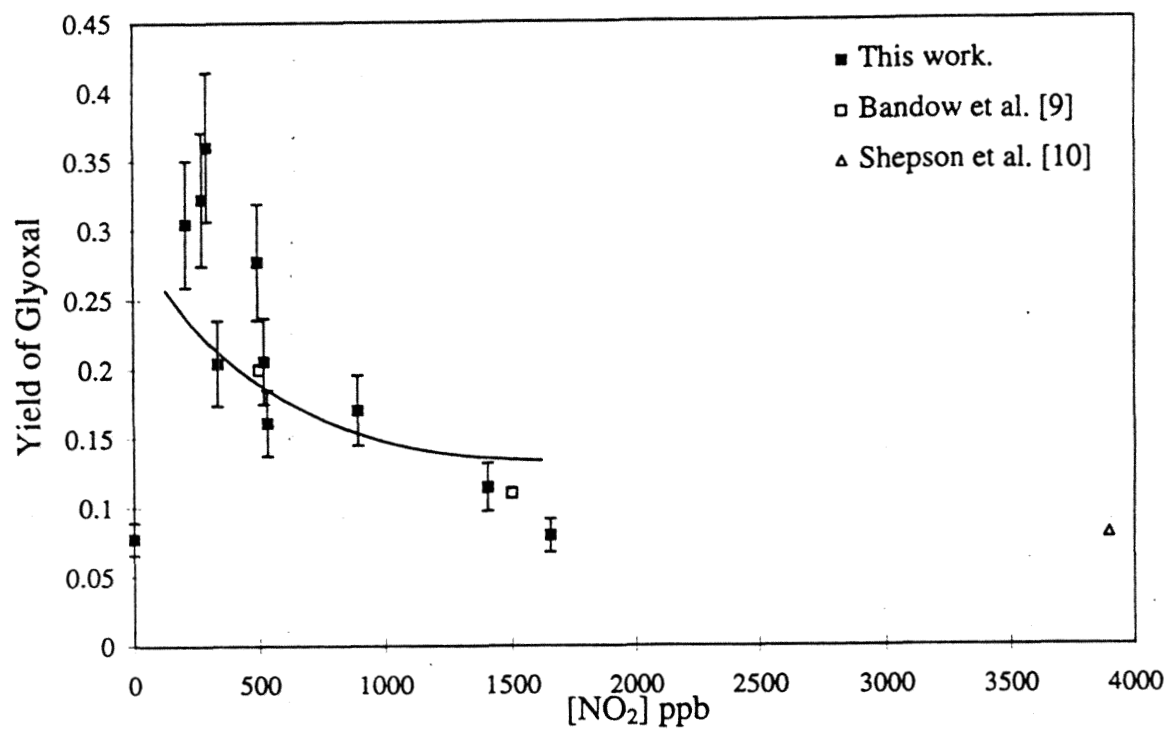
Figure 5.2: Toluene Photooxidation- Glyoxal
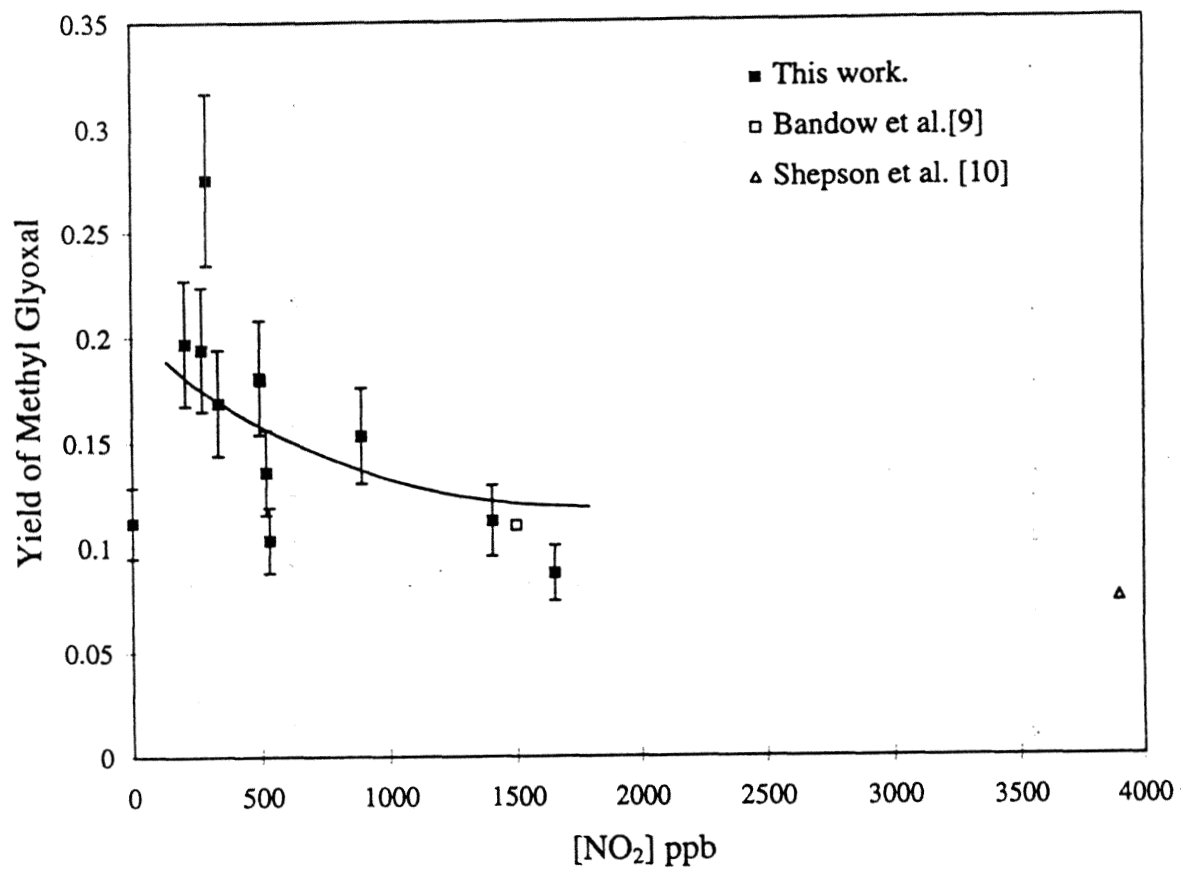
Figure 5.3: Toluene Photooxidation- Methyl Glyoxal
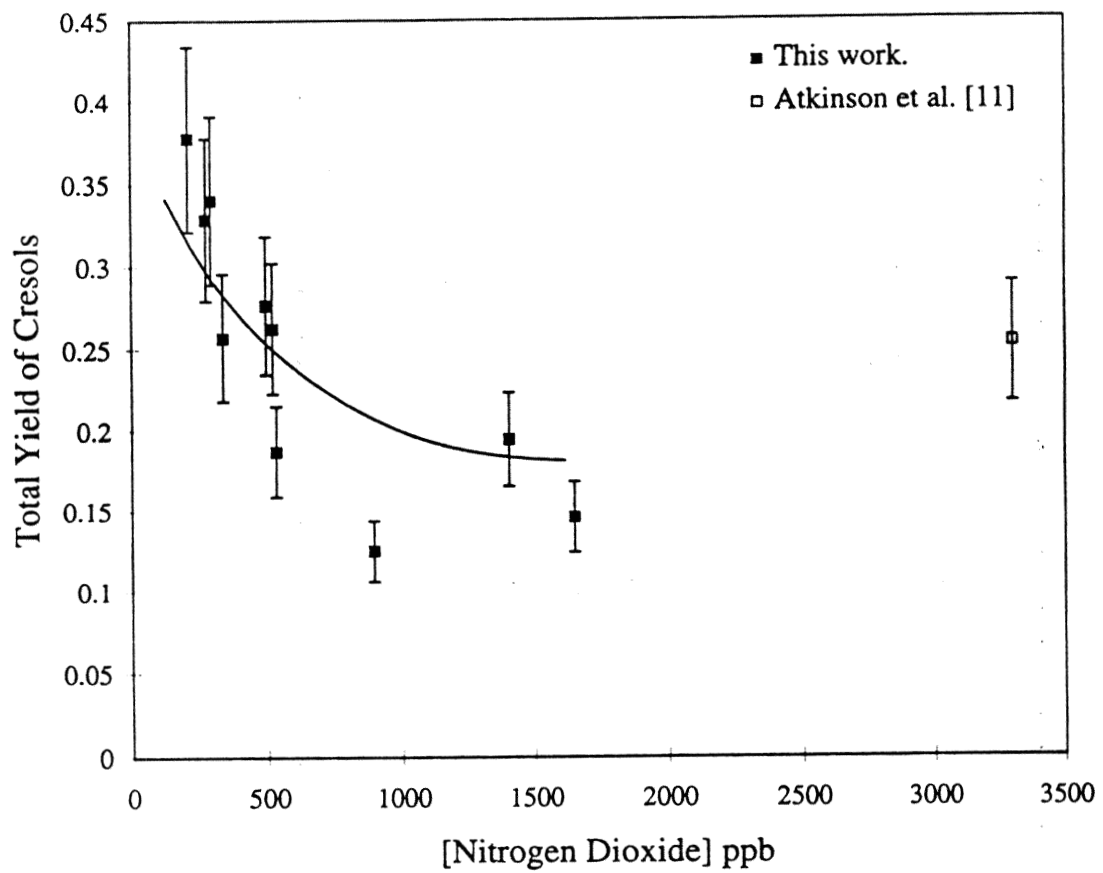
Figure 5.4: Toluene Photooxidation- Cresols
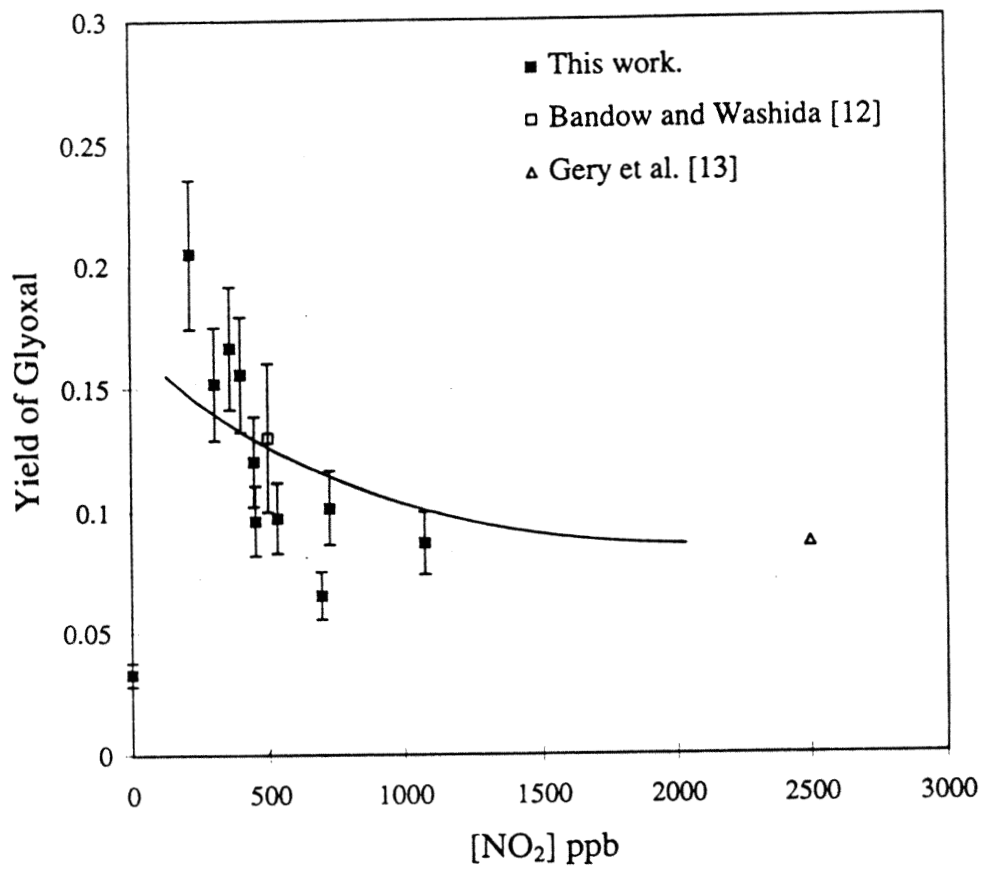
Figure 5.5: *m*-xylene Photooxidation- Glyoxal
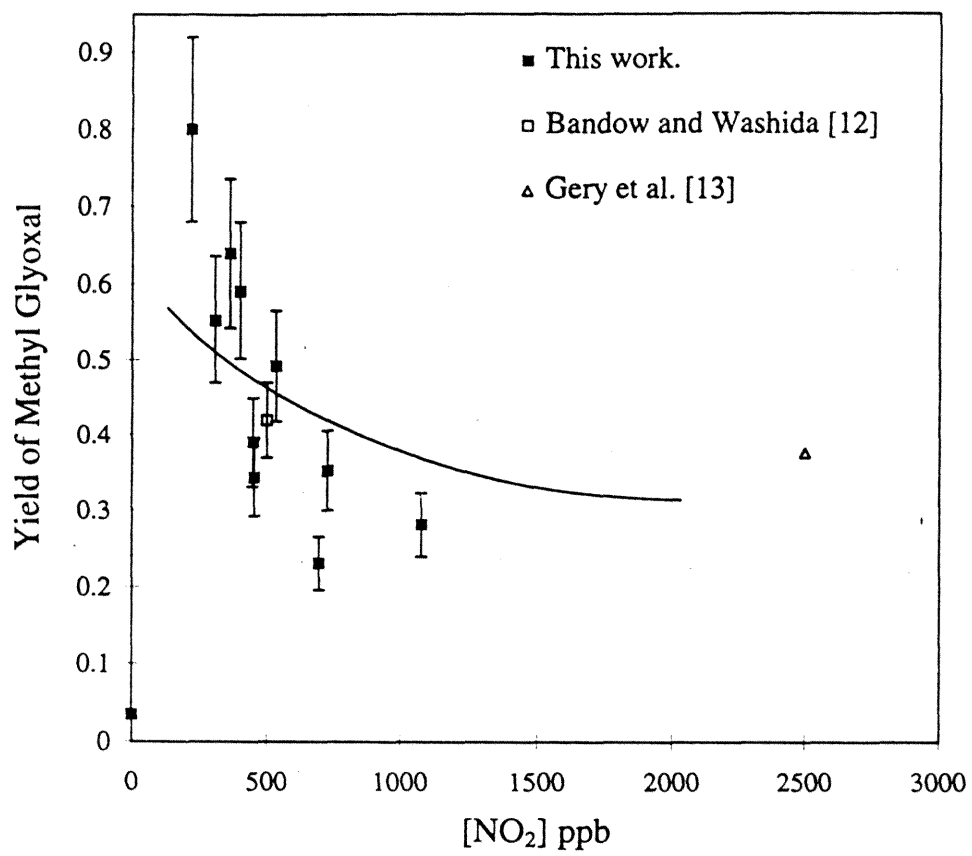
Figure 5.6: *m*-xylene Photooxidation- Methyl Glyoxal
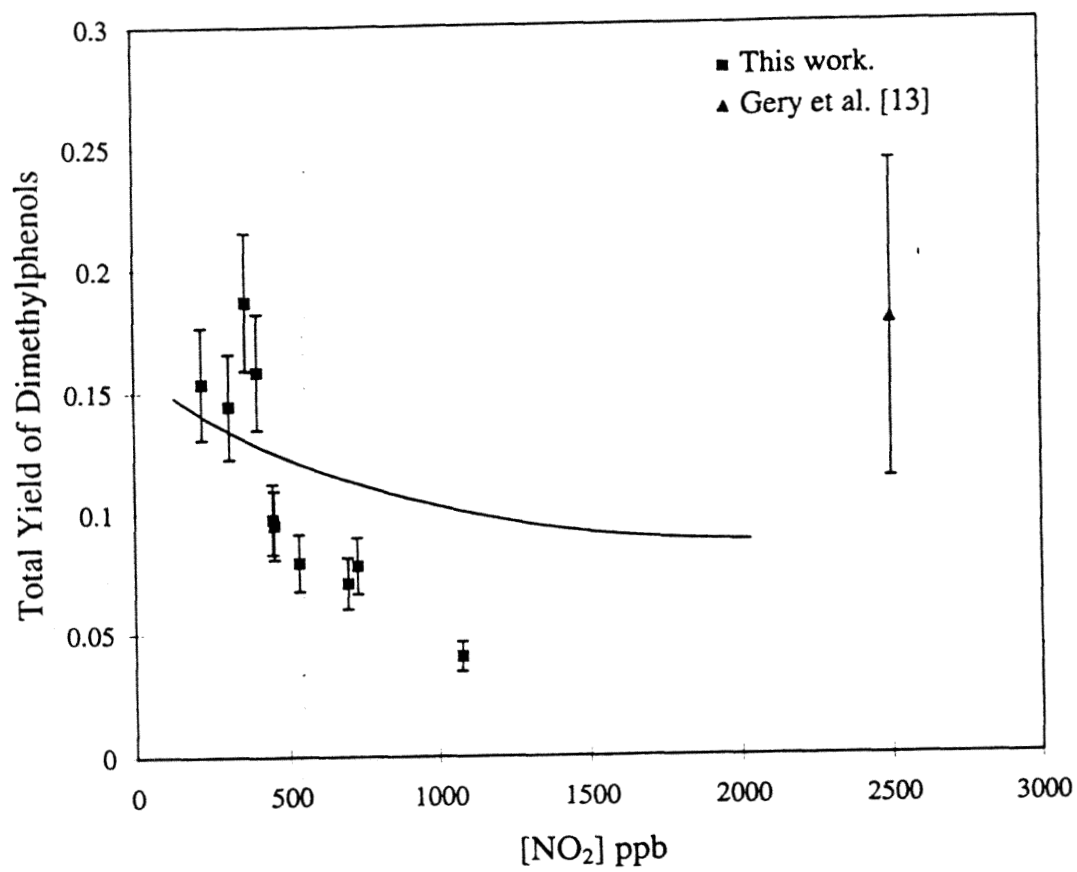
Figure 5.7: *m*-xylene Photooxidation- Dimethylphenols
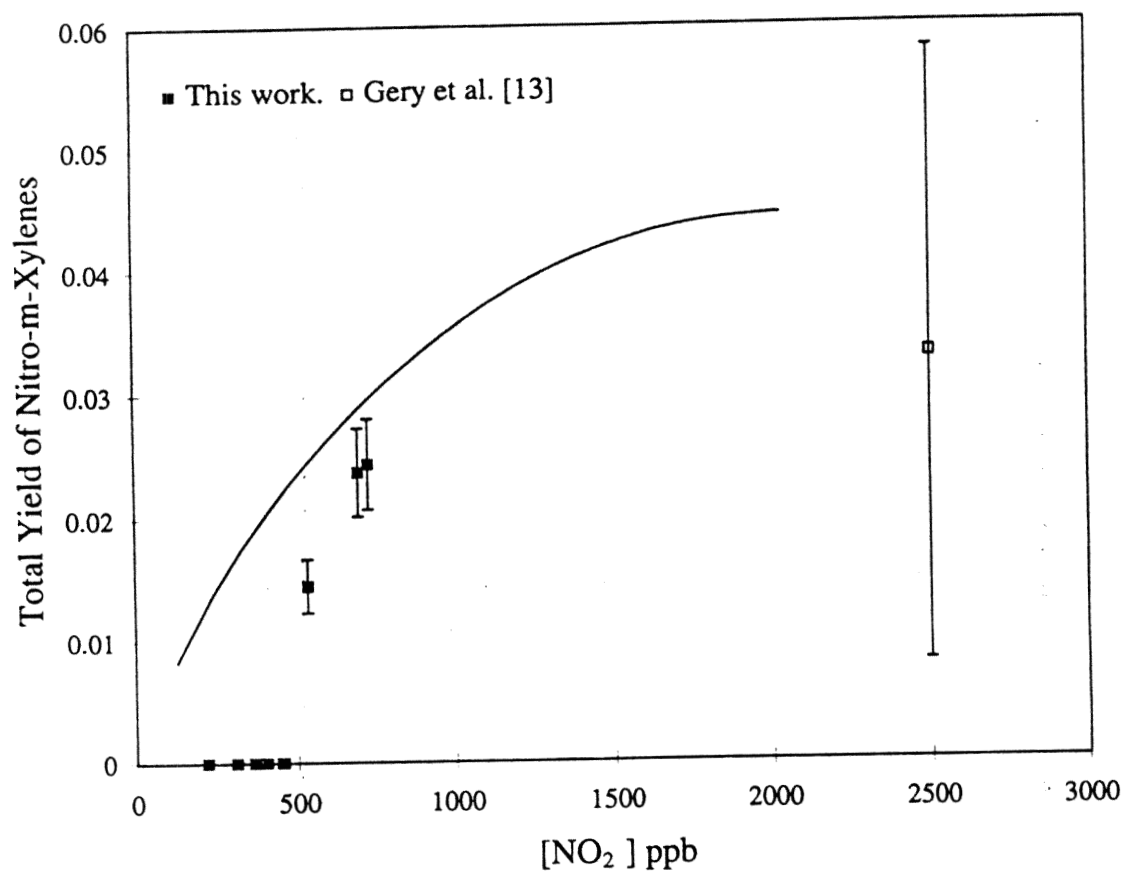
Figure 5.8: *m*-xylene Photooxidation- Nitro-*m*-xylene
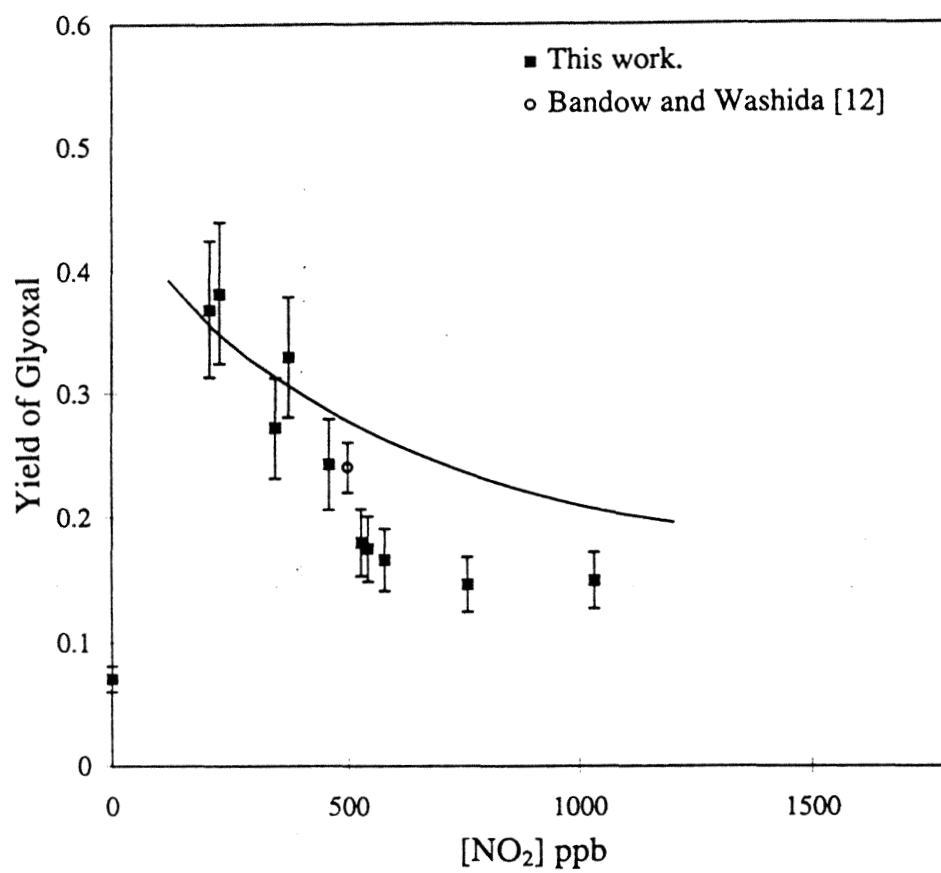
Figure 5.9: *p*-xylene Photooxidation- Glyoxal
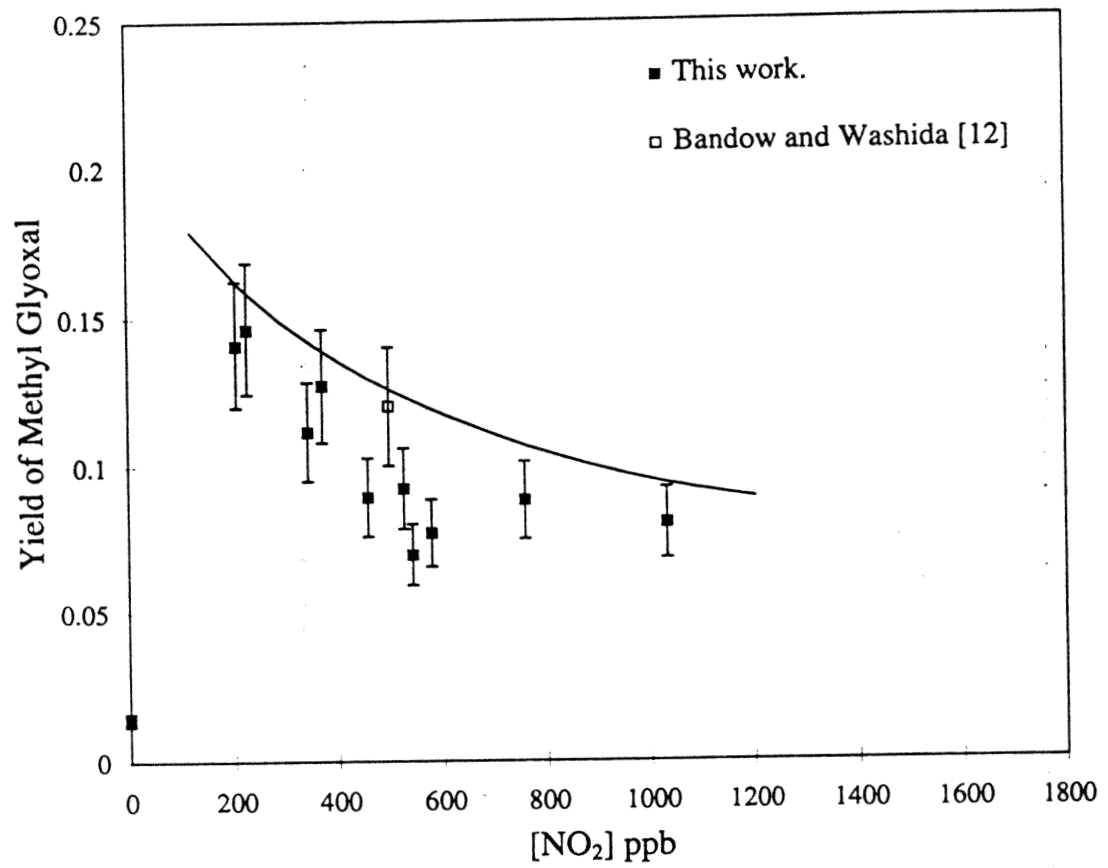
Figure 5.10: *p*-xylene Photooxidation- Methyl Glyoxal
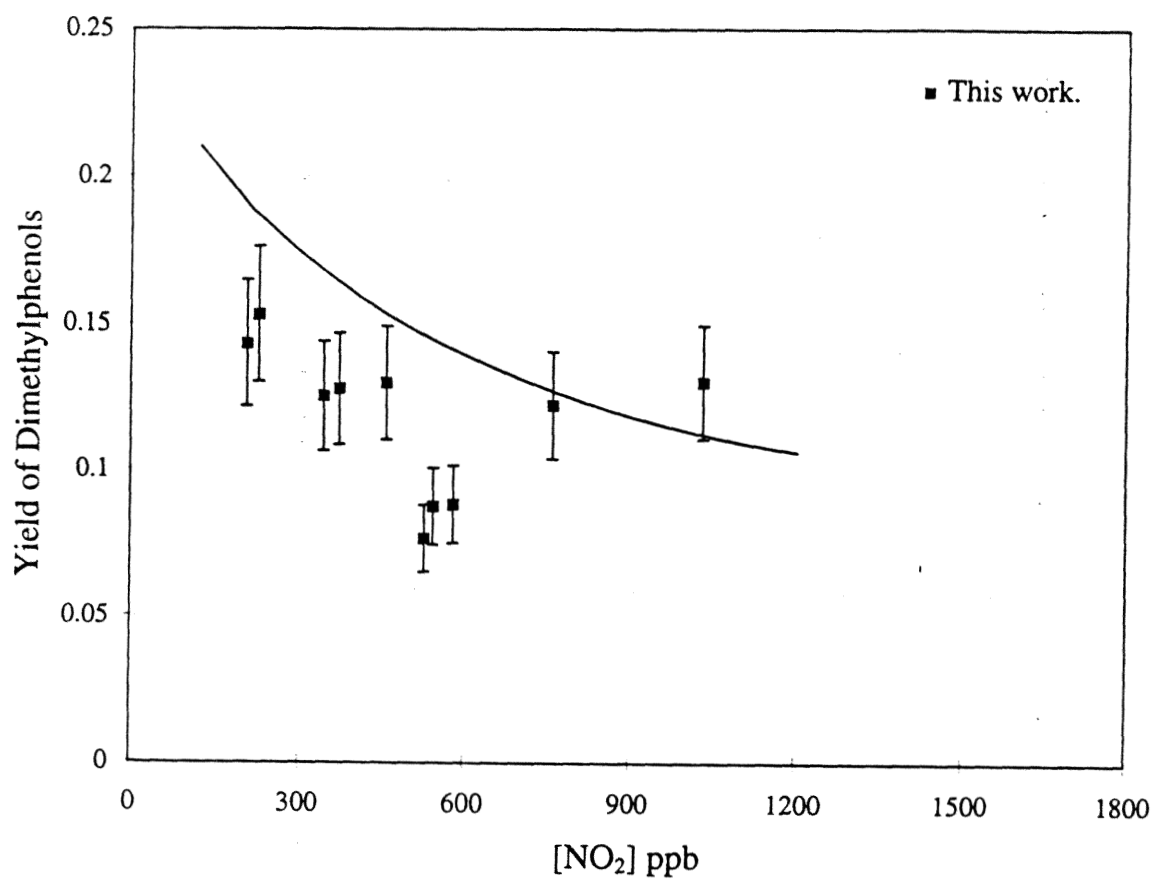
Figure 5.11: *p*-xylene Photooxidation- Dimethylphenol

Table 5.4: OH radical rate constants used to correct product yields.

Compound	Rate constant @ 298K [3, 4] $(cm^3molecule^{-1}s^{-1})$
Aromatics	
Toluene	5.96×10^{-12}
m-xylene	2.36×10^{-11}
p-xylene	1.43×10^{-11}
Products	
Glyoxal	1.14×10^{-11}
Methyl Glyoxal	1.72×10^{-11}
o-Cresol	4.2×10^{-11}
m-Cresol	6.4×10^{-11}
p-Cresol	4.7×10^{-11}
2,4-Dimethylphenol	7.15×10^{-11}
2,6-Dimethylphenol	6.59×10^{-11}
2,5-Dimethylphenol	8×10^{-11}
Nitro-*m*-xylene	0.95×10^{-125}

is used to derive a correction factor. Raw yields are multiplied by this correction factor, F to obtain a corrected yield. Rate constants used in Equation (5.1) for compounds identified in this work are given in Table 5.4. Presented in Table 5.5 are the ranges determined for F for each of the products quantified in the studies presented in this work. It should be noted that the correction factor, F, increased with increasing NO_2 concentration, and that uncertianties in F due to uncertainties in the rate constants, k_1 and k_2, were not taken into account.

For the three aromatics, several general trends can be discerned. As the NO_2 concentration increases, yields of ring fragmentation products and phenolic compounds decrease. In the case of *m*-xylene, an increase in the nitroaromatic yield is noticed. These observations suggest that the pathways

Table 5.5: Ranges of correction values, F, used for each quantified product.

Aromatic	Product	F Range
Toluene	Glyoxal	1.03 - 1.95
	Methyl Glyoxal	1.05 - 2.59
	Cresols	1.12 - 6.16
m-Xylene	Glyoxal	1.01 - 1.13
	Methyl Glyoxal	1.02 - 1.21
	Dimethylphenols	1.06 - 1.94
	Nitro-m-Xylene	1.003 - 1.006
p-Xylene	Glyoxal	1.02 - 1.25
	Methyl Glyoxal	1.02 - 1.39
	Dimethylphenols	1.11 - 3.48

forming ring fragmentation and phenolic compounds are in competition with those forming nitroaromatic compounds. Yields of ring fragmentation products and phenolic compounds formed in the absence of NO_x are lower than the product yield corresponding to the lowest NO_2 concentration. This is likely a result of the fact that peroxy radical-radical interactions in NO_x-free systems produce additional products as compared to those in peroxy radical-NO reactions.

Previous yield data reported in the literature fall in the high NO_2 concentration regime relative to the present experiments. It should be noted that while the present study extends the data concerning the aromatic product yields to lower NO_2 concentrations, these concentrations are still, at their lowest value, approximately a factor of two higher than that of NO_2 in urban areas. Difficulties were encountered in performing even lower level NO_2 experiments with the CH_3ONO-NO-aromatic systems because of the difficulty in accurately distinguishing small changes in aromatic concentration.

5.4 Aromatic Photooxidation Mechanisms

Reaction mechanisms (excluding the reactions of products) for toluene, m-xylene and p-xylene were developed to provide a direct comparison between the experimental product data (corrected for losses due to OH reaction) and the mechanisms. The mechanisms were executed using the SAPRC Atmospheric Photochemical Mechanism Preparation Program[12]. A detailed description of the modeling program, its development and implementation, is available [12].

A generalized mechanism for aromatic reactions following OH radical addition is given in Figure 5.12. The major issues faced in preparing detailed mechanisms for each of the aromatics are determination of the following:

(1) OH + Aromatic branching ratio (addition versus abstraction).

(2) Branching ratio of the MHCD radical reaction with O_2 and NO_2.

(3) Branching ratio of the MHCD + O_2 reaction (phenolic compounds vs. peroxy radical formation leading to ring-fragmentation products).

(4)Branching ratio of the MHCD + NO_2 reaction.

Each of these issues, except the first, is addressed by analysis of product data and is discussed subsequently. Branching ratios and absolute rate constants for the OH-abstraction versus OH-addition pathway for each of the aromatics studied are available [4].

Mechanisms for the primary reactions of toluene, m-xylene, and p-xylene, are presented in Tables 5.7 - 5.9, and structures for the species used in the mechanisms are presented in Table 5.6. The names and structures used in the p-xylene mechanism are identical to those in the m-xylene mechanism, with
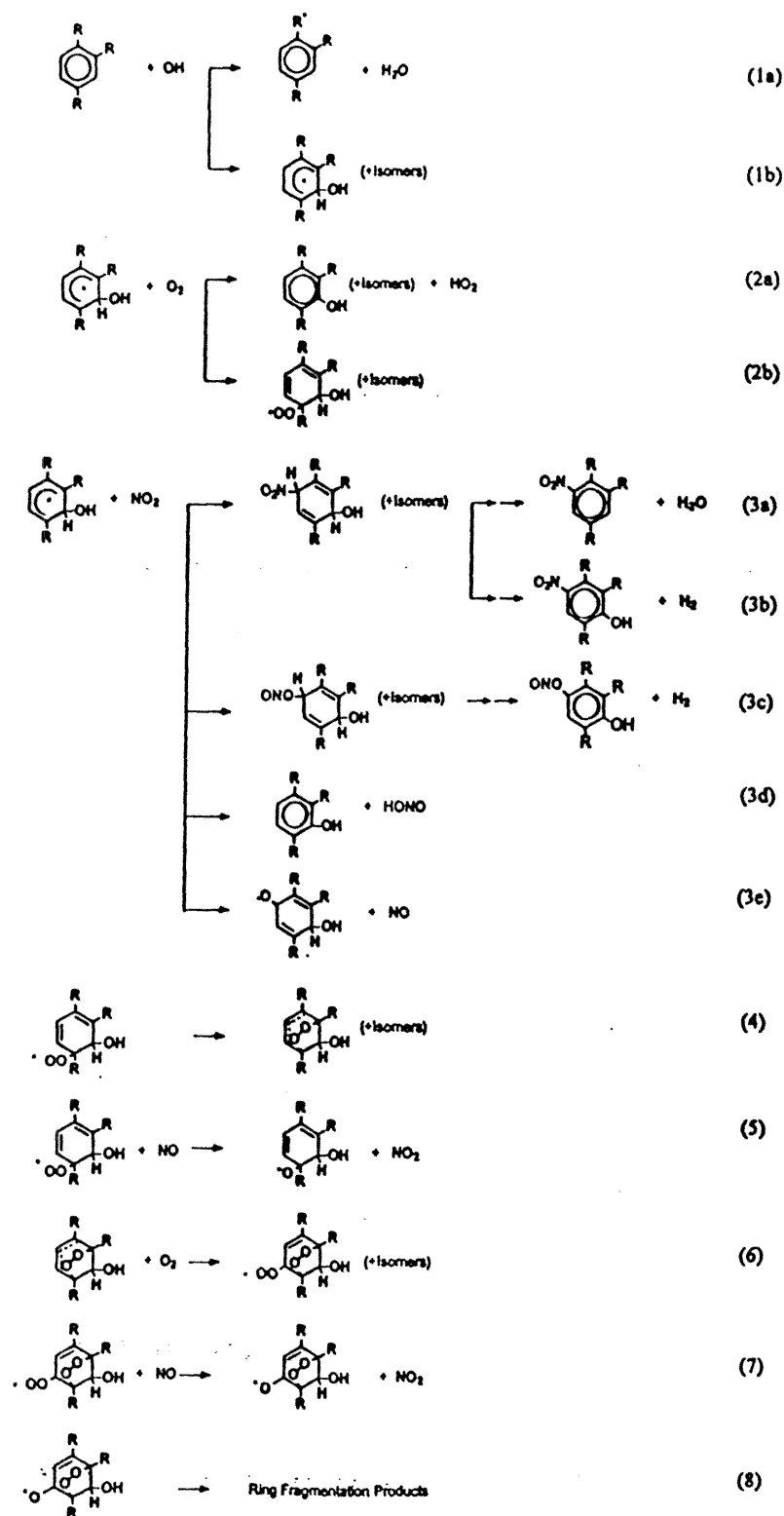
Figure 5.12: Reactions in a generalized mechanism of Aromatic-OH photooxidation. "R" represents either an H atom or a CH_3 group, depending on the aromatic considered.

the exception that the substituent methyl groups are in the para rather than meta position. While the mechanisms listed do not include the secondary reactions of the primary products, in full atmospheric models these additional reactions would normally be included.

Table 5.6: Names and structures of species appearing in the aromatic mechanisms of Tables 5.7, 5.8, and 5.9.

Table 5.7: Toluene Mechanism

No.	Reaction	Rate Constant, 298 K (cm^3, molecule, s units)
	Methyl Nitrite Photolysis	
MN1)	$CH_3ONO + HV \rightarrow CH_3O + HCHO$	Experiment
MN2)	$CH_3O + O_2 \rightarrow HCHO + HO_2$	1.9×10^{-15}
MN3)	$HO_2 + NO \rightarrow OH + NO_2$	3.7×10^{-12}
	Primary Reactions of Toluene	
TA1)	$TOL + OH \rightarrow TOL\text{-} + H2O$	5.07×10^{-13}
TA2)	$TOL\text{-} + O_2 \rightarrow TOL\text{-}O_2$	1×10^{-12}
TA3)	$TOL\text{-}O_2 + NO \rightarrow NO_2 + TOL\text{-}O$	7.91×10^{-12}
TA4)	$TOL\text{-}O_2 + NO \rightarrow TOL\text{-}ONO_2$	9.89×10^{-13}
TA5)	$TOL\text{-}O + O_2 \rightarrow BENZALD + HO_2$	9.5×10^{-15}
TA6)	$TOL\text{-}O + NO_2 \rightarrow TOL\text{-}ONO_2$	3.8×10^{-11}
TA7)	$TOL\text{-}O_2 + TOL\text{-}O_2 \rightarrow 2\ TOL\text{-}O + O_2$	2.5×10^{-13}
TB1)	$TOL + OH \rightarrow MHCD$	5.9×10^{-12}
TB2a)	$MHCD + O_2 \rightarrow CRES + HO_2$	3.18×10^{-16}
TB2b)	$MHCD + O_2 \rightarrow MHCD\text{-}O_2$	4.46×10^{-16}
TB3a)	$MHCD + NO_2 \rightarrow NTOL$	3.6×10^{-11}
TB3b)	$MHCD + NO_2 \rightarrow Products$	3.6×10^{-11}
TB4)	$MHCD\text{-}O_2 + NO \rightarrow NO_2 + MHCD\text{-}O$	8.9×10^{-12}
TB5)	$MHCD\text{-}O + O_2 \rightarrow PRODUCT1 + HO_2$	7×10^{-15}
XB6)	$MHCD\text{-}O + NO_2 \rightarrow MHCD\text{-}ONO_2$	3.8×10^{-11}
TB7)	$MHCD\text{-}O_2 + MHCD\text{-}O_2 \rightarrow 2\ MHCD\text{-}O + O_2$	5×10^{-15}
TB8)	$MHCD\text{-}O_2 \rightarrow BCYLRAD$	8×10^4
TB9)	$BCYLRAD + O_2 \rightarrow MHCD2\text{-}O_2$	1×10^{-12}

TB10) $MHCD2\text{-}O_2 + NO \rightarrow NO_2 + MHCD2\text{-}O$ 8.9×10^{-12}

T11a) $MHCD2\text{-}O \rightarrow METHGLY + C4H4O2$ PHOT. $= NO_2$

T11b) $MHCD2\text{-}O \rightarrow GLYOXAL + C5H6O2$ 8.8×10^3

TB12) $MHCD2\text{-}O + NO_2 \rightarrow MHCD2\text{-}ONO_2$ 2.36×10^3

TB13) $MHCD2\text{-}O_2 + MHCD2\text{-}O_2 \rightarrow 2\ MHCD2\text{-}O + O_2$ 3×10^{-11}

    5×10^{-15}

Inorganic Reactions

1) $NO_2 + HV \rightarrow NO + O$ PHOT. $= NO_2$

2) $O + O_2 + M \rightarrow O_3 + M$ 6.093×10^{-34}

3A) $O + NO_2 \rightarrow NO + O_2$ 6.459×10^{-12}

3B) $O + NO_2 \rightarrow NO_3 + M$ FALLOFF F= 0.600, N= 1.000

    K0: 3.232×10^{-03} 0.00 -4.000

    KI: $3.229\times110^{+04}$ 0.00 -1.000

4) $O_3 + NO \rightarrow NO_2 + O_2$ 1.977×10^{-12}

5) $O_3 + NO_2 \rightarrow O_2 + NO_3$ 1.379×10^{-13}

6) $NO + NO_3 \rightarrow 2\ NO_2$ 1.690×10^{-11}

7) $NO + NO + O_2 \rightarrow 2\ NO_2$ 3.284×10^{-39}

8) $NO_2 + NO_3 \rightarrow N_2O_5$ FALLOFF F= 0.600, N= 1.000

    K0: $7.901\times10^{+02}$ 0.00 -6.300

    KI: $2.202\times10^{+03}$ 0.00 -1.500

9) $N_2O_5 + RCON8 \rightarrow NO_2 + NO_3$ 8.995×10^{26} x k_8

10) $N_2O_5 + H_2O \rightarrow 2\ HNO_3$ 9.933×10^{-22}

11) $NO_2 + NO_3 \rightarrow NO + NO_2 + O_2$ 4.946×10^{-15}

12A) $NO_3 + HV \rightarrow NO + O_2$ PHOT. $= NO_3NO$

12B) $NO_3 + HV \rightarrow NO_2 + O$ PHOT. $= NO_3NO_2$

13A) $O_3 + HV \rightarrow O + O_2$ PHOT. $= O_3O3P$

13B) $O_3 + HV \rightarrow O*1D2 + O_2$ PHOT. $= O_3O1D$

14) $O*1D2 + H_2O \rightarrow 2\ OH$ 2.185×10^{-10}

15) $O*1D2 + M \rightarrow O + M$ 1.907×10^{-11}

16) $OH + NO \rightarrow HONO$ FALLOFF F= 0.600, N= 1.000

		K0: $2.514 \times 10^{+02}$ 0.00 -4.600
		KI: $2.202 \times 10^{+04}$ 0.00 -1.500
17)	$HONO + HV \rightarrow OH + NO$	PHOT. = HONO
18)	$OH + NO_2 \rightarrow HNO_3$	FALLOFF F= 0.600, N= 1.000
		K0: $9.337 \times 10^{+02}$ 0.00 -5.200
		KI: $3.523 \times 10^{+04}$ 0.00 -2.300
19)	$OH + HNO_3 \rightarrow H_2O + NO_3$	6.425×10^{-15}
20)	$HNO_3 + HV \rightarrow OH + NO_2$	PHOT. = HNO_3
21)	$OH + CO \rightarrow HO_2 + CO_2$	2.384×10^{-13}
22)	$OH + O_3 \rightarrow HO_2 + O_2$	1.584×10^{-12}
24)	$HO_2 + NO_2 \rightarrow HNO_4$	FALLOFF F= 0.600, N= 1.000
		K0: $6.464 \times 10^{+03}$ 0.00 -5.200
		KI: $6.899 \times 10^{+03}$ 0.00 -2.400
25)	$HNO_4 + RCON24 \rightarrow HO_2 + NO_2$	4.558×10^{26} x k_{24}
27)	$HNO_4 + OH \rightarrow H_2O + NO_2 + O_2$	1.293×10^{-12}
28)	$HO_2 + O_3 \rightarrow OH + 2 O_2$	1.091×10^{-14}
29A)	$HO_2 + HO_2 \rightarrow HO_2H + O_2$	2.190×10^{-13}
29B)	$HO_2 + HO_2 + M \rightarrow HO_2H + O_2$	1.894×10^{-33}
29C)	$HO_2 + HO_2 + H_2O \rightarrow HO_2H + O_2 + H_2O$	3.109×10^{-34}
29D)	$HO_2 + HO_2 + H_2O \rightarrow HO_2H + O_2 + H_2O$	2.682×10^{-54}
30A)	$NO_3 + HO_2 \rightarrow HNO_3 + O_2$	SAME K AS 29A
30B)	$NO_3 + HO_2 + M \rightarrow HNO_3 + O_2$	SAME K AS 29B
30C)	$NO_3 + HO_2 + H_2O \rightarrow HNO_3 + O_2 + H_2O$	SAME K AS 29C
30A)	$NO_3 + HO_2 + H_2O \rightarrow HNO_3 + O_2 + H_2O$	SAME K AS 29D
31)	$HO_2H + HV \rightarrow 2 OH$	PHOT. = H_2O_2
32)	$HO_2H + OH \rightarrow HO_2 + H_2O$	3.276×10^{-12}
33)	$OH + HO_2 \rightarrow H_2O + O_2$	4.573×10^{-11}

Table 5.8: *m*-xylene Mechanism

No.	Reaction	Rate Constant, 298 K
		(cm^3, molecule, s units)
Methyl Nitrite Photolysis		
MN1)	CH$_3$ONO+ HV $\rightarrow$ CH$_3$O + HCHO	Experiment
MN2)	CH$_3$O + O$_2$ $\rightarrow$ HCHO + HO$_2$	1.9x10^{-15}
MN3)	HO$_2$ + NO $\rightarrow$ OH + NO$_2$	3.7x10^{-12}
Primary Reactions of m-*xylene*		
XB1)	OH + MXYL $\rightarrow$ DMHCD	2.3x10^{-11}
XB2a)	DMHCD + O$_2$ $\rightarrow$ HO$_2$ + DMPHEN	2x10^{-16}
XB2b)	DMHCD + O$_2$ $\rightarrow$ DMHCD-O$_2$	1x10^{-12}
XB3a)	DMHCD + NO$_2$ $\rightarrow$ NMXYL + H2O	See text
XB3b)	DMHCD + NO$_2$ $\rightarrow$ Products	See text
XB4)	DMHCD-O$_2$ + NO $\rightarrow$ DMHCD-O + NO$_2$	8.9x10^{-12}
XB5)	DMHCD-O + O$_2$ $\rightarrow$ PRODUCT1 + HO$_2$	7x10^{-15}
XB6)	DMHCD-O + NO$_2$ $\rightarrow$ DMHCD-ONO$_2$	3.8x10^{-11}
XB7)	DMHCD-O$_2$ + DMHCD-O$_2$ $\rightarrow$ 2 DMHCD-O + O$_2$	5x10^{-15}
XB8)	DMHCD-O$_2$ $\rightarrow$ BCYLRAD	8x10^4
XB9)	BCYLRAD + O$_2$ $\rightarrow$ DMHC2-O$_2$	1x10^{-12}
XB10)	DMHC2-O$_2$ + NO $\rightarrow$ NO$_2$ + DMHC2-O	8.9x10^{-12}
X11a)	DMHC2-O $\rightarrow$ METHGLY + C5H6O2	9x10^2
X11b)	DMHC2-O $\rightarrow$ GLYOXAL + C6H8O2	2.45x10^2
XB12)	DMHC2-O + NO$_2$ $\rightarrow$ DMHC2-ONO$_2$	3.8x10^{-11}
XB13)	DMHC2-O$_2$ + DMHC2-O$_2$ $\rightarrow$ 2 DMHC2-O + O$_2$	5x10^{-15}
XA1)	OH + MXYL $\rightarrow$ MXY- + H$_2$O	7.2x10^{-13}
XA2)	MXY- + O$_2$ $\rightarrow$ MXY-O$_2$	1.0x10^{-12}

XA3) $MXY-O_2 + NO \rightarrow NO_2 + MXY-O$ $8.01x10^{-12}$

XA4) $MXY-O_2 + NO \rightarrow MXY-ONO_2$ $0.89x10^{-12}$

XA5) $MXY-O + O_2 \rightarrow HO_2 + MTOLALD$ $9.5x10^{-15}$

XA6a) $MXY-O + NO_2 \rightarrow MXY-ONO_2$ $3.8x10^{-11}$

XA6b) $MXY-O + NO \rightarrow MXY-ONO$ $3.8x10^{-11}$

XA7) $MXY-O_2 + MXY-O_2 \rightarrow 2\ MXY-O + O_2$ $2.5x10^{-13}$

Inorganic Reactions

Same as in the Toluene mechanism.

Table 5.9: *p*-xylene Mechanism

No.	Reaction	Rate Constant, 298 K
		(cm^3, molecule, s units)
	Methyl Nitrite Photolysis	
MN1)	CH$_3$ONO+ HV $\rightarrow$ CH$_3$O + HCHO	Experiment
MN2)	CH$_3$O + O$_2$ $\rightarrow$ HCHO + HO$_2$	1.9x10^{-15}
MN3)	HO$_2$ + NO $\rightarrow$ OH + NO$_2$	3.7x10^{-12}
	p-*xylene Mechanism*	
XB1)	OH + PXYL = DMHCD	1.36x10^{-11}
XB2)	DMHCD + O$_2$ $\rightarrow$ HO$_2$ + DMPHEN	2x10^{-16}
XB3a)	DMHCD + NO$_2$ $\rightarrow$ NPXYL + H2O	4x10^{-11}
XB3b)	DMHCD + NO$_2$ $\rightarrow$ DMPHEN + HONO	3x10^{-11}
XB4a)	DMHCD + O$_2$ $\rightarrow$ DMHCD-O$_2$	1x10^{-12}
XB4b)	DMHCD-O$_2$ $\rightarrow$ DMHCD + O$_2$	6x10^6
XB5)	DMHCD-O$_2$ + NO $\rightarrow$ DMHCD-O + NO$_2$	8.9x10^{-12}
XB6)	DMHCD-O + O$_2$ $\rightarrow$ PRODUCT1 + HO$_2$	7x10^{-15}
XB15)	DMHCD-O + NO$_2$ $\rightarrow$ DMHCD-ONO$_2$	3.8x10^{-11}
XB7)	DMHCD-O$_2$ + DMHCD-O$_2$ $\rightarrow$ DMHCD-O + DMHCD-O	5x10^{-15}
XB8)	DMHCD-O$_2$ $\rightarrow$ BCYLRAD	8x10^4
XB9)	BCYLRAD + O$_2$ $\rightarrow$ DMHC2-O$_2$	1x10^{-12}
XB10)	DMHC2-O$_2$ + NO $\rightarrow$ NO$_2$ + DMHC2-O	8.9x10^{-12}
X11a)	DMHC2-O $\rightarrow$ METHGLY + C5H6O2	9x10^2
X11b)	DMHC2-O $\rightarrow$ GLYOXAL + C6H8O2	2.45x10^2
XB12)	DMHC2-O + NO$_2$ $\rightarrow$ DMHC2-ONO$_2$	3.8x10^{-11}
XB13)	DMHC2-O$_2$ + DMHC2-O$_2$ $\rightarrow$ 2 DMHC2-O + O$_2$	5x10^{-15}
XA1)	OH + PXYL $\rightarrow$ PXY- + H$_2$O	7.2x10^{-13}

XA2)	PXY- + O_2 → PXY-O_2	1.0×10^{-12}
XA3)	PXY-O_2 + NO → NO_2 + PXY-O	6.3×10^{-12}
XA4)	PXY-O_2 + NO → PXY-ONO_2	0.7×10^{-12}
XA5)	PXY-O + O_2 → HO_2 + PTOLALD	7.0×10^{-15}
XA6)	PXY-O + NO_2 → PXY-ONO_2	1.5×10^{-11}
XA7)	PXY-O_2 + PXY-O_2 → 2 PXY-O + O_2	2.5×10^{-13}

Inorganic Reactions

Same as in the Toluene mechanism.

5.4.1 Aromatic-OH Adduct Reaction with O_2

The overall rate constant, k_2, for O_2 reaction with the MHCD radical has been estimated [6, 13]. Direct measurements of the O_2 reaction of hydroxy-cyclohexadienyl and methylhydroxycyclohexadienyl radicals have been made, and estimates of the rate constant are $2x10^{-16}$ and $5x10^{-16}$ $cm^3molecule^{-1}s^{-1}$, respectively[13]. Direct measurements of the dimethylhydroxycyclohexadi-enyl (DMHCD) radical reaction with O_2 have not been conducted, but an indirect estimate of the rate constant of this reaction is $2.3x10^{-16}$ cm^3 $molecule^{-1}$ s^{-1}[6].

To determine the overall rate constant for the DMHCD $+O_2$ reaction, product yields predicted by the mechanism for each aromatic were compared to those determined experimentally as the value for k_2 was varied between $1x10^{-16}$-$1x10^{-15}$ $cm^3molecule^{-1}s^{-1}$. It should be noted that the value used for k_3, the rate constant for the aromatic-OH adduct reaction with NO_2, was 3×10^{-11} $cm^3molecule^{-1}s^{-1}$, as will be discussed in the subsequent section. Resulting yield data were plotted versus average NO_2 concentration. The branching ratio, $R1 = \frac{k_{2a}}{k_{2b}}$, was estimated from experimental data as the ratio of the yield of phenolic compounds to the sum of the methyl glyoxal and glyoxal yields. Average branching ratios for the rate constant of reaction 2 for toluene, m-xylene, and p-xylene, determined by averaging the R1 values of all of our experimental data for each aromatic, were 0.78, 0.20, and 0.36, respectively. The lines in Figures 5.5- 5.7 and 5.9-5.11 are the yields predicted by the mechanisms using the best fit DMHCD radical $+ O_2$ rate constant of approximately $2x10^{-16}$ $cm^3molecule^{-1}s^{-1}$. This value is in agreement with

the estimate of k_2 of Atkinson et al. [6] for o-xylene. The rate constant of the MHCD + O_2 reaction from toluene photooxidation, determined by best fits to the experimental data, is approximately $1\text{x}10^{-16}$ cm^{3}molecule^{-1}s^{-1}. This value is somewhat lower than the direct measurements of Knispel et al. [13] of $5\text{x}10^{-16}$ cm^{3}molecule^{-1}s^{-1}. Figures 5.2- 5.4 show the results of the mechanism predictions for products formed from toluene photooxidation.

5.4.2 Aromatic-OH Adduct Reaction with NO$_2$

The NO$_2$ pathway, reaction 3 in Figure 5.12, was assumed to have an overall rate constant of $3\text{x}10^{-11}$ cm^{3}molecule^{-1}s^{-1}[4]. If it is assumed that the NO$_2$ pathway proceeds to exclusively form the nitroaromatic compound, then nitroaromatic yields are obtained that are an order of magnitude higher than those measured in the present or in previous studies. This can clearly be seen in Figure 5.13 where the results of the mechanism predicting the exclusive formation of the nitroaromatic (k_3=$3\text{x}10^{-11}$ cm^{3}molecule^{-1}s^{-1}) are compared to that which produces the best fit of the nitro-m-xylene data, with k_3=$3\text{x}10^{-12}$ cm^{3}molecule^{-1}s^{-1}. Because this value has been determined experimentally, we must conclude that there is an additional pathway involving the substituted MHCD radicals and NO$_2$. This conclusion is consistent with the results of the *ab initio* calculations of Andino et al. [5], and the data of Atkinson et al.[6]. The branching ratio, $\frac{k_{3a}}{k_{total}}$, is determined by fitting the experimental and predicted values of nitro-m-xylene formed in the photooxidation of m-xylene while varying k_{3a}. Results indicate a branching ratio, $\frac{k_{3a}}{k_{total}}$ of approximately 0.1, consistent with the data of Atkinson et al.

[6].

Several pathways have been suggested for the reaction of the aromatic-OH adduct with NO_2 [5, 6]. The recent theoretical study of Andino et al. [5] has narrowed the possible pathways down to the four that are represented in Figure 5.12 as reactions 3a-d, based on calculations using toluene as an example. Possible pathways for the aromatic-OH adduct-NO_2 reaction were evaluated based on barrier heights and overall ΔH_{rxn} [5]. The ΔH_{rxn} for the first steps of pathways 3a-3c, and overall pathways 3d and 3e for toluene are -26.3, -26.3, -24.5, -52.8, and +38.3 kcal/mol, respectively. The barrier heights for pathways 3a,b (first step), 3c (first step), and 3d are 5, 1, 2 kcal/mol, respectively. Note that Reactions 3c and 3e are assumed to have the same transition state. Based on this information for the intial steps of Reactions 3a-3c, and the overall Reactions 3d and 3e, the only pathway that can be unambiguously excluded is Reaction 3e, because of its endothermic nature. The decreasing yield of phenolic compounds observed in the present experimental study as average $[NO_2]$ increases is not consistent with a significant pathway for phenolic compound formation from aromatic-OH adduct reaction with NO_2, namely, reaction 3d. The study of Atkinson et al. [6], which examined the effect of NO_2 on the phenolic compound yield only from the toluene reaction, suggest a slight increase in phenolic compound yield as $[NO_2]$ increases. The hydroxy nitroaromatics are products of phenolic compound reaction with OH radicals, thus, it is impossible to determine the contribution of hydroxy nitroaromatics resulting from Reaction 3 by experiment alone.
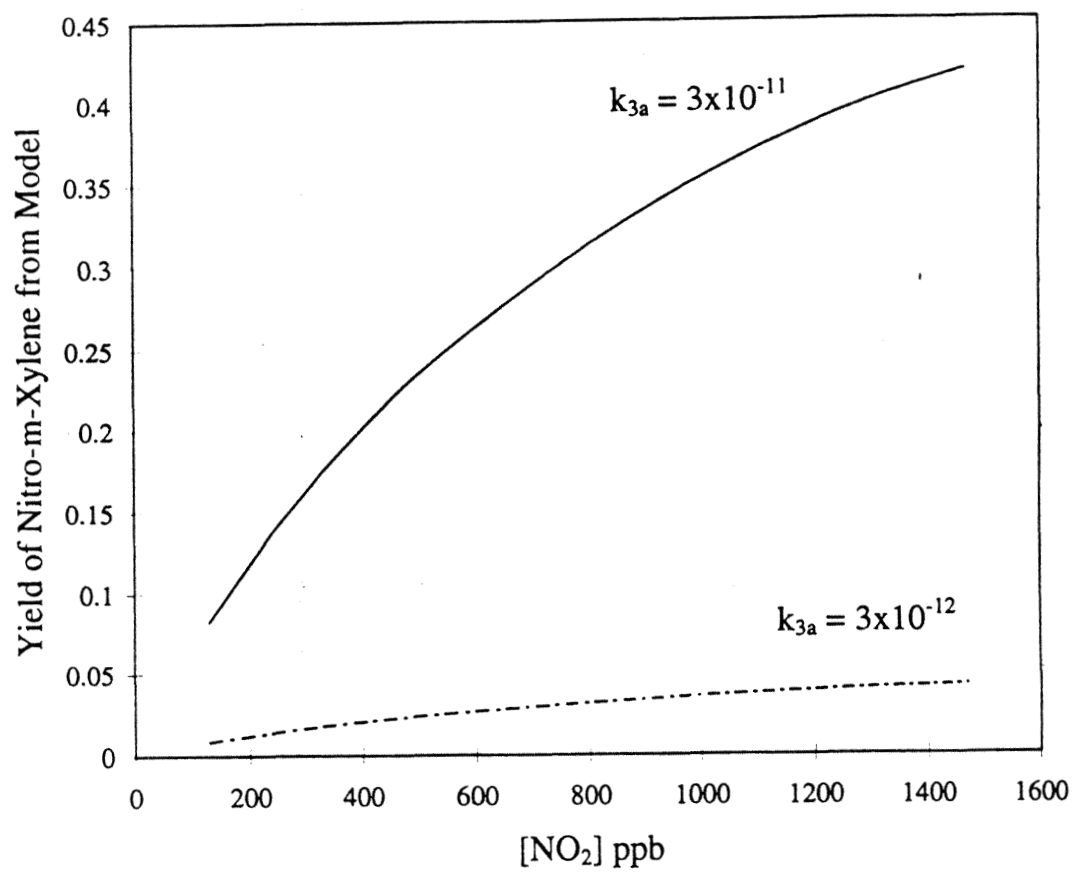
Figure 5.13: Nitro-m-xylene formation simulated based on two assumed values of the rate constant k_{3a}.

5.4.3 Ring Fragmentation Products

Andino et al. [5] showed that each bicyclic oxy radical (generalized structure shown in Reaction 8 of Figure 5.12) isomer for toluene, m- and p-xylene leads to the formation of either glyoxal and a larger ring fragmentation product, or methyl glyoxal and another large ring fragmentation product. The relative formation yields of each of these bicyclic oxy radical isomers is not known, but since each isomer is believed to lead either to glyoxal or methyl glyoxal, a rate constant ratio can be determined for the decomposition step from the glyoxal and methyl glyoxal yields. An estimate of the decomposition rate constant for the bicyclic oxy radicals (Reaction 8 of Figure 5.12) leading to the formation of methyl glyoxal is made by analogy with alkoxy radicals that decompose to form a secondary alkyl radical and a carbonyl compound[14]. On this basis, the rate constant for $k_{8a} = 8.8 \times 10^3$ s^{-1}. The ratio, R2=k_{8a}/ k_{8b}, is assumed to be equal to the ratio, [Methyl Glyoxal]/[Glyoxal]. The R2 values for toluene, m-xylene, and p-xylene are determined from the data as 0.68, 3.72, and 0.45, respectively, and the resulting rate constants for each step appear in the mechanisms. These values for R2 are in excellent agreement with those calculated from literature data [4].

5.5 Implications for Atmospheric Aromatic Photooxidation Mechanisms

The present work serves to support the recent work of Atkinson et al.[6] and Knispel et al.[13] concerning the kinetics of the reaction of the aromatic-OH

adduct with O_2. In addition, we have shown a clear effect of NO_2 on the products formed in the addition pathway of aromatic reactions. However, if the relative atmospheric concentrations of NO_2 and O_2 are considered, it is clear that the aromatic-OH adduct reaction with NO_2 is negligible under atmospheric conditions. Under the typically high NO_2 conditions of laboratory chamber studies, the reactions of NO_2 with the aromatic-OH adduct are, however, significant. Nitroaromatic formation only accounts for approximately 10% of the aromatic-OH reaction with NO_2. This point is reflected in Tables 7, 8, and 9 for each of the aromatics studied in this work.

Acknowledgements

Bibliography

[1] Lurmann, F.W. and Main, H.H., "Analysis of the Ambient VOC Data Collected in the Southern Air Quality Study," Final Report, Contract No. A832-130. State of California Air Resources Board, Sacramento, 1992.

[2] National Research Council, "Rethinking the Ozone Problem in Urban and Regional Air Pollution", National Academy Press, Washington D.C. , 1991.

[3] Atkinson, R., J. Phys. Chem. Ref. Data., 1989, Monograph 1,1.

[4] Atkinson, R., J. Phys. Chem. Ref. Data, 1994, Monograph 2, 1.

[5] Andino, J.M., Smith, J.N., Flagan, R.C., Goddard III, W.A., Seinfeld, J.H., J.Phys. Chem., 1995, Submitted for publication.

[6] Atkinson, R., Aschmann, S.M, Int. J. Chem. Kinet., 1994, 26, 929.

[7] Atkinson, R. , Aschmann, S.M., Arey, J., Shorees, B. J. Geophys. Res., 1992, 97, 6065.

[8] Grosjean,D., Williams,E.L., Seinfeld, J.H., *Env. Sci. Tech.*, **1992**, *26*, 1526.

[9] Hakola, H., Arey, J., Aschmann, S.M., Atkinson,R., *J. Atmos. Chem.* , **1994**, *18*, 75.

[10] Druzik, C.M., Grosjean,D., Van Neste, A., Parmar, S.S., *Int. J. Environ. Anal. Chem.*, **1990**, *38*, 495.

[11] Atkinson, R., Aschmann,S.M., Carter,W.P.L., Winer,A.M., Pitts Jr., J.N., *J.Phys. Chem.*, **1982**, *86*, 4563.

[12] Carter, W.P.L.. Documentation for the SAPRC Atmospheric Photochemical Mechanism Preparation and Emissions Processing Programs for Implementation in Air-Shed Models, California Air Resources Board, Contract No. A5-122-32, October 1988.

[13] Knispel,R., Koch,R., Siese,M., Zetzsch,C., *Ber. Bunsenges. Phys. Chem.*, **1990**, *94*, 1375.

[14] Atkinson, R., *Atmos. Environ.*, **1990**, *24A*, 1.

[15] Tuazon, E., Mac Leod, H., Atkinson, R., Carter, W.P.L. , *Environ. Sci. Tech.*, **1986** *20*, 383.

[16] Dumdei, B., Kenny, D., Shepson, P.B., Kleindienst, T.E., Nero, C., Cupitt, L., Claxton,, L., *Environ. Sci. Tech.*, **1988**, *22*, 1493.

[17] Bandow, H., Washida,N., Akimoto, H., *Bull. Chem. Soc. Jpn.*, **1985**, *58*, 2531.

[18] Shepson,P.B, Edney,E.O., Corse,E. , *J. Phys. Chem.*, **1984**, *88*, 4122.

[19] Atkinson,R. Aschmann,S.M, Arey, J., Carter,W.P.L., *Int. J. Chem. Kinet.*, **1989**, *21*, 801.

[20] Bandow,H., Washida,N., *Bull. Chem. Soc. Jpn.*, **1985**, *58*, 2541.

[21] Gery,M.W., Fox,D., Kamens,R.M.., Stockburger,L., *Environ. Sci. Technol.*, **1987**, *21*, 339.

[22] Atkinson,R., Aschmann,S.M., Arey, J., *Int. J.Chem. Kinet.*, **1991**, *23*, 77.

Chapter 6

Photooxidation of m-Ethyltoluene and 1,2,4 Trimethylbenzene: A Product Study

Abstract

The OH-initiated photooxidaton of 1,2,4-trimethylbenzene and *m*-ethyltoluene have been investigated in the Caltech Indoor Photochemical Reactor. These studies are the first studies of the products resulting from *m*-ethyltoluene photooxidation, and are the only studies reporting ring retaining products for the 1,2,4-trimethylbenzene system. Products identified from the *m*-ethyltoluene system include acetaldehyde, glyoxal, methyl glyoxal, 2-ethyl-4-methylphenol, 4-ethyl-2-methylphenol, 1-(3-methylphenol) ethanone, 3-methyl benzaldehyde, and ethylbenzaldehyde. Products identified from 1,2,4-trimethylbenzene photooxidation include acetaldehyde, glyoxal, methyl glyoxal, 2,4- dimethylbenzaldehyde, 3,4- dimethylbenzaldehyde, 2,5- dimethylbenzaldehyde, 2,3,6-trimethylphenol, and 2,4,5-trimethylphenol.

6.1 Introduction

Aromatics are an important class of compounds in urban air. Notably, in the Southern California Air Quality Study of 1987, aromatics were found to compromise approximately 25% of the carbon in the south coast air basin.[1] The aromatics that are focused on in this study, m-ethyltoluene and 1,2,4-trimethylbenzene, were found to be in the top 25 of the most abundant species (based on carbon) during the summer and fall episodes, respectively, of the SCAQS study. Despite the prevalence of these compounds in the atmosphere and their importance in ozone formation, the reaction mechanisms of these species are one of the greatest uncertainties in atmospheric chemical models[2]. Aromatics are capable of reacting with OH radicals, O_3 and NO_3. However, the major atmospheric sink of these species is reaction with the OH radical. The OH rate constants for m-ethyltoluene and 1,2,4-trimethylbenzene are 1.92×10^{-11} and 3.25×10^{-11} $cm^3 molecule^{-1} s^{-1}$, respectively [4].

Approximately 10% of the hydroxyl radical reaction with an aromatic proceeds via the abstraction route, the remainder by addition[4]. The abstraction route produces ring-retaining products such as aromatic aldehydes and nitrated compounds. The first step in the abstraction channel of toluene (as an example) is shown in Figure 6.1. The addition route results in ring fragmentation products such as dicarbonyls and ring-retaining products such as nitroaromatics and phenols. The results of two previous studies identifying some of the ring fragmentation products resulting from the photooxidation of 1,2,4-trimethylbenzene are presented in Table 6.1. In general, addition to

Table 6.1: 1,2,4 Trimethylbenzene Photooxidation Products: Molar Yields

Compound	Yield	Reference
Formaldehyde	0.18 ± 0.01	[6]
Glyoxal	0.078 ± 0.005	[6]
	0.048 ± 0.005	[7]
Methylglyoxal	0.37 ± 0.01	[6]
	0.357 ± 0.017	[7]
Biacetyl	0.11 ± 0.01	[6]
3-Hexene-2,5 dione	Detected	[6]

the aromatic ring occurs at positions meta to the carbon that is substituted with an electron donating group[5]. The first step in the OH addition channel of toluene, as an example, is shown in Figure 6.1.

Molecular oxygen and NO_2 can react with the resulting substituted methyl-hydroxycyclohexadienyl (MHCD) radical. Present indications are that the O_2 pathway proceeds via two routes: addition to form a peroxy radical and abstraction to form a phenolic type compound. The peroxy radical stabilizes itself by cyclicizing. The cyclized radical adds oxygen, forming another peroxy radical which subsequently undergoes a series of favorable β scission reactions to form ring fragmentation products. Recently, through *ab initio* calculations, Andino et al. [5] identified the favored intermediate species formed in the OH-initiated photooxidation of several aromatic comounds, including *m*-ethyltoluene and 1,2,4-trimethylbenzene, and examined their ring fragmentation pathways. The experimental results presented in this paper are directly compared to those predicted by the *ab initio* calculations of Andino et al. [5] for the addition pathways of aromatics, and to proposed mechanisms, based on current knowledge [4], for the abstraction pathways.
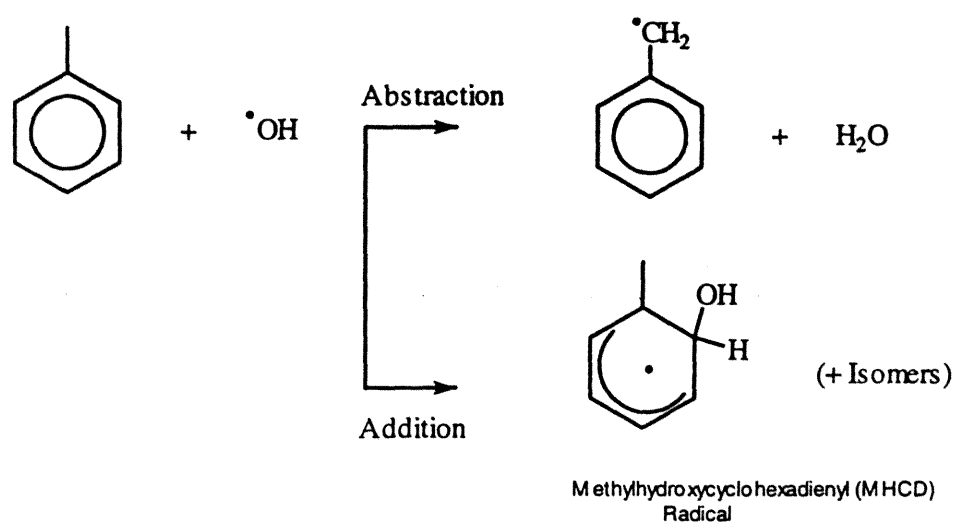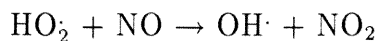
Figure 6.1: Initial reactions of the OH-initated reaction of toluene.

6.2 Experimental

The Caltech Indoor Photochemical Reactor has been described in detail elsewhere[1]. Briefly, the chamber is a 1 m^3 reactor composed of 2 mil FEP Teflon. Artificial light (two banks of 24 Sylvania F30T8BL black lamps) is used to initiate the chemistry within the chamber. The lamps are mounted on a cylindrical surface to provide for uniformity in irradiation. The light intensity within the chamber can be adjusted by varying the number of lamps that are used (minimum of 2 lamps, and maximum of 48 lamps). Typical irradiation times for 1,2,4-trimethylbenzene and m-ethyltoluene were 1-3 min. and 0.5-4 min., respectively.

To study the hydroxyl radical-aromatic reactions in the presence of NO$_x$, methyl nitrite was introduced to the chamber along with the aromatic of interest via a calibrated glass vacuum manifold. Methyl nitrite generates OH radicals according to the following reactions:

$$CH_3ONO + h\nu \rightarrow CH_3O^{\cdot} + NO$$
$$CH_3O^{\cdot} + O_2 \rightarrow HCHO + HO_2$$
$$HO_2^{\cdot} + NO \rightarrow OH^{\cdot} + NO_2$$
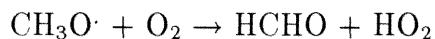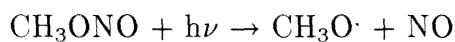
In order to minimize ozone production, and maximize the conversion of peroxy radicals to alkoxy radicals, NO was added to the chamber. Typical starting mixing ratios were 4-5 ppm aromatic, 1-5 ppm CH$_3$ONO, and 1 ppm NO. 1,2,4-Trimethylbenzene and m-ethyltoluene were obtained from Aldrich with stated purities of 99+%, 99+%. All were used without further purification.

---

[1]See Chapter 2.

Nitric oxide was taken from a standard cylinder (generated by Scott-Marin). Methyl nitrite was prepared by the dropwise addition of 50% sulfuric acid to a saturated methanol/sodium nitrite solution [8]. Using high purity N_2, the resulting gas was bubbled through a NaOH solution to neutralize the acid, and then passed through $CaCl_2$ to dry it. The nitrite was trapped in a bulb which was immersed in a dry ice/ethanol slush bath, purified using a vacuum manifold, and stored at liquid N_2 temperatures.

To study the aromatic-OH reactions in the absence of NO_x, ozone- olefin reactions were used to generate OH radicals. The olefin-ozone reaction has been shown to yield significant amounts of hydroxyl radicals.[9] α-Pinene was chosen because its photooxidation products have been reasonably well charaterized, and it produces a high yield of OH radicals. [9] [10] [11].Hydroxyl radical yield from the ozone reaction is 0.85, much higher than other readily available alkenes and monoterpenes. Thus, dark reactions of ozone, α-pinene, and aromatic were conducted. The ozone was produced by an ozone generator (Enmett Inc.), and α-pinene was purchased from Aldrich with a stated purity of 99%. It was used without further purification.

The chamber was sampled periodically for analyses by the on-line ozone analyzer (Dasibi 1008) and NO_x analyzer (Thermo Environmental Model 42). Samples were also collected onto Tenax packed stainless steel tubes for desorption and subsequent analysis by GC-FID. Desorption was accomplished using a Tekmar Model 6000 Aerotrap desorber with an attached cryofocusing unit. The column used in the GC-FID was a J&W Scientific DB-5 column of dimension 30 m x 0.25 mm x 0.25 μm. The GC-FID oven temperature was held at 50° C for 1 min. and increased by 20° C/min. until a final tempera-

ture of 275° C. The oven was then held at 275° C for 1 min.. The GC-FID was calibrated for the aromatics by using standard cylinders (generated by Scott-Marrin) of each aromatic. Standard concentrations of the aromatic were introduced into a small (4 liter) teflon bag. Tube samples were taken from this bag, and analyzed in the same manner as the experimental samples.

At the end of each experiment, a sample from the chamber was collected on a 2,4-dinitrophenylhydrazine (DNPH) impregnated C_{18} cartridge. The samples were eluted using 3 ml of acetonitrile, and analyzed using a Hewlett Packard Model 1090 Series II liquid chromatograph, with a diode array detector. A reversed phase Axxiom LC column of dimension 0.5 μm x 150 cm was used to obtain adequate separation. HPLC grade acetonitrile and water were used as the solvents in a ratio of 55% to 45%, with a total flowrate of 1 ml/min. Typical observed pressures were between 109 and 112 mbar.

Authentic DNPH derivatized carbonyl standards for the LC were purchased from Radian Corporation for comparison to the experimental samples. Standards for DNPH-glyoxal and DNPH-methyl glyoxal were synthesized in our laboratory according to the method of Druzik et al. [12].

Additional experiments were conducted to positively identify additional products formed during the photoxidation of m-ethyltoluene and 1,2,4 trimethylbenzene from mass spectral data. Experiments were conducted in the same manner as indicated above. However, the tenax tube samples collected were desorbed into a Hewlett Packard GCD (Model G1800A). The column used was a HP5, of dimensions 30 m x 0.25 mm x 0.25 μm.

6.3 1,2,4-Trimethylbenzene Photooxidation

6.3.1 Ring-Retained Products

Each of the three substituent methyl groups of 1,2,4-trimethylbenzene are possible sites for OH abstraction of an H atom. The resulting radicals are expected to react with O_2 to form the corresponding ring-retained aromatic aldehydes[4]. Figure 6.2 details the abstraction channel for 1,2,4-trimethylbenzene. The LC chromatograms did not show any evidence for high molecular weight carbonyls. However, the GCD analyses, which were found to be more sensitive to the detection of products than the DNPH technique or the GC-FID analyses, showed positive evidence for the presence of 2,4-dimethylbenzaldehyde, 3,4-dimethylbenzaldehyde, and 2,5- dimethylbenzaldehyde. Shown in Figure 6.3 is a selected portion of a typical GCD chromatogram for 1,2,4-trimethylbenzene photooxidation. The mass spectral fingerprints of the detected dimethylbenzaldehydes were compared to the spectral library of the GCD (Wiley) for positive identification.

The results of *ab initio* calculations performed by Andino et al. [5] indicate that the preferred sites for OH addition to the ring of 1,2,4 trimethylbenzene are the 3- and 5-positions. Shown in Figure 6.4 are all of the possible reacton pathways for the trimethylhydroxycyclohexadienyl radical reaction with O_2 to form the trimethylphenols. Figure 6.3 shows positive evidence for the formation of only two phenolic compounds, 2,3,6-trimethylphenol and 2,4,5-trimethylphenol, consistent with the predictions based on theory of Andino et al. [5].
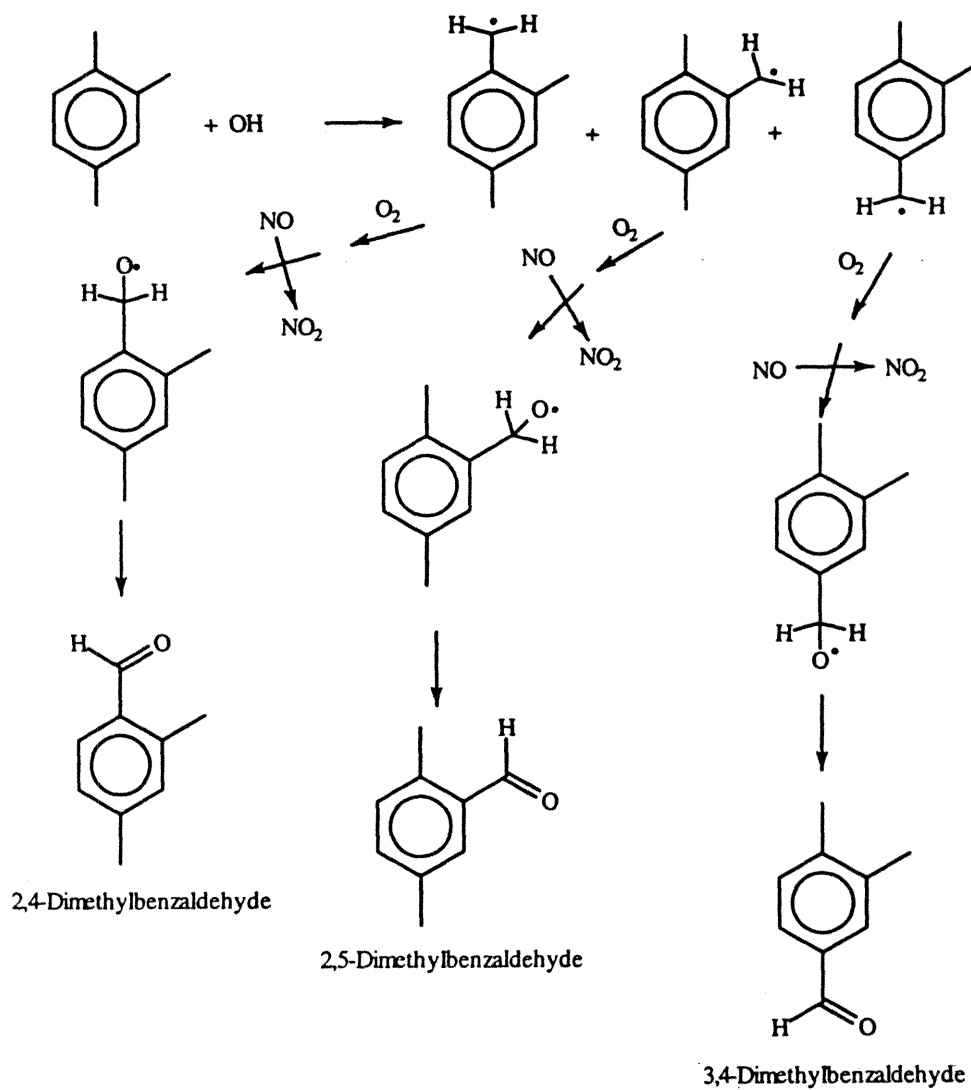
Figure 6.2: Abstraction pathway for 1,2,4-trimethylbenzene. Depicted are all of the possible radicals formed from the abstraction pathway of 1,2,4-trimethybenzene and their reactions with O_2 to form the corresponding aromatic aldehydes.

193

Figure 6.3: GCD chromatogram of products formed from the photooxidation of 1,2,4-trimethylbenzene. Depicted are the benzaldehydes and the trimethylphenols.

Figure 6.4: Pathways for the reaction of isomers of the trimethylhydroxycyclohexadienyl radical with O_2. Depicted are all of the possible trimethylphenols formed from each path.

6.3.2 Ring-Fragmentation Products and the NO$_2$ Effect

LC data show positive evidence for the formation of acetaldehyde, glyoxal, and methyl glyoxal. Methyl glyoxal and glyoxal have previously been identified as products of 1,2,4-trimethylbenzene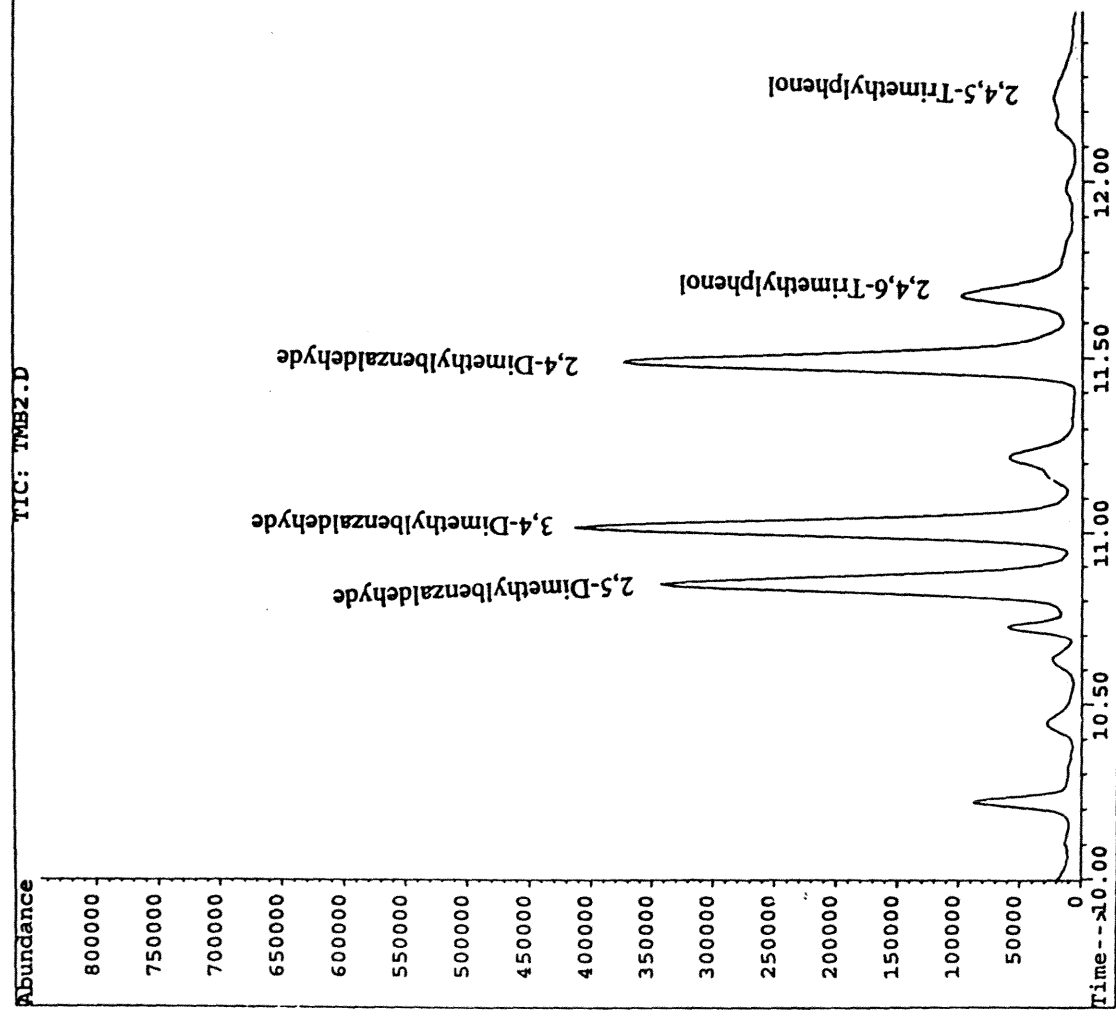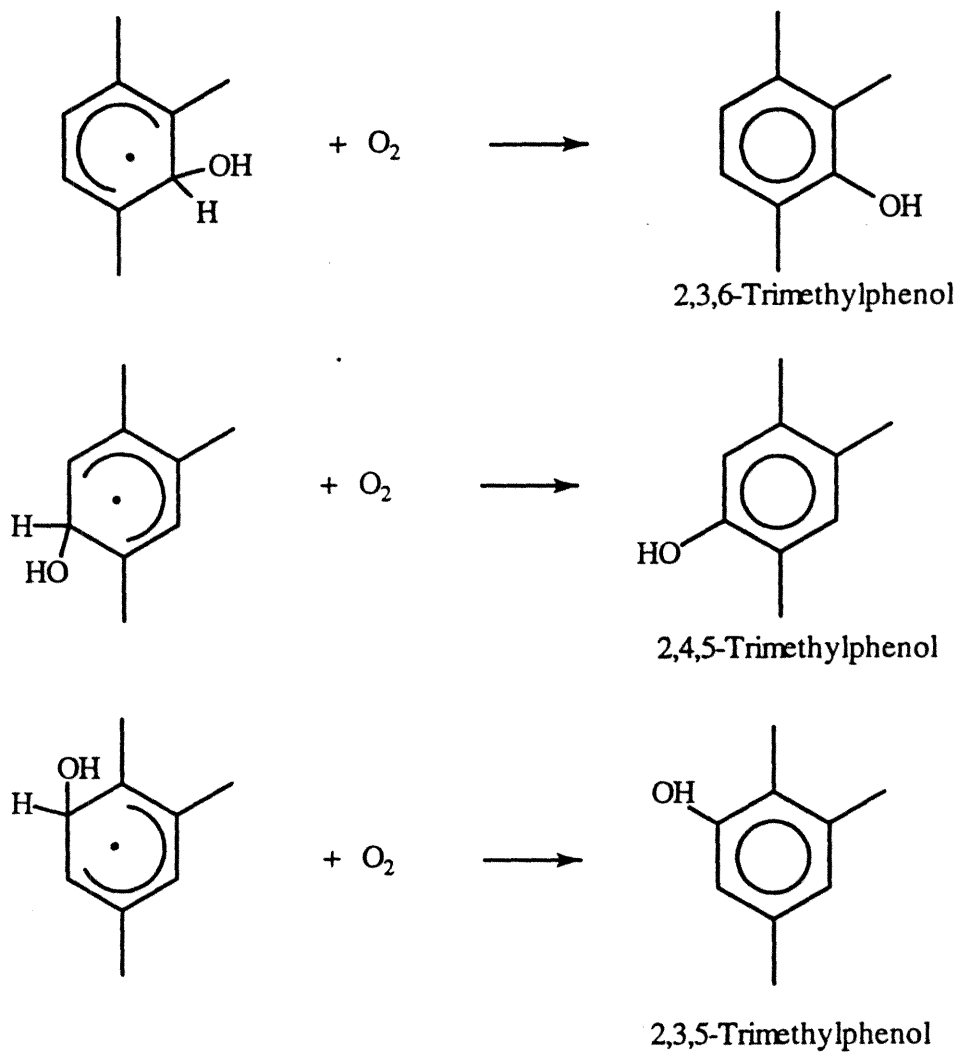 photooxidation (see Table 6.1 and references within). Both products are ring fragmentation products of the bicyclic peroxy radicals formed after intial OH addition to the ring [5]. Figure 6.5 shows the mechanisms of an initial 1,2,4-trimethylbenzene-OH adduct leading to the formation of methyl glyoxal. An analogous path exists for the formation of glyoxal. A path does not exist for the primary formation of acetaldehyde from 1,2,4-trimethylbenzene photooxidation, thus, it must be a result of secondary reaction.

The yields of glyoxal, methyl glyoxal, and acetaldehyde were determined by comparison with authentic DNPH-derivatized samples. Product yields were corrected for secondary reactions with OH according to the method of Atkinson et al. [13], using the following equation:

$$ F = \frac{k_1 - k_2}{k_1} \frac{1 - \frac{[Aromatic]_t}{[Aromatic]_o}}{\frac{[Aromatic]_t}{[Aromatic]_o}^{\frac{k_2}{k_1}} - \frac{[Aromatic]_t}{[Aromatic]_o}} \tag{6.1} $$

where k_1 and k_2 are the rate constants of the following reactions:

(1) Aromatic + OH $\rightarrow$ Product

(2) Product + OH $\rightarrow$ Secondary Products .

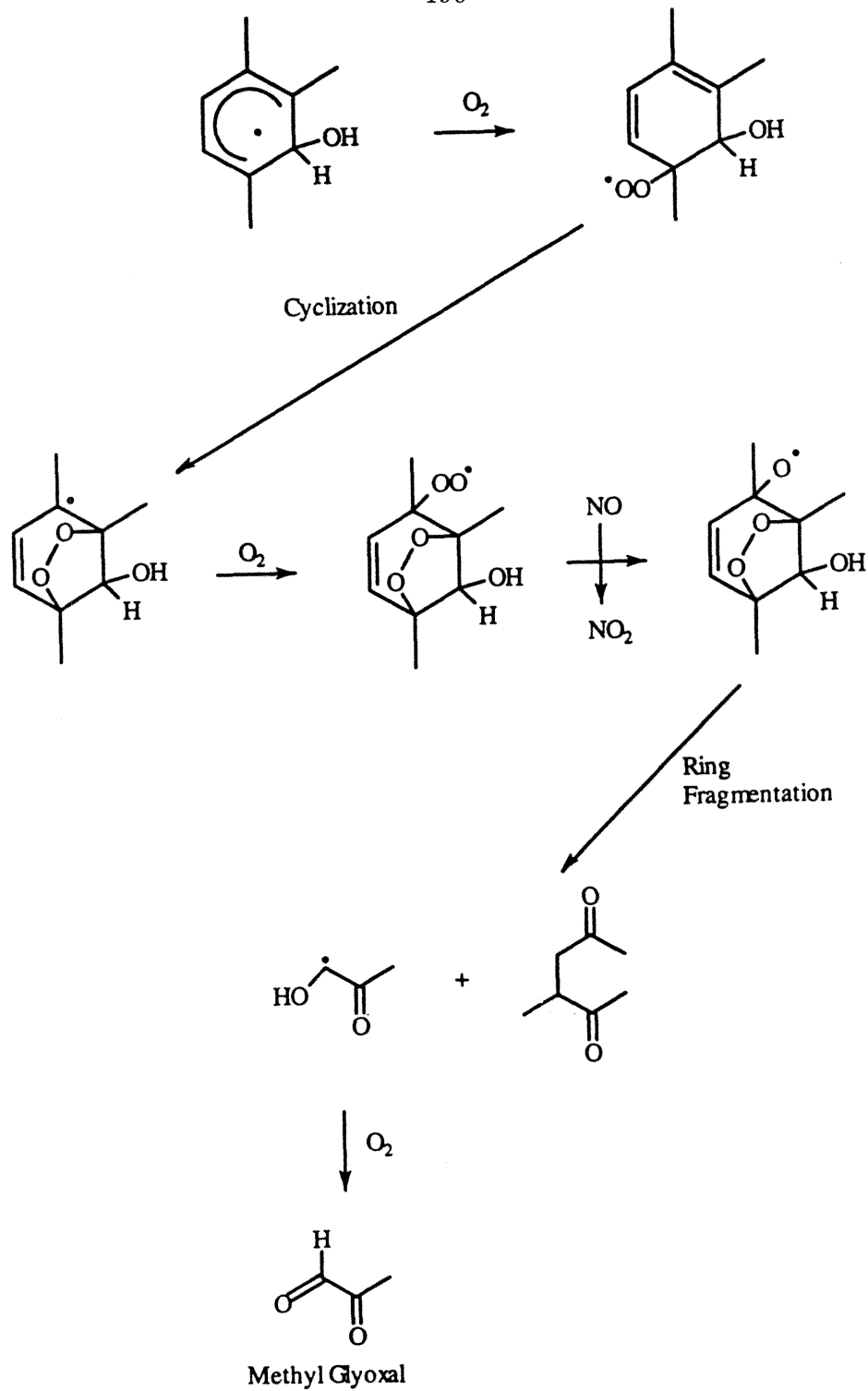Corrected yields were determined by multiplying the raw yields by the factor,

Figure 6.5: Depicted is the proposed mechanism for the formation of ring-fragmentation products from the photooxidation of 1,2,4-trimethylbenzene.

F. The rate constants for the ring fragmentation products, acetaldehyde, glyoxal, and methyl glyoxal are 1.58×10^{-11} [4], 1.14×10^{-11} [14], and 1.72×10^{-11} [14], respectively, with units of $cm^3 molecule^{-1} s^{-1}$.

Average NO_2 concentrations were determined using the following equation, incorporating the contribution of methyl nitrite photolysis and NO to NO_2 conversion to the total NO_2 concentration in the system:

$$\overline{[NO_2]} = \tfrac{1}{n} \sum_n ([CH_3ONO]_o (1 - e^{-ktn}) + \Delta[NO]_n)$$

where: k = photolysis rate constant for methyl nitrite, as measured experimentally, $\Delta[NO]_n = [NO]_o - [NO]_t$, and n = number of data points. Average NO_2 concentrations for 1,2,4-trimethylbenzene ranged from 200 to 800 ppb. Plots of yields of the ring-fragmentation products versus average $[NO_2]$ formed in 1,2,4-trimethylbenzene photooxidation are presented in Figures 6.6- 6.8. Note that the points at $[NO_2] = 0$ are from the ozone-α-pinene-1,2,4-trimethylbenzene experiments. From Figures 6.6- 6.8, a decrease in the yield of ring-fragmentation products is noticed as the average concentration of NO_2 increases, indicating the existence of a competing pathway for NO_2 reaction.
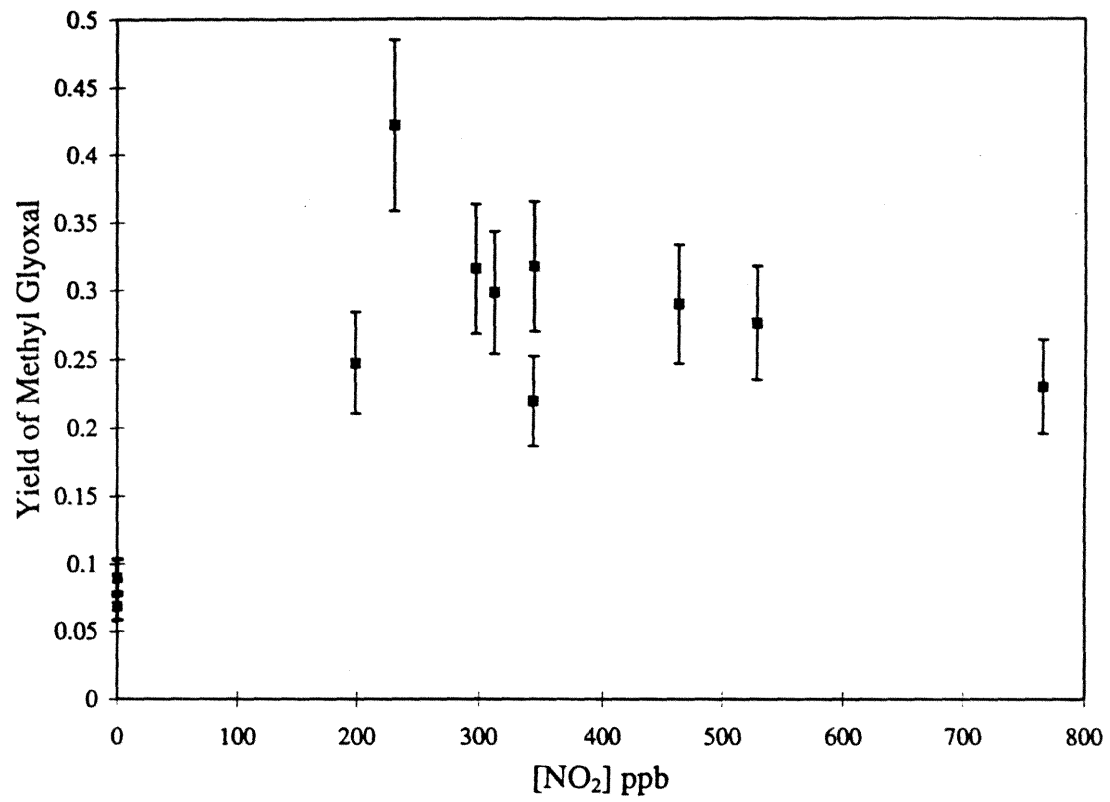
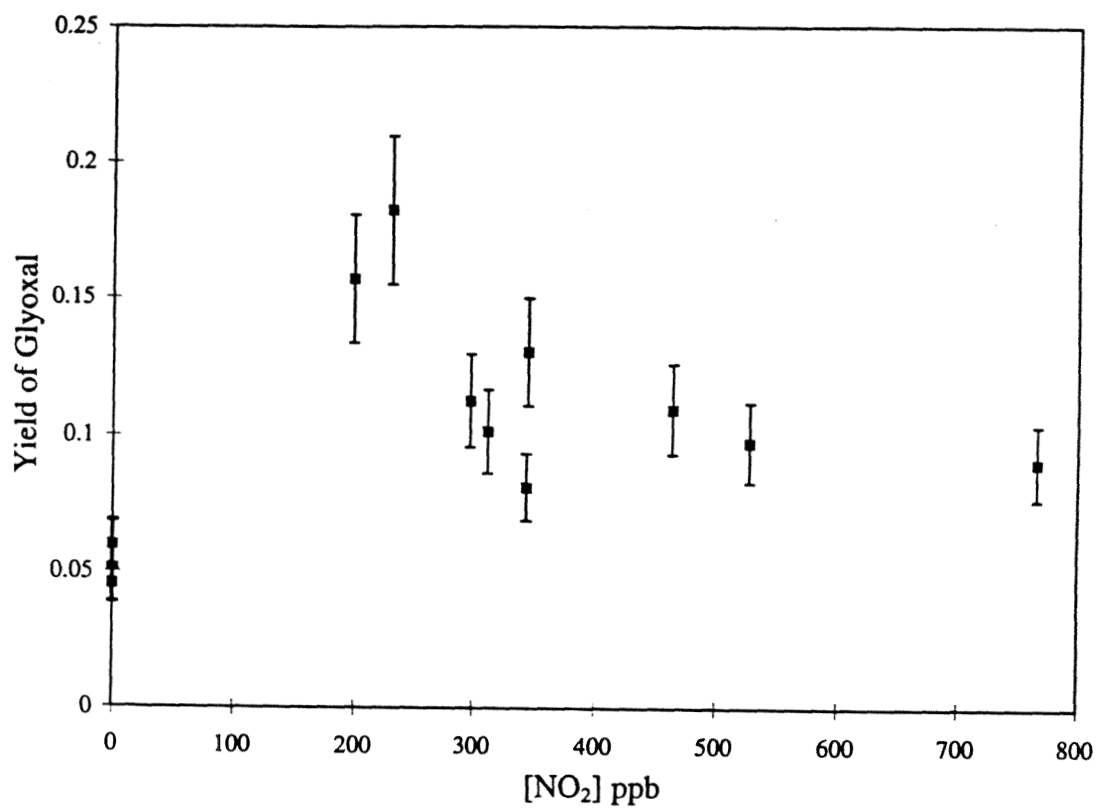Figure 6.6: 1,2,4 Trimethylbenzene Photooxidation Results: Methyl Glyoxal

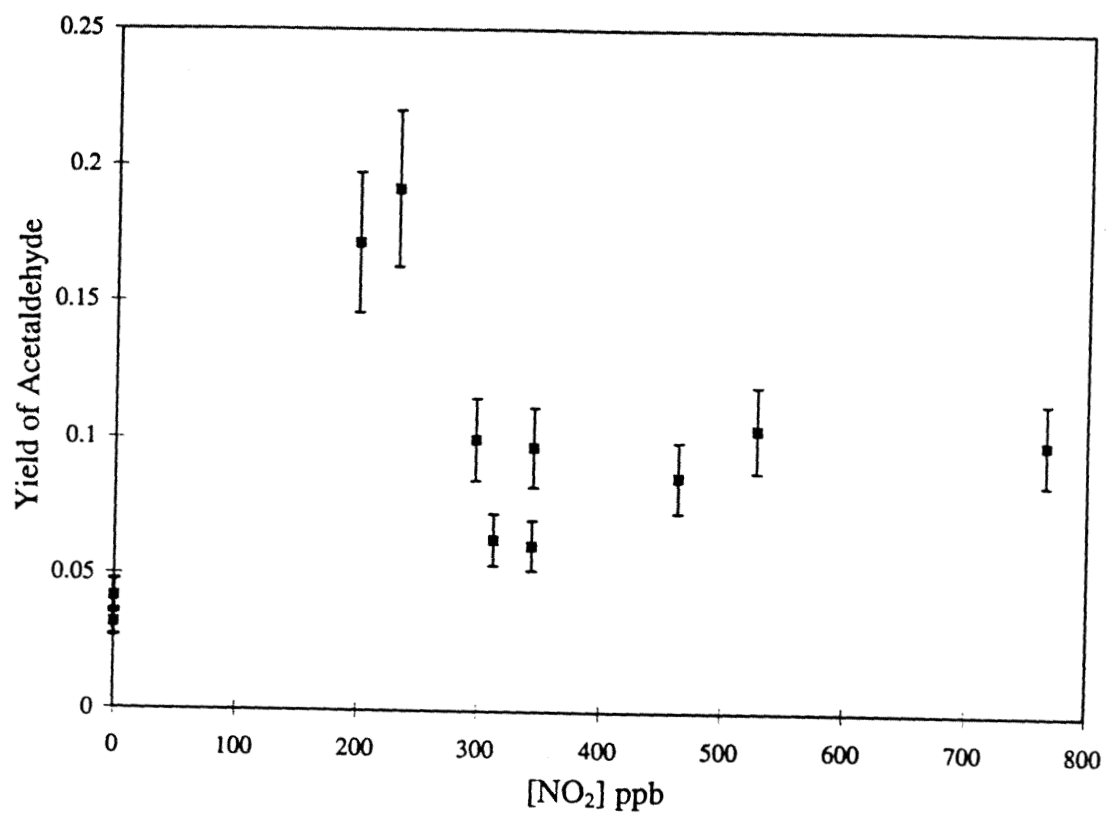Figure 6.7: 1,2,4 Trimethylbenzene Photooxidation Results: Glyoxal

Figure 6.8: 1,2,4 Trimethylbenzene Photooxidation Results: CH_3CHO

6.4 *m*-Ethyltoluene Photooxidation

6.4.1 Ring-Retained Products

As mentioned previously, the studies presented here are the first product studies of the photooxidation of *m*-ethyltoluene. Abstraction of a hydrogen from *m*-ethyltoluene can occur at a variety of sites. The resulting radicals can react with O_2 to eventually form aromatic aldehydes. These reactions are depicted in Figure 6.9. As with the case of 1,2,4-trimethylbenzene, high molecular weight carbonyls were not detected in the LC chromatograms. However, GCD results indicate the formation of 1-(3-methylphenyl)-ethanone, ethylbenzaldehyde, and 3-tolualdehyde from comparisons with library spectra. As indicated in Figure 6.9, 3-tolualdehyde formation may be the result of two different reaction pathways for radical (c).

The results of *ab initio* calculations performed by Andino et al. [5] indicate that the preferred sites for OH addition to the ring of *m*-ethyltoluene are the 2-, 4- and 6-positions. The reactions forming the ethyl-methylphenols from *m*-ethyltoluene are analogous to those depicted in Figure 6.4 for 1,2,4-trimethylbenzene photooxidation. Comparisons of mass spectra to library spectra indicated the presence of 2-ethyl-4-methylphenol, 4-ethyl-2-methylphenol, and 2-ethyl-6-methylphenol from OH addition to the 4-, 6-, and 2-positions of *m*-ethyltoluene, respectively. A section of a typical GCD total ion chromatogram depicting the reaction products for the abstraction and addition pathways for *m*-ethyltoluene appears in Figure 6.10.
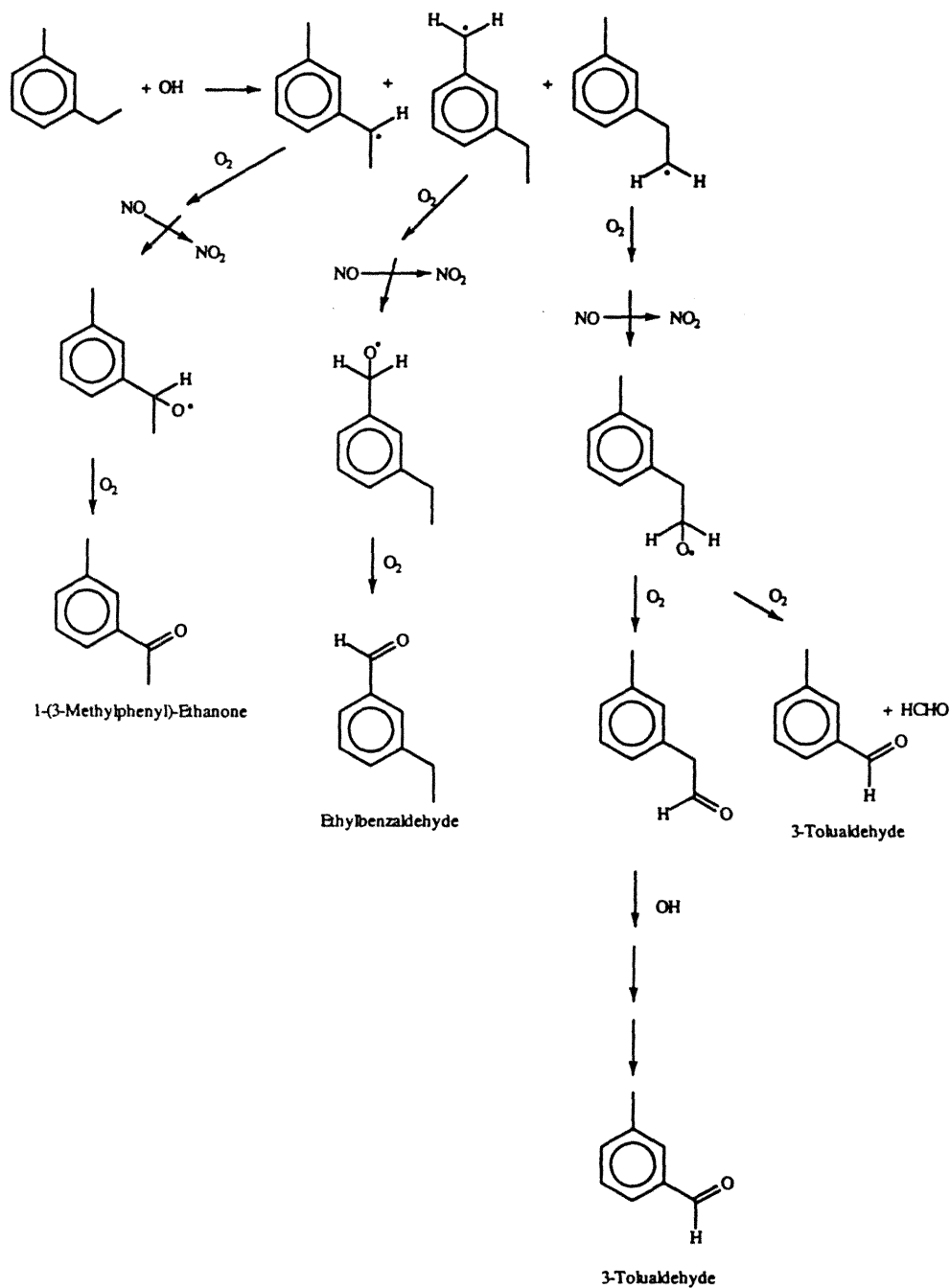
Figure 6.9: Depicted are the radicals resulting from the OH abstraction pathways for *m*-ethyltoluene and the subsequent formation of aromatic aldehydes.
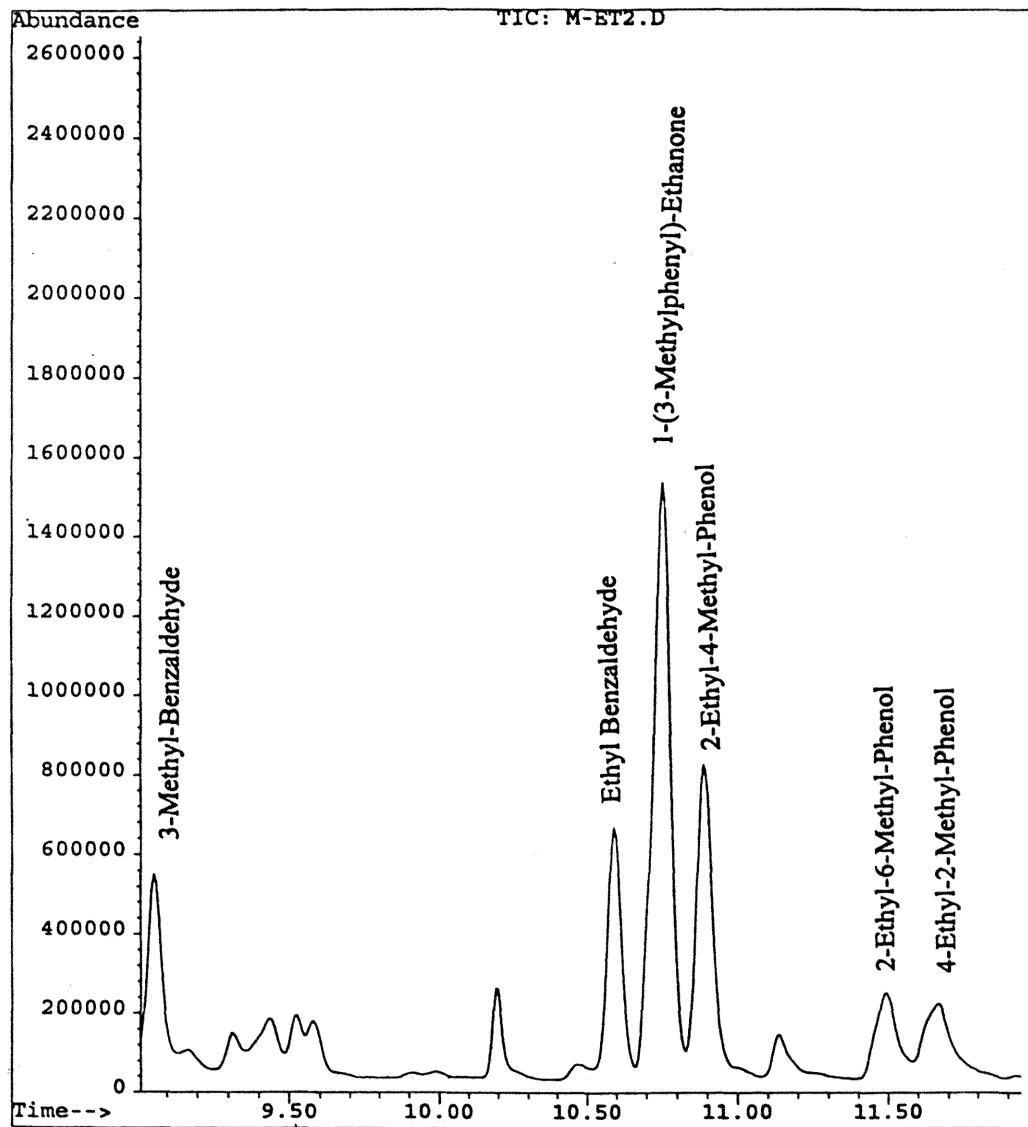
Figure 6.10: GCD chromatogram of products formed from the photooxidation of *m*-ethyltoluene. Depicted are the ring-retained carbonyls and the phenolic compounds.

6.4.2   Ring-Fragmentation Products and the NO$_2$ Effect

LC data show positive evidence for the formation of acetaldehyde, glyoxal, and methyl glyoxal. Both methyl glyoxal and glyoxal are formed as a result of ring fragmentation of the bicyclic peroxy radicals formed after intial OH addition to the m-ethyltoluene [5]. The pathways are analogous to those depicted in Figure 6.5 for 1,2,4-trimethylbenzene. Acetaldehyde is believed to be formed as a secondary product from one of the C$_7$ ring fragmentation products, or from ethyl glyoxal, another possible ring fragmentation product predicted by Andino et al. [5]. The yields of glyoxal, methyl glyoxal, and acetaldehyde were determined by comparison with authentic DNPH-derivatized samples. Product yields were corrected for secondary reactions with OH according to the method of Atkinson et al. [13], using Equation 6.1.

Average NO$_2$ concentrations were determined using the method presented in the 1,2,4-trimethylbenzene section, and ranged from 250 to 650 ppb. Plots of ring-fragmentation product yields resulting from m-ethyltoluene photooxidation versus average [NO$_2$] are presented in Figures 6.11- 6.13. The plots for glyoxal and acetaldehyde indicate that there is no clear effect of NO$_2$ on product formation within the range of NO$_2$ concentrations considered in this work. However, the methyl glyoxal data show a slight decrease in yield with increasing average [NO$_2$]. These results, when compared with the results from the 1,2,4-trimethylbenzene system and the results for toluene, m- and p-xylene from Andino et al. [5] may indicate that as the order of substitution

at a particular site increases (i.e. in going from a methyl substituted carbon to an ethyl substituted carbon), the effect of NO_2 on ring-fragmentation product yields decreases. This suggestion is plausible given that in the case of methyl substituted aromatics (such as 1,2,4-trimethylbenzene), only two possible pathways for ring fragmentation exsit, one forming glyoxal (and a C_7 carbonyl), and the other forming methyl glyoxal (and a C_6 carbonyl). m-Ethyltoluene, on the other hand, has three different possible pathways: formation of glyoxal and a C_7 carbonyl, methyl glyoxal and a C_6 carbonyl, and ethyl glyoxal and a C_5 carbonyl. Thus, the effect of NO_2 on any one possible pathway would be mitigated by the existence of several different pathways.

6.5 Conclusions

1,2,4-Trimethylbenzene and m-ethyltoluene are important aromatics which have been detected in urban air. As such, their photooxidaton products are important. This study provides the first information on the ring-retained and ring-fragmented products observed during the photooxidation of m-ethyltoluene. In addition, the first evidence for ring-retained products from the 1,2,4-trimethylbenzene system are reported. The yields of ring fragmentation products identified in the 1,2,4-trimethylbenzene system are in excellent agreement with those of previous studies. These product data serve to increase the available information for the reactions pathways of substituted aromatics.

The effect of NO_2 on the ring-fragmentation products of 1,2,4- trimethyl-
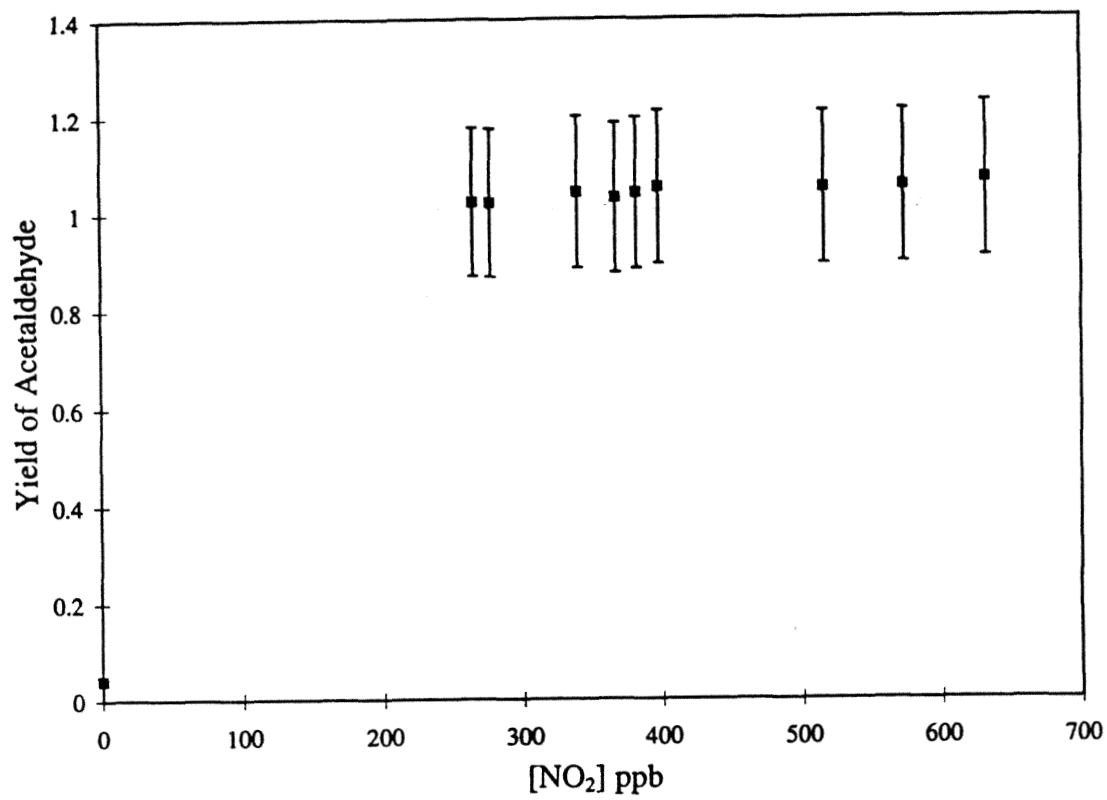
Figure 6.11: *m*-Ethyltoluene Photooxidation Results: CH₃CHO
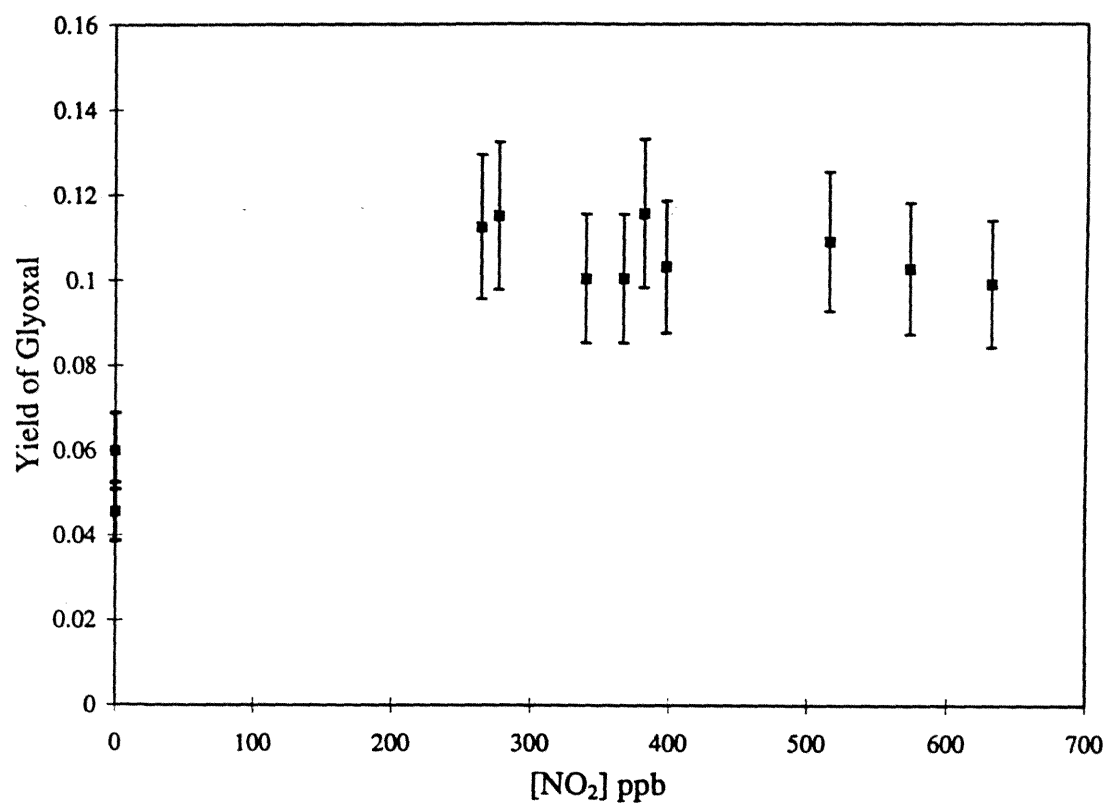
Figure 6.12: *m*-Ethyltoluene Photooxidation Results: Glyoxal
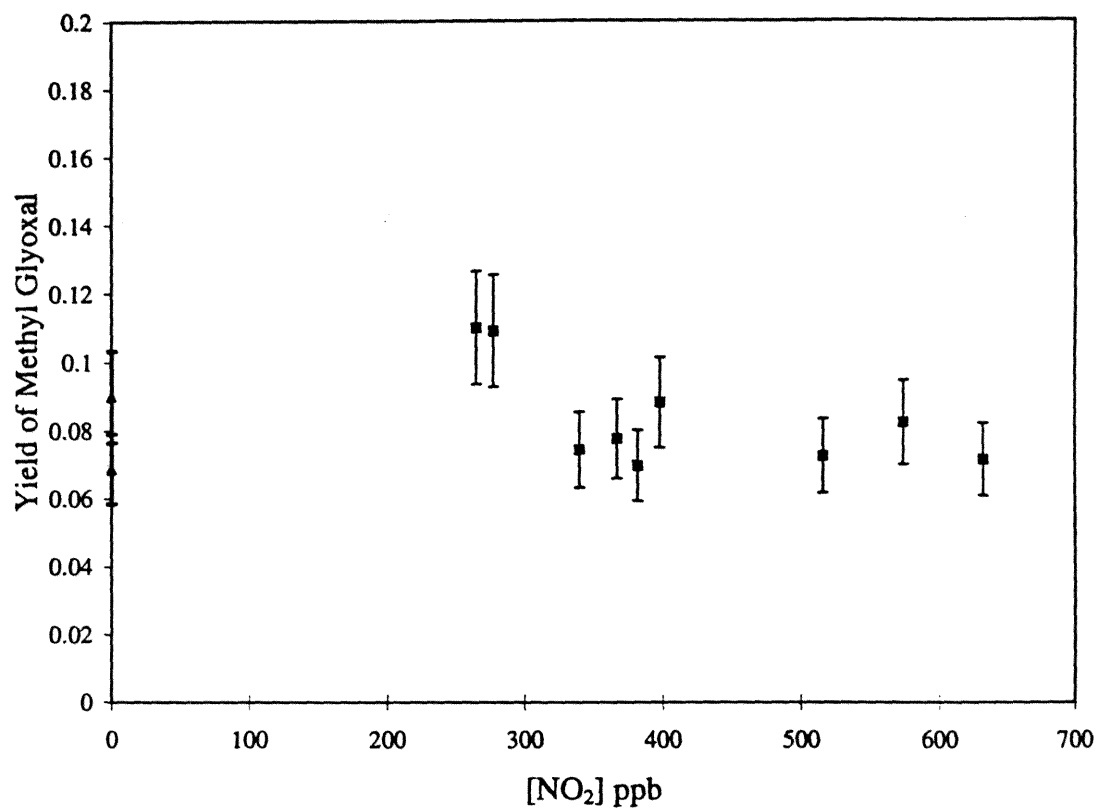
Figure 6.13: *m*-Ethyltoluene Photooxidation Results: Methyl Glyoxal

benzene and *m*-ethyltoluene was also examined. The yields of the ring-fragmentation products formed from the 1,2,4-trimethylbenzene system decreased with increasing average NO_2 concentration. However, only the yield of methyl glyoxal from *m*-ethyltoluene photooxidation decreased with increasing NO_2, and the decrease was almost negligible.

Acknowledgements

Bibliography

[1] Lurmann, F.W. and Main, H.H., "Analysis of the Ambient VOC Data Collected in the Southern Air Quality Study," Final Report, Contract No. A832-130. State of California Air Resources Board, Sacramento **1992**.

[2] National Research Council, "Rethinking the Ozone Problem in Urban and Regional Air Pollution", National Academy Press, Washington D.C. , **1991**.

[3] Atkinson, R., *J. Phys. Chem. Ref. Data.*, **1989**, *Monograph 1*, 1.

[4] Atkinson, R., *J. Phys.Chem. Ref. Data*, **1994**, *Mongraph 2*, 1.

[5] Andino, J.M., Smith, J.N., Flagan, R.C., Goddard III, W.A., Seinfeld, J.H., *J.Phys. Chem.*, **1995**, Submitted for publication .

[6] Bandow, H., Washida,N., *Bull. Chem. Soc. Jpn.*, **1985**, *58*, 2549.

[7] Tuazon, E., Mac Leod, H., Atkinson, R., Carter, W., *Environ. Sci. Tech.*, **1986**, *20*, 383.

[8] Taylor, W.D., Allston, T.D., Moscato, M.J., Fazekas, G.B., Ko-
zlowski,R., Takacs,G.A., *Int. J. Chem. Kinet.,*, **1980**, *12*, 231.

[9] Atkinson, R. , Aschmann, S.M., Arey, J., Shorees, B., *J. Geophys. Res.,*
1992, *97*, 6065.

[10] Grosjean,D., Williams,E.L., Seinfeld, J.H., *Env. Sci. Tech.*, **1992**, *26*,
1526.

[11] Hakola, H., Arey, J., Aschmann, S.M., Atkinson,R., *J. Atmos. Chem.*,
1994, *18*, 75.

[12] Druzik, C.M., Grosjean,D., Van Neste, A., Parmar, S.S., *Int. J. Environ.
Anal. Chem.*, **1990**, *38*, 495.

[13] Atkinson, R., Aschmann,S.M., Carter,W.P.L., Winer,A.M., Pitts Jr.,
J.N., *J.Phys. Chem.*, **1982**, *86*, 4563.

[14] Atkinson, R., *J. Phys. Chem. Ref. Data.*, **1989**, *Monograph 1*, 1.

[15] Atkinson, R., *Int. J. Chem. Kinet.*, **1987**, *19*, 799.

[16] Kwok, E.S.C., Atkinson, R., *Atm. Environ.*, **1995**, *24*, 1685.

Chapter 7

Conclusions

A new indoor photochemical reactor was designed and constructed to study detailed gas-phase kinetics and mechanisms. This system was used to study the photooxidation of branched alkanes and aromatic compounds, the results of which have been presented in this thesis. The development of an indoor system for detailed gas-phase studies serves to complement the outdoor system which has traditionally been available at Caltech for studies of gas to particle conversions. The development of this new and smaller indoor system launches the Air Pollution/Aerosols group at Caltech into a wide variety of new research areas involving gas-phase atmospheric chemistry.

Studies of the branched alkanes, 2,2,4-trimethylpentane and 2,2,5- trimethylhexane were conducted, and the results presented in Chapter 3. The first determination of the rate constant for 2,2,5-trimethylhexane was made, and the result is in excellent agreement with the value predicted from the structure reactivity relationship[1, 2]. The product studies were aimed at elucidating the gas-phase mechanism of 2,2,4-trimethylpentane and 2,2,5-trimethylhexane in particular, and providing additional information on the reactions of alkoxy radicals in general. Experimentally observed product yields were compared to those predicted from mechanisms developed for each alkane studied in this work. The results of these comparisons indicated that the 1,5-H atom isomerization reaction pathway is a significant atmospheric sink for many of the large alkoxy radicals formed in the two alkane systems. Rate constant estimates were made for the 1,4 H-atom isomerization pathways based on the reactions of 2,2,4-trimethylpentane, and are consistent with previous estimates based on data from straight chain alkanes. These studies serve to expand the available database for the reactions of large alkanes, and indicate

that currently available kinetic data for alkanes provide reasonable fits to experimental results.

This thesis also focused on the photooxidation of aromatic hydrocarbons. Theoretical and experimental studies were carried out on the OH-initiated photooxidation of toluene, m-xylene, p-xylene, m-ethyltoluene, and 1,2,4-trimethylbenzene. The theoretical studies presented in Chapter 4 provide the first, unambiguous determination of the intermediates formed in aromatic-OH systems. *Ab initio* calculations were performed on proposed reaction intermediates, and the lowest energy structures were identified. Where possible, predictions based on theory were compared to available experimental data. Particular reactions were examined in detail to determine the most likely paths. In particular, the aromatic-OH adduct reaction with NO_2 was examined. Based on the results, three pathways for this reaction were found to be likely. Previous indications were that the aromatic-OH adduct reaction proceeded by one pathway, forming only the nitroaromatic[3]. In addition, the reactions of the aromatic peroxy radical were investigated. Previous indications were that the peroxy radical preferentially cyclicized rather than reacting with NO to form the oxy radical. Theoretical results indicated that both of these reactions should be included in overall mechanisms for aromatic-OH reaction. Thus, Chapter 4 elucidated the structures of the intermediates formed, and suggested additional reaction pathways.

Experimental studies on toluene, m-, and p-xylene presented in Chapter 5 focused on the effect of NO_2 on the products formed during the OH-initiated photooxidation of the aromatics. Results showed a positive indication for an effect of NO_2 on products in all three systems. Full mechanisms for the

aromatics were developed and tested against experimental data. While a NO_2 effect was noticed in the experimental systems, and predicted results show the same phenomenon, rate constant fits indicate that, under atmospheric conditions, the reaction of the aromatic-OH adduct with NO_2 is insignificant as compared to reaction with O_2. The mechanisms developed also support the data presented in Chapter 4 concerning the NO_2 reactions of aromatics. Based on comparisons of observed and predicted data, additional pathways for the NO_2 reaction with the aromatic-OH adduct were necessary in order to explain the observed nitroaromatic yields. The results of this chapter extend the available information regarding the effect of NO_2 on product yield, and provide an updated and detailed mechanism for aromatic photooxidation.

The gas-phase photooxidations of m-ethyltoluene and 1,2,4- trimethylbenzene were examined in Chapter 6. These studies represent the first product study for the m-ethyltoluene system, and only the second study for the 1,2,4-trimethylbenzene system. Both studies provide the first identifications of ring-retaining products formed, and are in excellent agreement with those predicted from the theoretical study of Chapter 4. Ring fragmentation products identified in the 1,2,4-trimethylbenzene system in these studies are consistent with those found in previous studies. The information obtained from these studies serves to further validate the theoretical predictions of Chapter 4, and to extend the available information on aromatic-OH photooxidation mechanisms. Additional work is, however, required to fully determine the effects of NO_2 on ring-retained compounds.

Although this thesis provides insight into the photooxidation of large alkanes (alkoxy radical reactions, in particular) and aromatics, there is still

much information to be gained in both cases. Alkoxy radical isomerizations have been found to be important for branched and straight chain alkanes. However, alkoxy-type radicals formed from other classes of compounds have yet to be investigated, and should be focused on in the future. While much information has been gained about aromatic-OH photooxidation from the data of Chapter 4 in particular, additional experimental evidence is needed in order to confirm the mechanism of photooxidation. Techniques that are capable of directly monitoring the reactions of the short-lived intermediates should be extremely helpful in confirming the aromatic reaction mechanism and identifying additional products of photooxidation. These new analytical techniques are currently being developed within the analytical chemistry field, and should prove to be quite useful to the atmospheric chemistry field.
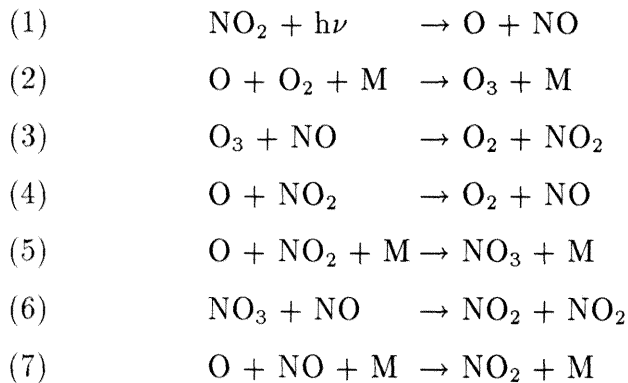
Bibliography

[1] Atkinson, R., *Int. J. Chem. Kinet.*, **1987**, *19*, 799.

[2] Kwok, E.S.C., Atkinson, R., *Atm. Environ.*, **1995**, *24*, 1685.

[3] Atkinson, R., Lloyd, A., *J. Phys. Chem. Ref. Data*, **1984**, *13*, 315.

Appendix A

Calculation of the Photolysis Rate Constant, k_1

A.1 Reactions of NO$_2$

(1)   NO$_2$ + hν $\rightarrow$ O + NO

(2)   O + O$_2$ + M $\rightarrow$ O$_3$ + M

(3)   O$_3$ + NO $\rightarrow$ O$_2$ + NO$_2$

(4)   O + NO$_2$ $\rightarrow$ O$_2$ + NO

(5)   O + NO$_2$ + M $\rightarrow$ NO$_3$ + M

(6)   NO$_3$ + NO $\rightarrow$ NO$_2$ + NO$_2$

(7)   O + NO + M $\rightarrow$ NO$_2$ + M

A.2 Calculations

$$
\frac{d[NO_2]}{dt} = -k_1[NO_2] + k_3[O_3][NO] - k_4[O][NO_2]
$$
$$
-k_5[O][NO_2][M] + 2k_6[NO_3][NO] + k_7[O][NO][M] \quad \text{(A.1)}
$$

If we assume that [O$_3$], [NO$_3$], and [O] are at pseudo-steady state, then :

$$
\frac{d[O_3]}{dt} = k_2[O][O_2][M] - k_3[O_3][NO] = 0
$$

Therefore:

$$
[O_3] = \frac{k_2[O][O_2][M]}{k_3[NO]} \quad \text{(A.2)}
$$

$$\frac{d[NO_3]}{dt} = k_5[O][NO_2][M] - k_6[NO_3][NO] = 0$$

Therefore:

$$[NO_3] = \frac{k_5[O][NO_2][M]}{k_6[NO]} \qquad (A.3)$$

$$\frac{d[O]}{dt} = k_1[NO_2] - k_2[O][O_2][M] - k_4[O][NO_2] - k_5[O][NO_2][M] - k_7[O][NO][M] = 0$$

$$[O] = \frac{k_1[NO_2]}{k_2[O_2][M] + k_4[NO_2] + k_5[NO_2][M] + k_7[NO][M]}$$

$$[O] = \frac{k_1[NO_2]}{D} \qquad (A.4)$$

Substituting equations A.2, A.3 and A.4 into equation A.1 gives:

$$\begin{aligned}\frac{d[NO_2]}{dt} &= \frac{-k_1[NO_2]D + k_1k_2[NO_2][O_2][M] - k_1k_4[NO_2]^2}{D} \\ &+ \frac{k_1k_5[NO_2]^2[M] + k_1k_7[NO_2][NO][M]}{D}.\end{aligned} \qquad (A.5)$$

Simplifying equation A.5 and rearranging gives:

$$\frac{d[NO_2]}{dt} = \frac{-2k_1k_4[NO_2]^2}{D} \qquad (A.6)$$

and:

$$\frac{d[NO_2]}{\frac{d[NO_2]}{dt}} = \frac{D}{k_4[NO_2]} \tag{A.7}$$

where:

$$\frac{D}{k_4[NO_2]} = 1 + \frac{k_2[O_2][M]}{k_4[NO_2]} + \frac{k_5[M]}{k_4}$$
$$+ \frac{k_7[NO][M]}{k_4[NO_2]}. \tag{A.8}$$

Making the following definitions:

$$R_1 = \frac{k_5[M]}{k_4}$$

$$R_2 = \frac{k_7[M]}{k_4}$$

$$R_3 = \frac{k_2[M]}{k_4}$$

Then:

$$\frac{-2k_1}{\frac{d(\ln[NO_2])}{dt}} = 1 + \frac{R_3[O_2]}{[NO_2]} + R_1 + \frac{R_2[NO]}{[NO_2]} \tag{A.9}$$

Defining: $[NO] = [NO]_o + [NO_2]_o - [NO_2]$

$$\Delta t = t_{final} - t_{initial}$$

Integrating equation A.9, and assuming that the initial NO and O_2 con-

centrations are zero gives:

$$k_1 = \frac{1}{2\Delta t} \left\{ [1 + R_1 - R_2] \ln \frac{[NO_2]_o}{[NO_2]} + R_2 \left(\frac{[NO_2]_o}{[NO_2]} - 1 \right) \right\} \qquad (A.10)$$

This last equation is a measure of the light intensity.

Appendix B

Experimental Protocol

This appendix is intended as a general guide for future users of the Indoor Photochemical Reactor. It is not intended to be an exhaustive, step-by-step manual for performing an experiment. Instead, it is written to provide the user with helpful suggestions before and during the running of experiments in the indoor system. Before reading this, it would be helpful to have reviewed the following reference materials:

- Thermo Environmental Inc., Manual for NO_x monitor, Model 42.

- Dasibi Inc., Manual for O_3 monitor, Model 1003-PC.

- Labtech Inc, Manual for Notebook (data acquisition program).

- Hewlett Packard, Manuals for GC-FID, Model 5890.

- Tekmar, Manual for Aerotrap 6000 and Cryofocusing unit.

- Waters Inc., Waters Sep-Pak DNPH-Silica Cartridge Care and Use Manual

B.1   Before an Experiment

There are several proceedures which should be completed before running an experiment. These proceedures are listed in the subsequent subsections.

B.1.1 NO_x Monitor Calibration

A detailed description of the calibration proceedure for the NO_x monitor appears in the manual for the instrument. The reader is referred to section

III of the manual for details. After calibration, the results should be plotted and calibration factors should be entered into Labtech Notebook's data acquisition program (blocks 1,2, and 3). Full calibrations should be repeated whenever the monitor begins to drift. Span and zero checks should be conducted at the start of each day of experiments. Comparison of the results of the daily zero and span checks to the full calibration curve will determine when the instrument has drifted beyond a reasonable amount. The NO_x monitor manual lists <10% as a reasonable drift, but <5% is a better value to follow. Typical drifts for the NO_x monitor attached to the indoor system have been less than 1-3% over as long as a two month period.

B.1.2 O_3 Analyzer Calibration

The O_3 analyzer is taken to the Air Quality Management District for full calibration once a year. They will provide a calibration curve which can then be used in Labtech Notebook's data acquisition program (block 4).

B.1.3   GC-FID Calibration

Every organic compound studied should be calibrated on the GC-FID. A full calibration should be performed at least once to determine whether the compound is linear over the range of concentrations considered. If the GC-FID is left on over the course of the study of the hydrocarbon of interest, one need only conduct a one or two point calibrations (using duplicate points)

on a daily basis. Leaving the GC-FID on over the course of an experiment ensures that all FID gas flows and response factors remain essentially the same over the course of the experimental study. We have found that the GC-FID Series II attached to the indoor system is quite stable over time.

B.2 Running an Experiment

B.2.1 Admitting Reactants

There are three primary methods of admitting reactants to the chamber. Reactants can be admitted from a standard gas cyclinder, from the vacuum manifold, and from what has been termed as the "evaporation" bulb (see Figure 2.6). The most important point to remember when admitting reactants is to make sure that the teflon lines from the gas cylinders, vacuum manifold or the evaporation buld are fully flushed with scrubbed air after the reactant has been admitted. This added flushing ensures that the reactant has reached the chamber and that there are no remnants of reactant in the teflon lines, vacuum manifold or evaporation bulb.

Nitric Oxide.

Nitric oxide is admitted using the high concentration NO cylinders available in the laboratory. It is important to measure the flowrate of the NO and the time taken to admit the reactant. An estimate of the concentration admitted to the chamber can be made by using the following formula:

$$[NO] \text{ ppm} = \frac{F*t*[NO]_{cylinder}}{V_{bag}}$$

where:

F= flowrate of NO from the cylinder (liters/min),

t= time (in min.) taken to admit the reactant,

$[NO]_{cylinder}$ = concentration of the standard cylinder of NO, and

V_{bag} = volume of the teflon chamber (in liters).

Methyl Nitrite.

Methyl nitrite is stored in a cold finger in liquid nitrogen, and is admitted through the vacuum manifold. Before admitting methyl nitrite to the chamber it is important to utilize the manifold to purify the methyl nitrite. Using the technique of freezing-pumping-thawing the cold finger one or two times works well. Before admitting the methyl nitrite, it is important that it be sufficiently thawed. The pressure guage on the manifold can be used to admit a known amount of reactant to one of the calibrated bulbs on the manifold. Assuming ideal gas behavior, the partial pressure of methyl nitrite in the bag can be determined using the following relationship:

$$P_{chamber} = \frac{P_{manifold} * V_{manifold}}{V_{chamber}} \qquad (B.1)$$

where P and V are the partial pressures and volumes of methyl nitrite in either the chamber or the glass bulb on the vacuum manifold. (The volume of the glass bulb on the vacuum manifold can be calibrated using a gravimetric technique, i.e. placing water in the bulb, weighing the bulb, and computing

the volume.) By flowing scrubbed air to the manifold and through the bulb containing the reactant, the methyl nitrite is admitted to the chamber. It is important to let the air flow through the manifold for a while to ensure that the reactant has been completely admitted to the chamber.

Hydrocarbon

Hydrocarbons are admitted using the evaporation bulb. A known amount of pure, liquid hydrocabon is injected to the evaporation bulb. The bulb is connected to the scrubbed air supply. While flowing air over the liquid, the bulb is gently heated using a heat gun. Again, it is important to continue flowing scrubbed air through the bulb even after all of the liquid has evaporated.

B.2.2 Sampling From the Bag

Once the sampling valve on the chamber and the appropriate valves on the glass sampling manifold are opened, gas samples from the chamber can be obtained. The only caution to be given during sampling concerns the start of the experiment. It is extrememly important that the user wait until the system is fully stabilized and well mixed before proceeding with an experiment. The user will have to perform several experiments to determine exactly how long of a delay is needed to ensure stabilization. Two things to monitor are the NO_x monitor values and the hydrocarbon concentrations. It is important that the t=0 hydrocarbon peak areas for the GC-FID be within a few percent. If the user finds that the concentrations of reactants decrease over

time, and the system has had time to mix, radical sources within the chamber have probably reached high concentrations. It is then necessary to either re-condition the bag or change the bag. It is often best to simply change the bag.

B.3   Teflon Chamber

B.3.1   Deciding When to Change a Bag

One cannot really place a time limit on the frequency of bag changing since the frequency depends upon what has been placed in the bag and how often the bag has been used. As mentioned previously, though, it is important to change the bag when radical sources become too high. To test for the presence of radical sources, the user should irradiate a bag containing only air. The analytical instruments should be used to monitor the concentrations of O_3, NO_x, and hydrocarbon present in the bag. If there are significant radical sources in the bag, one should see an increase in the O_3 concentration over time. The bag should be changed if radical sources are found to be significant. In addition, one can make a visual inspection of the bag. Obviously, if there are any damages to the bag, it is important to immediately replace and condition the bag.

B.3.2   Making a New Chamber

Teflon (2 mil, FEP) is purchased directly from duPont in rolls that are 58 in. wide. Two sheets, each 6 ft. long , are cut from the 58 in. roll of teflon.

These two sheets of teflon are heat sealed along the long edges with the 14 in. Vertrod Inc. heat sealer available in the roof lab. It is important to place the seals within one inch from the edge of the teflon, or the user may encounter problems placing the teflon over the circular plates that form the top and bottom of the chamber. To strengthen the seals, it is wise to either make double seals on each edge or to reinforce the edges with teflon tape.

B.3.3   Conditioning the Bag

It is important to fully condition the chamber before performing experiments, since FEP teflon is a source of CO and volatile residues (Kelly, 1982 ; Killus and Whitten, 1990). To condition the chamber, fill the bag with NO_2 and air, and photolyze. Alternatively, the system can be filled with O_3 and air and photolyzed. It is crucial to fully flush the bag with scrubbed air after the conditioning process. The bag is considered to be fully conditioned when radical sources are insignificant (see the section entitled "Deciding when to change a bag".)

B.4   2,4 Dinitrophenylhydrazine Analyses

The 2,4 dinitrophenylhydrazine (DNPH) method has been used extensively to collect and identify gas-phase carbonyl compounds. Gas samples from the indoor chamber are collected onto cartridges impregnated with an acidic DNPH solution. DNPH selectivly reacts with aldehydes and ketones according to the reaction pictured in Figure B.1.
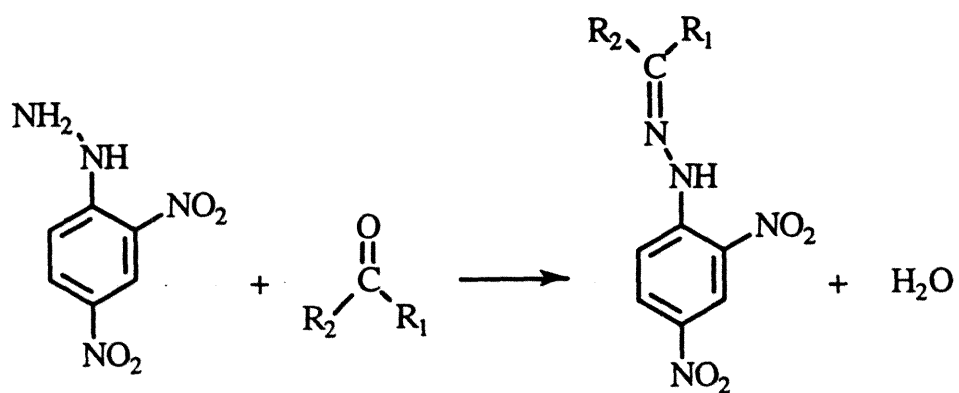
Figure B.1: 2,4 Dinitrophenylhydrazine Derivatization Reaction

The DNPH cartridge samples which are collected are eluted with 3 ml of acetonitrile, and analyzed using high performance liquid chromatography. To determine product yields, DNPH derivatized standards for all identified carbonyl compounds are required. These DNPH derivatized carbonyls are not always readily available. Radian corporation has many of the simpler carbonyls such as formaldehyde, acetone, and acetaldehyde, but they do not have many other monocarbonyls, nor do they carry dicarbonyls such as glyoxal and methyl glyoxal.

B.4.1   DNPH-Carbonyl Derivatization

Several monocarbonyls are readily available from Aldrich chemical company. They can be used without further purification, since many of them have stated purities of 95% or greater. The method for derivatization presented here is adapted from the Standard Operating Procedure for Carbonyl Analysis by HPLC from DGA, Inc., Ventura California. An additional proceedure is available in the Waters Sep-Pak DNPH-Silica Cartridge Care and Use Manual . The first step in the generating the DNPH derivative is to create an acidic DNPH solution. This is done by combining 0.5g of DNPH in 2ml of H_2SO_4 and 3ml of water. Add 10 ml of ethanol to this solution. Next, prepare the carbonyl solution by adding 0.5 g of the monocarbonyl to 20 ml of ethanol. Add the DNPH acidic solution to the carbonyl solution. A precipitate will form within a few minutes. This precipitate is the hydrazone of the monocarbonyl. Purification of the derivative may be necessary. A qualitative standard of derivative and acetonitrile can be synthesized and tested

on a liquid chromatograph to determine the purity of the hydrazone. To purify the derivative, recrystallize it using a minimum amount of methanol. If necessary, heat the solution to make it supersaturated. Once the solution begins to cool, fine, needlelike crystals of the derivative will form. Vacuum filter the crystals from the solution with methanol. A bit of ether can be used to speed the drying process of the crystals. Care should be taken during the crystallization process to avoid contact with sources of carbonyls.

Dicarbonyls such as glyoxal and methyl glyoxal are also available from Aldrich. These can be used without further purification. The same method for generating monocarbonyl derivatives can be used to generate 1,2 dicarbonyl DNPH derivatives. In this case, however, 1.25 gm of the dicarbonyl should be used in the carbonyl solution. It was found that the dicarbonyls required recrystallization. The procedure mentioned above can be used to recrystallize the dicarbonyl derivative.

Standard solutions, stable for up to several months, can be formed with acetonitrile. To prepare the standard solutions, it is best to start with a highly concentrated solution (approximately 200 $\frac{\mu g}{ml}$, as carbonyl) and dilute with acetonitrile until the desired concentration range is reached. The following formula can be used to calculate the concentration of the standard:

$$\text{Concentration}, \frac{\mu g}{mL} \text{ as carbonyl} = \frac{mg\,of\,hydrazone}{mL\,of\,Acetonitrile} \text{ x } \frac{MW\,carbonyl}{MW\,hydrazone} \text{ x } 10^3 \; .$$

Note that dicarbonyls will be double derivatized by the DNPH. This fact must be taken into account when calculating the concentrations of the standards.

To check the quality of the standards, calibrations curves should be generated for each DNPH carbonyl standard synthesized in the laboratory. These

curves should be linear. As an example, the calibration curves for several glyoxal and methyl glyoxal standards are presented in Figure B.2.

B.4.2 Calculation of Carbonyl Yields

Once the carbonyl standards have been synthesized, experimetal yields can be calculated. To do so, use the following formula:

$$Concentration(ppb) = \frac{PeakHeigth_{exp} - PeakHeight_{blank}}{x} * \frac{V_{eluate}}{V_{gas}} * \frac{1}{y}$$

where:

$PeakHeight_{exp}$= Peak Height of compound from the

experimental sample

$PeakHeight_{blank}$= Peak Height of compound from the

blank sample

x= Response factor for 1 $\frac{\mu g}{ml}$ of carbonyl standard

V_{eluate}= Volume of eluate (ml)

V_{gas}= Volume of gas collected onto the cartridge (m^3)

y= Conversion factor from $\frac{\mu g}{m^3}$ to ppb for the carbonyl

Conversion factors have been calculated for several carbonyls, and are tabulated in Table B.1.
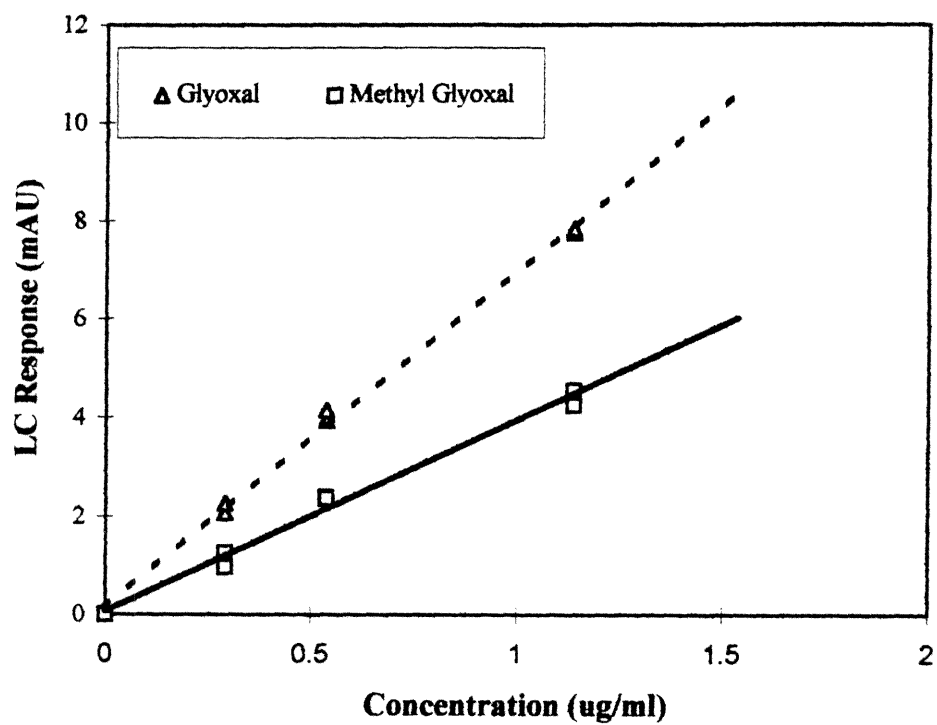
Figure B.2: Calibration curves for DNPH-glyoxal and DNPH-methyl glyoxal standards synthesized at Caltech

Table B.1: Conversion Factors for Selected Carbonyls

Carbonyl	Conversion Factor
Acetaldehdye	1.80
Acetone	2.37
Benzaldehyde	4.33
3,3-Dimethylbutyraldehyde	4.10
2,2-Dimethyl-1-propanal	3.52
Formaldehyde	1.23
Glyoxal	2.37
Methyl Glyoxal	2.94
2-Methyl-1-propanal	2.95
3-Methyl-1-butanal	3.52
Tolualdehyde	4.91

B.4.3 Interferences with the DNPH Technique

High levels (approximately 100 ppb) of ozone have been found to interfere with the accurate collection of DNPH samples. In order to elimnate the effect of O_3 on the DNPH cartridges, it is important to install a KI trap in-line between the glass sampling manifold and the DNPH cartridge. Experiments with and without the trap in place should be conducted by the user to convince oneself of the effectiveness of the KI trap. A full description of the construction of a KI ozone scrubber appears in the reference, "Waters Sep-Pak DNPH Silica Cartridge Care and Use Manual", published by Waters Inc., and available with every box of DNPH silica cartridges.

Appendix C

Energies of Aromatic Intermediates

In order to provide the reader with a more complete view of the steps leading to bicyclic radical formation, we have included energy "trees", indicating the possible radicals from each of the steps leading to bicyclic radical formation for the five aromatics studied in chapter 4. Toluene data appear in Figures C.1- C.3, m-xylene data in Figures C.4- C.6, p-xylene data in Figure C.7, 1,2,4 trimethylbenzene data in Figures C.8- C.10, and m-ethyltoluene data in Figures C.11- C.14.
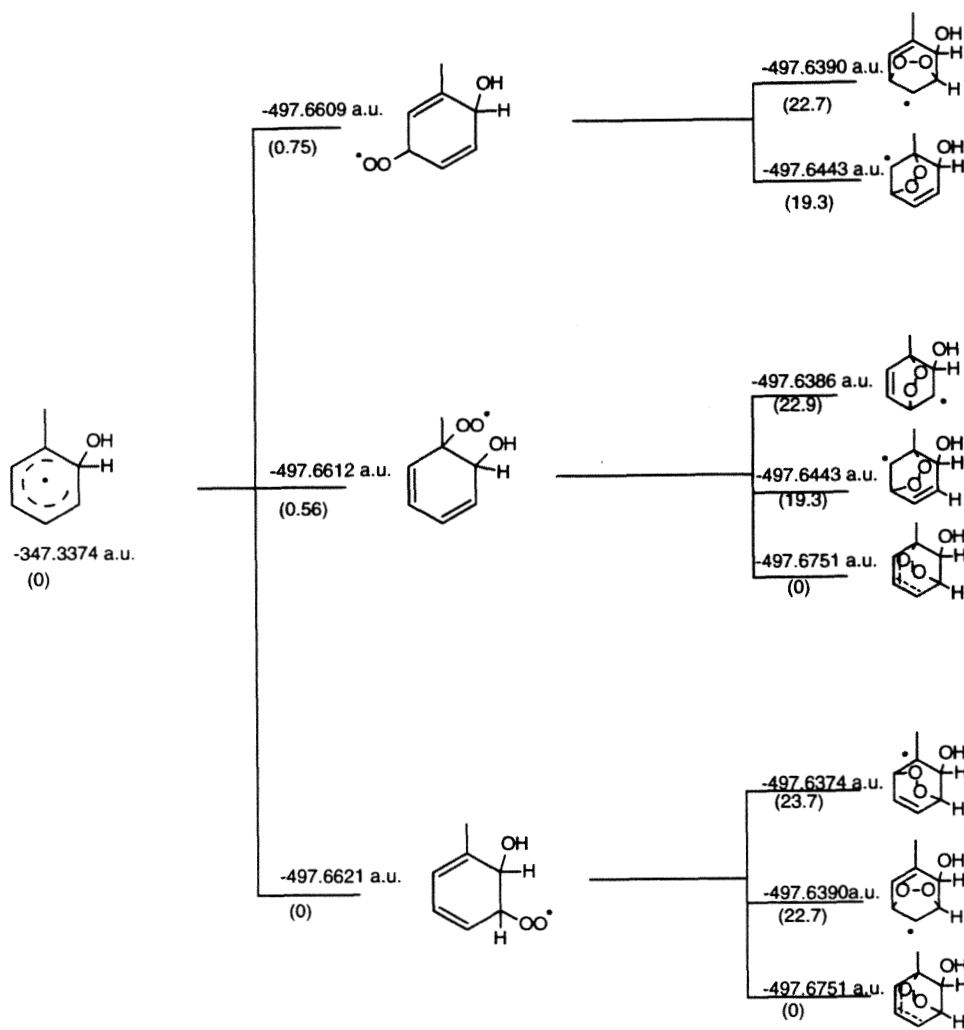
Figure C.1: Energy diagrams for toluene radicals.
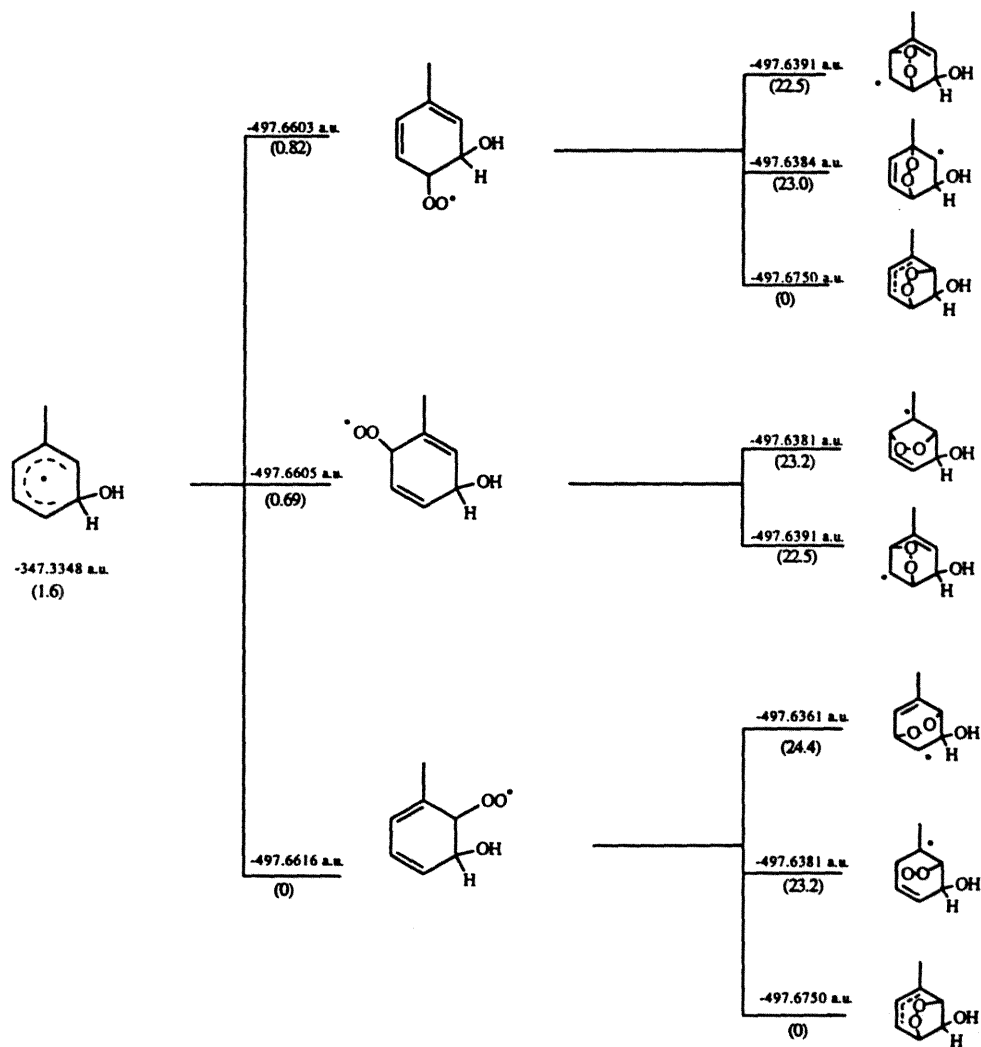
Figure C.2: Energy diagrams for toluene radicals.
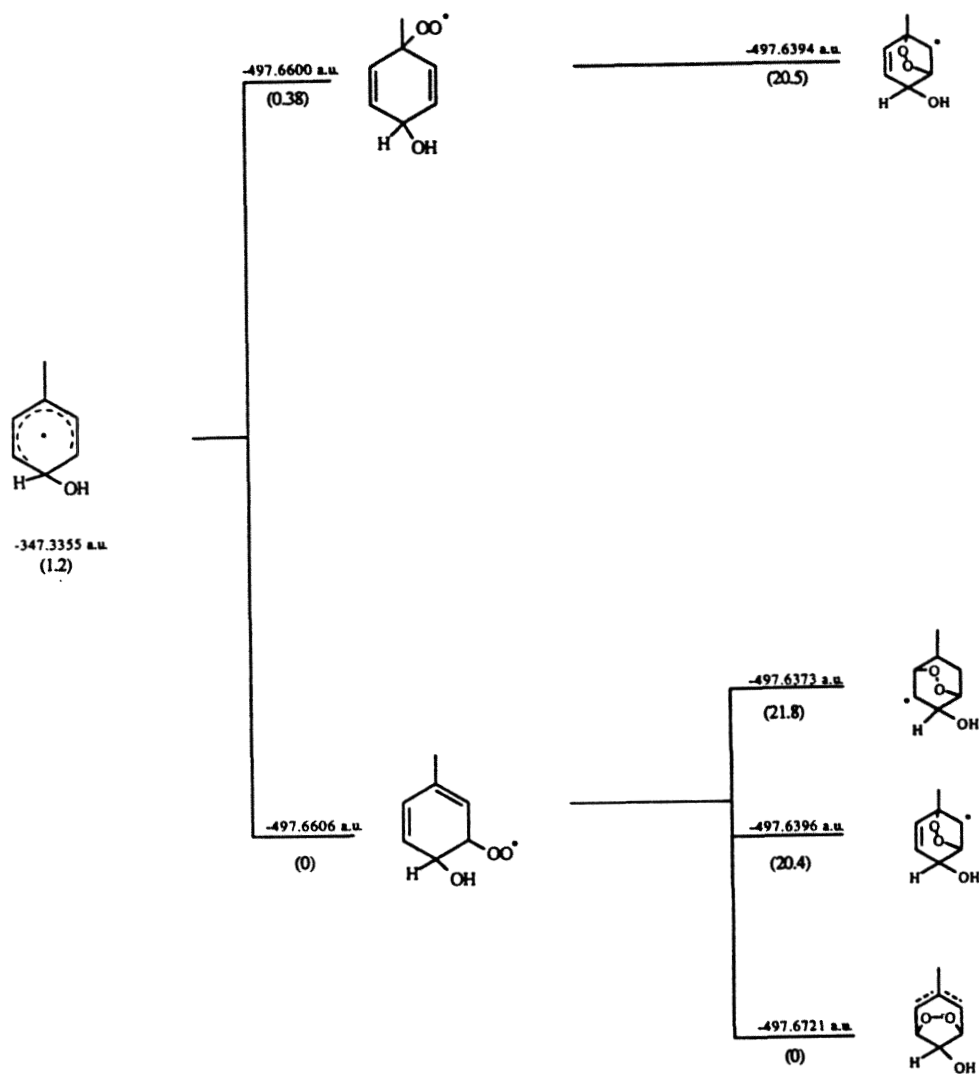
Figure C.3: Energy diagrams for toluene radicals.
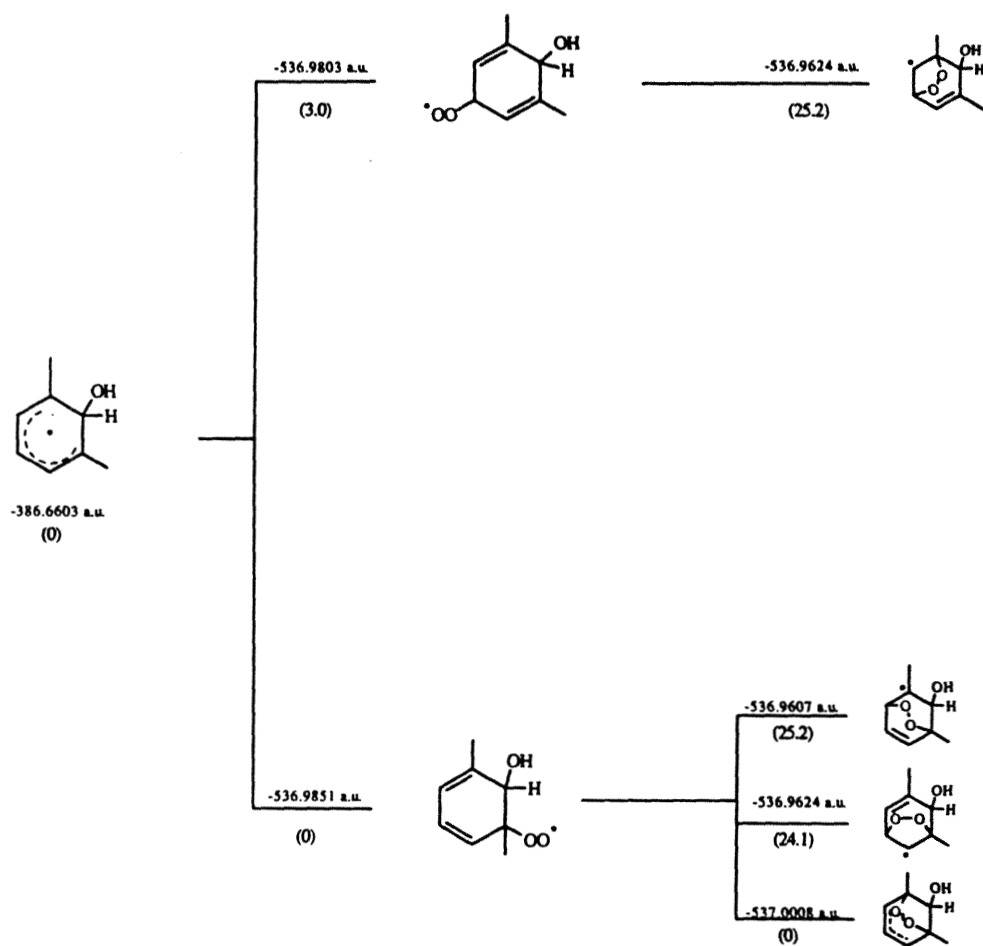
Figure C.4: Energy diagrams for m-xylene radicals.
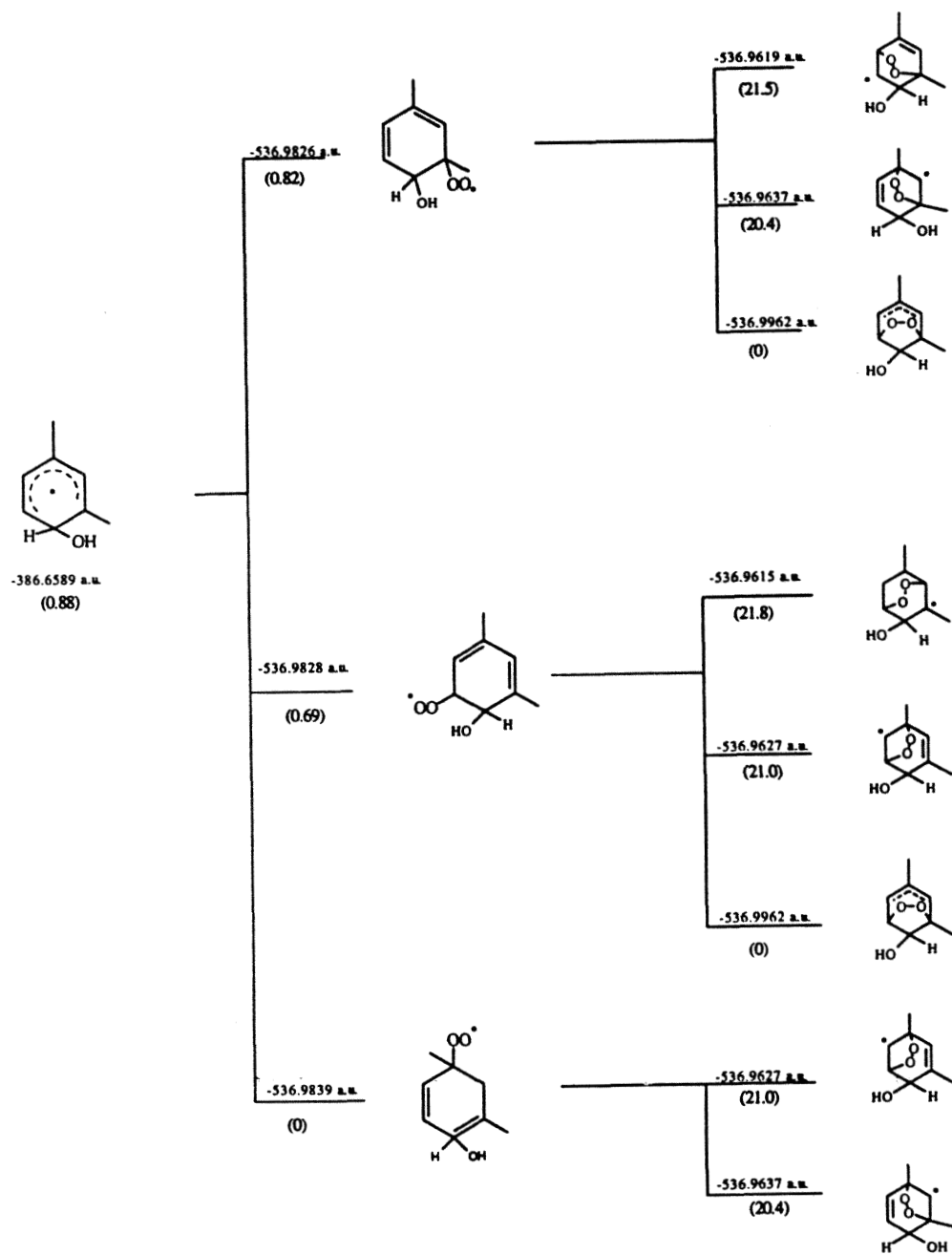
Figure C.5: Energy diagrams for m-xylene radicals.
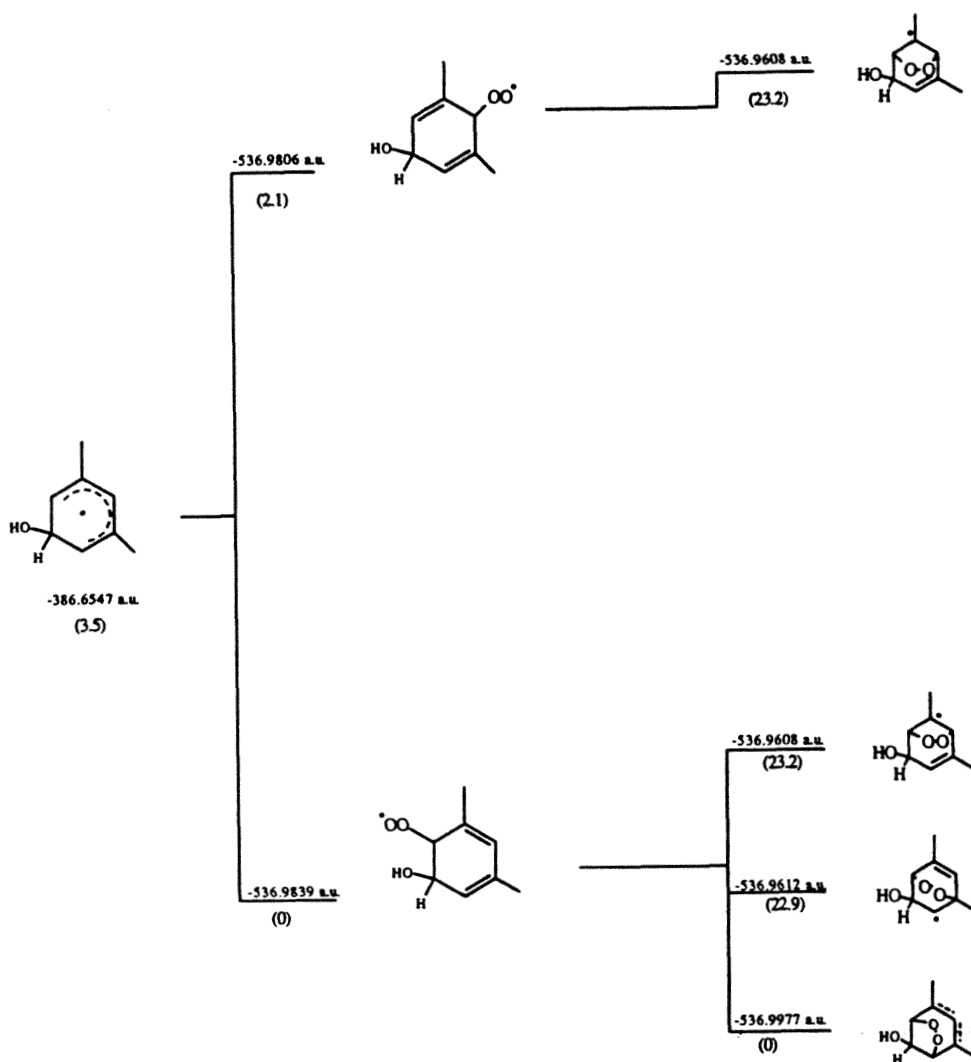
Figure C.6: Energy diagrams for m-xylene radicals.
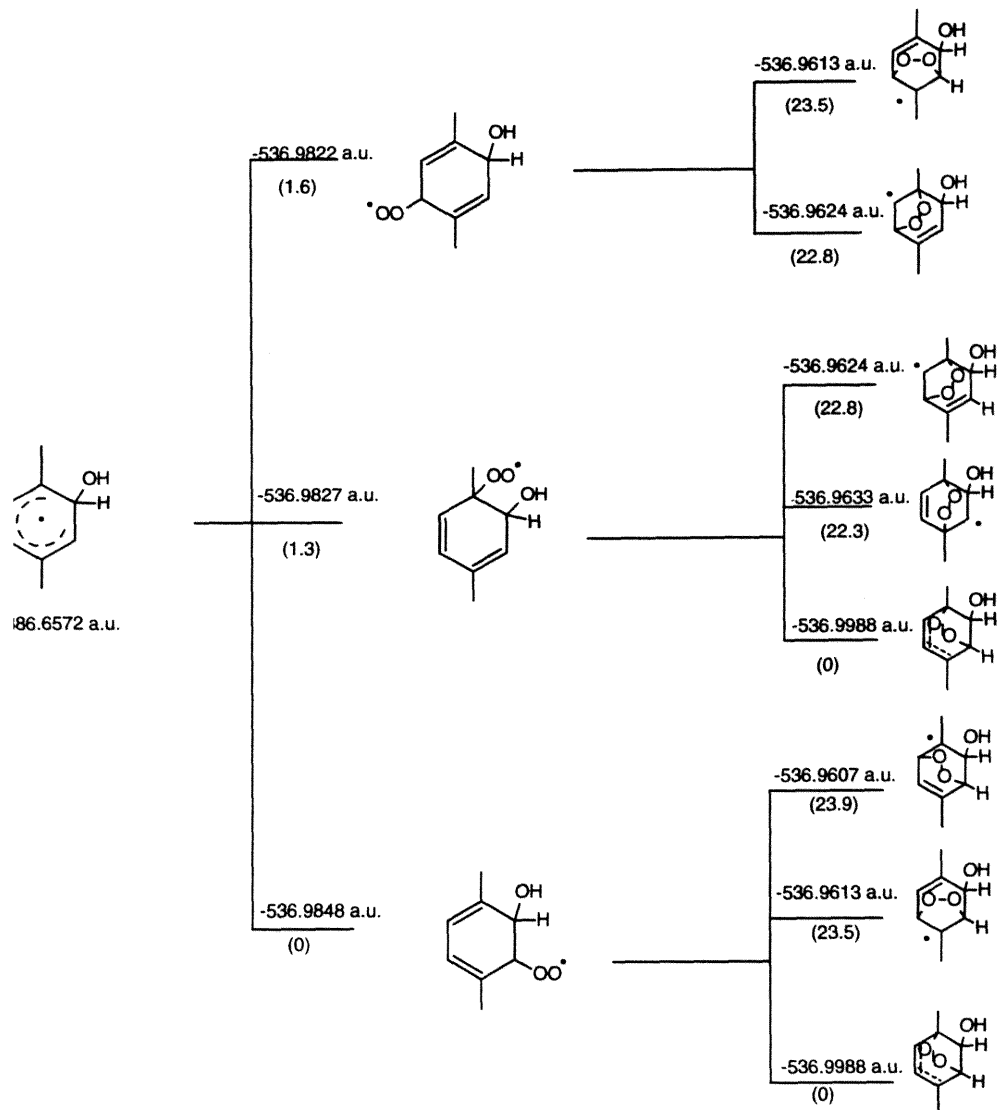
Figure C.7: Energy diagrams for p-xylene radicals.
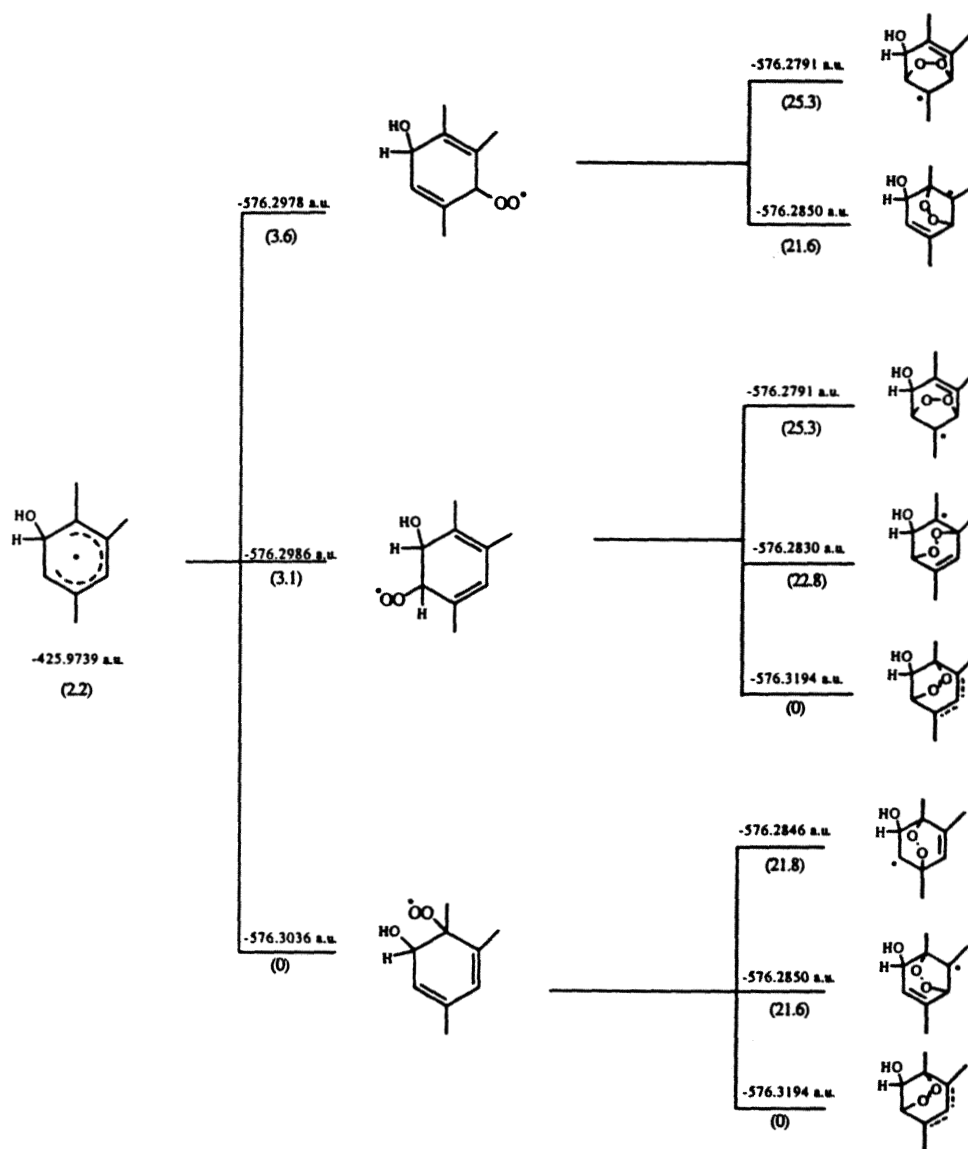
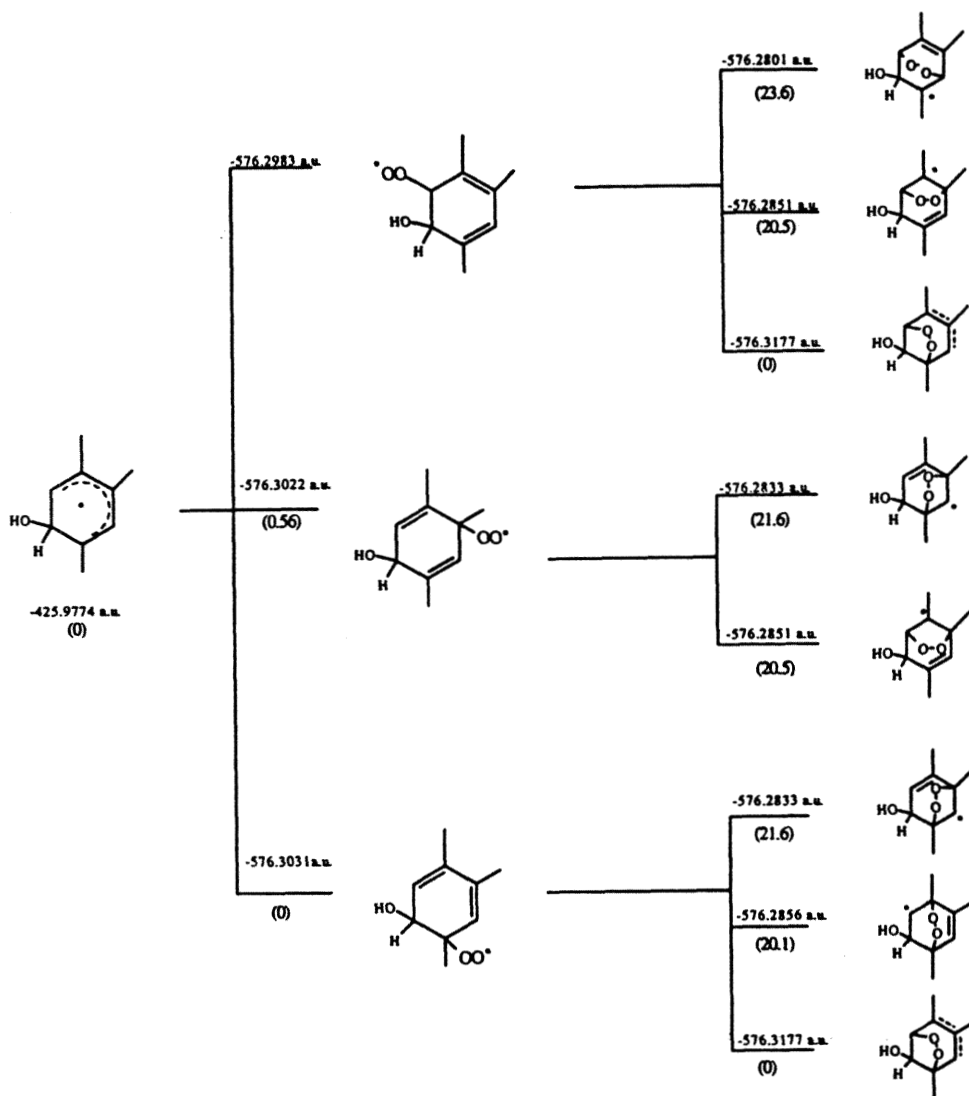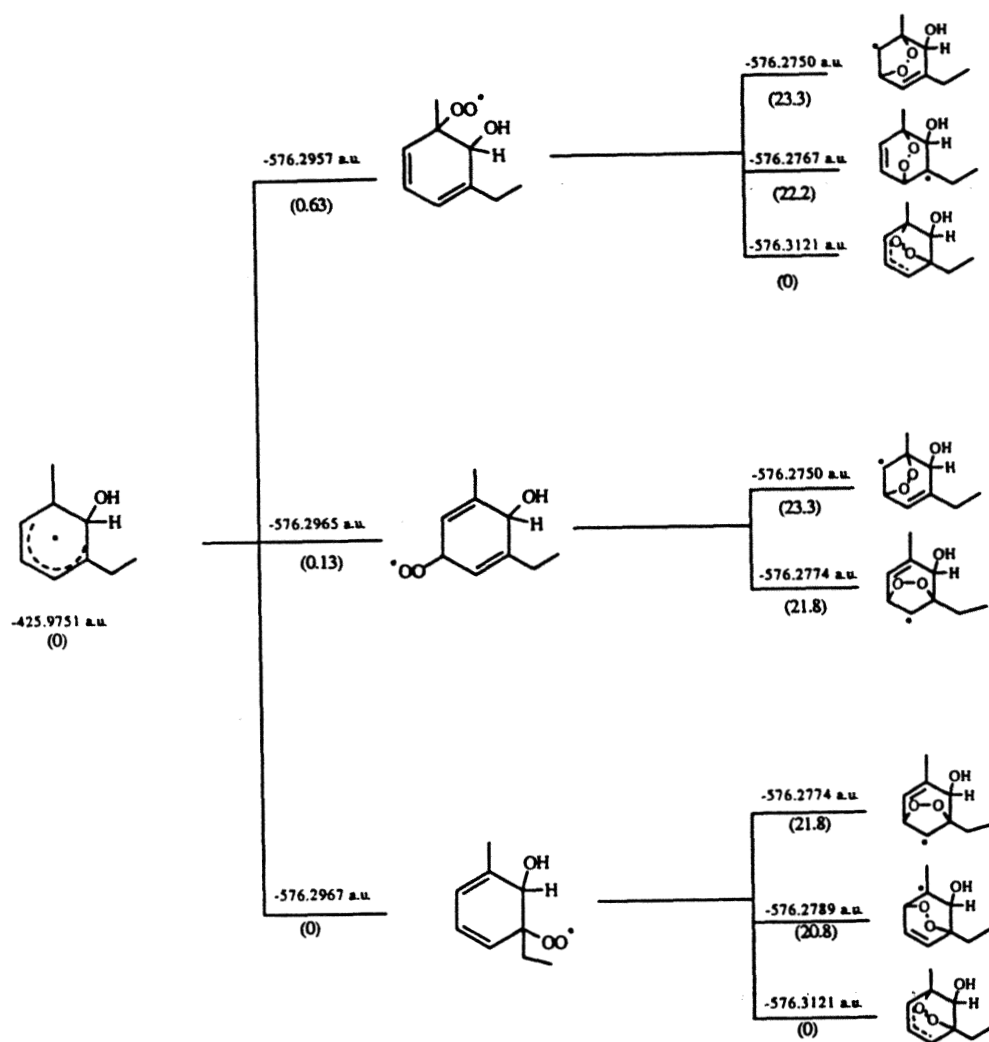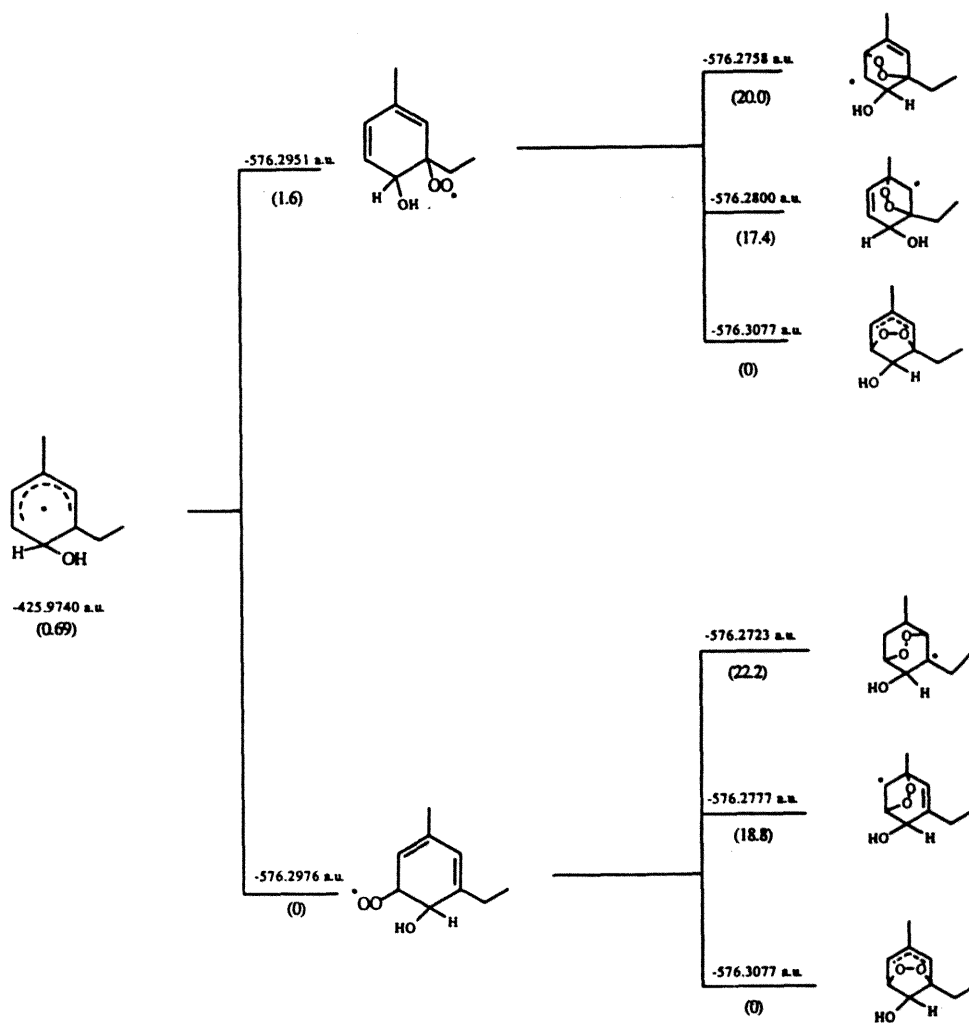Figure C.8: Energy diagrams for 1,2,4 trimethylbenzene radicals.
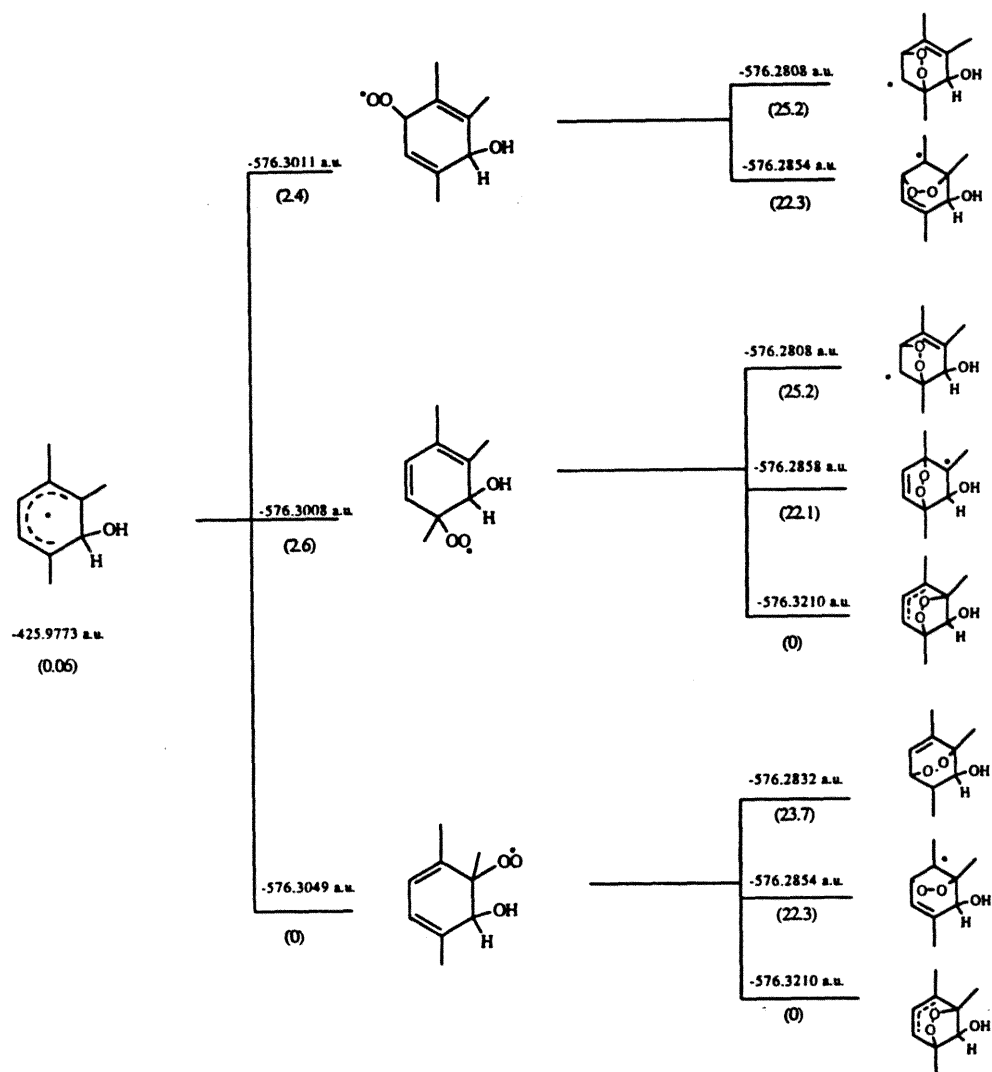
Figure C.9: Energy diagrams for 1,2,4 trimethylbenzene radicals.

Figure C.10: Energy diagrams for 1,2,4 trimethylbenzene radicals.

Figure C.11: Energy diagrams for m-ethyltoluene radicals.
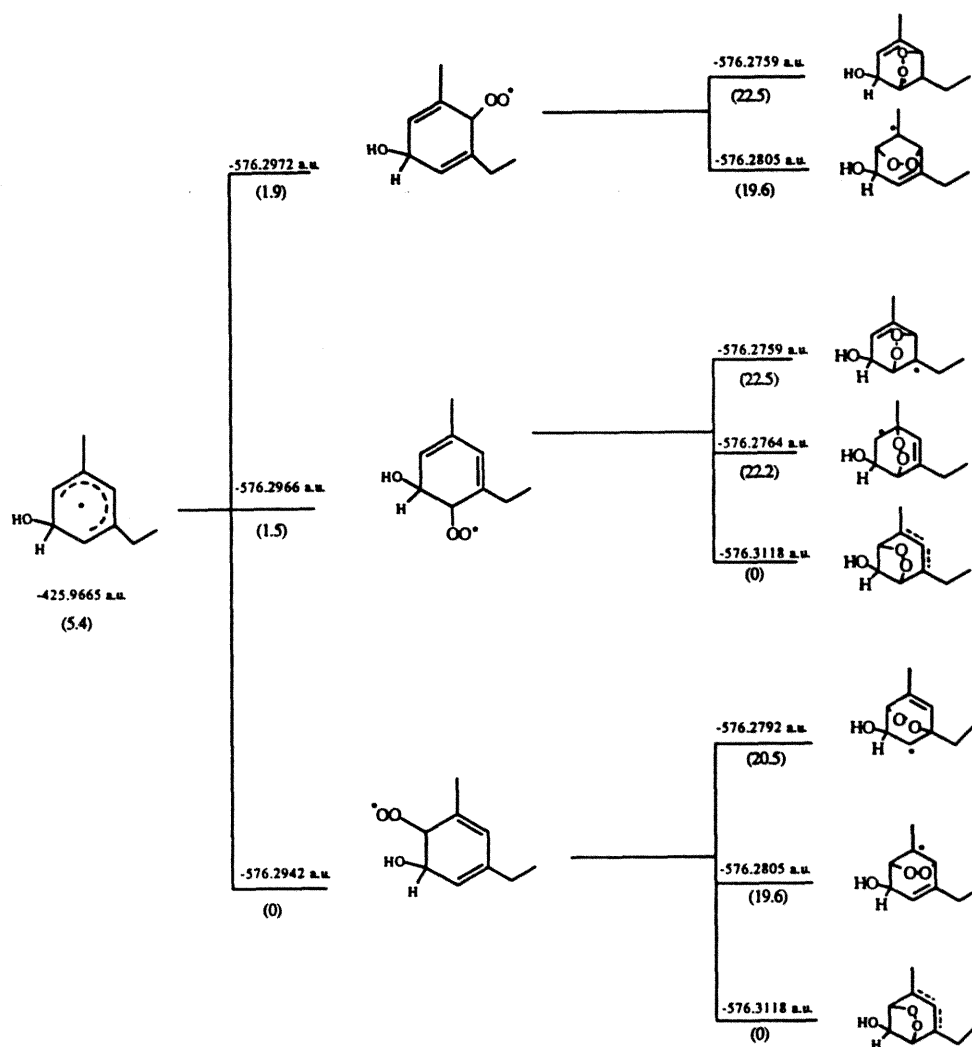
Figure C.12: Energy diagrams for m-ethyltoluene radicals.

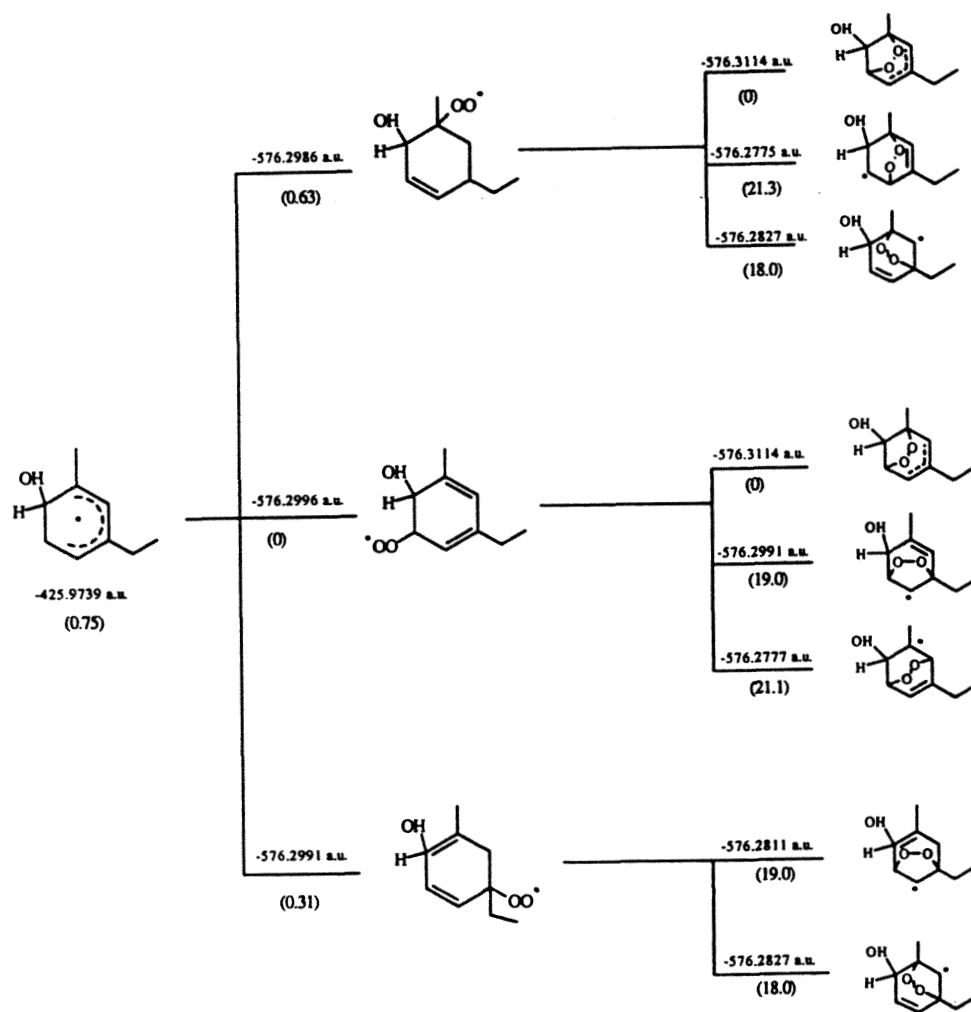Figure C.13: Energy diagrams for m-ethyltoluene radicals.

Figure C.14: Energy diagrams for m-ethyltoluene radicals.

Appendix D

Calculation of the Average [NO$_2$]

The expression used to calculate the average value of NO_2, $\overline{[NO_2]}$, was determined as :

$$\overline{[NO_2]} = \tfrac{1}{n} \sum_{i=1}^{n} ([CH_3ONO]_o(1\text{-} e^{-kt_i}) + \Delta[NO]_i)$$

where: k = photolysis rate constant for methyl nitrite, as measured

experimentally

$\Delta[NO] = [NO]_o - [NO]_t$
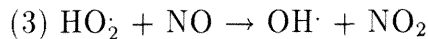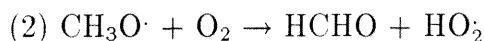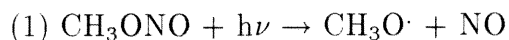
n = number of data.

This appendix presents a derivation of this formula.

In a system with methyl nitrite and NO, the NO_2 concentration at any point in time can be approximated by the formula,

$[NO_2]$ = Contribution from CH_3ONO + contribution from NO .

Methyl nitrite photolyzes according to the following reactions:

(1) $CH_3ONO + h\nu \rightarrow CH_3O\cdot + NO$

(2) $CH_3O\cdot + O_2 \rightarrow HCHO + HO_2^{\cdot}$

(3) $HO_2^{\cdot} + NO \rightarrow OH\cdot + NO_2$

Given these reactions, it is evident that the concentration of NO_2 from this source is simply the difference between the initial and final concetrations of CH_3ONO. While it is easy to determine the inital concentration of CH_3ONO, it is difficult to determine the final concentration by experiment alone. Thus, it is helpful to relate the final concentration of CH_3ONO to the inital concentration. This can be done by developing the rate equations for methyl

nitrite photolysis using Reactions 1-3. The rate expression for the photolysis of methyl nitrite can be stated as follows:

$$\frac{d[CH_3ONO]}{dt} = -k_1[CH_3ONO].$$ (D.1)

Rearranging this equation and integrating gives:

$$\int_{t_o}^{t} \frac{d[CH_3ONO]}{[CH_3ONO]} = \int_{t_o}^{t} -k_1 dt,$$ (D.2)

and

$$\ln \frac{[CH_3ONO]_t}{[CH_3ONO]_{t_o}} = -k_1 t,$$ (D.3)

which leads to

$$[CH_3ONO]_t = [CH_3ONO]_{t_o} \exp^{-k_1 t}$$ (D.4)

Substituting Equation D.4 into the expression for $[NO_2]$ gives the following expression:

$$NO_2 = [CH_3ONO]_o (1 - \exp^{-k_1 t}) + \text{contribution from NO}.$$

If we make the assumption that all of the NO is used to reduce peroxy radicals ($RO_2^·$) to oxy radicals ($RO^·$), forming one NO_2 radical in the process, then the contribution to the concentration of NO_2 from NO is simply the difference between the starting and final concentrations of NO, $\Delta[NO]$. Thus, the expression for $[NO_2]$ becomes:

$$NO_2 = [CH_3ONO]_o(1 - \exp^{-k_1 t}) + \Delta[NO]. \qquad (D.5)$$

Note that the assumption that all of the NO is used to reduce peroxy radicals to oxy radicals as opposed to forming the nitrate is reasonable given rate constant considerations for each path (see *J.Phys. Chem Ref. Data*, Monograph 2, 1995).

Summing over all of the readings, and dividing by the number of data points determined in time, t, results in the expression for the average NO_2 concentration,

$$\overline{[NO_2]} = \tfrac{1}{n} \sum_{i=1}^{n} ([CH_3ONO]_o(\ 1 - e^{-kt_i}) + \Delta[\ NO]_i)\ .$$